USGS
science for a changing world

Prepared in cooperation with the Nevada Division of Water Resources

Hydraulic Characterization of Carbonate-Rock and Basin-Fill Aquifers near Long Canyon, Goshute Valley, Northeastern Nevada

Scientific Investigations Report 2021-5021

U.S. Department of the Interior
U.S. Geological Survey

Cover: View looking eastward at the Johnson Springs wetland complex from the Pequop Mountains (left), and Big Spring discharge at Weir 8 (W-08) (right), Goshute Valley, northeastern Nevada. Photographs by Philip M. Gardner, U.S., Geological Survey, October 2017.

Hydraulic Characterization of Carbonate-Rock and Basin-Fill Aquifers near Long Canyon, Goshute Valley, Northeastern Nevada

By C. Amanda Garcia, Keith J. Halford, Philip M. Gardner, and David W. Smith

Prepared in cooperation with the Nevada Division of Water Resources

Scientific Investigations Report 2021–5021

U.S. Department of the Interior
U.S. Geological Survey

U.S. Geological Survey, Reston, Virginia: 2021

Suggested citation:
Garcia, C.A., Halford, K.J., Gardner, P.M., and Smith, D.W., 2021, Hydraulic characterization of carbonate-rock and basin-fill aquifers near Long Canyon, Goshute Valley, northeastern Nevada: U.S. Geological Survey Scientific Investigations Report 2021–5021, 99 p., https://doi.org/10.3133/sir20215021.

Associated data for this publication:
Nelson, N.C., Halford, K.J., and Garcia, C.A., 2021, MODFLOW-2005 and PEST models used to simulate the 2016 carbonate-rock aquifer test and characterize hydraulic properties of carbonate-rock and basin-fill aquifers near Long Canyon, Goshute Valley, northeastern Nevada: U.S. Geological Survey data release, https://doi.org/10.5066/P9JI8NQF.

Smith, D.W., Garcia, C.A., Halford, K.J., and Gardner, P.M., 2021, Appendixes and supplemental data—Hydraulic characterization of carbonate-rock and basin-fill aquifers near Long Canyon, Goshute Valley, northeastern Nevada, 2011–16: U.S. Geological Survey data release, https://doi.org/10.5066/P9P1P7QV.

ISSN 2328-0328 (online)

Acknowledgments

The authors gratefully acknowledge Newmont Mining Corporation and SRK Consulting for providing aquifer test data at pumping wells, long-term water-level data at monitoring wells, piezometers, and springs, and the Long Canyon geologic model. The authors gratefully acknowledge the efforts of U.S. Geological Survey colleagues Tracie R. Jackson and William G. Eldridge who contributed technical review to improve the accuracy and effectiveness of the report presentation, and Nora Nelson for assisting with documentation of the model archive of the data release.

Contents

Figures

Tables

Conversion Factors

U.S. customary units to International System of Units

Multiply	By	To obtain
	Length	
inch (in.)	25.4	millimeter (mm)
foot (ft)	0.3048	meter (m)
mile (mi)	1.609	kilometer (km)
	Area	
square foot (ft^2)	0.0929	square meter (m^2)
square mile (mi^2)	2.59	square kilometer (km^2)
acre	4,047	square meter (m^2)
	Volume	
gallon (gal)	3.7854	liter (L)
acre-foot (acre-ft)	1,233	cubic meter (m^3)
	Flow rate	
gallon per minute (gal/min)	0.2642	liter per minute (L/min)
acre-foot per year (acre-ft/yr)	1,233	cubic meter per year (m^3/yr)
foot per year (ft/yr)	0.3048	meter per year (m/yr)
cubic foot per second (ft^3/s)	0.02832	cubic meter per second (m^3/s)
	Radioactivity	
picocurie per liter (pCi/L)	0.037	becquerel per liter (Bq/L)
	Specific capacity	
gallon per minute per foot ([gal/min]/ft)	0.2070	liter per second per meter ([L/s]/m)
	Hydraulic conductivity	
foot per day (ft/d)	0.0000035	meter per second (m/s)
foot per day (ft/d)	0.3048	meter per day (m/d)
	Transmissivity*	
foot squared per day (ft^2/d)	0.09290	meter squared per day (m^2/d)

International System of Units to U.S. customary units

Multiply	By	To obtain
	Length	
micron (µ)	0.00003937	inch (in.)
meter (m)	3.281	foot (ft)
kilometer (km)	0.6214	mile (mi)
	Volume	
milliliter (mL)	0.03381402	ounce, fluid (fl. oz)
liter (L)	33.81402	ounce, fluid (fl. oz)
cubic meter (m^3)	0.0008107	acre-foot (acre-ft)
	Mass	
gram (g)	0.03527	ounce, avoirdupois (oz)

Temperature in degrees Celsius (°C) may be converted to degrees Fahrenheit (°F) as follows:

$$°F = (1.8 \times °C) + 32.$$

Temperature in degrees Fahrenheit (°F) may be converted to degrees Celsius (°C) as follows:

$$°C = (°F - 32) / 1.8.$$

Datums

Vertical coordinate information is referenced to the North American Vertical Datum of 1988 (NAVD 88).

Horizontal coordinate information is referenced to the North American Datum of 1983 (NAD 83).

Altitude, as used in this report, refers to distance above the vertical datum.

Supplemental Information

Transmissivity: The standard unit for transmissivity is cubic foot per day per square foot times foot of aquifer thickness [(ft^3/d)/ft^2]ft. In this report, the mathematically reduced form, foot squared per day (ft^2/d), is used for convenience.

Specific conductance is given in microsiemens per centimeter at 25 degrees Celsius (µS/cm at 25 °C).

Concentrations of chemical constituents in water are given in either milligrams per liter (mg/L) or micrograms per liter (µg/L).

Concentrations of dissolved gases are reported in cubic centimeters of gas at standard temperature and pressure per gram of water (ccSTP/g). Tritium concentration is reported in tritium units (TU) where 1 TU is equal to one molecule of ^3HHO per 10^{18} molecules of H_2O or 3.2 picocuries per liter. Carbon-14 activity is reported as percent modern carbon (pMC). Stable-isotope ratios are reported as delta (δ) values, which are parts per thousand or permil (‰) difference(s) from a standard.

Abbreviations

bls	below land surface
BP	before present
CE	closed-system equilibration
CO2	carbon dioxide
COOP	cooperative observer network
DEM	Digital-Elevation Model
ET	evapotranspiration
H_{avg}	mid-point recharge altitude
H_{max}	maximum recharge altitude
H_{min}	minimum recharge altitude
HTZ	highly transmissive zone
integrated LC model	integration of LC-SS and LC-MWAT2016 models
JSWC	Johnson Springs wetland complex
LC-MWAT2016 model	Long Canyon Multiple-well Aquifer Test 2016 model
LC-SS model	Long Canyon Steady State model
MODFLOW	Modular Three-Dimensional Finite-Difference Groundwater Flow Model
MNW	multi-node well
NGT_{avg}	mid-point noble-gas recharge temperature
NGT_{max}	maximum noble-gas recharge temperature
NGT_{min}	minimum noble-gas recharge temperature
permil	parts per thousand
pMC	percent modern carbon
ppm	parts per million
PEST	Parameter ESTimation
PRISM	Parameter-elevation Regressions on Independent slopes Model
RMS	root-mean-square
R^2	coefficient of determination
SNOTEL	SNOpack TELemetry
USGS	U.S. Geological Survey
^3H	tritium
TU	tritium units

Hydraulic Characterization of Carbonate-Rock and Basin-Fill Aquifers near Long Canyon, Goshute Valley, Northeastern Nevada

By C. Amanda Garcia, Keith J. Halford, Philip M. Gardner, and David W. Smith

Abstract

Understanding groundwater flow and pumping effects near pending mining operations requires accurate subsurface hydraulic characterization. To improve conceptual models of groundwater flow and development in the complex hydrogeologic system near Long Canyon Mine, in northwestern Goshute Valley, northeastern Nevada, the U.S. Geological Survey characterized the hydraulic properties of carbonate rocks and basin-fill aquifers using an integrated analysis of steady-state and stressed aquifer conditions informed by water chemistry and aquifer-test data. Hydraulic gradients and groundwater-age data in northern Goshute Valley indicate carbonate rocks in the Pequop Mountains just west and south of the Long Canyon Mine project area constitute a more permeable and active flow system than saturated rocks in the northern Pequop Mountains, western Toano Range, and basin fill. Permeable carbonate rocks in the northern Pequop Mountains, in part, discharge to the Johnson Springs wetland complex (JSWC), where mean groundwater ages range from 500 to 2,400 years and samples all contain a small fraction of modern waters, relative to mean ages of 8,600 to more than 22,000 years for most groundwater sampled to the north and east. Recharge to the JSWC occurs from a roughly 27-square-mile area in the upgradient Pequop Mountains to the west, composed mostly of permeable carbonate rock and fractured quartzite, and bounded by low-permeability shales and marbleized and siliclastic rocks.

Single-well aquifer-test analyses provided transmissivity estimates at pumped wells. Transmissivity estimates ranged from 7,000 to 400,000 feet squared per day (ft^2/d) in carbonate rocks and from 2,000 to 80,000 ft^2/d in basin fill near the Long Canyon Mine. Water-level drawdown from multiple-well aquifer testing and rise from unintentional leakage into the overlying basin-fill aquifer were estimated and distinguished from natural fluctuations in 93 pumping and monitoring sites using analytical water-level models. Leakage of disposed aquifer-test pumpage occurred south of the aquifer test area through an unlined irrigation ditch. Drawdown was detected at distances of as much as 3 miles (mi) from pumping wells at all but one carbonate-rock site, at basin-fill sites on the alluvial fan immediately downgradient from pumping wells, and in Big Spring and spring NS-05. Similar drawdowns in carbonate rocks within the drawdown detection area suggest all wells penetrate a highly transmissive zone (HTZ) that is bounded by low-permeability rocks. Drawdown was not detected in carbonate rocks to the west of Canyon fault, in any basin-fill sites on the valley floor east of the Hardy fault, or at volcanic sites to the north, indicating that these major fault structures and (or) permeability contrasts between hydrogeologic units impeded groundwater flow or obscured pumping signals. Alternatively, unintentional leakage might have obscured drawdown at basin-fill sites on the valley floor, where water-level rise was detected at nine sites over 3 mi.

Consistent hydraulic properties were estimated by simultaneously interpreting steady-state flow during predevelopment conditions and changes in groundwater levels and springflows from the 2016 carbonate-rock aquifer test with an integrated groundwater-flow model. Hydraulic properties were distributed across carbonate rocks, basin fill, volcanic rocks, and siliciclastic rocks with a hydrogeologic framework developed from geologic mapping and hydraulic testing. Estimated transmissivity distributions spanned at least three orders of magnitude in each rock unit. In the HTZ, simulated transmissivities ranged from 10,000 to 23,000,000 ft^2/d, with the most transmissive areas occurring around Big Spring. Comparatively low carbonate-rock transmissivities of less than 10,000 ft^2/d were estimated in the northern Pequop Mountains and poorly defined values of less than 1,000 ft^2/d were estimated in the western Toano Range. Transmissivities in basin fill ranged from less than 10 to 80,000 ft^2/d and were minimally constrained by the 2016 carbonate-rock aquifer test because poorly quantified leakage affected water levels more so than pumping. The most transmissive areas were informed by single-well aquifer tests along the eastern edge of the Pequop Mountains near Long Canyon Mine and could be indicative of a hydraulic connection between basin fill and more transmissive underlying carbonate rocks. Simulated transmissivities of volcanic and low-permeability rocks mostly are less than 1,000 ft^2/d. The estimated hydraulic-property distributions and informed interpretation of hydraulic connections among hydrogeologic units improved the characterization and representation of groundwater flow near the Long Canyon Mine.

Introduction

The Long Canyon Mine project area in northwestern Goshute Valley, northeastern Nevada (fig. 1), requires groundwater pumping from the carbonate-rock aquifer to sustain ongoing open-pit and underground gold mining and processing activities that are projected to continue beyond 2024 (Bureau of Land Management, 2014). Long-term pumping can alter hydraulic gradients in a groundwater-flow system, which, in turn, can affect spring discharge rates, surface-water flow, other well users, and the overall groundwater budget in a hydrographic area. Accurate subsurface hydrologic characterization is essential for understanding groundwater-flow paths and evaluating pumping effects on the hydrologic system near the Long Canyon Mine project area.

Groundwater beneath northwestern Goshute Valley flows through basin-fill and carbonate rocks that have been offset along the eastern flank of the Pequop Mountains by range-front faults (Golder Associates Inc., 2012). The Johnson Springs wetland complex (JSWC) occurs within the Long Canyon Mine Project area just south and west of existing and proposed pumping wells open to the carbonate-rock aquifer (fig. 2). The JSWC is composed of more than 80 springs, the largest of which is Big Spring, and provides habitat for the relict dace (*Relictus solitarius*), an endemic species in east-central and northeastern Nevada (Wildlife Action Plan Team, 2012). Outflow from the JSWC, and potential gaining reaches from the basin-fill aquifer, contribute to perennial surface-water flow in Hardy Creek (fig. 2) (Global Hydrologic Services, Inc., 2010; Golder Associates Inc., 2012).

Hydraulic testing and characterization of hydrogeologic units and structures to evaluate groundwater flow and effects of groundwater development for mining operations in Long Canyon have been ongoing since 2011 (Golder Associates Inc., 2012). Hydraulic connections between the carbonate-rock aquifer and several springs within the JSWC, most notably Big Spring, have been recognized through aquifer testing (Barnett Intermountain Water Consulting and others, 2011; Golder Associates Inc., 2012) and stable isotope data (Mayo and Associates, 2013). Prior to 2016, aquifer testing within the carbonate-rock aquifer was limited to a few days to minimize effects on Big Spring discharge and relict dace habitat. Short-duration testing, in turn, limited the volume of aquifer investigated.

During summer 2016, the Long Canyon Mine conducted a large-scale carbonate-rock aquifer test to improve understanding of groundwater-flow paths and more accurately characterize bulk hydraulic properties of the groundwater-flow system. Increased pumping duration and distance between pumping and monitoring sites during the 2016 test increased the aquifer volume investigated with respect to previous aquifer tests. Additional unintentional stresses to the adjacent (or overlying) basin-fill aquifer during the 2016 test were generated by discharge of aquifer-test water into a leaky irrigation ditch and water supplementation to Big Spring to protect aquatic species.

Aquifer-test data from complex hydrogeologic units frequently are interpreted using numerical models to evaluate heterogeneous hydraulic properties of the groundwater-flow system. Numerical simulations that combine estimated drawdowns from aquifer testing with knowledge of the hydrogeologic framework and steady-state hydrologic budget provide a more accurate characterization of complex groundwater systems than numerical models alone (Walton, 2008; Yobbi and Halford, 2008). The flexibility of numerical models allows for hydraulic characterization of hydrogeologic units and structural features and for evaluation of structural effects on drawdown behavior (Renard, 2005).

The U.S. Geological Survey (USGS), in cooperation with the Nevada Division of Water Resources, characterized the hydraulic properties of carbonate-rock and basin-fill aquifers near the Long Canyon Mine project area (fig. 1) using two numerical stress-response models and water-chemistry data. Stress-response models that simulated the steady-state conditions in the groundwater flow system and transient responses during the 2016 carbonate-rock aquifer test were interpreted simultaneously. Existing and new water-chemistry data collected during this study were combined to delineate the predevelopment contributing area to Big Spring and the JSWC.

Purpose and Scope

The purpose of this report is to present estimated hydraulic-property distributions and the presence and absence of hydraulic connections for aquifers and hydrogeologic units near and downgradient from the Long Canyon Mine project area (fig. 1). Hydraulic properties of carbonate-rock and basin-fill aquifers were estimated with stress-response models that simulated steady-state flow and responses to a large-scale aquifer test. Simulated hydrologic components include likely groundwater recharge and discharge from Goshute and Independence Valleys and the predevelopment contributing area to Big Spring and the JSWC. Representative groundwater discharge from Goshute and Independence Valleys was determined by comparing previous groundwater discharge estimates to measured discharges in the Long Canyon Mine project area. The predevelopment contributing area to Big Spring was delineated with water chemistry from selected wells and a potentiometric surface. Water-level and spring-discharge changes from pumping 140 million gal during the 2016 carbonate-rock aquifer test were differentiated from environmental water-level fluctuations with analytical models. Transmissivities around individual wells were estimated at 48 sites with 7 single-well pumping aquifer tests, 19 specific-capacity estimates, and 22 slug tests.

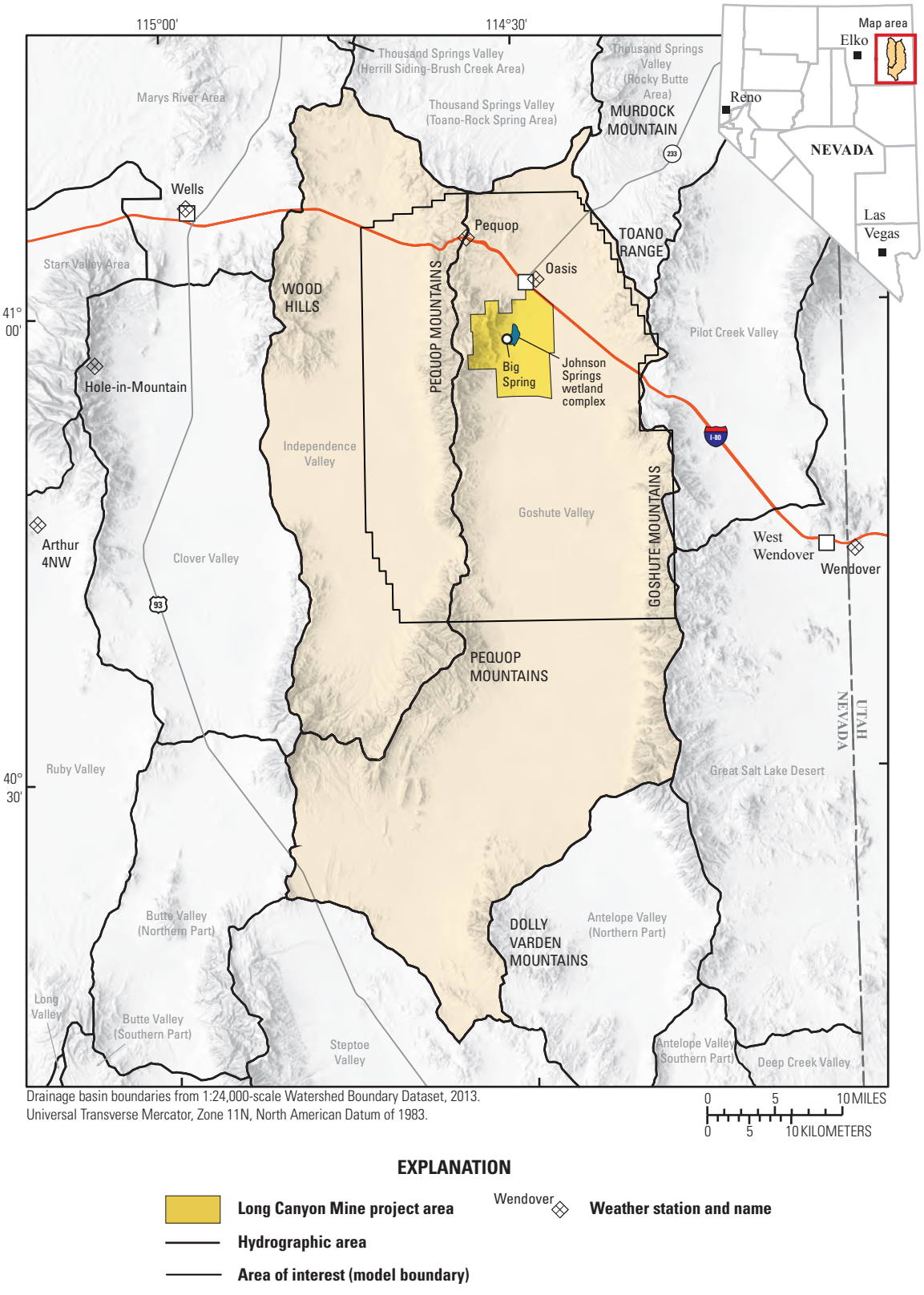

Figure 1. Location of study area, Long Canyon Mine project area, area of interest, and weather stations, Long Canyon, Goshute Valley, northeastern Nevada.

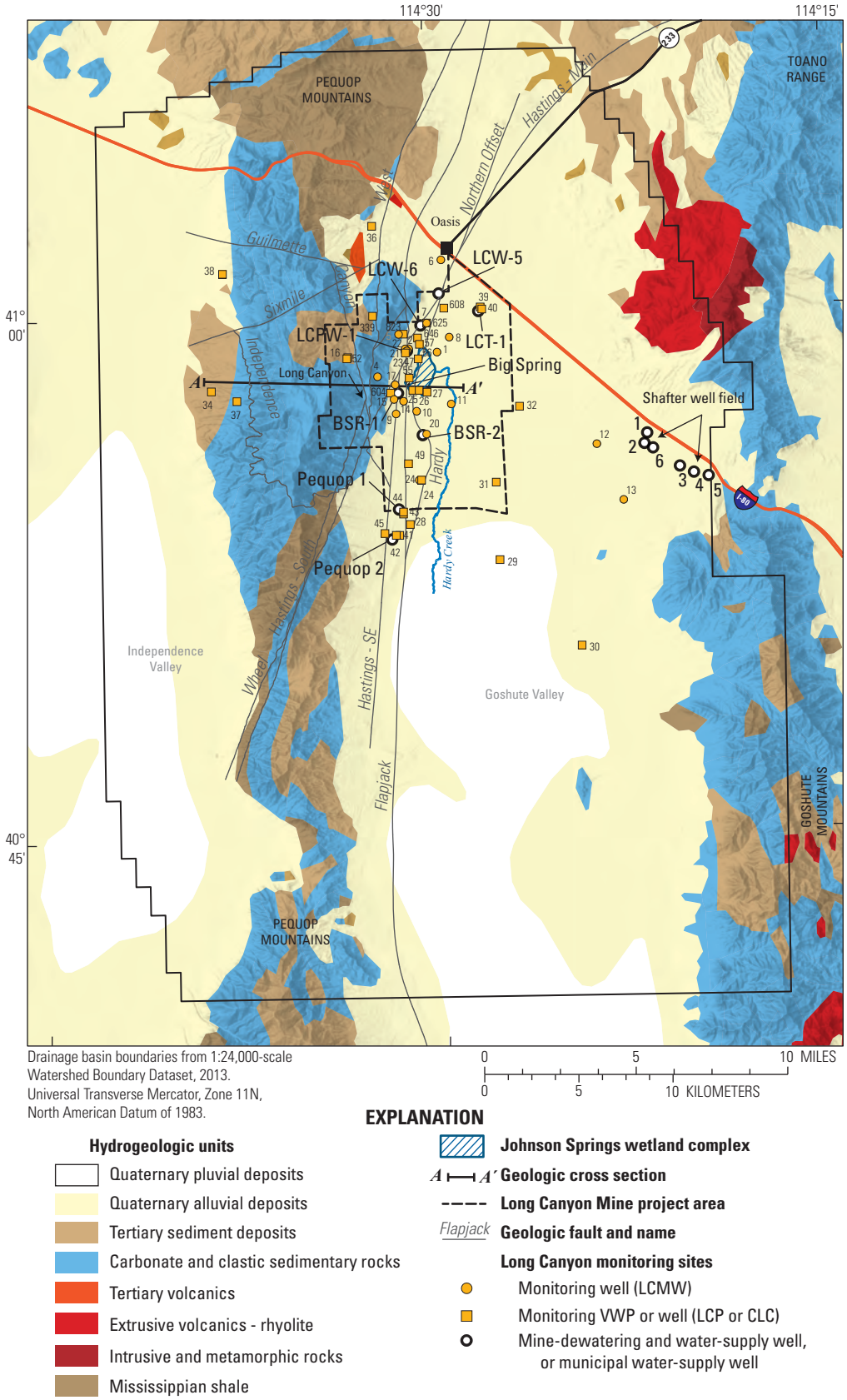

Figure 2. Surface geology and selected monitoring well and vibrating-wire piezometer (VWP) sites, Long Canyon, Goshute Valley, northeastern Nevada. See figures 3 and 26 for cross section *A*–*A'*. Well and VWP name prefixes are shown in parentheses.

Bulk hydraulic properties were estimated by simultaneously calibrating two three-dimensional numerical groundwater-flow models to steady-state and transient stresses. These models simulated steady-state (predevelopment) conditions and changes in groundwater levels and springflows from the 2016 carbonate-rock aquifer test. Transmissivity, specific yield, and storage coefficient distributions in eastern Independence Valley and northern Goshute Valley were estimated by simultaneously calibrating numerical groundwater-flow models. Water-chemistry data are archived in the USGS National Water Information System (U.S. Geological Survey, 2019). Drawdown observations, pumping datasets, groundwater-flow models, and supporting documentation are available in USGS data release reports by Nelson and others (2021) and Smith and others (2021).

Description of Study Area

The study area is composed of three overlapping areas including the Long Canyon Mine project area, the larger area of interest, and the full extent shown in figure 1 that encompasses areas within and adjacent to Goshute and Independence Valleys. The Long Canyon Mine project area, located in Goshute Valley about 65 mi east of Elko, Nevada, and 28 mi northwest of West Wendover, Nevada, bounds the mineral resource, but mine water development and disposal activities extend across northern Goshute Valley. Data within and adjacent to Goshute and Independence Valleys were used to conceptualize the groundwater flow system and the area of interest represents the groundwater-flow model extent, which encompasses all mining activities in Goshute Valley.

The Long Canyon Mine project area lies on the east-facing slope of the Pequop Mountains, which range in elevation from 9,255 ft at the highest point along the divide to 5,590 ft on the valley floor. The ridge of the Pequop Mountains forms the boundary between Goshute Valley (954 mi^2) to the east and Independence Valley to the west (345 mi^2). Goshute Valley is north-northeast trending, bordered to the north, south, and east by Murdock Mountain, the Dolly Varden Mountains, the Goshute Mountains, and the Toano Range, respectively. The JSWC is located in northeastern Goshute Valley near the transition from alluvial fan to valley floor (fig. 2). The spring complex is composed of Big Spring, its primary discharge point, and numerous secondary springs and seeps. The spring complex is home to the relict dace (*Relictus solitarius*), a threatened fish species that is native to the perennial system.

The climate of the study area is arid to semi-arid, characteristic of a high desert region. The climate is characterized by warm summers and cold winters, large fluctuations in daily and annual temperatures, and low precipitation and humidity. In Oasis, Nevada, located at the northern edge of the Long Canyon Mine project area, 30-year (1981–2010) average summertime maximum temperatures are 87 °F, whereas average wintertime minimum temperatures are about 10 °F (National Climatic Data Center, 2017). Annual precipitation in Oasis, Nevada, averages about 9 in. (1981–2010) and occurs throughout the year (National Climatic Data Center, 2017).

Most streams in the study area are ephemeral and flow only for brief periods after infrequent intense rainfall and during and shortly after spring snowmelt (Global Hydrologic Services, Inc., 2010). Flow is generally from west to east from the Pequop Mountains toward the valley floor; however, most flow infiltrates the fractured bedrock or the alluvial fan before reaching the valley floor (Golder Associates Inc., 2012). Streams originating in the JSWC are the only perennial surface-water features in northern Goshute Valley. These perennial streams are fed by Big Spring and numerous smaller springs and seeps that discharge along a roughly 1.5-mi transect trending north-northeast along the eastern range front of the Pequop Mountains (fig. 2). Some streamflow is diverted for irrigation by ranches near the Long Canyon Mine project area or is consumed by vegetation within the spring complex. Perennial streamflow from the JSWC converges into Hardy Creek, which flows several miles south until surface water ultimately is consumed by vegetation or lost to evaporation or subsurface percolation (Global Hydrologic Services, Inc., 2010; Golder Associates Inc., 2012).

Discharge from Big Spring has been measured by the cities of Wendover, Utah, and West Wendover, Nevada, during 2007–17. Big Spring discharge averaged about 1,100 gal/min (2.5 ft^3/s; 1,800 acre-ft/yr) but varied seasonally in response to upgradient winter precipitation and recharge (Paul Pettit and Stephanie Douglas, Newmont Mining Corporation, written commun., 2017). Average discharge over the same period from all other springs in the JSWC (other than Big Spring) was about 600 gal/min (970 acre-ft/yr; see section, "Groundwater Flow").

Previous Investigations

Multiple independent groundwater resource studies in Goshute and Independence Valleys provide a foundation for characterizing the hydrogeology of the study area. The earliest study, Eakin and others (1951), provided a reconnaissance estimate of the groundwater budget in Goshute, Antelope, and Independence Valleys. Harrill and others (1988) synthesized previous Great Basin groundwater studies into a hydrologic atlas as part of the USGS Regional Aquifer System Analysis. The hydrologic atlas by Harrill and others (1968) adopted recharge estimates for Goshute and Independence Valleys from Eakin and others (1951) and based interbasin flow estimates on published water budgets and knowledge of hydrogeologic units and hydraulic potential. Nichols (2000) estimated average-annual groundwater discharge and recharge in Goshute and Independence Valleys. Groundwater discharge was estimated using remote sensing and extrapolated evapotranspiration (ET) measurements made in central and southern Nevada, whereas recharge was estimated using a modified Maxey-Eakin method. Heilweil and Brooks (2011) and Brooks

and others (2014) also estimated groundwater discharge and recharge in Goshute and Independence Valleys as part of a regional groundwater flow study of the Great Basin. Although estimates from these studies provided insight into basin-level water budgets, Brooks and others (2014) noted that the regionally based estimates should not be used for water-resource management at the basin level because localized estimates often are based on regional rather than localized trends and observations.

Long Canyon hydrogeologic investigations began with Global Hydrologic Services, Inc. (2010), which provided a principal understanding of groundwater-flow paths, water chemistry, and hydraulic properties in the Long Canyon Mine project area (fig. 1). Multiple-well aquifer testing in Long Canyon began in 2011 with a 2-day test in carbonate-rock aquifer well LCPW-1 (Barnett Intermountain Water Consulting and others, 2011), followed by a 2-week test in basin-fill well *BSR-2* in 2012 (Golder Associates Inc., 2012; fig. 2). Golder Associates Inc. (2012) provided a hydrogeologic characterization of the Long Canyon Mine project area that included water budget estimates and hydraulic properties of basin-fill and carbonate-rock aquifers based on multiple- and single-well aquifer tests and slug tests. Estimated water-budget components for northern Goshute Valley (Golder Associates Inc., 2012) were based on Nichols (2000) and a modified Maxey-Eakin method (Maxey and Eakin, 1951) by Epstein and others (2010) that incorporated more than 70 reconnaissance-level and measurement-based recharge estimates across Nevada, including those from Nichols (2000). Golder Associates Inc. (2012) incorporated existing hydrogeologic data in a numerical groundwater-flow model that extended across northern Goshute Valley.

Monitoring Network and Data Collection

A network of 276 sites located within and adjacent to Goshute Valley and Independence Valley was used to characterize the hydraulic properties of carbonate-rock and basin-fill aquifers in the study area (fig. 2; Smith and others, 2021, appendix 1). Sites include mine-dewatering and water-supply wells, municipal water-supply wells, and monitoring wells (typically with a prefix of *LCMW*), vibrating-wire piezometers (VWPs; typically with prefixes of *CLC* or *LCP*), well drillers' logs, springs (with prefixes of *W*, *F*, *NS*, *CS*, or *SS*), and weather stations. Site data were used to evaluate long-term steady-state groundwater conditions and stressed conditions during aquifer testing. Data include withdrawal rates from pumping wells; water levels at pumping wells, monitoring wells, and VWPs; spring stage and discharge; specific capacity; water chemistry; and precipitation. Aquifer tests include one multiple-well test and seven single-well tests. The multiple-well aquifer-test includes simultaneous pumping in carbonate-rock wells LCW-6 and LCPW-1 during summer 2016. The seven single-well aquifer tests occurred during 2012, 2014, 2015, and 2016 in wells BSR-2, LCPW-1, LCT-1, Pequop-1, Pequop-2, LCW-5, and LCW-6.

Some monitoring sites occur at the same (X,Y) location but at different depths, often in different hydrogeologic units. For example, borehole LCMW-09 has two well completions: LCMW-09S and LCMW-09D, where *S* and *D* represent shallow and deep completions in the borehole, respectively. VWPs such as sites LCP-27A-C are present at three separate depths, where *A* is the deepest piezometer and *C* is the shallowest piezometer.

VWPs differ from conventional monitoring wells because piezometers are grouted in place with a cement-bentonite mixture (Mikkelsen and Green, 2003). Formation pore pressures are transmitted within minutes through the cement-bentonite mixture and are measured with VWPs. Lag between changes in formation pore pressures and measured changes is minimal, despite low permeabilities of the cement-bentonite mixture because wellbore storage is absent (Penman, 1961). Water-level altitudes measured with a VWP and in a comparable conventional well can differ by 2–3 ft at a depth of 50 ft below land surface (bls; McKenna, 1995). Water-level changes measured with a VWP and a conventional well typically will agree, except when pore pressures are affected by curing of the overlying grout in a borehole because the pressure from the entire saturated water column above a VWP must be measured. Water-levels typically are measured at a lower resolution with VWPs than with a transducer in a conventional well.

Stage and discharge measurements downgradient from Big Spring and lesser springs within the JSWC were made within stream channels or pools using flumes, weirs, and stilling wells during aquifer testing. Triangular V-notch and rectangular weirs (prefix *W*) are located downstream from spring orifices or from pipes and culverts that conveyed water from multiple springs. Flumes (prefix *F*) measure combined springflow captured by drainage ditches or channels (SRK Consulting, 2017). Stilling wells measure pool or channel stage downstream from springs denoted as north springs (NS), central springs (CS), or south springs (SS). Descriptions of springflow measurement sites are shown in table 1. Big Spring discharge is measured at W-08. Downstream from W-08, Big Spring discharge is partially diverted for irrigation at Big Springs Ranch (southeast of Big Spring) and the remainder flows into the JSWC (table 1).

Water-level sampling rates differed based on the purpose of the measurement. High frequency (sub-daily) monitoring in a subset of wells, piezometers, and springs (or streams) occurred during aquifer testing only. Water levels in most monitoring wells were measured monthly between aquifer tests and piezometers were measured daily. Continuous daily flow measurements at Big Spring have been made by the cities of Wendover, Utah, and West Wendover, Nevada, since 2006.

SRK Consulting and Newmont Mining Corporation (written commun., 2017) monitored water levels at 118 sites located in northern Goshute Valley (fig. 2) during the combined LCW-6 and LCPW-1 multiple-well aquifer test,

Table 1. Description of springflow measurement sites, Long Canyon, Goshute Valley, northeastern Nevada.

[Locations of sites are shown in figure 16. **Measured flow:** JSWC, Johnson Springs wetland complex; ET, evapotranspiration]

Site name	Structure	Measured flow
F-01	Flume	Combined flows from multiple springs in the north springs area and is downstream from F-04.
F-02	Flume	Residual outflow from the JSWC as it converges into Hardy Creek. Measured flow represents total springflow in the JSWC less that lost to ET or downward percolation.
F-03	Flume	Combined flows from multiple springs in the south springs area, parts of Big Spring flow diverted through the north ditch, and possible overflow from Big Spring pond.
F-04	Flume	Combined flows from multiple springs in the north springs area.
W-01	Weir	Combined flows from multiple springs in the central springs area including flow measured at W-02, W-04, W-05 and W-06, and parts of Big Spring diverted through the north ditch.
W-02	Weir	Combined flows from multiple springs in the central springs area.
W-03	Weir	North ditch flow diverted from Big Spring.
W-04	Weir	Combined flows from multiple springs in the central springs area.
W-05	Weir	Combined flows from multiple springs in the central springs area.
W-06	Weir	Flow from one spring in the central springs area.
W-07	Weir	Flow from one spring in the central springs area.
W-08	Weir	Flow from Big Spring. Downgradient from W-08, flow is partially diverted into north and south ditches and the remainder flows into a pond to the east. North ditch mostly drains into JSWC in the south springs area and a residual amount drains into the central springs area. South ditch flows toward Big Springs Ranch for irrigation. Pond overflow drains into the south springs area.

hereinafter referred to as the carbonate-rock aquifer test. Water levels were monitored in 102 wells and piezometers, whereas discharge and (or) stage were monitored at 16 spring (or stream) sites. Sub-daily monitoring during the carbonate-rock aquifer test began during April–May 2016, and data through January 2018 were used for the analysis presented in this report.

Well development and constant-rate aquifer testing in carbonate-rock wells LCW-6 and LCPW-1 are summarized in table 2. The primary water-bearing units open to LCW-6 and LCPW-1 are limestone and dolomite from the Ordovician Pogonip Group (Smith and others, 2021, appendix 2). Well LCW-6 was pumped from July 27 to August 10, 2016, and from August 19 to September 8, 2016. Well LCPW-1 was pumped from August 8 to 10, 2016, and from August 19 to September 8, 2016. Well LCW-6 was pumped at constant rates averaging 1,140 and 1,100 gal/min for 12 and 20 days, respectively. Well LCPW-1 was pumped at constant rates averaging 2,590 and 2,750 gal/min for 2 and 20 days, respectively. Withdrawal from wells LCPW-1 and LCW-6 totaled about 140 million gallons (table 2). A 2-day multiple-well aquifer test also occurred in carbonate-rock well LCPW-1 in 2011 (Barnett Intermountain Water Consulting and others, 2011), but this test was excluded from the integrated analysis because the 2011 test was repeated during the 2016 carbonate-rock aquifer test. Location information for all monitoring sites is provided in Smith and others (2021, appendix 1). Detailed information on well construction for pumping and monitoring wells and VWPs is provided in Smith and others (2021, appendix 2). Construction information was obtained primarily through written communications from Newmont Mining Corporation.

Table 2. General pumping schedule of wells LCW-6 and LCPW-1 during the 2016 carbonate-rock aquifer test in Long Canyon, Goshute Valley, northeastern Nevada, July–September 2016.

[**Start date/time and End date/time:** Start and end of pumping from Newmont Mining Corporation aquifer-test reports. **Approximate volume discharged:** The volume of water discharged from the pumping well between the start and end times. **Approximate discharge rate:** Represents the pumping rate when the pump was on during the period of analysis; value based on data collected from in-line flowmeter. **Abbreviations:** gal/min, gallons per minute; Mgal, million gallons; hhmm, time in 24-hour format in Pacific Daylight Time; NA, not applicable]

Pumping-well name	Start date/time	End date/time	Aquifer-test description	Approximate volume discharged (Mgal)	Approximate discharge rate (gal/min)	Notes
LCW-6	07-27-16, 1225 hours	07-28-16, 1715 hours	Well development and step testing	1.1	NA	None
LCW-6	07-29-16, 0901 hours	08-10-16, 0900 hours	Constant-rate test	19.6	1,139	Test truncated owing to spring supplementation complications.
LCW-6	08-19-16, 1940 hours	09-08-16, 1200 hours	Constant-rate test	31.8	1,096	
LCPW-1	08-08-16, 0631 hours	08-10-16, 0430 hours	Constant-rate test	7	2,592	Test truncated owing to generator failure.
LCPW-1	08-19-16, 0702 hours	09-08-16, 1200 hours	Constant-rate test	80.2	2,756	

Hydrogeology

The study area (Goshute Valley) is located within the Basin and Range physiographic province. The area has undergone periods of deformation with contraction and extension, forming a deep fault-blocked central valley bordered primarily by carbonate-clastic mountain ranges (Thorman, 1970; Coats, 1987). Structurally, the Pequop Mountains and Toano Ranges include low- and high-angle normal and reverse faults (Ketner and others, 1998; Camilleri, 2010; fig. 3). Miocene to Quaternary Basin and Range normal faulting created a deep structural basin that accumulated alternating Tertiary to Quaternary age pluvial, volcanic, and alluvial sediments, collectively referred to as basin fill (Camilleri, 2010). Basin-fill sediments are underlain by bedrock consisting mainly of carbonate and clastic sedimentary rocks of Cambrian to Pennsylvanian age.

Geologic Units

Geologic units and formations were classified and reported based on similar hydrogeologic characteristics and inferred potential of the rock unit to transmit groundwater. Geologic units described herein extend west-east from the eastern half of Independence valley to the western edge of the Toano Range, and north-south from northern to central Goshute Valley (fig. 2). Hydrogeologic units, ordered in decreasing age, include: (1) carbonate and clastic sedimentary rocks of Cambrian to Pennsylvanian age, (2) volcanic rocks of Eocene age, and (3) sedimentary and volcanic deposits (basin fill) of Tertiary to Quaternary age (figs. 2 and 3). Approximate depths of hydrogeologic units are limited to total depth of monitoring or exploration wells and gravity survey estimates by (Paul Pettit and Stephanie Douglas, Newmont Mining Corporation, written commun., 2017). Supplemental descriptions of rock units and structure are available in Thorman (1970), Coats (1987), McCollum and Miller (1991), Ketner (1997), Ketner and others (1998), Camilleri (2010), and Golder Associates Inc. (2012).

Carbonate and Clastic Sedimentary Rocks

Ordovician and Cambrian to Pennsylvanian carbonate and clastic sedimentary rocks of Goshute Valley mainly consist of (1) Dunderberg Shale (Cd), (2) Notch Peak Formation (OCnp), (3) Pogonip Group (Op), (5) Eureka Quartzite (Oe) (fig. 3) and (5) Ely Limestone (Pe) . The Ordovician and Cambrian Dunderberg Shale is a metamorphosed phyllitic shale, with thin limestone beds, in the Pequop Mountains and Toano Range (Ketner, 1997). The shale formation ranges in thickness from 350 to 1,200 ft, outcropping south of Long Canyon (Camilleri, 2010). Although wells near Long Canyon do not penetrate the Dunderberg Shale, which is overlain by the Notch Peak Formation, shale permeability is assumed to be much lower than overlying carbonate rocks (Sweetkind and others, 2010; Golder Associates Inc., 2012).

The Ordovician and Cambrian Notch Peak Formation is of shallow marine origin and characterized by alternating layers of massive-to-thinly-bedded limestone overlain by massive dolomite. Golder Associates Inc. (2012) reported that the upper massive dolomite formation contains highly permeable

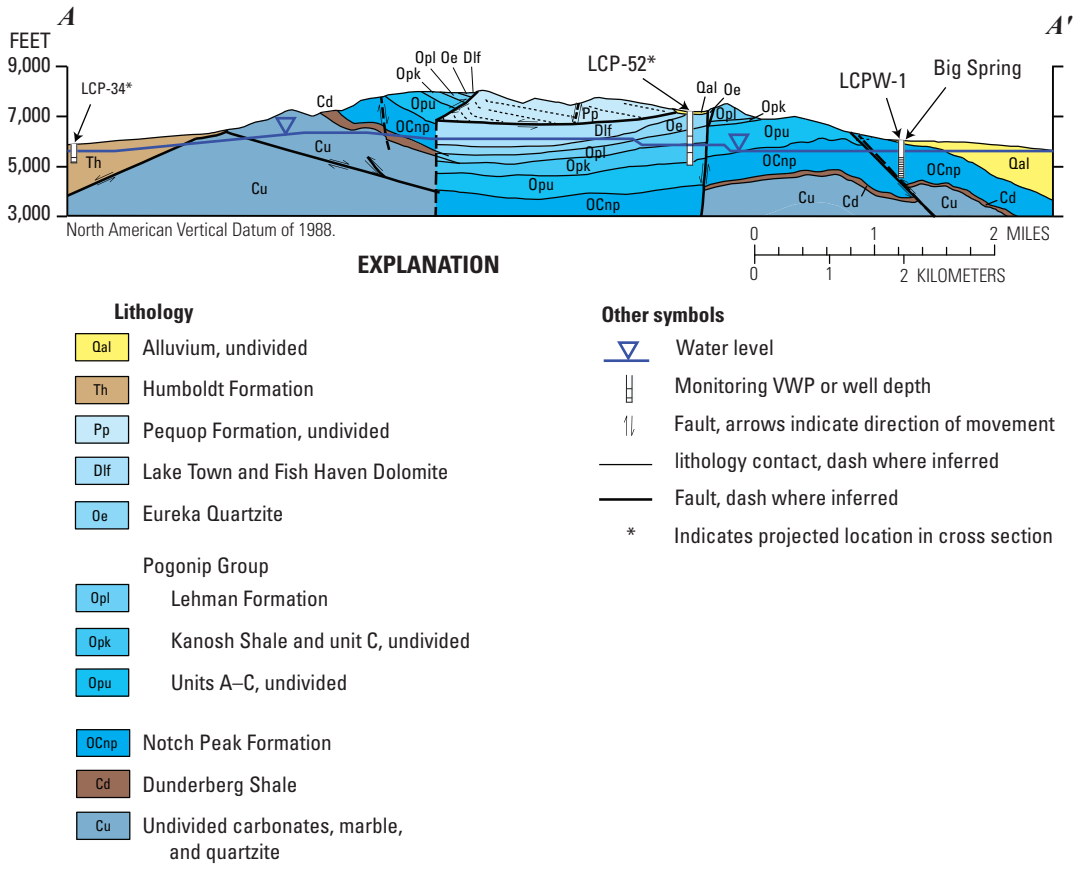

Figure 3. Geologic units beneath the Pequop Mountains, Long Canyon, and Goshute Valley, northeastern Nevada (modified from Camilleri [2010]). Trace of cross section *A–A′* is shown in figure 2.

caves and dissolution breccia zones for transmitting groundwater. The Notch Peak Formation is about 2,000 ft thick based on geophysical surveys (Camilleri, 2010), although the deepest well penetrating this unit in the study area extends to a depth of 765 ft bls (well LCMW-09D). An erosional unconformity defines the upper boundary of the formation, which is overlain by limestone from the Pogonip Group.

Pumping wells LCPW-1 and LCW-6, and an additional 14 monitoring wells and VWPs, are at least partially completed in the Notch Peak Formation (Smith and others, 2021, appendix 2). Well LCPW-1 is fully completed in the Notch Peak Formation, with the upper 460 ft of perforations in dolomite and the lower 560 ft of perforations in limestone. The lower 230 ft of the 1,244-ft-long perforated casing in LCW-6 penetrates the Notch Peak Formation, with the upper 168 ft of perforations in Notch Peak dolomite and the lower 62 ft in Notch Peak limestone. During aquifer testing at LCPW-1 in 2011, drawdown was detected more than 1 mi from the pumping well, indicating that the Notch Peak Formation is hydraulically connected among wells (Barnett Intermountain Water Consulting and others, 2011). Decreasing springflow during the 2011 LCPW-1 aquifer test also indicates that the Notch Peak Formation discharges, in part, to Big Spring.

The Ordovician Pogonip Group is as thick as 5,900 ft and is composed of five main units and several unit combinations in the Pequop Mountains and Toano Range. The base consists of three units, units A–C, composed of calcite and marble varying from laminated to massive with a combined thickness of about 1,600 ft (Camilleri, 2010). Units A–C are overlain by the Kanosh Shale (up to 160-ft thick) consisting of phyllite with subordinate limestone and marble (Camilleri, 2010). Overlying the Kanosh sequence is the Lehman Formation, a fossiliferous and silty limestone 500–680-ft thick, representing the youngest formation in the group, along with combinations of undivided Lehman Formation, Kanosh Shale, and unit C. The Pogonip Group is overlain by the Eureka Quartzite, with a sharp boundary marked by talus deposits of weathered quartzite (Golder Associates Inc., 2012). Seventeen wells and piezometers penetrate the highly transmissive Pogonip Group, including the upper 1,014 ft of perforations in pumping well LCW-6 (Smith and others, 2021, appendix 2).

The Ordovician Eureka Quartzite is fine grained, well-rounded, cross-bedded orthoquartzite cemented with silica. The quartzite is highly resistant to weathering and constitutes ridges in the Pequop Mountains. The Eureka Quartzite generally is near 300-ft thick (Camilleri, 2010), but extends to a depth of more than 515 ft bls near sites LCP-52A–B.

The Eureka Quartzite is overlain by sparse outcrops of the Laketown dolomite and Fish Haven dolomite in the Pequop Mountains.

The Mississippian Chainman Shale (or Mississippian shale in fig. 2) is an organic-rich shale outcropping on the central Pequop Mountains and on the west side of the Goshute Mountains (Lawrence and others, 2007). The unit thickness is greater than 3,600 ft in the Goshute Valley (Camilleri, 2010) and is estimated to be greater than 6,000 ft in the Great Basin (Lawrence and others, 2007).

The Pennsylvanian Ely Limestone is a cherty-conglomerate, fossiliferous limestone that outcrops in central Goshute Valley on the western edge of the Toano Range (Ketner and others, 1998) and in northern Goshute Valley in the Pequop Mountains north of Interstate 80 (Henry and Thorman, 2015). Unit thickness is less than 200 ft in the Pequop Mountains (Camilleri, 2010) but likely varies with metamorphism and extensional and erosional thinning (Ketner and others, 1998; Henry and Thorman, 2015).

Volcanic Rocks

Tertiary volcanic rocks are located 2 mi north of Long Canyon in the Pequop Mountains and other extrusive volcanic rocks are located 2.5 mi north of Interstate 80 in the southern end of the Toano Range (Brooks and others, 1995; Ketner, 1997; figs. 2 and 3). During the mid-Tertiary period, tectonic extension and normal faulting created a down-faulted depositional setting. The extension coincided with volcanism resulting in the accumulation of crystal-rich rhyolite ash-flow tuffs, andesite ash-flow breccia, rhyolite ash-flow tuff, and hornblende rhyolite north of Long Canyon and west of Oasis (Brooks and others, 1995). The alternating volcanic rocks have varying degrees of welding, alteration, and disaggregation. The maximum thickness of the Tertiary volcanic unit is estimated at 3,940 ft (Brooks and others, 1995). Piezometer site LCP-36–D penetrates the upper 575 ft of this unit. Piezometers or monitoring wells were not completed in the Miocene aged rhyolitic flows in the Toano Range, and the unit thickness is unknown.

Intrusive Rocks

Intrusive units outcrop on the southeastern end of the rhyolitic flows in the Toano range and in the Goshute Mountains to the south. Although the outcrop of intrusive unit in the Toano Range is limited, the pluton is thought to extend across a much larger subsurface area (Ketner, 1997; fig. 2). The unit is descripted as quartz-monzonite and granodiorites of Jurassic to Miocene age. Thickness of the intrusive volcanics is unknown.

Sedimentary and Volcanic Basin-Fill Deposits

Thick sequences of Tertiary sedimentary deposits and Quaternary alluvial and pluvial deposits, or basin fill, overlay the carbonate bedrock and lesser amounts of Paleozoic clastic and Tertiary volcanic rocks in Goshute Valley (fig. 2 and 3). The complexly interbedded deposits of older eroded Tertiary rocks, Tertiary tuff, and younger Quaternary alluvium are undivided. The unit primarily consists of unconsolidated gravel, sand, and silt. In some areas, the basin fill includes thin (less than 10-ft thick) tuffaceous deposits; for example, at sites LCP-31A–C. The basin fill increases in thickness from the alluvial fan on the eastern slope of the Pequop Mountains toward the center of Goshute Valley, where it extends to more than 6,000 ft bls (Paul Pettit and Stephanie Douglas, Newmont Mining Corporation, written commun., 2017).The deepest basin-fill VWP extends to 1,790 ft bls (CLC-608A). Aquifer testing in basin fill indicates permeability decreases from the eastern flank of the Pequop Mountains toward the center of Goshute Valley (see section, “Single-Well Aquifer Tests”). Shafter municipal pumping wells (fig. 2) for the cities of West Wendover, Nevada, and Wendover, Utah, penetrate alluvial-fan deposits along the western edge of the Toano Range. A total of 73 monitoring wells and piezometers penetrate basin fill in Goshute Valley, where about one-half are open to alluvial-fan deposits and one-half are open to less permeable basin fill near the valley center.

Structural Features

The Pequop Mountains contain multiple thrust and normal faults that were formed during a complex structural history (Camilleri and Chamberlain, 1997; Camilleri, 2010; fig. 3). The main faults near the Long Canyon Mine project area, ordered by chronological age, include the Independence and other thrust faults, northeast trending Sixmile vertical fault, north-trending high-angle Canyon vertical fault, and numerous Basin and Range normal faults including Flapjack, Hastings, and Hardy faults (Golder Associates Inc., 2012; figs. 2 and 3). Faults and fractures may enhance or impede groundwater flow depending on juxtaposition of hydrogeologic units with similar or different permeabilities, respectively, or to a lesser extent where filled by fault gouge.

Groundwater Flow

Water movement in a groundwater-flow system is constrained by recharge, discharge, and hydraulic-property distributions. Recharge adds water to the groundwater system through direct infiltration of precipitation in the mountains and infiltration of streamflow and runoff. Groundwater discharge occurs in localized discharge areas through springflow and

seepage, transpiration by local phreatophytic vegetation, and by evaporation from soil and open water. Water levels, flow rates, flow directions between recharge and groundwater-discharge areas, and the magnitude of recharge and discharge components are constrained by hydraulic conductivities. Water chemistry analyses provide additional insight and constraints on interpretating groundwater-flow paths, flow rates, and contributing recharge areas.

Groundwater Discharge

Groundwater discharges define groundwater budgets for undeveloped basins because discharge, unlike recharge, can be observed directly as springflow, baseflow to streams, and as phreatophyte evapotranspiration (ET; Bredehoeft, 2007). The spatial distribution of groundwater discharge also is important because locations and magnitudes of discrete discharges affect estimated transmissivity distributions in aquifers.

Groundwater in Goshute and Independence Valleys discharges naturally in topographically low areas where groundwater is near land surface. Natural discharge occurs through springs and seeps, transpiration by phreatophytic vegetation, and by evaporation from soil. ET across a typical discharge area in the southwestern United States includes spring and seep flow. Water discharged from springs and seeps either evaporates or infiltrates downward toward the shallow water table where it potentially evaporates or is transpired by wetland or phreatophytic vegetation. The combined processes of evaporation and transpiration are collectively referred to as evapotranspiration (ET).

The amount and rate of water lost to the atmosphere by ET from groundwater-discharge areas varies with vegetation type and density, soil characteristics, and water-table depth (Laczniak and others, 1999, 2001, 2008; Reiner and others, 2002; DeMeo and others, 2003; Moreo and others, 2007; Allander and others, 2009). Typical groundwater-discharge areas include dry playa; moist bare soil; and areas with vegetation dominated by phreatophytic shrubs, grasses, rushes, and reeds. ET generally increases with increasing vegetation density and health, and soil moisture.

Previous studies in Nevada have applied various remote-sensing techniques within groundwater-discharge areas where satellite imagery, in combination with field mapping, was used to identify and group areas of similar vegetation and soil conditions (Smith and others, 2007; Allander and others, 2009; Garcia and others, 2015; Berger and others, 2016). Vegetation and soil groupings are assumed to represent areas with similar ET rates. Regional groundwater discharge is estimated volumetrically by grouping vegetation types in mapped groundwater-discharge areas, estimating the total ET from all groups, and subtracting non-groundwater contributions such as local precipitation and infiltrated floodwaters. Local precipitation and infiltrated floodwaters are assumed to evaporate locally, or supply plant needs when available (Laczniak and others, 1999).

Predevelopment groundwater discharge has been estimated for groundwater-discharge areas in Goshute and Independence Valleys (table 3). Eakin and others (1951) mapped groundwater-discharge areas, applied groundwater ET rates to the discharge areas, and measured 2,400 acre-ft/yr (or 1,500 gal/min; May–June 1948) of discharge from "Johnson Spring," which was interpreted to issue from Big Spring rather than the JSWC. In Goshute and Antelope Valleys, groundwater ET rates of 0.03 ft/yr for playa and sparse phreatophytic shrubs and 0.25 ft/yr for moderate shrub densities were applied; and in Independence Valley, groundwater ET rates of 0.1 ft/yr for sparse shrubs and 0.5 ft/yr for spring-fed areas were applied (Eakin and others, 1951). Natural groundwater discharge estimates totaled 9,725 acre-ft/yr in Goshute and Antelope Valleys (inclusive of spring discharge) and 9,500 acre-ft/yr in Independence Valley (table 3).

Nichols (2000) used Landsat-based vegetation indices from 1985 and 1989 to map and group vegetation within groundwater-discharge areas and estimate groundwater ET in northeastern Nevada (table 3). Groundwater ET estimates were extrapolated from 12 micrometeorological measurements of groundwater ET, most of which were made in southern Nevada and southeastern California. Measured groundwater ET rates ranged from 0.5 to 2.7 ft/yr. Vegetation areas mapped in 1985 and 1989 varied drastically in their assumed density and groundwater use, owing to large differences in Landsat-based vegetation indices. Large differences in vegetation indices, in turn, resulted in a 40–100 percent difference in estimated groundwater ET for the 2 years (42,500 and 63,500 acre-ft/yr in Independence Valley and 28,500 and 83,500 acre-ft/yr in Gohsute Valley; Nichols, 2000, table C17). Mean annual groundwater ET estimates from Nichols (2000, table C7) were much closer to the 1985 estimate in Independence valley and the average of 1985 and 1989 estimates for Goshute Valley (table 3).

Groundwater discharges from Goshute and Independence Valleys were notably different between Eakin and others (1951) and Nichols (2000). Total groundwater discharge from both valleys was estimated by Eakin and others (1951) as about 20,000 acre-ft/yr and by Nichols (2000) as about 90,000 acre-ft/yr (table 3). Most of the difference can be attributed to overestimated groundwater ET rates used in Nichols (2000) for areas with bare soil/playas and sparse (less than 10 percent) plant cover, which constituted 95 percent of the groundwater-discharge area delineated in Goshute and Independence Valleys. Recent estimates of groundwater ET for bare soil and playas made in north-central Nevada were less than 0.07 ft/yr based on eddy-covariance ET measurements and modeling studies (Garcia and others, 2015; Jackson and others, 2018), whereas recent estimates of groundwater ET for less than 10 percent plant cover made in north-central and north-eastern Nevada were 0.09–0.17 ft/yr (Moreo and others, 2007; Garcia and others, 2015; Berger and others, 2016), respectively. These recent estimates are comparable to the rates of 0.03 and 0.1 ft/yr reported by Eakin and others (1951) in areas of playa and sparsely distributed shrubs.

Table 3. Previous water-budget estimates for Goshute and Independence Valleys, northeastern Nevada.

[**Groundwater evapotranspiration:** Goshute Valley estimate includes evapotranspiration of spring discharge. **Abbreviations:** acre-ft/yr, acre-feet per year; –, not available]

Reference	Groundwater recharge (acre-ft/yr)			Natural groundwater discharge (acre-ft/yr)			
	Goshute Valley	Independence Valley	Total	Goshute Valley		Independence Valley	Total
				Springs	Groundwater evapotranspiration		
Eakin and others (1951)	[1]10,400	9,300	19,700	[3]2,525	[1]9,725	9,500	19,225
Harrill and others (1988)	[1]10,400	9,300	19,700	–	–	–	–
Nichols (2000)	41,000	50,000	91,000	–	42,500	47,000	89,500
Heilweil and Brooks (2011)	20,000	17,000	37,000	0	6,600	9,500	16,100
Golder Associates Inc. (2012)[2]	[2]17,953	–	–	2,423	[1,2]20,791	–	–
Brooks and others (2014)	20,000	19,000	39,000	0	7,000	15,000	22,000

[1]Value reported is total for Goshute and Antelope Valleys.

[2]Value based on Nichols (2000) and represents northern Goshute Valley only.

[3]Total spring discharge from the Johnson Springs Wetland Complex (including Big Spring).

Groundwater discharges estimated by Nichols (2000) from Goshute and Independence Valleys also are suspect because of conceptual errors. Reported groundwater discharges more than double between 1985 and 1989, which is conceptually inconsistent with regional groundwater discharge being steady (Jackson and Fenelon, 2018). The large increase in the Landsat-based vegetation index, which was attributed to an increase in plant biomass and groundwater use, more likely can be attributed to an increase in precipitation-based soil-water availability. An increase in soil-water availability is supported by annual precipitation measurements at Hole-in-Mountain SNOpack TELemetry (SNOTEL), where precipitation trends are assumed to represent regional recharge conditions that control groundwater levels in the study area, and at the Wells cooperative observer network (COOP) station, where precipitation is assumed to represent conditions on the valley floor of Goshute Valley (fig. 1, table 4). Annual precipitation at Hole-in-Mountain SNOTEL during the 5 years leading up to 1985 and 1989 was 1.2 and 0.9 times the 1918–2017 mean, respectively (44 in. from 1980 to 1984 and 31 in. from 1984 to 1988). A decrease in recharge-area precipitation from above average in 1985 to average in 1989 does not support the twofold increase in groundwater discharge estimated by Nichols (2000). At the Wells COOP precipitation site, annual precipitation increased from 7.9 in. in 1985 to 8.7 in. in 1989. An increase in valley-floor precipitation and resulting soil-water availability most likely caused the increase in plant biomass and Landsat-based vegetation index observed by Nichols (2000).

Recent spring discharge measurements from Big Spring support groundwater-discharge estimates from Eakin and others (1951). Reported discharge of 1,500 gal/min (2,400 acre-ft/yr) from Big Spring prior to 1951 is similar to recent (2007–17) discharge measurements at Big Spring that ranged from 300 to 2,600 gal/min and averaged 1,100 gal/min (1,770 acre-ft/yr). Slightly higher discharge during the 1940s could indicate a slightly wetter period compared to mean precipitation during 2007–17 (table 4). At sites across northeastern Nevada, mean precipitation during the 1940s was about 9 percent above the 100-year mean (1918–2017), whereas mean precipitation during 2007–17 was about 6 percent above the 100-year mean (table 4).

Long-term precipitation datasets overlapping the period characterized by Eakin and others (1951) (1940–49) and the Big Spring flow record (2007–17) were obtained from four local COOP sites and one SNOTEL site (table 4). None of the sites recorded the complete periods of interest (often a few to several years were missing); therefore, site measurements were linearly related to 4-km Parameter-elevation Regressions on Independent Slopes Model (PRISM) data, and the relation was applied to PRISM data from 1918 to 2017 to extrapolate long-term measurements. The extrapolated datasets were used to compute and compare mean annual precipitation during 1918–2017, 1940–49, and 2007–17.

Large interannual variability in Big Spring discharge corresponds with average to above-average winter precipitation, indicating that proximal snowmelt likely is the recharge source (fig. 4). During the period of record (November 2006–December 2017), discharge ranged from a minimum of 287 gal/min (December 2015) to a maximum of 2,606 gal/min (July 2017). Peak discharge within a year typically occurred between April and June, but peaks occurred only during 6 of the 11 years monitored. Peaks or spikes in discharge correspond with average to above-average winter precipitation measured during the previous winter at the Hole-in-Mountain SNOTEL site, located about 50 mi southwest of Big Spring. The largest spikes and long-term springflow recession curves correspond with higher winter precipitation that fell during

Table 4. Mean annual precipitation at long-term measurement sites in northeastern Nevada and northwestern Utah, 1918–2017.

[**Precipitation sites:** Long-term measurement sites from the National Weather Service (COOP) and U.S. Department of Agriculture Natural Resources Conservation Service (SNOTEL). **Linear relation with 4-kilometer PRISM data:** Linear relation used to extrapolate site data across the 1911–2017 record. Relations are between annual site measurements and 4-kilometer PRISM estimates. r^2, coefficient of determination. **Mean annual precipitation:** based on calendar year. **Abbreviations:** COOP, cooperative observer network; PRISM, Parameter-elevation Regressions on Independent Slopes Model; SNOTEL, SNOpack TELemetry]

Precipitation sites	Site type	Measurement record	Linear relation with 4-kilometer PRISM data			Mean annual precipitation (inches)		
			r^2	Slope	Intercept	1918–2017	1940–49	2007–17
Wendover Airport, Utah	COOP	1934–2016	0.73	0.86	-0.38	4.70	5.31	4.77
Arthur 4NW, Nevada	COOP	1926–2017	0.89	0.98	0.43	14.87	14.80	15.39
Wells, Nevada	COOP	1936–2003	0.96	1.09	-0.88	10.28	11.78	11.58
Oasis, Nevada	COOP	1988–2011	0.99	1.04	-0.30	9.21	10.07	9.58
Hole-in-Mountain, Nevada	SNOTEL	1982–2017	0.95	1.26	-1.54	35.45	3.45	36.00

water years[1] 2006, 2011, and 2017. Lesser spikes in spring discharge correspond with average winter precipitation and generally are superimposed on the larger springflow recession curve (fig. 4).

Variability of springflow and steep recession curves indicate that the contributing area upgradient from Big Spring has a limited extent. Flow is variable, with a recession index of 1,400 days per log-cycle, indicating that flow would decline an order of magnitude in less than 4 years if all recharge ceased. Recession indices cannot be determined on large regional springs where discharge is constant over multiple decades, such as Crystal Pool in Ash Meadows, Nye County, Nevada. Flow from Crystal Pool is extremely steady because the contributing area exceeds 2,000,000 acres (Halford and Jackson, 2020).

Estimated long-term (2006–17) discharge from all springs in the JSWC averaged 1,700 gal/min (2,740 acre-ft/yr). Synoptic discharges from all springs other than Big Spring totaled 400 and 900 gal/min (650 and 1,450 acre-ft/yr) during May 2016 and November 2017, respectively. Discharge from Big Spring averaged 700 and 2,000 gal/min (1,130 and 3,230 acre-ft/yr) during the synoptic measurements in May and November, respectively. Average discharge from all springs other than Big Spring totaled 600 gal/min (970 acre-ft/yr) and was estimated by scaling synoptic discharges to discharge from Big Spring.

Groundwater-discharge estimates used in this study were based on groundwater ET estimates from Eakin and others (1951) and spring-discharge measurements made during 2007–17. Although Heilweil and Brooks (2011) and Brooks and others (2014) also estimated groundwater discharge and recharge, these estimates are based on regional rather than localized trends and observations and therefore were not used in this study. Phreatophyte and playa discharge areas delineated by Nichols (2000) generally were used to distribute discharge estimates by Eakin and others (1951). Similarities between groundwater ET rates applied by Eakin and others (1951) and more recent estimates based on ET measurements and modeling studies (Moreo and others, 2007; Garcia and others, 2015; Berger and others, 2016, and Jackson and others, 2018), and between Big Spring discharge measurements made by Eakin and others (1951) and recent measurements made from 2007 to 2017, provide confidence in rates provided by Eakin and others (1951).

[1]A water year is the 12-month period from October 1, for any given year, through September 30 of the following year. The water year is designated by the calendar year in which it ends.

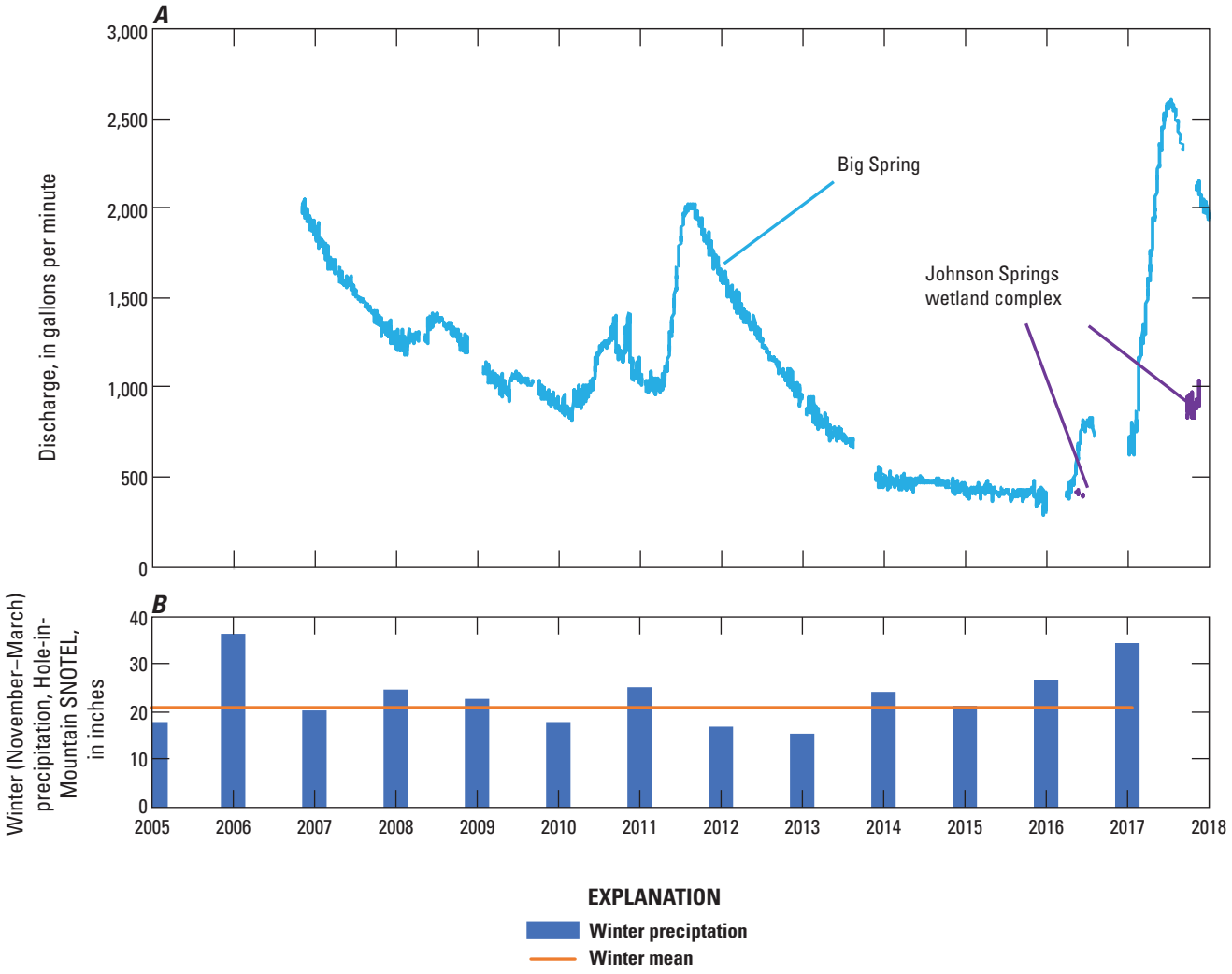

Figure 4. Discharge from Big Spring and the Johnson Springs wetland complex, and winter precipitation from Hole-in-Mountain SNOpack TELemetry (SNOTEL) station, northeastern Nevada, 2005–17.

Groundwater Recharge

Groundwater recharge is temporally and spatially variable in the study area. Most recharge is derived from winter precipitation in upland areas where the magnitude of recharge varies during wet and dry years and can be observed as distinct water-level rises in well hydrographs and rises in Big Spring discharge. Temporal recharge variations indicate seasonal and inter-annual precipitation variability. Spatially varying recharge is dependent on the permeability of saturated rocks and distribution of precipitation, where higher altitudes receive more precipitation. Total recharge is inclusive of recharge from direct infiltration and from runoff, where runoff can recharge along mountain fronts or through permeable stream channels downstream from the mountain front (Welch and others, 2007).

Long-term water-level fluctuations in primarily undeveloped groundwater systems indicate changes in storage that result from differences between recharge entering the system and discharge leaving the system. In the Great Basin, most groundwater discharges to springs, seeps, and phreatophyte areas are distant from recharge areas. Regional discharge is nearly constant from year to year because the regional gradient is insensitive to small (generally less than 10-ft) local water-level fluctuations in wells relative to the more than 100-ft head differences between recharge areas and distant discharge areas. Unlike discharge, recharge varies temporally and spatially, and primarily is the cause of annual to decadal water-level fluctuations in wells.

Recharge principally is from winter (October–March) precipitation during years with greater-than-average accumulation. During a typical winter with average or less-than-average precipitation, infiltrated precipitation mostly or entirely replenishes the soil-moisture reservoir depleted by ET during the previous summer. In these years, little to no water percolates below the root zone to support recharge. Following winters with greater-than-average precipitation (wet winters),

spring snowmelt replenishes the soil reservoir beyond its field capacity, allowing downward percolation below the root zone and into the groundwater system (Smith and others, 2017).

Early recharge estimates for Goshute, Independence, and Antelope Valleys were based on the Maxey-Eakin method (Maxey and Eakin, 1949). The Maxey-Eakin recharge approach assumes that recharge is proportional to mean annual precipitation, and the proportion of precipitation contributing to recharge increases with increasing elevation and precipitation. Maxey and Eakin (1949) estimated recharge volumes as the product of mapped precipitation intervals from the Hardman (1936) precipitation map and recharge coefficients that varied by interval. Recharge coefficients were determined by balancing recharge estimates against discharge estimates in valleys where groundwater discharges were measurable. Eakin and others (1951) estimated recharge rates of 10,400 acre-ft/yr for Goshute and Antelope Valleys and 9,300 acre-ft/yr for Independence Valley using recharge coefficients applied to the Hardman (1936) precipitation map. Interbasin flow estimates made in Eakin and others (1951) were determined by balancing differences between recharge and discharge and represent a small amount of occasional flow entering Goshute Valley from Steptoe Valley to the southwest.

Harrill and others (1988) estimated interbasin flow entering and exiting Goshute Valley using published water budgets and knowledge of hydrogeologic units and hydraulic potential. Minor amounts of interbasin flow were reported to enter Goshute Valley from Steptoe Valley and exit Goshute Valley to Antelope Valley. Eastward outflow from Goshute Valley to the Great Salt Lake Desert was limited to consolidated rocks and estimated as about 2,000 acre-ft/yr. A minor amount of inflow to Independence Valley was reported to occur from Clover Valley to the west.

Nichols (2000) estimated annual recharge volumes of 41,000 and 50,000 acre-ft in Goshute and Independence Valleys, respectively, using a modified Maxey-Eakin method that balanced recharge with discharge estimates from the same study (Nichols, 2000). Recharge coefficients developed by Nichols (2000) were applied to the 1961–90 PRISM precipitation map (Daly and others, 1994) and adjusted to balance recharge with discharge, and with interbasin flow estimates from previous studies (Eakin and others, 1951; Harrill and others,1988). Using revised recharge and discharge estimates, Nichols (2000) revised interbasin flow estimates. Nichols (2000) estimates of interbasin flow from Goshute to Antelope Valley and to the Great Salt Lake Desert were similar to estimates from Harrill and others (1988); however, excess recharge with respect to discharge in other basins resulted in sizable interbasin flow estimates of 4,000 acre-ft/yr from Steptoe to Goshute Valleys and 3,000 acre-ft/yr from Independence to Clover Valleys, the latter of which contradicts hydraulic gradients (see section, “Groundwater Levels” and Harrill and others [1988]).

Spatially distributed recharge rates were estimated in this study with a conceptual model of water availability and permeability of saturated rocks in recharge areas. Rates of infiltration below the root zone were assumed proportional to precipitation and assumed to increase as precipitation rates increased. Recharge rates were assumed to be equal to infiltration rates below the root zone and termed the ‘conceptual recharge rate.’ However, in areas where infiltration rates exceed rock permeability at the water table, infiltration normally is displaced downgradient along the contact to more permeable rock (Halford and Jackson, 2020). Infiltration displacement was not considered necessary for this study because recharge rates (fig. 5*A*) are unlikely to exceed the minimum rock hydraulic conductivity from aquifer tests of 0.007 ft/d, which equals a recharge rate of 2.6 ft/yr if distributed across the year, or about 0.9 ft/yr if recharge is constrained to a 4-month snowmelt-runoff period.

Recharge was distributed across Goshute, Independence, and Antelope Valleys and balanced against an estimated annual groundwater-discharge volume of 19,225 acre-ft (table 3; Eakin and others, 1951). Distributed recharge is conceptualized as a piecewise linear function of total annual precipitation (fig. 5). Precipitation was defined by the 1981–2010 PRISM precipitation distribution (PRISM Climate Group, 2012). A two-stage relation between precipitation and total potential recharge (from direct infiltration and runoff infiltration) was assumed. Annual precipitation estimates in the study area range from 0.6 to 2.7 ft/yr, where rates of less than 0.8 ft/yr occur on the valley floor and rates greater than 0.8 ft/yr occur in upland areas. Recharge was assumed not to occur on clay-rich valley floors. Therefore, the piecewise relation between recharge and precipitation exists for precipitation ranges of 0.8–2.7 ft/yr. An annual precipitation rate of 1.5 ft/yr demarcated the inflection point of the two-stage linear relation (fig. 5*A*). Proportions of annual precipitation contributing to recharge increase from 0 to 4 percent for 0.8 to 1.5 ft/yr of precipitation, and from 4 to 29 percent for 1.5 to 2.7 ft/yr of precipitation.

The two-stage relation approximates conceptual differences in water available for recharge, even if an inflection point of 1.5 ft/yr is arbitrary. About 40 percent (8,000 acre-ft/yr) of the total recharge to Independence, Goshute, and Antelope Valleys occurs in areas with precipitation rates of less than 1.5 ft/yr (fig. 5*B*). Precipitation rates greater than 1.5 ft/yr occur at higher altitudes where winter snowpack generates most of the recharge. A greater fraction of precipitation becomes recharge as precipitation increases and ET decreases with increasing altitude. All available water is assumed to infiltrate below the root zone and migrate to the water table.

Distribution and annual volume of recharge to the area of interest was defined by the conceptual recharge distribution for Goshute, Independence, and Antelope Valleys (fig. 6). Annual volume of recharge to Goshute, Independence, and Antelope Valleys was defined by annual groundwater-discharge (19,225 acre-ft; Eakin and others, 1951). A maximum recharge rate of 0.28 ft/yr occurred in the northern Pequop Mountains that divide Goshute and Independence Valleys (fig. 6). Annual volume of recharge to the area of interest totaled 8,000 acre-ft/yr.

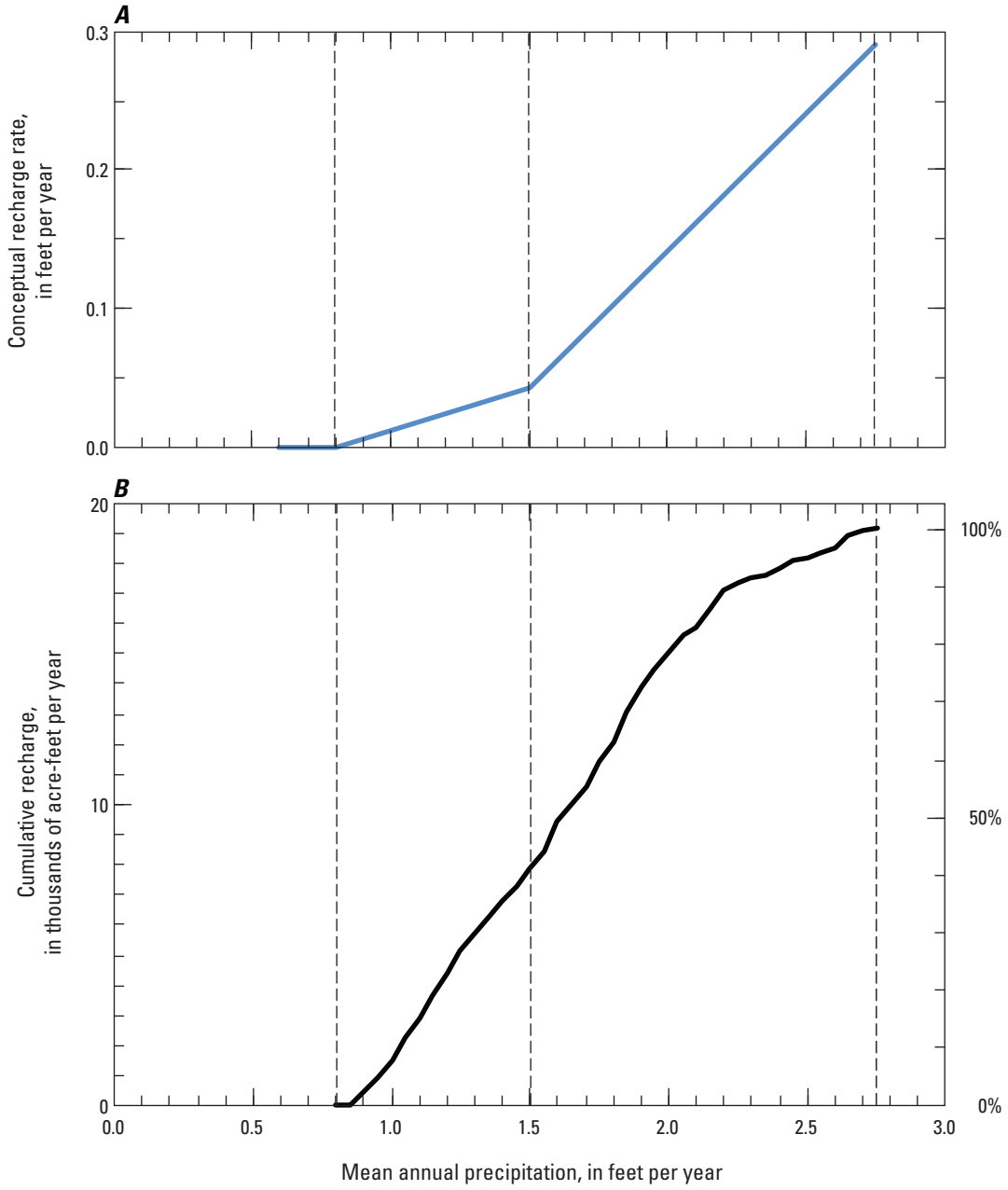

Figure 5. Relation between mean annual precipitation and (*A*) conceptual recharge rate from direct infiltration and runoff infiltration to the study area, and (*B*) cumulative recharge resulting from this relation, Long Canyon, Goshute Valley, northeastern Nevada. %, percent.

Groundwater Levels

Groundwater levels provide insight into the occurrence and movement of groundwater in a flow system. In confined aquifers, the groundwater potential or potentiometric surface is the altitude to which water will rise in tightly cased wells that tap a confined aquifer system (Lohman, 1972). In unconfined aquifers, such as parts of the basin-fill aquifer, the potentiometric surface is the water table. Groundwater flow is determined by hydraulic gradients, or changes in groundwater altitude with distance along flow paths. Potentiometric-surface maps that define the shape and gradient of the groundwater surface can be used to infer groundwater-flow patterns within carbonate-rock and basin-fill aquifers. Time-series of groundwater levels can highlight seasonal recharge and discharge patterns and long-term stresses on the flow system.

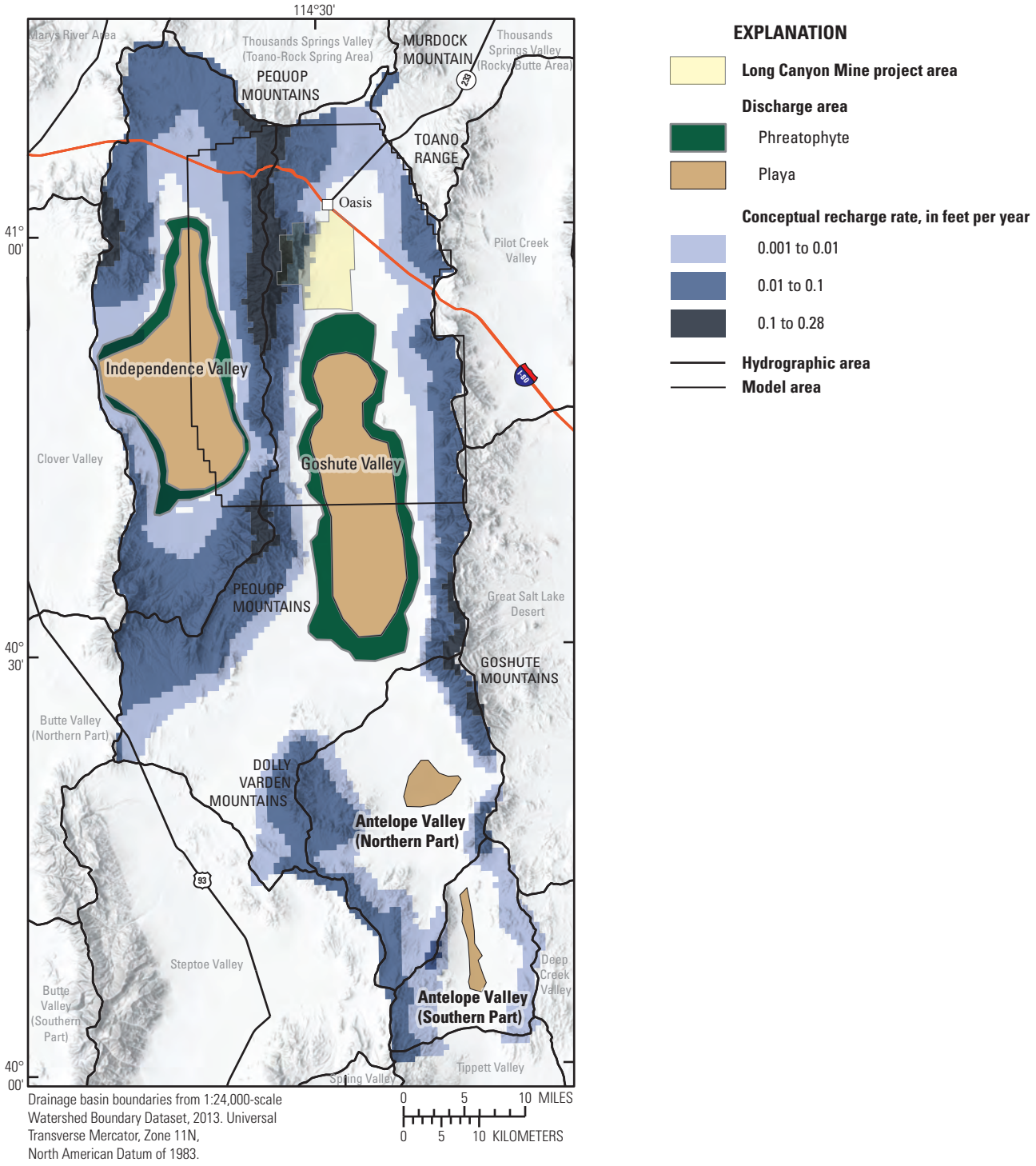

Figure 6. Conceptual recharge rates and distribution and areas of groundwater discharge in the study area, Long Canyon, Goshute Valley, northeastern Nevada.

Groundwater in Goshute and Independence Valleys generally flows from upland recharge areas toward valley lowlands where it is ultimately discharged by springs and through ET (fig. 7). A much smaller volume of groundwater flows across basin boundaries where hydraulic gradients support interbasin flow. Groundwater-level altitudes within, and west and south of the Long Canyon Mine project area, gradually decrease from more than 5,700 ft in the Pequop Mountains to less than 5,600 ft along the valley floors of Goshute and Independence Valleys over distances of several miles. In the Pequop Mountains north of the Long Canyon Mine project area, the hydraulic gradient steepens as groundwater levels sharply increase from 5,700 ft at the mountain front to 6,300 ft toward the mountain crest. Similarly, groundwater levels in northeastern Goshute Valley sharply increase toward the upper Toano Range from about 5,700 ft at the mountain front to more than 6,100 ft near the basin divide. The steeper hydraulic gradients in areas with similar rates of recharge are indicative of lower permeability hydrogeologic units north and east of the project area. More gradual hydraulic gradients within the Pequop Mountains west and south of the study area are coincident with more permeable carbonate rocks (fig. 2).

Hydraulic gradients indicate that groundwater moves away from the Pequop Mountains toward the valley floor of Goshute and Independence Valleys rather than as interbasin flow between the two basins (fig. 7). Along the western edge of Goshute Valley and south of the Long Canyon Mine project area, groundwater-level observations are sparse and hydraulic gradients are less certain. East of the Toano Range in Pilot Creek Valley, valley-floor groundwater levels are roughly 1,000 ft lower than in Goshute Valley. This steep hydraulic gradient between basins indicates potential for interbasin flow; however, the spring-pool altitudes of six flowing springs in the central and southern Toano Range vary from 6,095 to 6,350 ft (USGS sites 403820114143801, 403711114144901, 403747114163901, 402553114110701, and 402506114122901). These springs are at least 500–750 ft above groundwater-level altitudes in central and eastern Goshute Valley, indicating overall low permeability in the mountain block and limited groundwater movement from the mountain uplands toward the valleys on either side. Furthermore, the negligible hydraulic gradient across the more than 6,000-ft-thick valley-fill and playa deposits in central Goshute Valley likely precludes interbasin flow out of Goshute Valley to the east (fig. 7).

Groundwater-level time series data in Goshute Valley wells and piezometers show long- and short-term responses to climate and seasonal weather patterns. Continuous water-level monitoring near the Long Canyon Mine project area began in 2009, and spatial coverage continues to increase as new wells and piezometers are drilled. Water levels in most carbonate-rock, alluvial-fan, and volcanic-rock monitoring wells rise periodically in response to average or above-average winter precipitation (fig. 8). The most substantial water-level changes in carbonate-rock and alluvial-fan monitoring wells LCMW-02D and LCMW-02S, respectively, occurred during May–August 2011 and 2017, following above-average winter precipitation. Water levels measured in volcanic-rock piezometer LCP-36B also rose substantially following winter 2017 precipitation. Declining water levels observed in LCP-36B from the onset of monitoring in October 2012 to March 2016 likely show the natural decline (or recovery) from peak water levels associated with recharge following above-average winter precipitation during water year 2011. The common rising water-level response to above-average winter precipitation among carbonate-rock, alluvial-fan, and volcanic-rock observations indicates that most recharge likely occurs intermittently. Although trends are similar among these upland wells, the magnitude of water-level change following winter 2011 precipitation was an order of magnitude greater in volcanic rocks than in carbonate rocks and alluvial-fan material (40-ft decline in water levels in LCP-36B from 2011 to 2016, as compared to a 3–5-ft decline in water levels in wells LCMW-02D and LCMW-02S). This difference likely corresponds with the limited capacity of local volcanic rocks to store and transmit water compared to more transmissive carbonate rocks and alluvial-fan material.

Annual groundwater-level responses in volcanic rock to any amount of winter precipitation supports the assumption that these rocks are less permeable than surrounding carbonate rocks and alluvial-fan material. Water levels in piezometer LCP-36B, for example, rose annually during spring and summer, regardless of the magnitude of winter precipitation, and the magnitude of the rise always was proportional to the volume of precipitation from the previous winter (fig. 8). Rapid annual water-level responses to recent precipitation were attributed to changes in overlying pressure rather than high rates of direct recharge. Although a hydraulic connection exists between the volcanic-rock piezometer and the recharge source, water-level responses to winter precipitation are governed by the hydraulic diffusivity (the ratio of transmissivity to storativity) of the fractured rock. Therefore, the rapid water-level rises following even small amounts of winter precipitation are a pressure response in fractured rock that has very little capacity to store water compared to the carbonate rocks and alluvial-fan material. In addition to annual responses to winter precipitation, greater water-level responses to above-average winter precipitation in volcanic rocks and steeper hydraulic gradients in volcanic-rock mountain areas relative to those observed in carbonate rocks and alluvial-fan material west and south of the Long Canyon Mine project area indicate that these volcanic rocks generally are less permeable than carbonate rocks and alluvial-fan material throughout the study area.

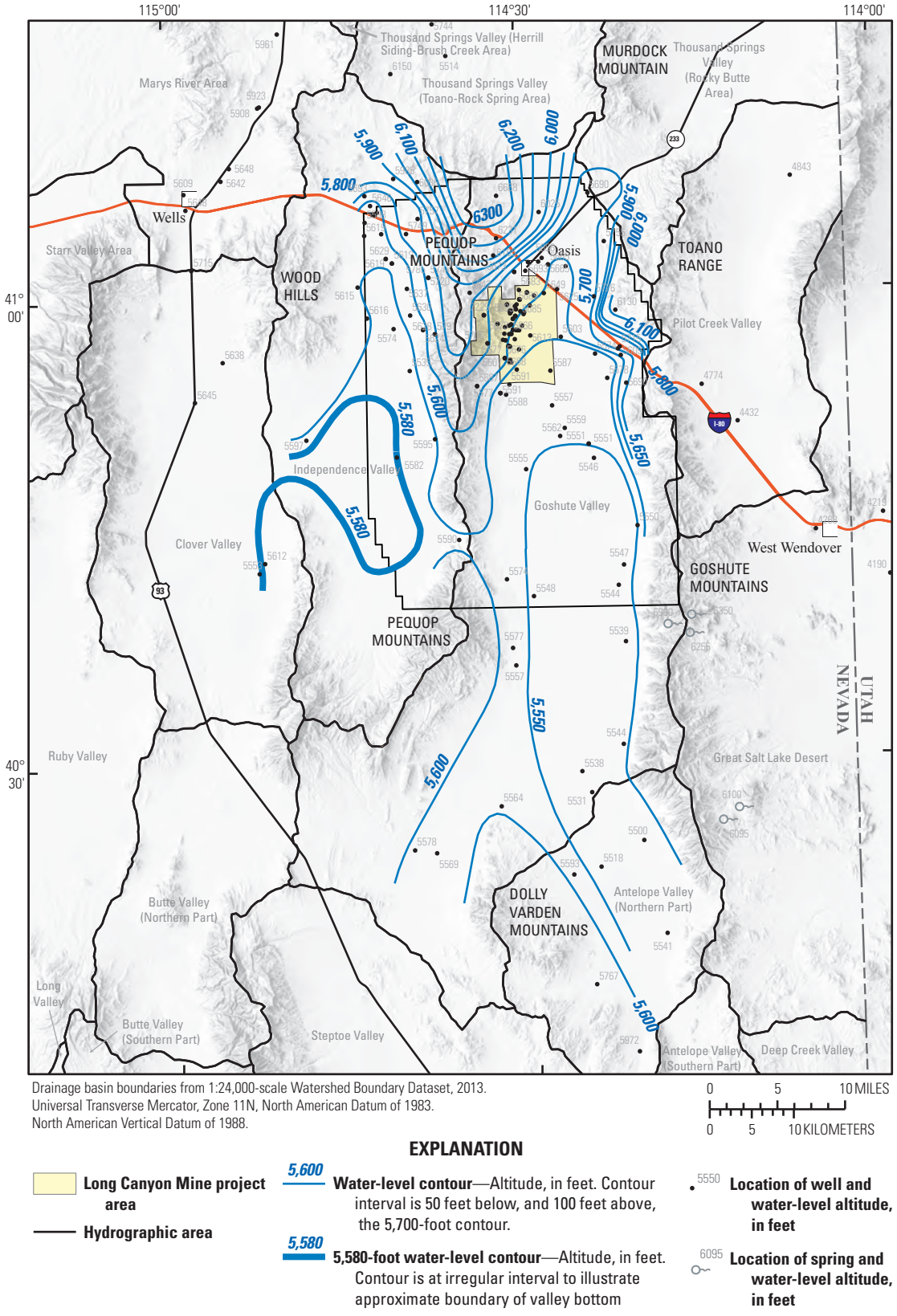

Figure 7. Potentiometric surface map for northern Goshute and Independence Valleys, Elko County, northeastern Nevada.

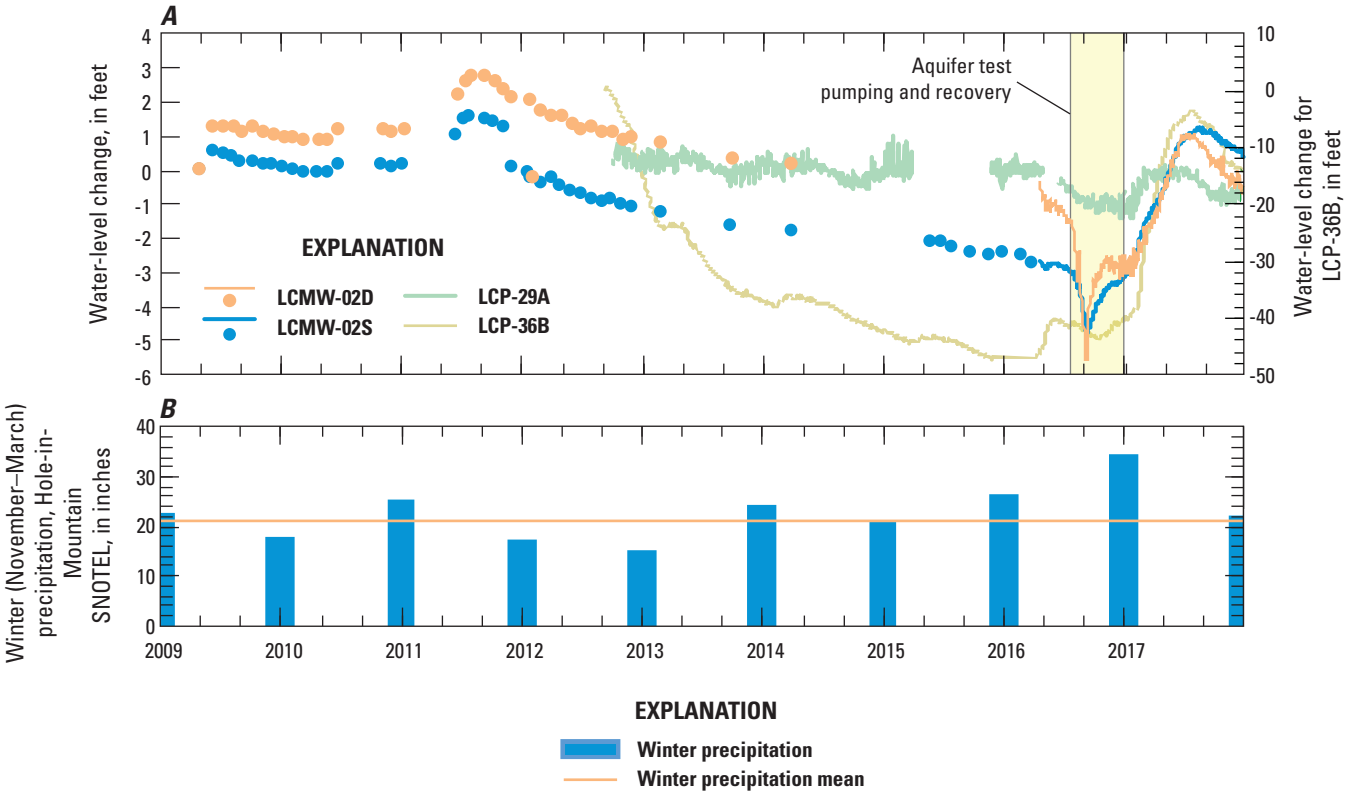

Figure 8. Long-term water-level change in carbonate-rock well LCMW-02D, alluvial-fan well LCMW-02S, valley-fill vibrating-wire piezometer LCP-29A, and volcanic-rock vibrating-wire piezometer LCP-36B, in Goshute Valley (*A*); and long-term winter precipitation at Hole-in-Mountain SNOpack TELemetry (SNOTEL) site, in Ruby Valley (*B*), northeastern Nevada, 2009–17.

Groundwater levels in valley fill (basin-fill deposits on the valley floor) fluctuate annually in response to discharge and recharge patterns driven by weather, but long-term (2012–17) trends remained relatively constant with time (fig. 8). Piezometer LCP-29A lies in the center of Goshute Valley, beneath phreatophytic shrubs and near the northern edge of the playa (fig. 2). Seasonal water-level declines in LCP-29A of 0.5–1 ft between the start and end of each growing season are responses to annual groundwater discharge through ET. The period of gradual water-table recovery after phreatophytes senesce is a result of lateral groundwater inflow from aquifer storage, as the storage reservoir is replenished with regional recharge.

Although long- and short-term groundwater responses to recharge and discharge provide insight into the hydraulic forces driving groundwater flow, these fluctuations minimally affect the steady-state system because the regional hydraulic gradient generally remains constant throughout northern Goshute and Independence Valleys. Regional discharge through ET is nearly constant from year to year because the hydraulic gradient in the discharge area is relatively insensitive to water-level fluctuations from recharge, which occur at the distant end of the groundwater system.

Selected Water Chemistry to Evaluate the Groundwater-Flow System

Groundwater samples collected from 12 sites within the study area were analyzed for selected dissolved and isotopic constituents to investigate sources of recharge, groundwater-flow paths, and mean groundwater ages near the Long Canyon Mine project area. The location of the sample sites is shown on figure 9 along with the location of 10 additional sites with water chemistry reported by Mayo and Associates (2013). The sites sampled in this study include six monitoring wells equipped with low-flow bladder pumps, four water-supply wells equipped with submersible pumps, and two springs (table 5). Samples were analyzed for dissolved major ions and selected trace elements that include calcium, magnesium, sodium, potassium, bicarbonate, sulfate, chloride, fluoride, bromide, silica, nitrate, arsenic, barium, boron, cesium, lithium, molybdenum, rubidium, strontium, and uranium. Samples also were analyzed for a suite of isotopic environmental tracers including the stable isotopes of oxygen ($\delta^{18}O$), hydrogen (δD), strontium ($^{87}Sr/^{86}Sr$) and carbon ($\delta^{13}C$); the radioactive isotopes of carbon (carbon-14, or ^{14}C) and hydrogen (tritium, ^{3}H); and dissolved noble gases including helium-3, helium-4, neon, argon, krypton, and xenon (^{3}He, ^{4}He, ^{20}Ne, ^{40}Ar, ^{84}Kr, and ^{129}Xe, respectively).

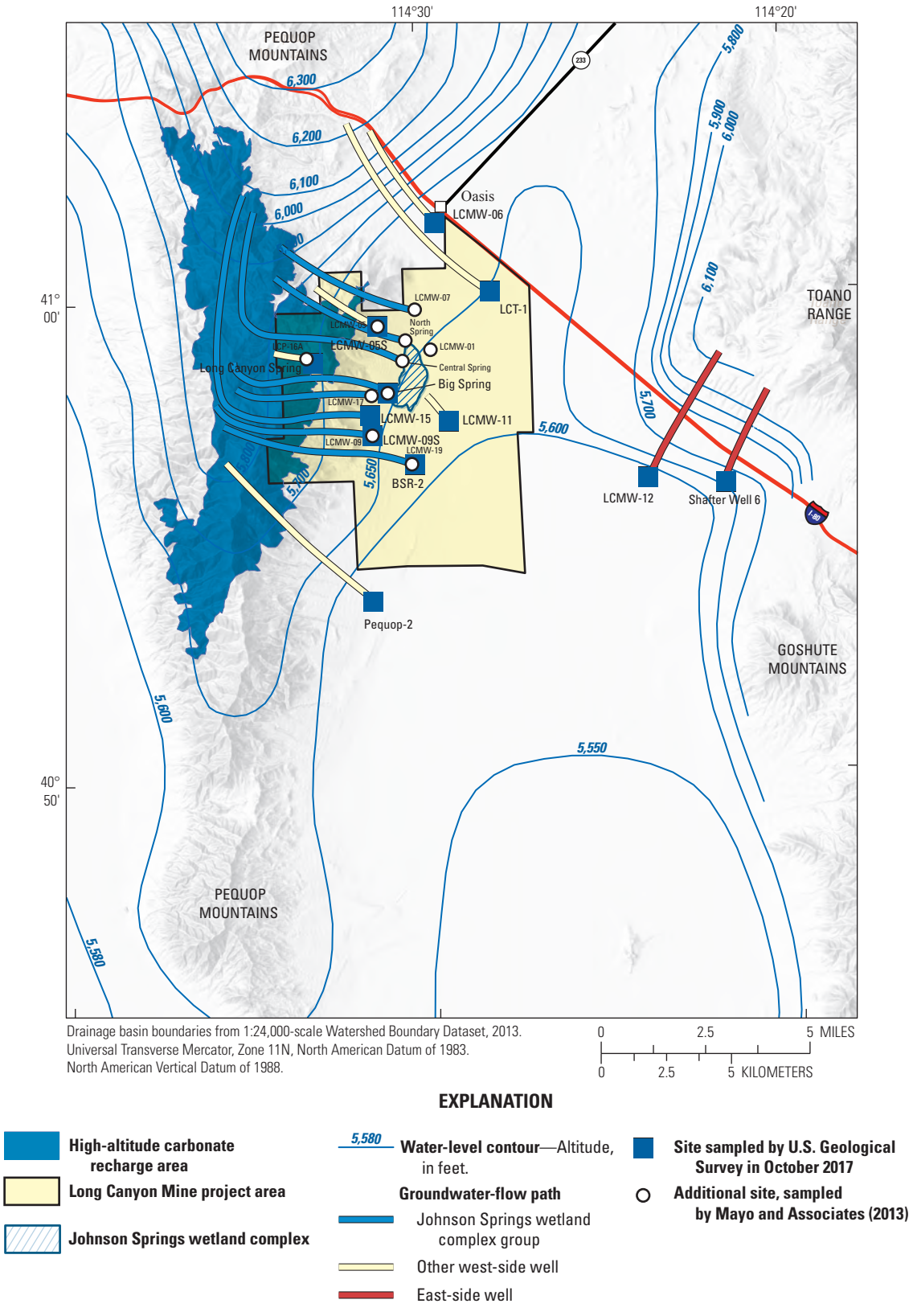

Figure 9. Groundwater sample sites and associated upgradient groundwater flow paths in Goshute Valley, Elko County, northeastern Nevada.

Table 5. Measured field parameters and dissolved concentrations of major ions for groundwater sampled in Goshute Valley, Elko County, northeastern Nevada.

[See figure 9 for locations and Smith and others, 2021, appendixes 1 and 2, for additional site information. **Abbreviations:** $CaCO_3$, calcium carbonate; JSWC, Johnson Springs wetland complex; USGS, U.S. Geological Survey; °C, degrees Celsius; µS/cm, microsiemens per centimeter at 25 degrees Celsius; µg/L, micrograms per liter; mg/L, milligrams per liter; <, less than; –, no information]

Site name	USGS site number	Sample date	Water temperature (°C)	Specific conductance (µS/cm)	pH (standard units)	Dissolved solids as sum of constituents (mg/L)	Sample group
LCMW-06	410132114293201	10-18-2017	10.1	555	7.3	486	Other west-side wells
LCT-1	410004114280401	10-17-2017	11.0	317	7.7	283	Other west-side wells
LCMW-05S	405924114311002	10-17-2017	13.3	666	7.5	494	Other west-side wells
Big Spring	405760114305701	10-19-2017	20.6	330	7.6	280	JSWC
LCMW-15	405732114312801	10-19-2017	19.8	317	7.5	272	JSWC
LCMW-09S	405707114312402	10-18-2017	21.8	318	7.5	278	JSWC
BSR-2	405629114301401	10-17-2017	15.5	324	7.7	286	JSWC
BSR-2, replicate	405629114301401	10-17-2017	15.5	324	7.7	277	JSWC
LCMW-11	405723114291701	10-18-2017	9.6	743	7.2	658	Other west-side wells
LCMW-12	405606114234901	10-18-2017	13.9	481	7.4	454	East-side wells
Shafter Well 6	405557114214101	10-19-2017	17.6	277	8.0	287	East-side wells
Pequop-2	405339114313001	10-19-2017	14.0	293	7.7	259	Other west-side wells
Long Canyon Spring	405839114325901	10-18-2017	9.8	629	7.1	571	Long Canyon Spring

Table 5. Measured field parameters and dissolved concentrations of major ions for groundwater sampled in Goshute Valley, Elko County, northeastern Nevada.—Continued

[See figure 9 for locations and Smith and others, 2021, appendixes 1 and 2, for additional site information. **Abbreviations:** $CaCO_3$, calcium carbonate; JSWC, Johnson Springs wetland complex; USGS, U.S. Geological Survey; °C, degrees Celsius; µS/cm, microsiemens per centimeter at 25 degrees Celsius; µg/L, micrograms per liter; mg/L, milligrams per liter; <, less than; –, no information]

Site name	USGS site number	Sample date	Calcium (mg/L as Ca)	Magnesium (mg/L as Mg)	Sodium (mg/L as Na)	Potassium (mg/L as K)	Sample group
LCMW-06	410132114293201	10-18-2017	70.8	20.7	23.1	2.00	Other west-side wells
LCT-1	410004114280401	10-17-2017	39.0	15.3	8.71	2.59	Other west-side wells
LCMW-05S	405924114311002	10-17-2017	70.2	22.1	36.0	2.29	Other west-side wells
Big Spring	405760114305701	10-19-2017	42.5	15.7	4.94	1.40	JSWC
LCMW-15	405732114312801	10-19-2017	40.9	14.7	5.14	1.50	JSWC
LCMW-09S	405707114312402	10-18-2017	41.7	14.7	4.61	1.52	JSWC
BSR-2	405629114301401	10-17-2017	42.1	15.7	5.44	1.52	JSWC
BSR-2, replicate	405629114301401	10-17-2017	41.5	15.7	5.33	1.60	JSWC
LCMW-11	405723114291701	10-18-2017	80.4	33.7	38.5	4.70	Other west-side wells
LCMW-12	405606114234901	10-18-2017	29.4	12.8	57.7	11.0	East-side wells
Shafter Well 6	405557114214101	10-19-2017	22.3	8.19	23.6	7.65	East-side wells
Pequop-2	405339114313001	10-19-2017	34.6	14.9	6.42	2.37	Other west-side wells
Long Canyon Spring	405839114325901	10-18-2017	88.2	21.8	23.6	1.70	Long Canyon Spring

Site name	USGS site number	Sample date	Alkalinity (mg/L as $CaCO_3$)	Bicarbonate (mg/L as HCO_3.)	Sulfate (mg/L as SO_4)	Chloride (mg/L as Cl)	Sample group
LCMW-06	410132114293201	10-18-2017	219	266	59.9	18.3	Other west-side wells
LCT-1	410004114280401	10-17-2017	144	176	16.4	3.28	Other west-side wells
LCMW-05.S.	405924114311002	10-17-2017	167	203	73.7	67.4	Other west-side wells
Big Spring	405760114305701	10-19-2017	155	188	11.2	2.72	JSWC
LCMW-15.	405732114312801	10-19-2017	148	180	12.1	3.36	JSWC
LCMW-09S	405707114312402	10-18-2017	154	187	12.1	2.55	JSWC
BSR-2	405629114301401	10-17-2017	157	191	12.5	2.83	JSWC
BSR-2, replicate	405629114301401	10-17-2017	150	183	12.5	2.84	JSWC
LCMW-11	405723114291701	10-18-2017	291	354	81.4	25.3	Other west-side wells
LCMW-12	405606114234901	10-18-2017	191	232	50.9	6.46	East-side wells
Shafter Well 6	405557114214101	10-19-2017	118	143	12.3	4.65	East-side wells
Pequop-2	405339114313001	10-19-2017	135	165	12.3	3.24	Other west-side wells
Long Canyon Spring	405839114325901	10-18-2017	301	365	18.0	17.2	Long Canyon Spring

Table 5. Measured field parameters and dissolved concentrations of major ions for groundwater sampled in Goshute Valley, Elko County, northeastern Nevada.—Continued

[See figure 9 for locations and Smith and others, 2021, appendixes 1 and 2, for additional site information. **Abbreviations:** CaCO3, calcium carbonate; JSWC, Johnson Springs wetland complex; USGS, U.S. Geological Survey; °C, degrees Celsius; µS/cm, microsiemens per centimeter at 25 degrees Celsius; µg/L, micrograms per liter; mg/L, milligrams per liter; <, less than; –, no information]

Site name	USGS site number	Sample date	Fluoride (mg/L as F)	Bromide (mg/L as Br)	Silica (mg/L as SiO_2)	Nitrate plus nitrite (mg/L as N)	Sample group
LCMW-06	410132114293201	10-18-2017	0.051	0.121	24.6	0.285	Other west-side wells
LCT-1	410004114280401	10-17-2017	0.200	0.026	21.5	0.429	Other west-side wells
LCMW-05S	405924114311002	10-17-2017	0.110	0.428	17.4	0.818	Other west-side wells
Big Spring.	405760114305701	10-19-2017	0.069	0.024	13.1	0.657	JSWC
LCMW-15	405732114312801	10-19-2017	0.080	0.028	13.4	0.451	JSWC
LCMW-09.S.	405707114312402	10-18-2017	0.080	0.023	13.4	0.418	JSWC
BSR-2	405629114301401	10-17-2017	0.070	0.025	13.9	0.454	JSWC
BSR-2, replicate	405629114301401	10-17-2017	0.075	0.023	13.6	0.478	JSWC
LCMW-11	405723114291701	10-18-2017	0.224	0.149	40.4	<0.040	Other west-side wells
LCMW-12	405606114234901	10-18-2017	1.37	0.053	52.7	<0.040	East-side wells
Shafter Well 6	405557114214101	10-19-2017	0.540	0.038	63.4	0.811	East-side wells
Pequop-2	405339114313001	10-19-2017	0.100	0.027	19.6	0.505	Other west-side wells
Long Canyon Spring	405839114325901	10-18-2017	0.267	0.092	34.5	1.000	Long Canyon Spring

Data Collection Methods

Field parameters were measured at water sample collection sites with a multi-parameter sonde. The sonde was used with a flow-through chamber connected to a discharge line near the well head for each of the 10 sampled wells. At the two sampled springs, the sonde was submerged (without the flow-through chamber) in flowing water near the discharge orifice.

Water samples were collected from wells using either the existing submersible pumps in production wells or the pre-installed low-flow bladder pumps in monitoring wells. Prior to sample collection, each well was purged of a minimum of three casing volumes of water and field parameters were monitored for stabilization. After purged wells stabilized, water was filtered as necessary prior to filling samples bottles. Samples were collected from springs as grab samples or by using a small submersible pump where field parameters were monitored to verify stabilization prior to sample collection.

Samples for dissolved major ions, trace constituents, strontium isotopes, and carbon-14 were filtered using 0.45-µ disposable filters and collected in clean polyethylene bottles after rinsing with native filtered water according to procedures described by U.S. Geological Survey (2018). Samples for dissolved metals and anion analysis were preserved with 7.7-normal nitric acid. Tritium samples were collected in 1-liter polyethylene bottles without head space. Stable isotopes of hydrogen and oxygen were collected in 60-mL glass bottles with polyseal caps without head space. Carbon-14 samples were collected in 1-L glass bottles, according to procedures described by the USGS National Water Quality Laboratory. Noble gas samples were collected in 3/8-in. diameter copper tubes according to the methods described by Stute and Schlosser (2000). Noble gas samples were not collected at sites where sample water contained bubbles indicating active degassing or sample re-equilibration with the atmosphere.

Major ions and trace constituents were analyzed by the U.S. Geological Survey at the National Water Quality Laboratory in Denver, Colorado. Stable isotopes of hydrogen and oxygen were analyzed by the U.S. Geological Survey at the Stable Isotope Laboratory in Reston, Virginia. Strontium isotope analyses were done by the Inductively Coupled Plasma Mass Spectrometry Lab at the University of Utah in Salt Lake City, Utah. Tritium analyses were done by the USGS Tritium Laboratory in Menlo Park, California, using the helium in-growth method (Clarke and others, 1976). Carbon-14 samples were analyzed at the National Ocean Sciences Accelerator Mass Spectrometry facility at the Woods Hole Oceanographic Institution in Woods Hole, Massachusetts.

Assessment of Dissolved Major-Ion and Trace-Element Compositions

Dissolved major-ion and trace-element concentrations were analyzed to evaluate groundwater-flow paths because they indicate the chemical evolution of water moving through the ground. Geology imparts unique chemical compositions to groundwater because the elements available for dissolution and reaction depend on the minerals present in the specific rocks and sediment that the water contacts. Therefore, waters with similar geochemical composition likely have come in contact with common geologic units along their flow path from points of recharge to the sampling location.

Dissolved solid concentrations of samples from all sites range from 259 to 658 milligrams per liter (mg/L) and are less than 300 mg/L for 7 of the 12 sites samples (table 5). Principal dissolved ions in most samples are calcium and bicarbonate, which are derived directly from dissolution of the abundant carbonate rocks throughout the study area and alluvium eroded from these rocks. Secondary dissolved ions in most samples are magnesium, sodium, sulfate, and chloride. A piper diagram shows the often-subtle differences in water types across the study area (fig. 10). The most notable feature of the diagram is that a group of samples plot in a tight cluster around the sample collected at Big Spring, the point of greatest discharge from the JSWC. Samples from Big Spring, carbonate-rock well LCMW-15, and alluvial-fan wells LCMW-09S and BSR-2 (Smith and others, 2021, appendix 2) are symbolized as belonging to the JSWC cluster of waters because of their similar major-ion composition. The remaining samples are grouped and symbolized according to their general location within the watershed: Other west-side wells (alluvial-fan and valley-fill wells LCMW-06, LCT-1, LCMW-05S, LCMW-11, and Pequop-2) also are located along the eastern front of the Pequop Mountains but are chemically distinct from JSWC waters, east-side wells (alluvial-fan wells LCMW-12, Shafter Well 6) are located downgradient from the Toano Range on the east side of Goshute Valley, and Long Canyon Spring (not shown in fig. 9) is an isolated and possibly perched spring located above 7,000 ft in the Pequop Mountains (fig. 9).

Seven of 10 samples reported by Mayo and Associates (2013) plot with the JSWC cluster, 3 of which are samples from the JSWC (North Spring, Central Spring, and Big Spring; fig. 10; table 6). The remaining Mayo and Associates samples that plot with the JSWC waters are from wells located along the eastern mountain front of the Pequop Mountains (alluvial-fan wells LCMW-07, LCMW-09S, and LCMW-19, and carbonate-rock well LCMW-17). The water chemistries from 11 samples within the JSWC major-ion cluster (collected during this study and by Mayo and Associates in 2013) define an area along the eastern front of the Pequop Mountains extending from LCMW-07 south to BSR-2. Nearly identical major-ion compositions among carbonate-rock and alluvial-fan samples within the JSWC cluster indicate that these waters have come in contact with similar geologic units along their flow paths and are likely part of a well-connected groundwater flow system in the Long Canyon Mine project area.

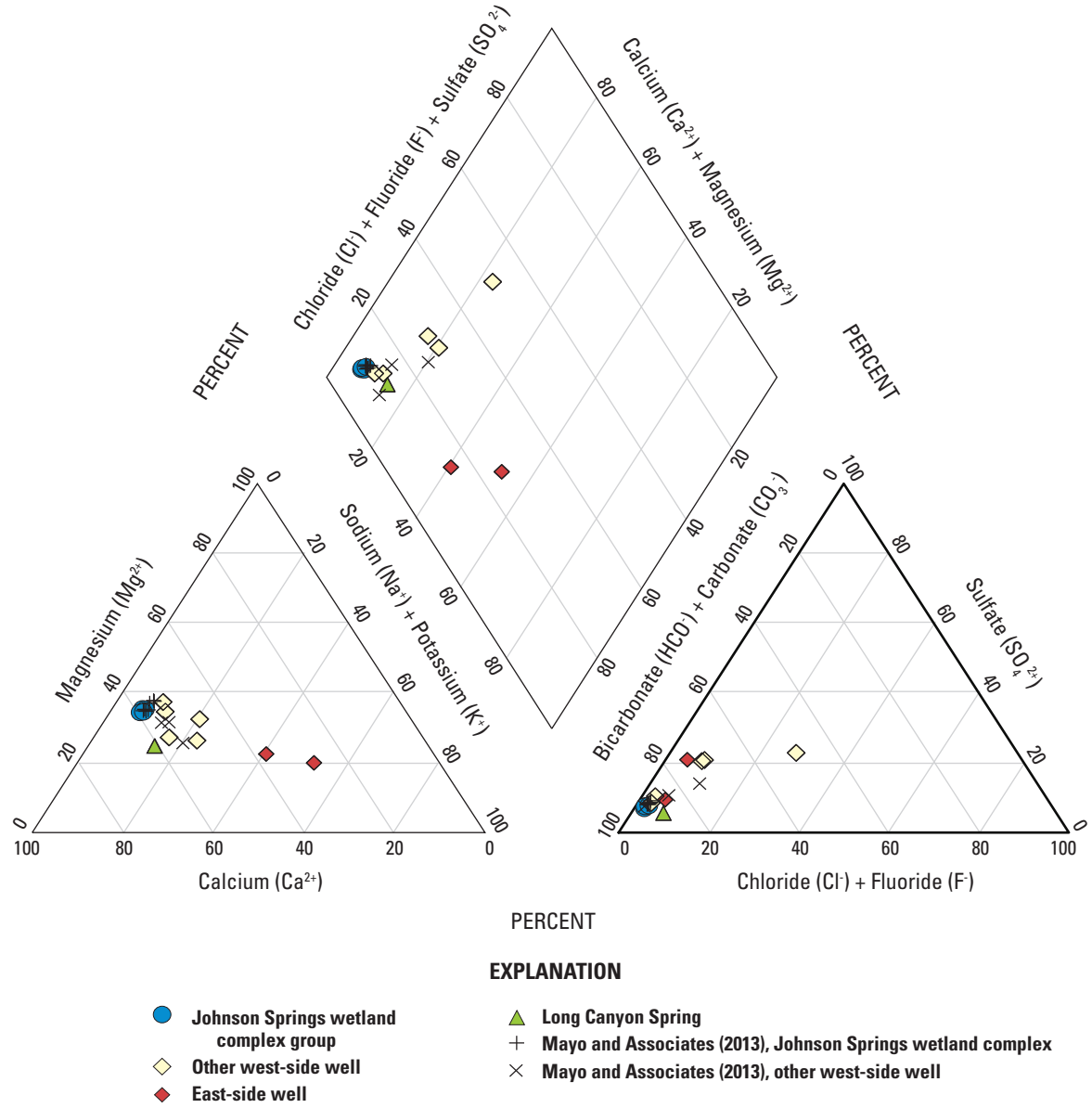

Figure 10. Major-ion composition for groundwater sampled in Goshute Valley, Elko County, northeastern Nevada.

Several samples grouped as other west-side wells have major-ion compositions like those of the JSWC cluster but are distinguished by their trace-element and isotopic composition (Long Canyon Spring, LCT-1, and Pequop-2, sampled during this study, and LCMW-01 and LCMW-05 sampled by Mayo and Associates in 2013). Major-ion compositions in east-side wells LCMW-12 and Shafter Well 6 and other west-side well LCMW-05S differ most from other wells sampled. The east-side waters contain notably higher fractions of sodium whereas the LCMW-05S sample contains elevated chloride and higher dissolved-solids when compared to other west-side and JSWC wells and springs. Distinct chemistry in east-side wells is expected because potentiometric contours indicate an east-to-west direction of groundwater flow in that area (fig. 7); therefore, waters would be in contact with different geologic units than west-side waters. The elevated chloride and higher dissolved-solids content in the LCMW-05S sample is anomalous given its upgradient proximity to the JSWC and indicates that it moves through a rock unit that JSWC waters do not come into contact with.

Table 6. Measured field parameters, major-ion concentrations, and selected isotopes reported by Mayo and Associates (2013) for groundwater sampled in Goshute Valley, Elko County, northeastern Nevada.

[See figure 9 for locations. **Sample Group:** JSWC, Johnson Springs wetland complex. **Abbreviations:** $\delta^{13}C$, ratio of carbon-13 to carbon-12 in sample compared to reference standard; ^{14}C, carbon-14; $\delta^{2}H$, ratio of hydrogen-2 (deuterium) to hydrogen-1 in sample compared to reference standard; $\delta^{18}O$, ratio of oxygen-18 to oxygen-16 in sample compared to reference standard; °C, degrees Celsius; mg/L, milligrams per liter; permil, parts per thousand; TU, tritium units; pmC, percent modern carbon; <, less than; –, no information]

Site name	Sample date	Water temperature (°C)	pH (standard units)	Dissolved solids as sum of constituents (mg/L)	Bicarbonate (mg/L as CO_{3-})	Calcium (mg/L as Ca)	Sample group
North Spring	03-20-2013	20.3	7.7	176	210	39.3	JSWC
Central Spring	03-20-2013	16.8	7.6	180	211	39.7	JSWC
Big Spring	03-11-2013	21.4	7.6	180	177	40.6	JSWC
LCMW-01	03-06-2013	10.7	8.2	225	254	47.6	Other west-side wells
LCMW-07	03-06-2013	22.5	8.1	186	207	39.3	JSWC
LCMW-19	03-26-2013	13.5	8.5	184	190	39.5	JSWC
1LCMW-05	03-18-2013	13.3	7.8	202	214	43.8	Other west-side wells
1LCMW-09	03-25-2013	21.6	8.4	180	186	38.6	JSWC
LCMW-17	03-11-2013	18.6	8.3	175	195	40.9	JSWC
LCP-16A	07-16-2013	–	8.1	223	170	54.2	Other west-side wells
LC-Snow	03-18-2013	–	–	–	–	–	Snow sample

Site name	Sample date	Magnesium (mg/L as Mg)	Sodium (mg/L as Na)	Potassium (mg/L as K)	Sulfate (mg/L as SO4)	Chloride (mg/L as Cl)	Fluoride (mg/L as F)	Sample group
North Spring	03-20-2013	16.4	5.7	2.0	16.8	3.5	0.13	JSWC
Central Spring	03-20-2013	16.0	5.2	1.6	14.9	3.5	0.13	JSWC
Big Spring	03-11-2013	15.0	5.0	1.5	12.3	2.8	0.10	JSWC
LCMW-01	03-06-2013	16.8	12.5	3.6	16.1	3.4	0.11	Other west-side wells
LCMW-07	03-06-2013	16.5	5.6	1.8	15.0	3.2	0.10	JSWC
LCMW-19	03-26-2013	14.7	5.6	1.5	14.3	3.4	0.12	JSWC
[1]LCMW-05	03-18-2013	14.9	10.6	1.7	21.3	8.6	0.15	Other west-side wells
[1]LCMW-09	03-25-2013	14.0	4.6	1.5	13.6	2.9	0.10	JSWC
LCMW-17	03-11-2013	14.9	5.4	1.7	13.5	2.9	0.10	JSWC
LCP-16A	07-16-2013	15.5	21.6	3.7	24.7	14.3	0.23	Other west-side wells
LC-Snow	03-18-2013	–	–	–	–	–	–	Snow sample

Table 6. Measured field parameters, major-ion concentrations, and selected isotopes reported by Mayo and Associates (2013) for groundwater sampled in Goshute Valley, Elko County, northeastern Nevada.—Continued

[See figure 9 for locations. **Sample Group:** JSWC, Johnson Springs wetland complex. **Abbreviations:** $\delta^{13}C$, ratio of carbon-13 to carbon-12 in sample compared to reference standard; ^{14}C, carbon-14; $\delta^{2}H$, ratio of hydrogen-2 (deuterium) to hydrogen-1 in sample compared to reference standard; $\delta^{18}O$, ratio of oxygen-18 to oxygen-16 in sample compared to reference standard; °C, degrees Celsius; mg/L, milligrams per liter; permil, parts per thousand; TU, tritium units; pmC, percent modern carbon; <, less than; –, no information]

Site name	Sample date	$\delta^{18}O$ (permil)	$\delta^{2}H$ (permil)	Tritium (^{3}H) (TU)	Carbon-14 (^{14}C (pmC)	$\delta^{13}C$ (permil)	Sample group
North Spring	03-20-2013	-17.5	-134	<1	21.1	-3.8	JSWC
Central Spring	03-20-2013	-17.2	-133	<1	26.9	-5.7	JSWC
Big Spring	03-11-2013	-17.2	-133	1.00	28.8	-6.8	JSWC
LCMW-01	03-06-2013	-17.3	-133	<1	40.5	-7.4	Other west-side wells
LCMW-07	03-06-2013	-17.2	-133	<1	20.9	-6.8	JSWC
LCMW-19	03-26-2013	-17.3	-133	<1	29.5	-7.1	JSWC
[1]LCMW-05	03-18-2013	-17.2	-133	<1	22.3	-6.9	Other west-side wells
[1]LCMW-09	03-25-2013	-17.3	-133	0.95	24.1	-6.1	JSWC
LCMW-17	03-11-2013	-17.2	-133	0.68	24.5	-7.1	JSWC
LCP-16A	07-16-2013	-17.0	-134	<1	7.1	-7.1	Other west-side wells
LC-Snow	03-18-2013	-17.6	-137	8.9	–	–	Snow sample

[1]Mayo and Associates (2013) does not state whether the shallow or deep completion was sampled.

Dissolved trace-element concentrations for samples collected during this study are shown in table 7 and plotted by water chemistry group on figure 11. Trace-element concentrations typically differ by one to two orders of magnitude for west-side and east-side samples. This is true even when considering only west-side samples, which presumably all represent groundwater recharged within about a 10-mi north-south length of the Pequop Mountains. Trace-element concentrations within the JSWC sample cluster, however, are distinct with negligible variability compared to the larger sample set (fig. 11). Although water from well Pequop-2 and the JSWC cluster have similar concentrations of major ions and some trace elements (boron, molybdenum, and uranium), water from Pequop-2 is clearly distinguishable from JSWC waters by its concentrations of cesium, lithium, and rubidium.

Dissolved strontium concentrations range from 163 to 1,120 µg/L, with the lowest concentrations in JSWC waters (163–171 µg/L) and no apparent spatial correlation for the remaining samples (table 7). Strontium isotope values ($^{87}Sr/^{86}Sr$) in groundwater samples are derived from the isotopic compositions of soluble soil constituents in recharge areas and subsequent modification by water-rock interactions during flow through aquifers (Paces and Wurster, 2014). A plot of strontium isotope ratios ($^{87}Sr/^{86}Sr$) compared to dissolved strontium concentrations indicates that JSWC waters are unique among the sample set, with low dissolved strontium and strontium isotope ratios enriched in ^{87}Sr (fig. 12). The unique strontium-isotope signature combined with the trace-element and dissolved major ion and chemistry of the JSWC water likely are influenced by geology of the mineralized rock zone in the central part of the Long Canyon Mine project area (Smith and others, 2011).

Estimating Mean Age of Groundwater with Tritium, Helium, and Carbon Isotopes

Radioactive tritium and carbon-14 concentrations along with stable isotopes of helium and carbon were used to evaluate the mean age of groundwater within the Goshute Valley groundwater basin. Tritium (^{3}H) is a radioactive isotope of hydrogen with a half-life of 12.32 years that can exist as part of a water molecule and is present in small concentrations in water worldwide. In this study, ^{3}H was used to detect the occurrence of modern (post-1950) groundwater and, combined with its radioactive decay product ^{3}He, to more accurately estimate groundwater age. The ^{3}H concentrations are reported in tritium units (TU), where 1 TU equals radioactive decay of about 3.2 picocuries per liter (piC/L). The ^{3}H concentration in precipitation in the study area is assumed to be similar to that measured by the Global Network of Isotopes in Precipitation monitoring station operated by the International Atomic Energy Agency in Salt Lake City, Utah. The ^{3}H concentrations in precipitation ranged from less than 10 to more than 3,200 TU from 1950 to 2005 (about 0.4–171 TU decay-corrected to 2017) with the peak resulting from above ground nuclear testing that began in the early 1950s (Gardner and Heilweil, 2014). For this study, water samples containing greater than 0.4 TU are assumed to have at least some modern fraction. The isotopes of helium (^{3}He and ^{4}He) were apportioned to concentrations that originated from the atmosphere (tritium decay,$^{3}He_{trit}$), and the Earth's crust (uranium/thorium-series decay, $^{4}He_{terr}$) (Solomon, 2000a, 2000b). In this analysis, the mantle was not considered as a source of helium gas.

Groundwater ^{3}H concentrations range from below detection (0.1 TU) to 3.4 TU for the 12 sites sampled during this study (table 8). Only two waters, LCMW-11 and Long Canyon Spring, are clearly modern with values of 1.5 and 3.4 TU, respectively. The sample from LCMW-11 has an apparent $^{3}H/^{3}He$ age of 34 years. Site LCMW-11 is a shallow basin-fill well (screened from 13 to 79 ft bls) yielding water that likely recharges along the mountain front and may contain a fraction of recharge from nearby overland runoff after periods of above-average precipitation, such as the winter preceding this sampling (2016–17). No dissolved noble gas sample was collected at Long Canyon Spring owing to apparent gas re-equilibration with the atmosphere. Without a measurement of ^{3}He, this sample can only be classified as *modern*. The remainder of the samples are classified simply as a *mixture* (containing a fraction of modern water) or as *premodern* with respect to apparent $^{3}H/^{3}He$ ages (table 8).

Tritium values greater than 0.4 TU identify a modern fraction of water in five samples located along the Pequop Mountain front (LCMW-05S, Big Spring, LCMW-15, LCMW-09S, and BSR-2). Tritium values less than 0.4 TU identify samples from LCMW-06, LCT-1, Pequop-2, LCMW-12, and Shafter Well 6 as clearly premodern. JSWC waters have tritium values ranging from 0.4 and 0.9 TU and are classified as mixtures containing a fraction of modern water. Mayo and Associates (2013) reported a tritium value of 8.9 TU for one snow sample, and despite having a higher detection limit of about 1 TU, reported tritium values in groundwater of less than 1 TU that were consistent with most other groundwater tritium concentrations measured during this study(tables 6 and 8).

Qualitative age dating with $^{4}He_{terr}$ is used in this study to help identify a premodern component of water in samples of mixed age. Solomon (2000b) reports average crustal $^{4}He_{terr}$ production rates ranging from 0.28 to 2.4 micro-cubic centimeters per cubic meter of rock or sediment at standard temperature and pressure (µccSTP/ m^3) per year, indicating that groundwater will not acquire significant concentrations of $^{4}He_{terr}$ (more than about 2×10^{8} micro-cubic centimeters per gram of water at standard temperature and pressure [µccSTP/g]) until it has been in contact with aquifer materials for more than 1,000 years. Samples classified as mixtures of modern and premodern water have $^{4}He_{terr}$ concentrations ranging from 1.98×10^{-8} to 2.84×10^{-8} ccSTP/g, confirming the presence of an old component (table 8). Samples classified as premodern have $^{4}He_{terr}$ concentrations ranging from 2.20×10^{-8} to 2.38×10^{-7} ccSTP/g. The modern sample from LCMW-11 had no detectible $^{4}He_{terr}$.

Table 7. Dissolved concentrations of selected trace elements for groundwater sampled in Goshute Valley, Elko County, northeastern Nevada.

[See figure 9 for site locations and Smith and others, 2021, appendixes 1 and 2, for additional site information. **USGS site number:** U.S. Geological Survey site number. **87Sr/86Sr:** strontium isotope ratio. Sample group: JSWC, Johnson Springs wetland complex. **Abbreviation:** µg/L, micrograms per liter]

Site name	USGS site number	Arsenic (µg/L as As)	Barium (µg/L as Ba)	Boron (µg/L as Bo)	Cesium (µg/L as Cs)	Lithium (µg/L as Li)	Sample group
LCMW-06	410132114293201	1.76	44.1	80	0.000	7.68	Other west-side wells
LCT-1	410004114280401	2.10	105	52	0.002	10.6	Other west-side wells
LCMW-05S	405924114311002	1.00	149	130	0.003	1.53	Other west-side wells
Big Spring	405760114305701	2.01	164	24	0.307	6.09	JSWC
LCMW-15	405732114312801	1.90	188	26	0.321	5.80	JSWC
LCMW-09S	405707114312402	1.90	197	24	0.275	6.29	JSWC
BSR-2	405629114301401	2.00	208	26	0.402	7.31	JSWC
BSR-2, replicate	405629114301401	1.98	211	26	0.398	6.68	JSWC
LCMW-11	405723114291701	12.5	124	86	0.000	21.7	Other west-side wells
LCMW-12	405606114234901	16.3	38.2	150	0.099	80.5	East-side wells
Shafter Well 6	405557114214101	4.00	102	86	0.190	24.8	East-side wells
Pequop-2	405339114313001	1.80	143	28	1.96	17.4	Other west-side wells
Long Canyon Spring	405839114325901	8.16	94.2	95	0.000	12.0	Long Canyon Spring

Site name	USGS site number	Molybdenum (µg/L as Mo)	Rubidium (µg/L as Rb)	Strontium (µg/L as Sr)	$^{87}Sr/^{86}Sr$	Uranium (µg/L as U)	Sample group
LCMW-06	410132114293201	0.209	1.53	186	0.70891	1.90	Other west-side wells
LCT-1	410004114280401	1.28	4.13	215	0.70928	1.27	Other west-side wells
LCMW-05S	405924114311002	2.03	1.15	377	0.70946	2.25	Other west-side wells
Big Spring	405760114305701	0.489	2.89	170	0.71023	0.930	JSWC
LCMW-15	405732114312801	0.524	2.81	163	0.71054	0.837	JSWC
LCMW-09S	405707114312402	0.537	2.81	164	0.71050	0.842	JSWC
BSR-2	405629114301401	0.399	3.26	171	0.71052	0.896	JSWC
BSR-2, replicate	405629114301401	0.44	3.34	169	0.71055	0.910	JSWC
LCMW-11	405723114291701	12.9	8.53	343	0.70997	2.38	Other west-side wells
LCMW-12	405606114234901	17.8	19.7	1,120	0.70946	2.10	East-side wells
Shafter Well 6	405557114214101	2.43	18.1	367	0.71015	14.6	East-side wells
Pequop-2	405339114313001	0.399	14.1	236	0.70994	1.02	Other west-side wells
Long Canyon Spring	405839114325901	0.785	0.93	329	0.70812	4.20	Long Canyon Spring

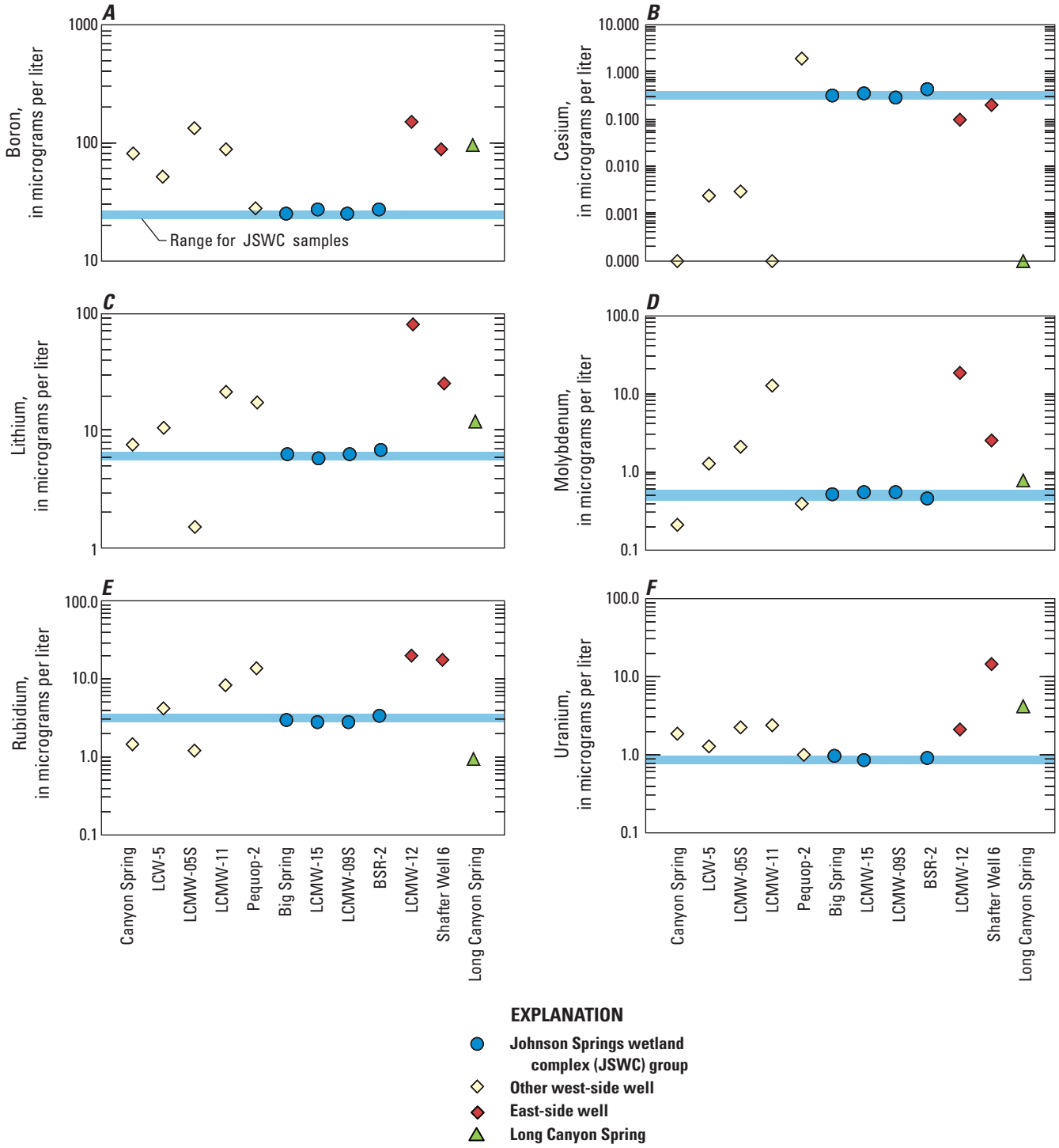

Figure 11. Selected trace-element concentrations for groundwater sites sampled in Goshute Valley, Elko County, northeastern Nevada.

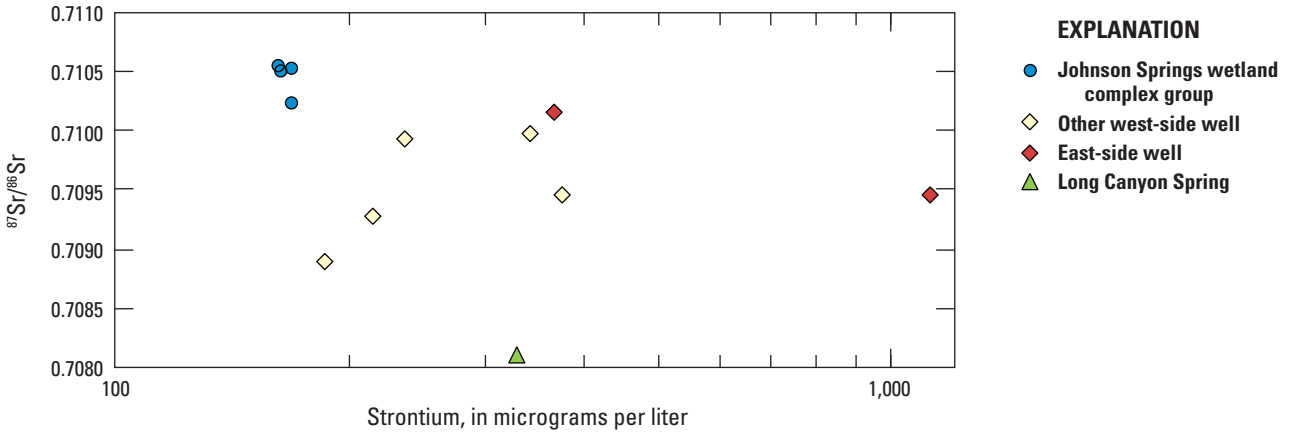

Figure 12. Strontium isotope ratios compared to dissolved strontium concentrations for groundwater sites sampled in Goshute Valley, Elko County, northeastern Nevada.

Radioactive ^{14}C was used to estimate the mean age of premodern water in the Goshute Valley groundwater basin. Unadjusted radiocarbon ages were calculated from non-normalized ^{14}C activities of dissolved inorganic carbon using the Libby half-life (5,568 years) and assuming an initial ^{14}C activity of 100 percent modern carbon (pMC). Radiocarbon age corrections were made using the revised Fontes and Garnier formula-based model as implemented by Han and Plummer (2013). The corrections are made to account for physical processes and chemical reactions other than radioactive decay that alter ^{14}C activity in the unsaturated zone and below the water table. Following the graphical method of Han and others (2012), a closed system equilibration model (representing reactions occurring below the water table limiting gas exchange with atmosphere) was assumed for all samples. Corrections were made using standard assumptions for the ^{14}C activities of carbonate minerals and soil gas carbon dioxide (CO_2; 0 and 100 pMC, respectively) and $\delta^{13}C$ of carbonate minerals (0 permil) (Plummer and Sprinkle, 2001; Kennedy and Genereux, 2007). A range of corrected ages was calculated based on the assumption of a range of $\delta^{13}C$ for soil-gas CO_2 of -19.5 to -22 permil, which is consistent with reported values for similar terrain in Utah (Cerling and others, 1991; Hart and others, 2010). Furthermore, this range of $\delta^{13}C$ produces near-zero corrected ^{14}C ages for waters shown to be modern by ^{3}H concentrations (LCMW-11 and Long Canyon Spring), validating the assumption. Because atmospheric ^{14}C has not been constant over time (de Vries, 1958), radiocarbon ages were then calibrated to years before present (BP) using the IntCal13 radiocarbon calibration curve (Reimer and others, 2013).

Carbon-14 activity of dissolved inorganic carbon in all samples ranges from 4.2 to 101 pMC and yields corrected radiocarbon ages ranging from modern to 22,400 years BP (table 8). A correlation showing decreasing ^{14}C activity with increasing $\delta^{13}C$ enrichment indicates significant water-carbonate mineral reaction and the necessity for radiocarbon age adjustments (fig. 13). There is a strong relation between ^{14}C and $\delta^{13}C$ for all samples from sites within or along the Pequop Mountain front (coefficient of determination [R^2]= 0.7). Samples from the two east-side wells (LCMW-12 and Shafter Well 6) have undergone considerably less $\delta^{13}C$ enrichment than all west-side waters, resulting from contact and reaction with different geologic units. JSWC waters plot in a tight cluster, indicating that they have undergone similar degrees of carbonate-mineral reaction and ^{14}C radioactive decay. Samples reported by Mayo and Associates (2013) classified as JSWC waters according to their dissolved major-ion chemistry (table 6) have similar ^{14}C activity with a somewhat larger spread of $\delta^{13}C$ values (fig. 13). Two of the three samples from Mayo and Associates (2013) with notable $\delta^{13}C$ enrichment are from North Spring and Central Spring, located at the head of the JSWC (not shown). If the samples were collected downstream from the spring orifice or if the spring discharge was low, these samples possibly underwent surface or near-surface processes that further altered the $\delta^{13}C$. Degassing of CO_2, carbonate precipitation, exchange with atmospheric CO_2, carbon uptake by aquatic organisms, methanogenesis, and methane oxidation are examples of these types of processes that can affect $\delta^{13}C$ of dissolved carbon in similar settings.

Minimum and maximum corrected radiocarbon ages for samples from the three wells categorized as JSWC waters (LCMW-15, LCMW-09S, BSR-2) are all very similar and range from 1,100 to 2,400 years BP. The range of corrected ages for Big Spring, also belonging to the JSWC group, is 500–1,400 years BP. The younger mean age for Big Spring water is not surprising given that all samples from the JSWC group were categorized as mixtures of modern and premodern water by their low ^{3}H and elevated $^{4}He_{terr}$ concentrations. Spring discharge typically integrates flow paths over a larger range of ages than discrete-depth well samples, which often represent a single flow path. The younger mean age for Big Spring water indicates that it contains a larger fraction of young water than the other samples constituting the JSWC cluster on figure 13.

Table 8. Stable- and radio-isotope data used to evaluate sources and estimate ages of groundwater sampled in Goshute Valley, Elko County, northeastern Nevada.

[See figure 9 for locations and Smith and others, 2021, appendixes 1 and 2, for additional site information. Premodern, groundwater that recharged prior to the mid-1950s. Modern, groundwater that recharged after the mid-1950s. Mixture, sample that contains a mixture of premodern and modern groundwater. **USGS site number:** U.S. Geological Survey site number. **R/Ra:** R is the $^{3}He/^{4}He$ ratio of the sample, and R_a is the $^{3}He/^{4}He$ ratio of air (1.384×10^{-6}). **Terrigenic Helium-4 ($^{4}He_{terr}$) and Tritiogenic Helium-3 ($^{3}He_{trit}$):** Interpreted value is derived using the Closed-Equilibrium dissolved gas model (Aeschbach-Hertig and others, 2000; Kipfer and others, 2002). Values are uncertain for premodern waters due to uncertain terrigenic $^{3}He/^{4}He$ ratio. **Corrected 14C age range:** Radiocarbon ages were corrected using the revised Fontes and Garnier model (Han and Plummer, 2013) and calibrated using the IntCal13 radiocalibration curve (Reimer and others, 2013). **Sample group:** JSWC, Johnson Springs wetland complex. **Abbreviations:** $\delta^{13}C$, ratio of carbon-13 to carbon-12 in sample compared to reference standard; ^{14}C, carbon-14; ccSTP/g, cubic centimeters per gram of water at standard temperature and pressure; $\delta^{2}H$, ratio of hydrogen-2 (deuterium) to hydrogen-1 in sample compared to reference standard; $\delta^{18}O$, ratio of oxygen-18 to oxygen-16 in sample compared to reference standard; permil, parts per thousand; pmC, percent modern carbon; TU, tritium units; years BP, years before present; –, no information]

Site name	USGS site number	$\delta^{18}O$ (permil)	$\delta^{2}H$ (permil)	Tritim (^{3}H) and precision (TU)	R/R_a	Measured helium-4 (^{4}He) (ccSTP/g)	Terrigenic helium-4 ($^{4}He_{terr}$) (ccSTP/g)	Sample group
LCMW-06	410132114293201	-16.6	-130	0.2 ± 0.1	0.94	4.28×10^{-08}	2.20×10^{-08}	Other west-side wells
LCT-1	410004114280401	-17.1	-131	0.1 ± 0.1	–	–	–	Other west-side wells
LCMW-05S	405924114311002	-16.6	-129	0.5 ± 0.1	–	–	–	Other west-side wells
Big Spring	405760114305701	-17.1	-130	0.9 ± 0.1	0.74	6.63×10^{-08}	2.20×10^{-08}	JSWC
LCMW-15	405732114312801	-17.1	-130	0.6 ± 0.1	0.73	6.32×10^{-08}	1.98×10^{-08}	JSWC
LCMW-09S	405707114312402	-17.0	-130	0.7 ± 0.1	0.68	7.41×10^{-08}	2.84×10^{-08}	JSWC
BSR-2	405629114301401	-17.1	-130	0.4 ± 0.1	0.74	6.34×10^{-08}	1.89×10^{-08}	JSWC
BSR-2, replicate	405629114301401	-17.1	-129	0.4 ± 0.1	0.75	6.30×10^{-08}	–	JSWC
LCMW-11	405723114291701	-15.8	-122	1.5 ± 0.1	1.35	4.54×10^{-08}	$0.00\times10^{+00}$	Other west-side wells
LCMW-12	405606114234901	-18.4	-145	0.1 ± 0.1	–	–	–	East-side wells
Shafter Well 6	405557114214101	-18.0	-140	0.1 ± 0.1	0.19	2.82×10^{-07}	2.38×10^{-07}	East-side wells
Pequop-2	405339114313001	-17.1	-130	0.04 ± 0.1	0.59	7.64×10^{-08}	3.02×10^{-08}	Other west-side wells
Long Canyon Spring	405839114325901	-15.8	-123	3.4 ± 0.2	–	–	–	Long Canyon Spring

Table 8. Stable- and radio-isotope data used to evaluate sources and estimate ages of groundwater sampled in Goshute Valley, Elko County, northeastern Nevada.—Continued

[See figure 9 for locations and Smith and others, 2021, appendixes 1 and 2, for additional site information. Premodern, groundwater that recharged prior to the mid-1950s. Modern, groundwater that recharged after the mid-1950s. Mixture, sample that contains a mixture of premodern and modern groundwater. **USGS site number:** U.S. Geological Survey site number. **R/Ra:** R is the $^{3}He/^{4}He$ ratio of the sample, and R_a is the $^{3}He/^{4}He$ ratio of air (1.384×10^{-6}). **Terrigenic Helium-4 ($^{4}He_{terr}$) and Tritiogenic Helium-3 ($^{3}He_{trit}$):** Interpreted value is derived using the Closed-Equilibrium dissolved gas model (Aeschbach-Hertig and others, 2000; Kipfer and others, 2002). Values are uncertain for premodern waters due to uncertain terrigenic $^{3}He/^{4}He$ ratio. **Corrected 14C age range:** Radiocarbon ages were corrected using the revised Fontes and Garnier model (Han and Plummer, 2013) and calibrated using the IntCal13 radiocalibration curve (Reimer and others, 2013). **Sample group:** JSWC, Johnson Springs wetland complex. **Abbreviations:** $\delta^{13}C$, ratio of carbon-13 to carbon-12 in sample compared to reference standard; ^{14}C, carbon-14; ccSTP/g, cubic centimeters per gram of water at standard temperature and pressure; $\delta^{2}H$, ratio of hydrogen-2 (deuterium) to hydrogen-1 in sample compared to reference standard; $\delta^{18}O$, ratio of oxygen-18 to oxygen-16 in sample compared to reference standard; permil, parts per thousand; pmC, percent modern carbon; TU, tritium units; years BP, years before present; –, no information]

Site name	USGS site number	Tritiogenic helium-3 ($^{3}He_{trit}$) (TU)	Apparent $^{3}H/^{3}He_{trit}$ age (years BP)	Carbon-14 (^{14}C) (pmC)	$\delta^{13}C$ (permil)	Unadjusted ^{14}C age (thousands of years BP)	Corrected ^{14}C age range (years BP)	Sample group
LCMW-06	410132114293201	2.9	Premodern	56.0	-10.5	5,000	Modern	Other west-side wells
LCT-1	410004114280401	–	Premodern	11.6	-7.2	17,000	9,000–10,200	Other west-side wells
LCMW-05S	405924114311002	–	Mixture	24.1	-7.3	11,000	2,000–3,300	Other west-side wells
Big Spring	405760114305701	2.9	Mixture	28.5	-7.3	10,000	500–1,400	JSWC
LCMW-15	405732114312801	1.6	Mixture	24.8	-6.9	11,000	1,100–2,200	JSWC
LCMW-09S	405707114312402	2.8	Mixture	24.1	-6.9	11,000	1,300–2,400	JSWC
BSR-2	405629114301401	1.5	Mixture	25.4	-7.2	11,000	1,100–2,300	JSWC
BSR-2, replicate	405629114301401	–	–	26.3	-7.2	11,000	1,200–2,200	JSWC
LCMW-11	405723114291701	8.6	34	78.1	-9.7	2,000	Modern	Other west-side wells
LCMW-12	405606114234901	–	Premodern	13.4	-10.55	16,000	11,600–12,900	East-side wells
Shafter Well 6	405557114214101	2.6	Premodern	4.2	-8.12	26,000	21,000–22,400	East-side wells
Pequop-2	405339114313001		Premodern	11.0	-6.74	18,000	8,600–9,900	Other west-side wells
Long Canyon Spring	405839114325901	–	Modern	101	-12.84	Modern	Modern	Long Canyon Spring

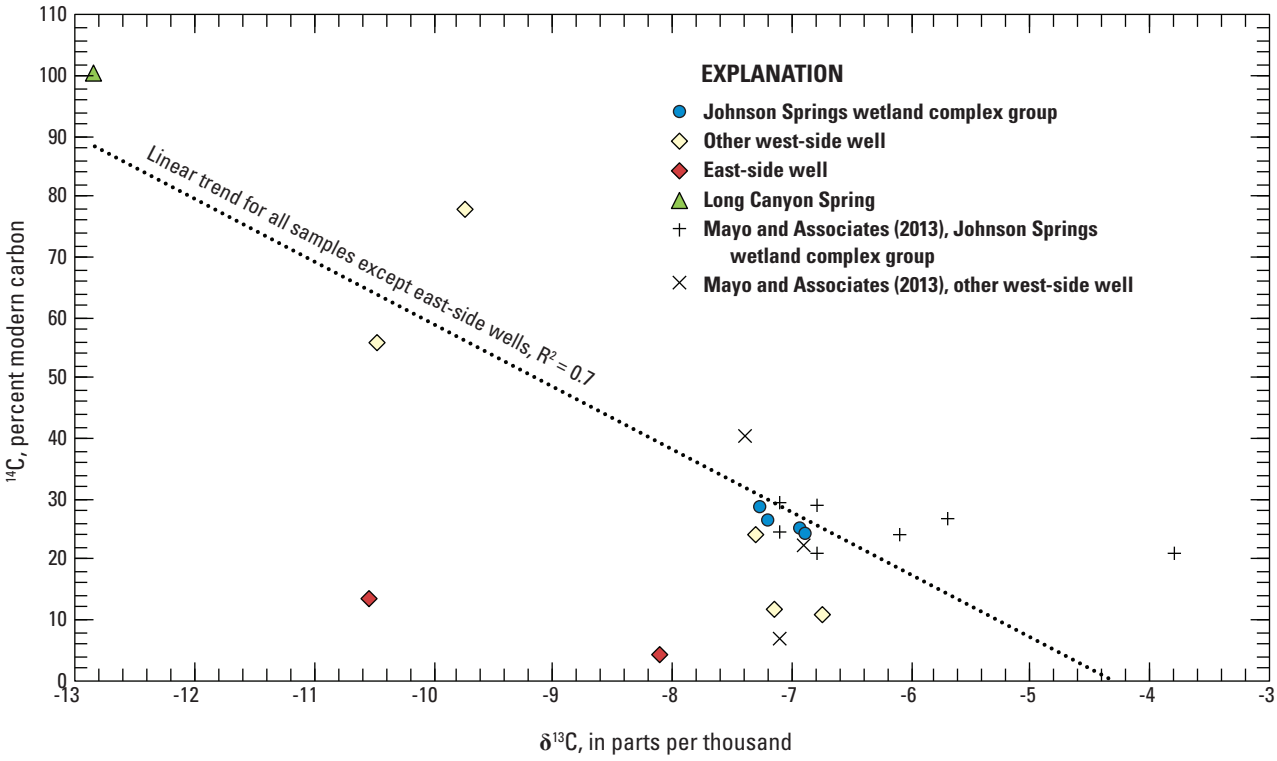

Figure 13. Carbon-14 (^{14}C) activity compared to stable carbon isotope ratios ($\delta^{13}C$), for groundwater sites sampled in Goshute Valley, Elko County, northeastern Nevada. R^2, coefficient of determination.

Age corrections for samples from LCMW-06, LCMW-11, and Long Canyon Spring indicate that these waters are modern. Modern age agrees with ^{3}H ages for LCMW-11 and Long Canyon Spring but is inconsistent with the premodern ^{3}H age for LCMW-06. The contradictory ^{3}H and ^{14}C ages for LCMW-06 indicate that this water is too old to date using ^{3}H and younger than can be resolved by radiocarbon dating in the aquifer setting where carbonate-mineral reaction leads to corrected-age uncertainties on the order of 500–1,000 years. As such, this sample is categorized simply as "premodern."

Remaining samples on the west side of the Goshute Valley include water from carbonate-rock well LCMW-05S (2,000–3,300 years BP), which is slightly older than water in the JSWC (500–2,400 years BP) and younger than waters from alluvial-fan and valley-fill wells Pequop-2 and LCT-1, respectively, which range from 8,600 to 10,200 years BP. Samples from east-side alluvial-fan wells LCMW-12 and Shafter Well 6 are clearly of Pleistocene age, with corrected radiocarbon ages of 11,600–22,400 years BP, indicating a less active groundwater-flow system on the east side of the Goshute Valley.

Evaluating Groundwater Sources with Stable Isotopes and Noble Gas Recharge Temperatures

The stable isotopes of water were used to better understand recharge sources to the groundwater basin. Stable isotopes are analyzed by measuring the ratio of the heavier, less abundant isotopes (^{18}O and ^{2}H) to the lighter, common isotopes (^{16}O and ^{1}H) that constitute a water sample. The values are reported as differences ($\delta^{18}O$ and $\delta^{2}H$) relative to a reference standard known as Vienna Standard Mean Ocean Water in permil (Craig, 1961a; Coplen, 1994). When $\delta^{2}H$ is plotted compared to $\delta^{18}O$, the proportional variation in ^{2}H and ^{18}O results in isotopic compositions of precipitation that plot along a linear trend termed a meteoric water line. For a location the size of the study area, samples sourced from precipitation falling at higher altitudes and (or) during the winter should be isotopically lighter (have more negative values) and plot lower and farther to the left along a meteoric water line, whereas samples sourced from precipitation falling at lower altitudes and (or) during the summer should be isotopically heavier (less negative values) and plot higher and farther to the right. Waters with more negative values (isotopically lighter) are said to be more "depleted" because they contain fewer of the heavy stable isotopes.

Stable-isotope compositions for the 12 sites sampled during this study range from -18.4 to -15.8 permil for $\delta^{18}O$ and from -145 to -122 permil for $\delta^{2}H$ (table 8). All waters plot along a meteoric trend between the global and arid-zone meteoric water lines (Craig, 1961b; Welch and Preissler, 1986), indicating that they represent precipitation that has not undergone significant evaporation (fig. 14). The range of $\delta^{2}H$ and $\delta^{18}O$ that represents modern high-altitude winter precipitation is bracketed by a snow sample collected by Mayo and Associates (2013) and the sample from Long Canyon Spring discharging from above 7,000 ft in the Pequop Mountains. Moreover, this range of values generally agrees with contours of $\delta^{2}H$ for cumulative winter precipitation across the Great Basin reported by Friedman and others (2002) and Smith and others (2002). Except for the east-side waters, all the samples fall within the range of modern high-altitude winter precipitation, indicating that snowmelt from high in the Pequop Mountains is the dominant source of recharge to western Goshute Valley. The two samples collected from wells on the east side of the valley (LCMW-12 and Shafter Well 6) notably are more-negative than all others, which agrees with their Pleistocene radiocarbon ages since precipitation would have been isotopically lighter during a cooler climate (fig. 14). Samples of JSWC water collected by the USGS in October 2017 continue to plot in a very tight cluster near -130 and -17.1 permil for $\delta^{2}H$ and $\delta^{18}O$. These values are all isotopically more negative than water from Long Canyon Spring, suggesting that the dominant recharge supplying the JSWC is snowmelt that accumulates above the Long Canyon Spring altitude of 7,149 ft. Samples collected by Mayo and Associates (2013) plot near the JSWC waters collected by the USGS in October of 2017 but are isotopically even more negative. The difference in isotopic values could be the result of the samples being collected years apart.

Although stable isotopes show that recharge to western Goshute Valley is dominated by high-altitude precipitation, taken alone, they are incapable of determining whether recharge occurred by infiltration directly to mountain bedrock or by seepage of water through streams and alluvium along the mountain front. The recharge mechanism can be evaluated using noble-gas recharge temperatures (NGTs, assumed to equal the temperature of groundwater recharge as it crosses the water table), derived from dissolved noble-gas concentrations (^{20}Ne, ^{40}Ar, ^{84}Kr, and ^{129}Xe). Interpretation of NGTs for this purpose assumes that a relation exists between recharge altitude (H_r) and recharge temperature that is like a typical air-temperature lapse rate, where recharge occurring at mountain altitudes will be cooler than recharge occurring in adjacent valleys. Noble gases dissolved in groundwater primarily are of atmospheric origin and their concentrations are governed by their solubility (with the possible addition of excess air) at the temperature, pressure, and salinity conditions as recharge crosses the water table. Because most noble-gas concentrations are geochemically inert, their concentrations and the groundwater NGTs derived from them should remain unchanged along a groundwater-flow path (Stute and Schlosser, 2000).

Noble-gas concentrations were interpreted using a closed-system equilibration (CE) model (Aeschbach-Hertig and others, 2000; Kipfer and others, 2002) to calculate NGTs.

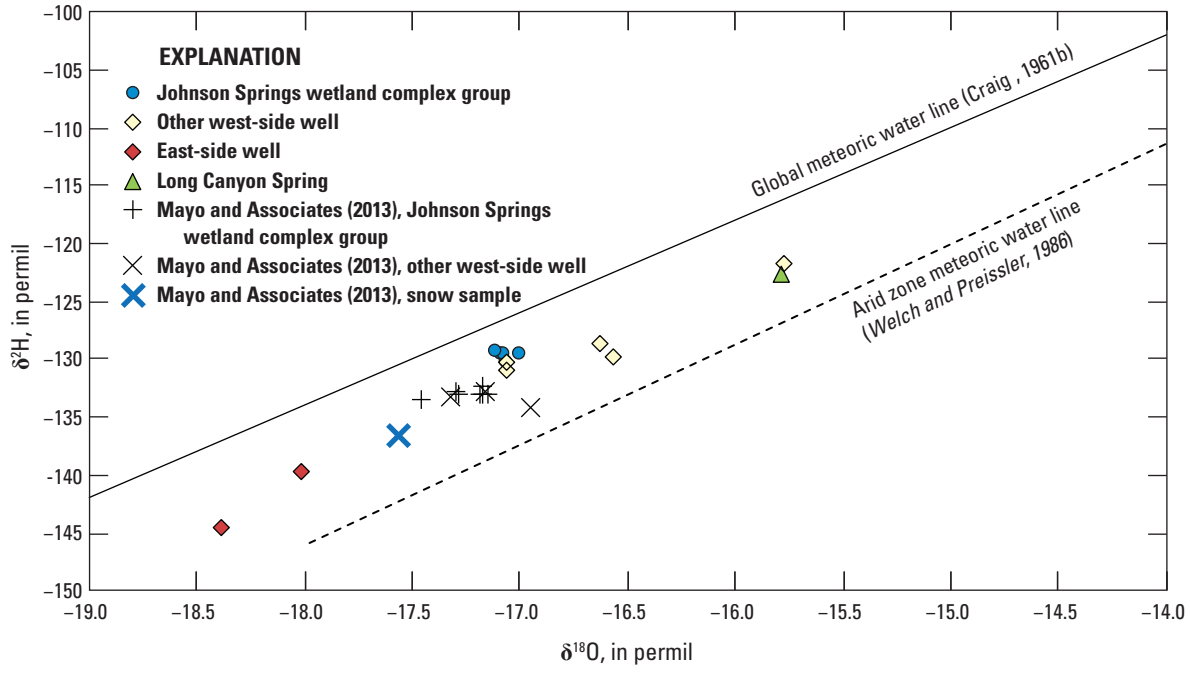

Figure 14. Stable hydrogen isotope ratios ($\delta^{2}H$) compared to stable oxygen isotope ratios ($\delta^{18}O$) for groundwater and one snow sample collected in Goshute Valley, Elko County, northeastern Nevada, permil, parts per thousand.

Recharge altitude (H; a proxy for barometric pressure) is an unknown parameter in this model, a typical situation in locations with high topographic relief. Because the NGTs and H are correlated, a range of NGTs was calculated for each sample, as described by Manning and Solomon (2003) and Manning (2011). This range consists of using a minimum recharge altitude (H_{min}), typically that of the sample site, to calculate a maximum noble-gas temperature (NGT_{max}). Conversely, the maximum recharge altitude (H_{max}) in a basin is used to calculate a minimum noble-gas recharge temperature (NGT_{min}). The H_{max} was assumed to be 8,000 ft in the mountains surrounding Goshute Valley. Average values (NGT_{avg}) also are calculated using the mid-point recharge altitude (H_{avg}) and often are assumed to best represent the actual recharge temperature of the sample with the minimum and maximum values representing a conservative range of uncertainty.

Dissolved noble-gas concentrations, NGTs, and CE model parameters and fit (A, F, and sum of χ^2) are presented for eight sample sites in table 9. The range of possible NGT values for each of the sites is shown on fig. 15, where the left and right points for each sample represent NGT_{min} and NGT_{max}, respectively. Values of NGT_{avg} range from 5.2 to 11.3 °C, with NGT_{min} and NGT_{max} values that range from 0.9 to 1.4 °C around the average.

Because NGTs represent estimates of recharge temperature (the water-table temperature at the location of recharge), they can be compared to measured water-table temperatures to evaluate whether samples represent mountain- or valley-altitude recharge. Physical water temperatures measured at six wells with open intervals located near or intersecting the top of the water surface are assumed to represent the water table and range from 9.6 to 22 °C, with an average of 14 °C (fig. 15). Values of NGT_{avg} for all but one site (Pequop-2) are less than even the coolest measured water-table temperature (from Long Canyon Spring at 7,149 ft in altitude), indicating that the point of recharge for nearly all JSWC and other west-side groundwater sample sites is confined to high altitudes. Water from the Shafter Well 6 well has the coolest NGT_{avg} of 5.2 °C, which is consistent with water of Pleistocene age. Along with depleted stable-isotope values, the cool NGTs for nearly all wells provide strong evidence for high-altitude snowpack and in-place recharge to the mountain block. Moreover, NGT_{min} values most closely represent the true recharge temperature of these waters. NGT_{min} values range from 4.3 to 7.6 °C for samples from all sites except Pequop-2 and are 2.6 °C less than to 0.7 °C greater than the average annual air temperature of 6.9 °C for two nearby weather stations located at mountain front altitudes of 6,030 and 5,830 ft (Western Regional Climate Center, 2019).

The Pequop-2 well has the warmest NGT of all sites sampled (NGT_{avg}=11.3±1.1 °C). However, NGT_{avg} is cooler than the measured water temperature of 14.0 °C and likely indicates recharge to an area where the water table is deep enough to be warmed by the natural geothermal gradient. A deeper water table is supported by information reported on the drillers log for a monitoring well (site LCP-66) located 2 mi upgradient from Pequop-2 at an altitude of 6,700 ft, which indicates a static water level of 1,031 ft bls and a water temperature of 12.8 °C (Nevada Division of Water Resources, 2017).

Groundwater Flow System

Coupled interpretations from geochemistry and potentiometric data, and mapped hydrogeology, provide insight into contributing recharge areas and groundwater-flow paths for waters moving through and adjacent to the western Long Canyon Mine project area. Dissolved major-ion and trace-mineral concentrations and strontium isotopic compositions identify a group of waters with very similar chemistry that likely results from contact with the mineralized bedrock zone in the Long Canyon Mine project area (figs. 10–12). These sites, categorized as JSWC waters, include four sites sampled during this study (Big Spring, LCMW-15, LCMW-09S, and BSR-2) and six sites sampled by Mayo and Associates (2013) (North Spring, Central Spring, Big Spring, LCMW-07, LCMW-19, LCMW-09, and LCMW-17).

Groundwater flow from the carbonate recharge area and through the Long Canyon Mine project area (fig. 9) is supported by the high transmissivity of the mineralized zone (SRK Consulting, 2017) and the geochemistry of JSWC waters. The approximate groundwater-flow paths drawn perpendicular to potentiometric contours upgradient from each of the sample locations are shown in figure 9. The high-altitude carbonate recharge area shown in figure 9 covers a 27 mi^2 area confined to altitudes above 7,200 ft. Stable isotope compositions ($\delta^{18}O$ and $\delta^{2}H$) and noble-gas recharge temperatures indicate that high-altitude precipitation is the source of all groundwater sampled on the west side of Goshute Valley (JSWC and other west-side wells) and that recharge predominantly occurred within the mountain block rather than along the mountain front. The high-altitude carbonate recharge area consists mostly of permeable carbonate rock and fractured quartzite and is bounded on the west by the Dunderberg Shale and a thick sequence of marbleized carbonate rocks, and on the southeast by the Chainman Shale and siliciclastic Diamond Peak Formation, all presumed to be low-permeability hydrogeologic units (both included in Mississippian shale in fig. 2; Camilleri, 2010). Groundwater-flow paths connecting the carbonate-rock recharge area to a relatively focused area of discharge along the mountain front suggests that a large permeable part of the high-altitude mountain block is connected to and drained by the JSWC.

Table 9. Dissolved noble-gas concentrations and related noble-gas temperature data for groundwater sampled in Goshute Valley, Elko County, northeastern Nevada.

[**Sample ID:** See figure 9 for locations and Smith and others, 2021, appendixes 1 and 2, for additional information. ID, identification. USGS site number: U.S. Geological Survey site number. **Modeled recharge parameters:** The complete set of estimated closed-system equilibration model parameters and fit (A, F, and of $\Sigma\chi 2$) are presented only for the H_{min}-NGT_{max}. These values are similar for the remaining H-NGT pairs for each sample. **Sample group:** JSWC, Johnson Springs wetland complex. **Abbreviations:** A, dimensionless ratio of the total volume of trapped (moist) air at the pressure and temperature of the free atmosphere to the volume of water; ccSTP/g, cubic centimeters at standard temperature and pressure per gram of water; °C, degrees Celsius; F, fractionation factor for partial dissolution of trapped air bubbles; H_{avg}, average recharge altitude; H_{rmax}, maximum recharge altitude; H_{rmin}, minimum recharge altitude; mmHg, millimeters of mercury; NGT_{avg}, average noble-gas recharge temperature; NGT_{max}, maximum noble-gas recharge temperature; NGT_{min}, minimum noble-gas recharge temperature; $\Sigma\chi^2$, sum of error-weighted misfit for each of the noble gases; –, noble gas sample not collected due to visible bubbles in sample water indicating active degassing]

Sample ID	USGS site number	Water temperature (°C)	Dissolved noble-gas concentrations				Sample group
			Neon-20 (^{20}Ne) (ccSTP/g)	Argon-40 (^{40}Ar) (ccSTP/g)	Krypton-84 (^{84}Kr) (ccSTP/g)	Xenon-129 (^{129}Xe) (ccSTP/g)	
LCMW-06	410132114293201	10.1	1.87×10^{-07}	3.45×10^{-04}	8.01×10^{-08}	1.15×10^{-08}	Other west-side wells
LCT-1	410004114280401	11.0	–	–	–	–	Other west-side wells
LCMW--05S	405924114311002	13.3	–	–	–	–	Other west-side wells
Big Spring	405760114305701	20.6	1.88×10^{-07}	3.31×10^{-04}	7.60×10^{-08}	1.12×10^{-08}	JSWC
LCMW-15	405732114312801	19.8	1.83×10^{-07}	3.19×10^{-04}	7.29×10^{-08}	1.08×10^{-08}	JSWC
LCMW-09S	405707114312402	21.8	1.93×10^{-07}	3.33×10^{-04}	7.73×10^{-08}	1.16×10^{-08}	JSWC
BSR-2	405629114301401	15.5	1.87×10^{-07}	3.17×10^{-04}	7.35×10^{-08}	1.09×10^{-08}	JSWC
BSR-2, replicate	405629114301401	15.5	1.87×10^{-07}	3.21×10^{-04}	7.54×10^{-08}	1.10×10^{-08}	JSWC
LCMW-11	405723114291701	9.6	2.00×10^{-07}	3.56×10^{-04}	8.19×10^{-08}	1.22×10^{-08}	Other west-side wells
LCMW-12	405606114234901	13.9	–	–	–	–	East-side wells
Shafter Well 6	405557114214101	17.6	1.95×10^{-07}	3.68×10^{-04}	8.36×10^{-08}	1.25×10^{-08}	East-side wells
Pequop-2	405339114313001	14.0	1.96×10^{-07}	3.36×10^{-04}	7.17×10^{-08}	1.03×10^{-08}	Other west-side wells
Long Canyon Spring	405839114325901	9.8	–	–	–	–	Long Canyon Spring

Table 9. Dissolved noble-gas concentrations and related noble-gas temperature data for groundwater sampled in Goshute Valley, Elko County, northeastern Nevada.—Continued

[**Sample ID:** See figure 9 for locations and Smith and others, 2021, appendixes 1 and 2, for additional information. ID, identification. **USGS site number:** U.S. Geological Survey site number. **Modeled recharge parameters:** The complete set of estimated closed-system equilibration model parameters and fit (A, F, and of $\Sigma\chi 2$) are presented only for the H_{min}-NGT_{max}. These values are similar for the remaining H-NGT pairs for each sample. **Sample group:** JSWC, Johnson Springs wetland complex. **Abbreviations:** A, dimensionless ratio of the total volume of trapped (moist) air at the pressure and temperature of the free atmosphere to the volume of water; ccSTP/g, cubic centimeters at standard temperature and pressure per gram of water; °C, degrees Celsius; F, fractionation factor for partial dissolution of trapped air bubbles; H_{avg}, average recharge altitude; H_{rmax}, maximum recharge altitude; H_{rmin}, minimum recharge altitude; mmHg, millimeters of mercury; NGT_{avg}, average noble-gas recharge temperature; NGT_{max}, maximum noble-gas recharge temperature; NGT_{min}, minimum noble-gas recharge temperature; $\Sigma\chi^2$, sum of error-weighted misfit for each of the noble gases; –, noble gas sample not collected due to visible bubbles in sample water indicating active degassing]

Sample ID	USGS site number	Modeled recharge parameters					Sample group
		Hmin (feet)	[1]NGTmax (°C)	A[1]	F[1]	$\Sigma\chi^2$	
LCMW-06	410132114293201	5,892	8.3	0.0244	0.80	0.00	Other west-side wells
LCT-1	410004114280401	–	–	–	–	–	Other west-side wells
LCMW--05S	405924114311002	–	–	–	–	–	Other west-side wells
Big Spring	405760114305701	5,682	8.8	0.0015	0.00	0.01	JSWC
LCMW-15	405732114312801	5,837	10.0	0.0014	0.00	0.06	JSWC
LCMW-09S	405707114312402	5,784	8.3	0.0018	0.00	0.38	JSWC
BSR-2	405629114301401	5,641	10.4	0.0016	0.00	0.82	JSWC
BSR-2, replicate	405629114301401	–	–	–	–	–	JSWC
LCMW-11	405723114291701	5,626	6.7	0.0062	0.55	0.00	Other west-side wells
LCMW-12	405606114234901	–	–	–	–	–	East-side wells
Shafter Well 6	405557114214101	5,863	6.1	0.0248	0.81	0.00	East-side wells
Pequop-2	405339114313001	5,690	12.4	0.0335	0.73	0.00	Other west-side wells
Long Canyon Spring	405839114325901	–	–	–	–	–	Long Canyon Spring

Table 9. Dissolved noble-gas concentrations and related noble-gas temperature data for groundwater sampled in Goshute Valley, Elko County, northeastern Nevada.—Continued

[**Sample ID:** See figure 9 for locations and Smith and others, 2021, appendixes 1 and 2, for additional information. ID, identification. **USGS site number:** U.S. Geological Survey site number. **Modeled recharge parameters:** The complete set of estimated closed-system equilibration model parameters and fit (A, F, and of $\Sigma\chi 2$) are presented only for the H_{min}-NGT_{max}. These values are similar for the remaining H-NGT pairs for each sample. **Sample group:** JSWC, Johnson Springs wetland complex. **Abbreviations:** A, dimensionless ratio of the total volume of trapped (moist) air at the pressure and temperature of the free atmosphere to the volume of water; ccSTP/g, cubic centimeters at standard temperature and pressure per gram of water; °C, degrees Celsius; F, fractionation factor for partial dissolution of trapped air bubbles; H_{avg}, average recharge altitude; H_{rmax}, maximum recharge altitude; H_{rmin}, minimum recharge altitude; mmHg, millimeters of mercury; NGT_{avg}, average noble-gas recharge temperature; NGT_{max}, maximum noble-gas recharge temperature; NGT_{min}, minimum noble-gas recharge temperature; $\Sigma\chi^2$, sum of error-weighted misfit for each of the noble gases; –, noble gas sample not collected due to visible bubbles in sample water indicating active degassing]

Sample ID	USGS site number	Modeled recharge parameters				Sample group
		H_{avg} (feet)	[1]NGT_{avg} (°C)	H_{max} (feet)	[1]NGT^{min} (°C)	
LCMW-06	410132114293201	6,946	7.4	8,000	6.5	Other west-side wells
LCT-1	410004114280401	–	–	–	–	Other west-side wells
LCMW-05S	405924114311002	–	–	–	–	Other west-side wells
Big Spring	405760114305701	6,841	7.5	8,000	6.5	SWC
LCMW-15	405732114312801	6,919	8.7	8,000	7.5	JSWC
LCMW-09S	405707114312402	6,892	7.1	8,000	5.8	JSWC
BSR-2	405629114301401	6,821	9.0	8,000	7.6	JSWC
BSR-2, replicate	405629114301401	–	–	–	–	JSWC
LCMW-11	405723114291701	6,813	5.7	8,000	4.6	Other west-side wells
LCMW-12	405606114234901	–	–	–	–	East-side wells
Shafter Well 6	405557114214101	6,932	5.2	8,000	4.3	East-side wells
Pequop-2	405339114313001	6,845	11.3	8,000	10.3	Other west-side wells
Long Canyon Spring	405839114325901	–	–	–	–	Long Canyon Spring

[1]Value derived using the Closed-Equilibrium dissolved gas model (Aeschbach-Hertig and others, 2000; Kipfer and others, 2002).

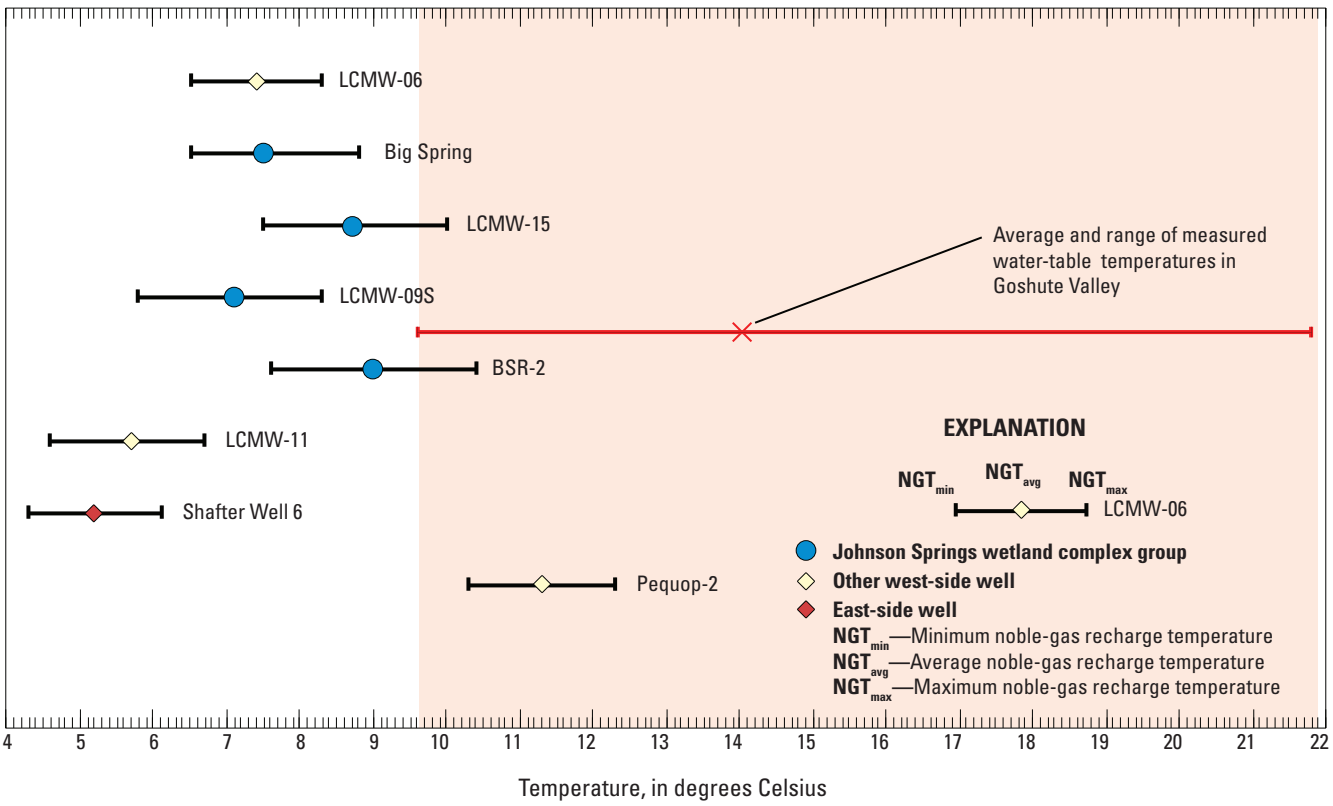

Figure 15. Noble-gas recharge temperatures for groundwater compared to measured water-table temperatures in Goshute Valley, Elko County, northeastern Nevada.

Groundwater-age data from the JSWC samples indicate mixtures of modern and premodern water with mean ages of 1,000–2,400 years BP for the wells and 500–1,400 BP years for Big Spring, indicating that groundwater traveled along similar-length subsurface flow paths (table 8). Variability in the mean ages of JSWC waters is a result of (1) the uncertainty associated with radiocarbon age-dating, and (2) the type of site sampled. Monitoring wells with low-flow pumps (LCMW-15 and LCMW-09S) sample waters from a relatively discrete depth, whereas samples from pumping wells and springs (BSR-2 and Big Spring) represent a more-integrated sample capturing water over a larger range of depth. A large spring like Big Spring typically represents a completely depth-integrated sample that captures a larger fraction of younger, shallow groundwater than other JSWC samples. Given the variability in sampled depths and lateral distance among sample sites that include JSWC waters, their mean ages and general geochemical compositions are remarkably similar.

The waters with younger ages (shorter subsurface travel times) than the JSWC group are Long Canyon Spring, LCMW-11, and LCMW-06, all of which are interpreted as having short flow paths from nearby points of recharge. Groundwater mean ages are significantly older for waters from LCT-1 and Pequop-2, ranging from 8,600 to 10,200 years. These pumping wells have similar screened intervals and are completed to greater depths than wells sampling JSWC waters, partially explaining their greater ages (Smith and others, 2021, appendix 2). However, their screen intervals overlap with those of BSR-2 and LCMW-15, and all JSWC waters are notably warmer than LCT-1 and Pequop-2 (table 5), suggesting that they represent water that has flowed to greater depths than LCT-1 and Pequop-2. Therefore, the considerably older waters from LCT-1 and Pequop-2 indicate a less active flow system north and south of the JSWC area of flow. Moreover, waters from LCT-1 and Pequop-2 are geochemically distinct from the JSWC waters, indicating that they do not flow through the mineralized zone of the Long Canyon Mine project area. The flow path associated with the sample from the Pequop-2 indicates that, although geochemically distinct, this water originates from the same high-altitude recharge zone as the JSWC waters. The natural (non-stressed) groundwater divide between the JSWC waters and Pequop Mountain recharge to the south likely lies between BSR-2 and Pequop-2 and might be influenced by the exposed Mississippian shale to the west (fig. 2).

Groundwater on the east side of Goshute Valley is the oldest of all water sampled during this study, with Pleistocene radiocarbon ages of 11,600–22,400 years BP for LCMW-12 and Shafter Well 6 (table 8; fig. 2). The Pleistocene ages of these waters are confirmed by $\delta^{18}O$ and $\delta^{2}H$ values, showing that they are isotopically lighter than any modern (or Holocene) recharge (fig. 14). Although Shafter Well 6 is

a deep production well (screened from 510 to 945 ft) that clearly captures deep water expected to be old, LCMW-12 is a relatively shallow monitoring well screened across the water table from 160 to 200 ft. The presence of Pleistocene water at all depths in the basin-fill aquifer in this part of the valley is indicative of a much-less active groundwater flow system than what is observed on the west side of Goshute Valley. Substantial eastern groundwater flow from Goshute Valley through the Toano Range is unlikely given Pleistocene ages and the northeast–southwest direction of groundwater flow. Under predevelopment conditions, all flow from the recharge area feeding the JSWC group of waters probably moved through the highly permeable mineralized zone of the Long Canyon Mine project area and discharged directly to the JSWC between North Spring and Big Spring, with lesser amounts discharging as ET in the associated wetlands. However, JSWC waters are observed as far as 0.7 mi north of North Spring in well LCMW-07 and as far as 1.4 mi south of Big Spring in wells LCMW-15, LCMW-09S, and BSR-2. The presence of JSWC waters may be the result of pumping—either for historical irrigation or associated with aquifer testing beginning in 2011 and continuing through 2016— that has drawn groundwater away from the focused area of steady-state discharge through connected permeable valley alluvium. If this is the case, extensive pumping from within the Long Canyon Mine project area could induce groundwater flow from an unknown distance to the north and south, regardless of distinct geochemical signals that seem to delineate the boundaries of a hydraulically connected JSWC flow system.

Aquifer Testing

Hydraulic properties of carbonate rocks and basin fill in the study area were determined from single- and multiple-well aquifer testing. Water-level drawdown observations at the pumped well during single- and multiple-well aquifer testing defined hydraulic-property estimates of hydrogeologic units near the well. Water-level change observations (such as drawdown and rise, and spring capture observations resulting from the 2016 multiple-well aquifer test in carbonate rocks) defined the hydraulic properties of hydrogeologic units and structures between pumping wells and monitoring sites and provided direct evidence of hydraulic connections between sites and across hydrogeologic units.

Single-Well Aquifer Tests

Single-well aquifer tests provide relatively certain estimates of hydraulic properties, such as transmissivity, around pumping wells because flow rates through pumped wells are known. Transmissivity describes the rate of groundwater movement through a section of aquifer and is expressed as the product of hydraulic conductivity and saturated aquifer thickness (Lohman, 1972). Multiple-well aquifer tests provide transmissivity estimates between pumping and monitoring sites, but certainty in the property distribution across hydrogeologic units is limited by heterogeneities between pumping and monitoring sites and elsewhere within the cone of depression.

In data-limited areas beyond the extent of aquifer testing, specific-capacity data and slug tests provide useful, albeit spatially limited, hydraulic information. Specific-capacity estimates from pump tests during well drilling and development provide insight into the productivity of hydrogeologic units around pumping wells, despite uncertain drawdown interpretations. Slug tests provide estimates of hydraulic conductivity in the immediate vicinity of the well screen that can be translated to transmissivity by assuming a representative saturated aquifer thickness. Hydraulic property estimates from specific-capacity data and slug tests typically are less certain than single-well aquifer tests because they represent only a small volume of aquifer material near the tested well.

Single-well aquifer tests were interpreted at seven pumping wells in the area of interest by the USGS and Newmont Mining Corporation: BSR-2, LCT-1, Pequop-1, Pequop-2, LCW-5, LCW-6, and LCPW-1 (table 10). Pumping and drawdown data were analyzed with the Cooper and Jacob (1946) method, which requires that drawdown shows a definitive linear slope when graphed on a semi-log plot over time. Transmissivity is inversely proportional to the slope of the line. The Cooper and Jacob (1946) method was evaluated during constant-rate pumping periods and occasionally during recovery periods (table 10).

Specific-capacity and slug-test interpretations near the Long Canyon Mine project area provide additional hydraulic property estimates. Specific-capacity estimates were determined as the ratio of discharge and drawdown reported on 19 driller's logs and translated to transmissivity using an empirical relation equal to 380 times specific capacity ([gal/min]/ft) (Frus and Halford, 2018). Twenty-two slug tests were analyzed (Smith and others, 2021) and included as transmissivity observations to add hydraulic control where limited data are available in the integrated analysis (see section, "Integrated Estimation of Recharge and Hydraulic-Property Distributions with Numerical Models"). Slug tests were analyzed using multiple approaches depending on the dataset (Bouwer and Rice, 1976; Barker and Black, 1983; Springer and Gelhar, 1991; Hyder and others, 1994; Butler, 1998; McElwee and Zenner, 1998; Butler and Garnett, 2000). Transmissivity estimates from specific-capacity data and slug tests are provided in table 10.

Table 10. Transmissivity estimates from single-well aquifer tests, slug tests, and specific-capacity data, Long Canyon, Goshute Valley, northeastern Nevada.

[**Test well:** Listed in alphabetical order following test type. **Geologic unit:** Geologic units in contact with open casing or open annulus. Qa sediments (basin fill) are distinguished as alluvial fan and valley fill (near the valley center). **Method:** Method used to compute transmissivity. Equation used for specific-capacity data from Frus and Halford (2018). **Abbreviations:** Qal, alluvium undivided; Tv, Tertiary volcanics; Op, Ordovician Pogonip Group; OCnp, Ordovician and Cambrian Notch Peak Formation; Cd, Cambrian Dunderberg Shale; SC, specific capacity; ST-PRH, slug test - pneumatic rising head; ST-FHS, slug test - falling head slug; ST-RHS, slug test - rising head slug; SWAT, single-well aquifer test; ft^2/d, feet squared per day; <, less than; >, greater than]

Test well	Geologic unit	T (ft^2/d)	Test type	Method
BSR-2	Qal - alluvial fan	40,000	SWAT	Cooper and Jacob (1946), recovery
LCPW-1	OCnp - carbonate	400,000	SWAT	Cooper and Jacob (1946), recovery
LCT-1	Qal - valley fill	2,000	SWAT	Cooper and Jacob (1946), recovery
LCW-5	Qal - alluvial fan	3,400	SWAT	Cooper and Jacob (1946), pumping
LCW-6	Op - carbonate	7,000	SWAT	Cooper and Jacob (1946), pumping
Pequop 1	Qal - alluvial fan	80,000	SWAT	Cooper and Jacob (1946), pumping
Pequop 2	Qal - alluvial fan	10,000	SWAT	Cooper and Jacob (1946), pumping
LCMW-01	Qal - valley fill	429.5	ST-PRH	Hyder and others (1994)
LCMW-02D	Op - carbonate	6,228.8	ST-PRH	McElwee and Zenner (1998)
LCMW-02S	Qal - alluvial fan	648.8	ST-PRH	Hyder and others (1994)
LCMW-04	OCnp - carbonate	296.5	ST-PRH	Hyder and others (1994)
LCMW-05D	OCnp - carbonate	116.4	ST-PRH	Hyder and others (1994)
LCMW-05S	Op - carbonate	9.1	ST-PRH	Hyder and others (1994)
LCMW-06	Qal - alluvial fan	258.5	ST-FHS	Bouwer and Rice (1976)
LCMW-07	Qal - alluvial fan	58.7	ST-FHS	Bouwer and Rice (1976)
LCMW-08	Qal - valley fill	2,446.5	ST-FHS	Bouwer and Rice (1976)
LCMW-09D	OCnp - carbonate	84.6	ST-PRH	Barker and Black (1983)
LCMW-09S	Qal - alluvial fan	123.4	ST-PRH	Barker and Black (1983)
LCMW-10	Qal - alluvial fan	185.0	ST-FHS	Bouwer and Rice (1976)
LCMW-11	Qal - valley fill	2,616.0	ST-RHS	Bouwer and Rice (1976)
LCMW-12	Qal - valley fill	0.6	ST-FHS	Bouwer and Rice (1976)
LCMW-13	Qal - alluvial fan	16.4	ST-FHS	Bouwer and Rice (1976)
LCMW-14	Qal - alluvial fan	181.9	ST-FHS	Bouwer and Rice (1976)
LCMW-15	Op - carbonate	5,592.9	ST-FHS	Springer and Gelhar (1991)
LCMW-17	OCnp - carbonate	2,341.4	ST-PRH	McElwee and Zenner (1998)
LCMW-21D	OCnp - carbonate	1,978.6	ST-PRH	McElwee and Zenner (1998)
LCMW-21S	Op - carbonate	459.0	ST-FHS/RHS	Bouwer and Rice (1976)
LCMW-23D	Op, OCnp - carbonate	682.0	ST-PRH	Butler (1998)
LCMW-23S	Qal - alluvial fan	21.3	ST-FHS	Bouwer and Rice (1976)
N000680	Qal	<190	SC	SC × 380
N000703	Qal	1,500	SC	SC × 380
N000977	Qal	340	SC	SC × 380
N001429	Qal	570	SC	SC × 380
N004446	Qal	76	SC	SC × 380
N009553	Qal	13	SC	SC × 380
N009744	Unknown - igneous	11	SC	SC × 380
N009819	Unknown - carbonate	190	SC	SC × 380
N013294	Tv	84	SC	SC × 380
N014752	Quartzite	6,700	SC	SC × 380

Table 10. Transmissivity estimates from single-well aquifer tests, slug tests, and specific-capacity data, Long Canyon, Goshute Valley, northeastern Nevada.—Continued

[**Test well:** Listed in alphabetical order following test type. **Geologic unit:** Geologic units in contact with open casing or open annulus. Qa sediments (basin fill) are distinguished as alluvial fan and valley fill (near the valley center). **Method:** Method used to compute transmissivity. Equation used for specific-capacity data from Frus and Halford (2018). **Abbreviations:** Qal, alluvium undivided; Tv, Tertiary volcanics; Op, Ordovician Pogonip Group; OCnp, Ordovician and Cambrian Notch Peak Formation; Cd, Cambrian Dunderberg Shale; SC, specific capacity; ST-PRH, slug test - pneumatic rising head; ST-FHS, slug test - falling head slug; ST-RHS, slug test - rising head slug; SWAT, single-well aquifer test; ft²/d, feet squared per day; <, less than; >, greater than]

Test well	Geologic unit	T (ft²/d)	Test type	Method
N026962	Unknown - carbonate	1,300	SC	SC × 380
N026972	Qal	4,100	SC	SC × 380
N049605	Cd - shale	510	SC	SC × 380
N069683	Qal	2,000	SC	SC × 380
N074220	Qal	3	SC	SC × 380
N109309	Unknown - carbonate	4,100	SC	SC × 380
N122892	Qal	560	SC	SC × 380
N123191	Qal	690	SC	SC × 380
N126309	Unknown - carbonate	>380	SC	SC × 380

Transmissivity estimates from single-well aquifer tests ranged from 2,000 to 400,000 ft²/d. The two transmissivity estimates in carbonate rocks differed by two orders of magnitude, from 7,000 ft²/d in LCW-6 to 400,000 ft²/d in LCPW-1 (table 10). Pumping well LCPW-1 is fully completed in the Ordivician and Cambrian Notch Peak Formation, with perforations in dolomite limestone. The lower 230 ft of the 1,244-ft-thick perforated casing in LCW-6 penetrates the Notch Peak Formation, whereas the upper 1,000 ft penetrates the overlying Ordovician Pogonip Group.

Basin-fill transmissivity estimates are highest (equal to or greater than 10,000 ft²/d) along the alluvial fan south of the JSWC (BSR-2, Pequop-1, and Pequop-2) and decrease by an order of magnitude to the north and northeast of the JSWC (LCW-5 and LCT-1, respectively; table 10, fig. 2). Pumping wells BSR-2 and Pequop-1 penetrate alluvial-fan material with transmissivities of 40,000 and 80,000 ft²/d, respectively. A transmissivity of 10,000 ft²/d was estimated in alluvial-fan well Pequop-2, located less than 1 mi south of Pequop-1. North and northeast of the JSWC, transmissivity ranged from 2,000 to 3,400 ft²/d in valley-fill and alluvial-fan material, respectively.

Transmissivity estimates exceeding 10,000 ft²/d in basin fill occur infrequently (Halford, 2016) and could highlight the influence of more transmissive carbonate rocks underlying wells BSR-2 and Pequop-1 near the Long Canyon Mine project area (fig. 2). Basin fill south of the JSWC likely is underlain by the Notch Peak Formation, as indicated in figure 3. If high-transmissivity estimates in LCPW-1 (400,000 ft²/d) are representative of carbonate rocks over a large spatial area, a stress-induced hydraulic connection between alluvial-fan material and underlying carbonate rocks would support the higher-than-average transmissivity estimates in wells BSR-2 and Pequop-1. A hydraulic connection between alluvial-fan material in BSR-2 and underlying carbonate rocks also is supported by nearly identical water chemistry in BSR-2 and carbonate-rock well LCPW-1.

Multiple-Well Aquifer Test

Multiple-well aquifer tests greatly increase the volume of rock characterized when compared with single-well tests alone. The multiple-well aquifer-test evaluated in this study includes simultaneous pumping in carbonate-rock wells LCW-6 and LCPW-1 during summer 2016 and observations in carbonate-rock and basin-fill sites across the study area. Additional stresses to the adjacent (or overlying) basin-fill aquifer during the 2016 test were generated by discharge of pumped water into a leaky irrigation ditch and water supplementation to Big Spring to maintain fish habitat.

Drawdowns between 91 pumping-well and monitoring-site pairs resulting from the 2016 carbonate-rock aquifer test were estimated using water-level models. Drawdowns between pumping wells and monitoring sites extended across a horizontal area of just over 3 mi². Water-level rise from ditch discharge and supplementation loss (or seepage loss of additional supplemented water to Big Spring and irrigation ditches) was estimated from 33 monitoring sites in 20 boreholes. Data collected during the 2016 carbonate-rock aquifer test were measured continuously and include withdrawal rates from pumping wells; water levels at pumping wells, monitoring wells, and VWPs; and spring stage and discharge (Smith and others, 2021, appendix 3). Background wells and piezometers were selected from monitoring sites that were assumed to be unaffected by well development and aquifer testing in Long Canyon and water-supply pumping throughout Goshute Valley. Background wells and VWPs monitor backgroundwater-level changes resulting from environmental

fluctuations only, and were distinguished from other monitoring wells and piezometers based on drawdown observations during aquifer testing.

Seepage Losses and Pumping-Induced Stresses

Pumping responses in basin-fill wells, piezometers, and possibly springs were obscured during the 2016 aquifer test by seepage losses of aquifer-test water discharged into a leaky irrigation ditch and additional water supplemented to Big Spring, and pumping from nearby water-supply wells. Aquifer-test water was discharged into an irrigation ditch located about 1.5 mi south of pumping well LCPW-1, and within 0.5 mi of the JSWC (fig. 16). A part of the discharge percolated downward into the subsurface along the ditch flow path, whereas the remainder ultimately merged with Hardy Creek more than 1 mi downstream (fig. 2). Seepage estimates made by Newmont Mining Corporation and SRK Consulting (Paul Pettit and Amy Prestia, respectively, written commun., August 24, 2016) indicate that approximately 40 percent of water discharged into the irrigation ditch infiltrated into the subsurface within the first half-mile. Downward percolation of this discharge recharged the shallow basin-fill aquifer and might have attenuated maximum declines in spring stage and pumping-induced drawdowns in shallow basin-fill wells and piezometers.

Big Spring was supplemented with water during and after the 2016 aquifer test to support wetland habitat and mitigate discharge reductions observed during previous aquifer testing in well LCPW-1 (Barnett Intermountain Water Consulting and others, 2011). Supplementation water was supplied at a semi-continuous rate of about 400 gal/min from August 4 to October 18, 2016.

Supplementation water was provided primarily by valley-fill well LCT-1 and alluvial-fan well LCW-5, and periodically supplemented by aquifer-test discharge water. About one-half of the supplementation water flowed through an irrigation ditch to the north from Big Spring pool through W-03. The remaining one-half of the supplementation water flowed into either an unlined irrigation ditch just south of Big Spring or into a holding pond just east of Big Spring, where it ultimately evaporated and percolated downward into the subsurface (Newmont Mining Corporation, written commun., 2017). Downward percolation of residual spring supplementation water also likely recharged the shallow basin-fill aquifer, further confounding pumping-signal detection in shallow basin-fill wells, piezometers, and possibly springs.

Additional stresses on the aquifer systems that might have interfered with the 2016 carbonate-rock aquifer test include numerous instances of pumping from nearby basin-fill water-supply wells. Long Canyon Mine supply wells LCT-1 and LCW-5, located about 2 and 1.2 mi northeast of aquifer-test well LCW-6, respectively (fig. 2), were pumped at average semi-continuous rates of about 500 and 200 gal/min, respectively, during the test. Well BSR-1, located about 1.3 mi southeast of aquifer-test well LCPW-1, was pumped intermittently during the test for drill water supply at an average rate of about 300 gal/min. Municipal water-supply wells for the cities of Wendover, Utah, and West Wendover, Nevada, pumped water from wells Pequop-1 and Pequop-2, located more than 5 mi south of LCPW-1, and from Shafter wells 1–6, located 8–11 miles east of the aquifer-test wells along the eastern edge of Goshute Valley (fig. 2). Municipal wells Pequop-1 and Pequop-2 pumped discontinuously at a combined rate of about 500 gal/min (computed as the average of September 2016 pumping rates), whereas Shafter wells pumped at a combined average rate of about 1,350 gal/min (Newmont Mining Corporation, written commun., 2017).

Water-Level Models and Drawdown Estimation

Drawdown and water-level rise from multiple-well aquifer testing were differentiated from environmental fluctuations using analytical water-level models (Halford and others, 2012; Garcia and others, 2013). Environmental fluctuations caused by barometric pressure and other natural forces on the aquifer system can obscure aquifer responses to anthropogenic stresses such as pumping and artificial recharge. Natural recharge can cause long-term rises and declines in water levels that are superimposed on short-term fluctuations from pumping and artificial recharge (Fenelon, 2000; Elliot and Fenelon, 2010). Water-level modeling provides a mechanism for distinguishing environmental fluctuations from anthropogenic stresses in hydrogeologic systems and improving aquifer-test interpretations (Halford and others, 2012; Garcia and others, 2013).

Water-level models analytically simulate all anthropogenic and environmental stresses simultaneously during the period of aquifer-test data collection, which allows for isolation of pumping stresses. The analysis period comprised antecedent non-pumping, pumping, and recovery periods. Theis (1935) modeled approximated anthropogenic signals such as pumping by transforming time-varying pumping schedules from pumping and water-supply wells into water-level drawdown responses.

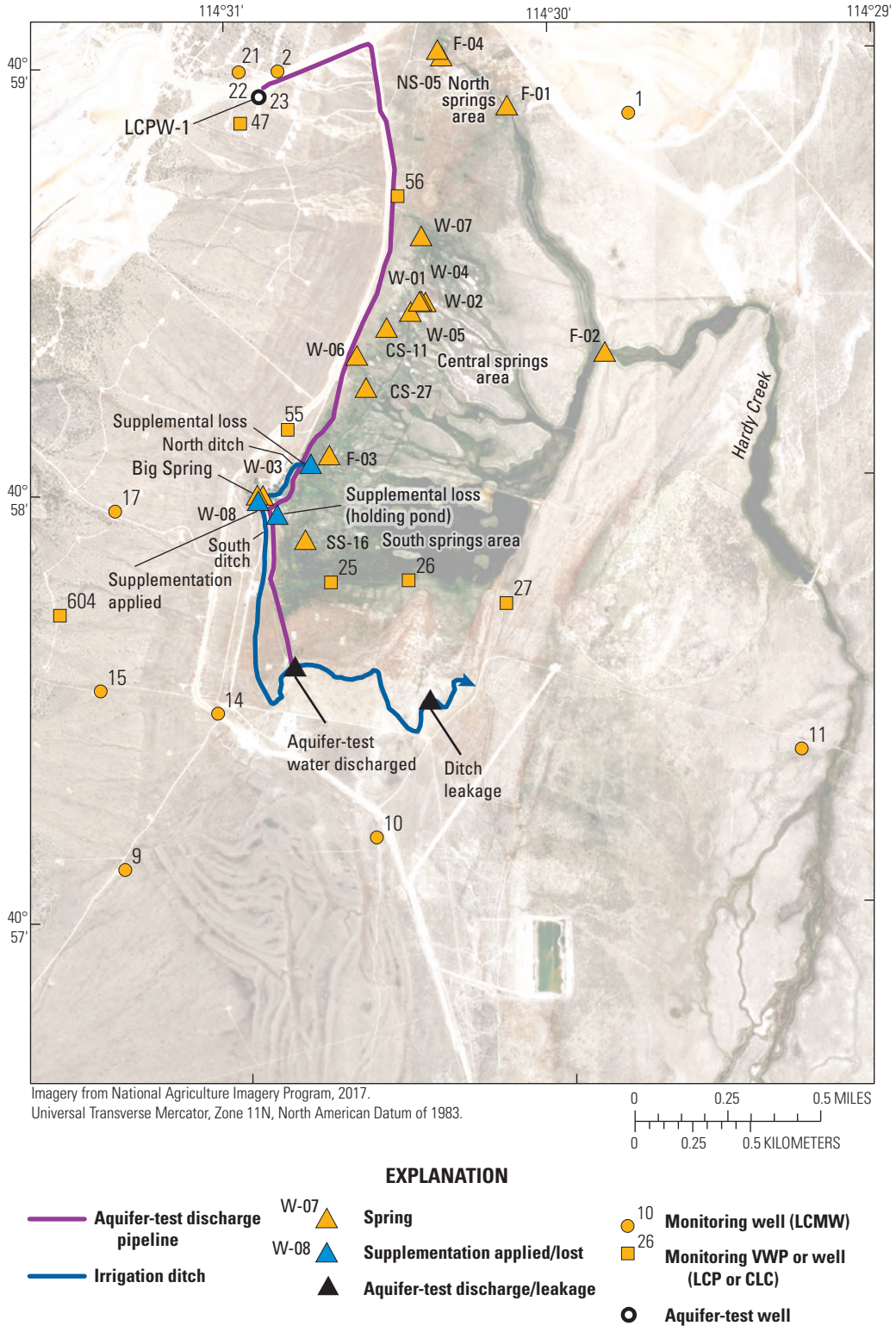

Figure 16. Locations of aquifer-test discharge pipeline, irrigation ditch, spring supplementation supply and loss, and selected monitoring sites, Long Canyon, Goshute Valley, northeastern Nevada. VWP, vibrating-wire piezometer. Well and VWP name prefixes are shown in parentheses.

Environmental water-level fluctuations were simulated with time series of barometric pressure and water levels from background VWPs LCP-29A–D and LCP-30A–D, and from background wells LCP-16A and LCMW-12 (fig. 2). Linear trends were used to model pre-pumping water levels where backgroundwater levels were insufficient. The background sites are assumed to be close enough to monitoring sites to be affected by similar environmental fluctuations, yet distant enough to be unaffected by pumping from wells LCW-6 and LCPW-1 and infiltration from ditch discharge and supplementation loss. Background sites LCP-29A–D, LCP-30A–D, and LCMW-12 were assumed to be unaffected by water-supply pumping on the eastern side of Goshute Valley (fig. 2). Well LCP-16A, which is screened in glacial till at nearly 2,000 ft above the screened interval of pumping wells (Smith and others, 2021, appendix 2), had a large recharge signal and was assumed to be unaffected by carbonate-rock pumping. Therefore, LCP-16A was used as a background VWP when analyzing drawdown and rise at monitoring sites with recharge signals. Water levels from background sites were critical because they were affected by barometric signals and seasonal and long-term climate trends. These effects also are assumed to be present in the monitoring sites. Water-supply pumping signals from wells LCT-1 and LCW-5, and irrigation well BSR-1 (fig. 2), were not simulated because water-supply pumping records were intermittent and pumping signals likely were correlated with aquifer-test pumping signals.

Theis models were generated from simplified pumping schedules to eliminate small pumping-rate fluctuations that minimally affect distant drawdowns. Simplified pumping schedules were considered acceptable for monitoring points because the aquifer responses to high-frequency changes in pumping (discharge) are attenuated by the aquifers (Garcia and others, 2013).

Rising water levels from ditch discharge and spring supplementation loss also were simulated using Theis models. Discharge and supplementation loss were simulated as localized recharge signals using discharge and loss records derived from pumping schedules, supplementation logs, seepage measurements (Newmont Mining Corporation, written commun., 2017), and continuous discharge measurements at monitoring sites W-03 and W-08 (fig. 16).

Analytically simulated water levels, which are the sum of all simulated stresses in the water-level model, were fit to measured water levels by minimizing the root-mean-square (RMS) error of differences between the analytically simulated and measured time series (Halford and others, 2012). Amplitude and phase of the hydrograph were adjusted in each time series that simulated environmental water-level fluctuations. Transmissivity and storage coefficient were adjusted to provide the best fit of simulated and measured water levels in the Theis models. However, estimated values of transmissivity and storage coefficient from the Theis model generally were not valid estimates of aquifer properties because the assumptions of the underlying Theis solution were violated. Drawdown (or rise) estimates are the summation of Theis models minus differences between simulated and measured water levels (residuals). Residuals represent all unexplained water-level fluctuations, during pumping and non-pumping periods.

Drawdown and rise detection were classified as not detected, detected, or ambiguous based on the signal-to-noise ratio (Garcia and others, 2013) and other factors (see Smith and others, 2021, appendix 3, for details). Signal and noise are defined herein as the maximum drawdown (or rise) occurring in a well during an aquifer test and the RMS error, respectively. At monitoring sites where pumping and "localized recharge" responses were observed, the larger response was used to compute the signal-to-noise ratio. Drawdown was classified as not detected where the signal-to-noise ratio was less than 5, indicating that drawdown could not be reliably differentiated from the noise. Drawdown or rise was classified as detected where the signal-to-noise ratio was greater than or equal to 10 and drawdown or rise was above a detection threshold of 0.05 ft. Drawdown or rise was classified as ambiguous when the signal-to-noise ratio ranged from 5 to less than 10. A signal-to-noise ratio greater than or equal to 10 was classified as ambiguous if drawdown or rise could be approximated as a linear trend, recovery was not observed, drawdown or rise was below the detection threshold, or because of likely correlation between pumping and "localized recharge" signals. Correlation between pumping and localized recharge signals is apparent in most models where both signals are observed because small and large pumping signals often are negated by equal localized recharge signals.

Simplified Pumping, Leakage, and Supplementation Loss Schedules

Water-level changes resulting from pumping wells LCW-6 and LCPW-1 were approximated using simplified pumping schedules. Schedules were simplified to 240 and 12 steps for pumping from wells LCW-6 and LCPW-1, respectively (fig. 17). The simplified schedules were sufficient to adequately simulate pumping responses in monitoring sites near and distant from pumping wells with Theis models.

Ditch leakage and spring supplementation loss rates were estimated using pumping schedules for wells LCW-6 and LCPW-1 (fig. 17), spring supplementation logs (fig. 18), and measured discharges at weirs W-03 and W-08 (fig. 19). Spring supplementation is water used to supplement big spring during aquifer testing. Discharge from aquifer testing was occasionally diverted and used to supplement Big Spring pool. These diversions totaled about 8.5 million gal. Ditch leakage was estimated as 40 percent of aquifer-test discharge and spring supplementation loss was estimated as 50 percent of spring supplementation. Ditch leakage and supplementation loss were each approximated with a single "localized recharge" point for the purpose of analytical modeling. The ditch leakage point was located at the mid-point of the one-half-mile ditch course where most leakage occurred (fig. 16). A single ditch leakage "recharge" point was adequate because the nearest monitoring site was located at least 0.25 mi from the leaky ditch course. Estimated ditch leakage totaled about 50 million gal (fig. 18).

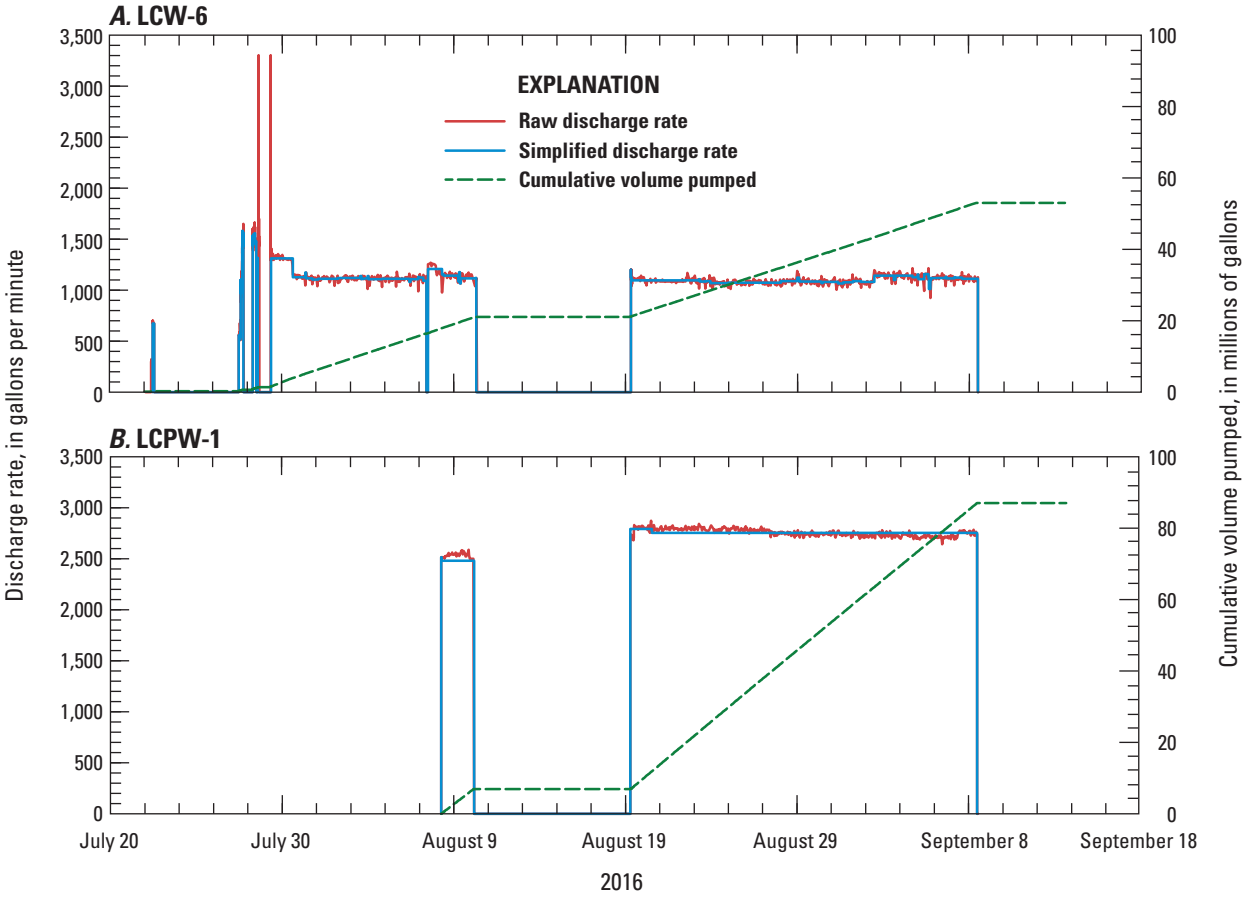

Figure 17. Raw and simplified pumping rates during aquifer testing in wells (*A*) LCW-6 and (*B*) LCPW-1, Long Canyon Mine project area, northeastern Nevada, July–September 2016. Data were binned into 240 (well LCW-6) and 12 (well LCPW-1) pumping steps for use in Theis models.

Infiltration of supplementation water was estimated using a combination of discharge rates measured at W-03 and W-08, and the general spring supplementation log (figs. 18 and 19). Big Spring pool was supplemented downgradient from W-08 and upgradient from W-03. Some supplementation water flowed northward through W-03, whereas the remainder either flowed into the irrigation ditch south of Big Spring or into the holding pond to the east. Flow through W-03 is derived from Big Spring and supplementation water from August 4 to October 18, 2016. Prior to supplementation and aquifer testing, the ratio of W-03 discharge to Big Spring (W-08) discharge averaged 1-to-2. Therefore, supplementation discharge flowing through W-03 was estimated by subtracting one-half of W-08 discharge from W-03 discharge. Once W-08 went dry, all W-03 flow was attributed to supplementation (fig. 19). Estimated supplementation discharge through W-03 was, on average, about one-half of the total water supplemented to Big Spring, indicating that about one-half of the total water applied could have infiltrated through the ditch to the south or through the holding pond to the east. Therefore, the entire supplemental discharge rate measured at W-03 was used to estimate the loss rate to the subsurface from all supplemental discharge in water-level models. The supplementation loss point was located immediately east of Big Spring pond (fig. 16). Estimated supplementation loss totaled about 18 million gal (fig. 18).

Drawdown Observations

Simulated water levels represent the sum of applicable time series including barometric pressure, backgroundwater levels, long-term linear trends, pumping responses, and localized recharge responses from ditch leakage and supplementation losses. Barometric pressure was measured at the Pequop weather station (fig. 1; Smith and others, 2021, appendix 1), located about 1 mi south of LCPW-1. Pumping and localized recharge responses were simulated with Theis models that used simplified pumping schedules of LCW-6 and LCPW-1 (fig. 17) and estimated "localized recharge" schedules for ditch leakage and supplementation loss (fig. 18).

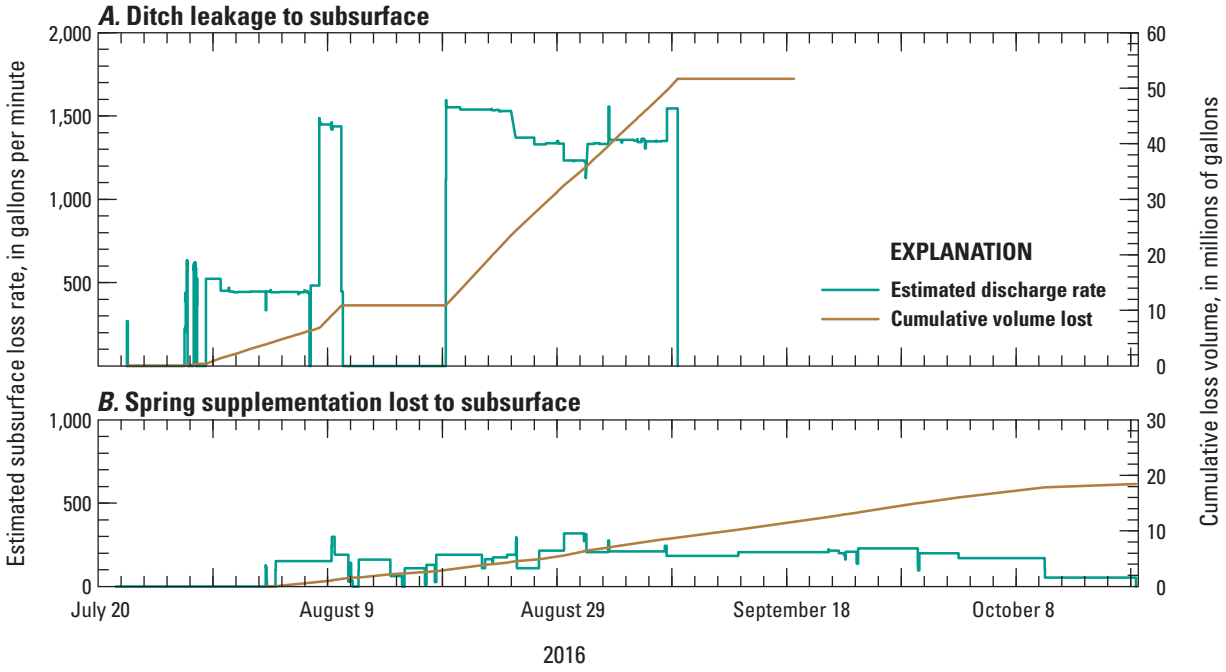

Figure 18. Estimated subsurface loss rates of pumped water discharged into an irrigation ditch (*A*), and supplementation water applied to Big Spring during the carbonate-rock aquifer test (*B*), Long Canyon Mine project area, northeastern Nevada, July–October 2016. Ditch leakage was estimated at about 40 percent of the total water discharged; spring supplementation loss estimated was at about 50 percent of the supplementation water applied.

The combined effect of pumping or "localized recharge" into multiple subsurface zones can be estimated with a certainty proportional to the RMS error where only drawdown or water-level rise was estimated. Differentiating between the drawdown response of pumping wells LCW-6 and LCPW-1 was not attempted. An attempt was made to differentiate drawdown from pumping and water-level rise from discharge leakage and supplementation losses, but the magnitude of estimates is highly uncertain because the two signals are inversely correlated.

Simulated water levels and spring stage matched measured values with RMS errors of 0.02–0.46 ft for monitoring wells, 0.02–0.43 ft for VWPs, and 0.003–0.02 ft for springs located more than 500 ft from pumping wells (Smith and others, 2021, appendix 3). Drawdown was detected at 42 monitoring sites as far as 3 mi from the nearest pumping well (fig. 20). Excluding pumping wells and LCMW-22D, maximum detected drawdown estimates ranged from 1.0 to 5.5 ft in monitoring wells and 1.2 to 4.8 ft in VWPs, and stage declines of 0.05 to 0.4 ft at springs (Smith and others, 2021, appendix 3). Maximum drawdowns of 275 and 16 ft were observed in pumping wells LCW-6 and LCPW-1, respectively (table 10). In monitoring well LCMW-22D, located less than 300 ft from LCPW-1, maximum detected drawdown was 23 ft. Substantial drawdown at LCMW-22D, with respect to adjacent monitoring wells (LCMW-22S, LCMW-23D, and LCMW-23S), indicates that a permeable conduit connects this well and pumping well LCPW-1 (fig. 20; Smith and others, 2021, appendix 3) (Newmont Mining Corporation, written commun., 2017). Drawdown was classified as ambiguous for 20 monitoring sites owing to unmeasured environmental fluctuations, low signal-to-noise ratios, and a lack of simulated drawdown recovery (see Smith and others, 2021, appendix 3, for details). Drawdown was classified as not detected for 34 monitoring sites (fig. 20; Smith and others, 2021, appendix 3).

Drawdown or spring capture was detected definitively at all carbonate-rock monitoring sites east of the Canyon fault and north of the Long Canyon Mine project area boundary, at all but two basin fill monitoring sites (LCP-55B and LCP-49A) completed in alluvial-fan material, at the single monitoring site completed in Ordovician and Cambrian Dunderberg Shale (CLC-604A), and at five springs (figs. 20 and 21). Negligible drawdown detection at carbonate-rock monitoring site LCP-52, located just west of the Canyon fault and within 2 mi of LCPW-1, indicates that the fault either impedes or diverts flow, or that the carbonate rocks surrounding the monitoring site have lower permeability than carbonate rocks east of the Canyon fault. Carbonate-rock monitoring sites with drawdown detections (and located east of the Canyon fault) are completed in either the deepest two formations in the Pogonip Group or the underlying Notch Peak Formation, whereas monitoring sites LCP-52A and LCP-52B are completed in the shallower Pogonip Group (Smith and others, 2021, appendix 2; Newmont Mining Corporation, written commun., 2016). In addition to formation differences, the water level at the LCP-52 monitoring site rose more than 10 ft

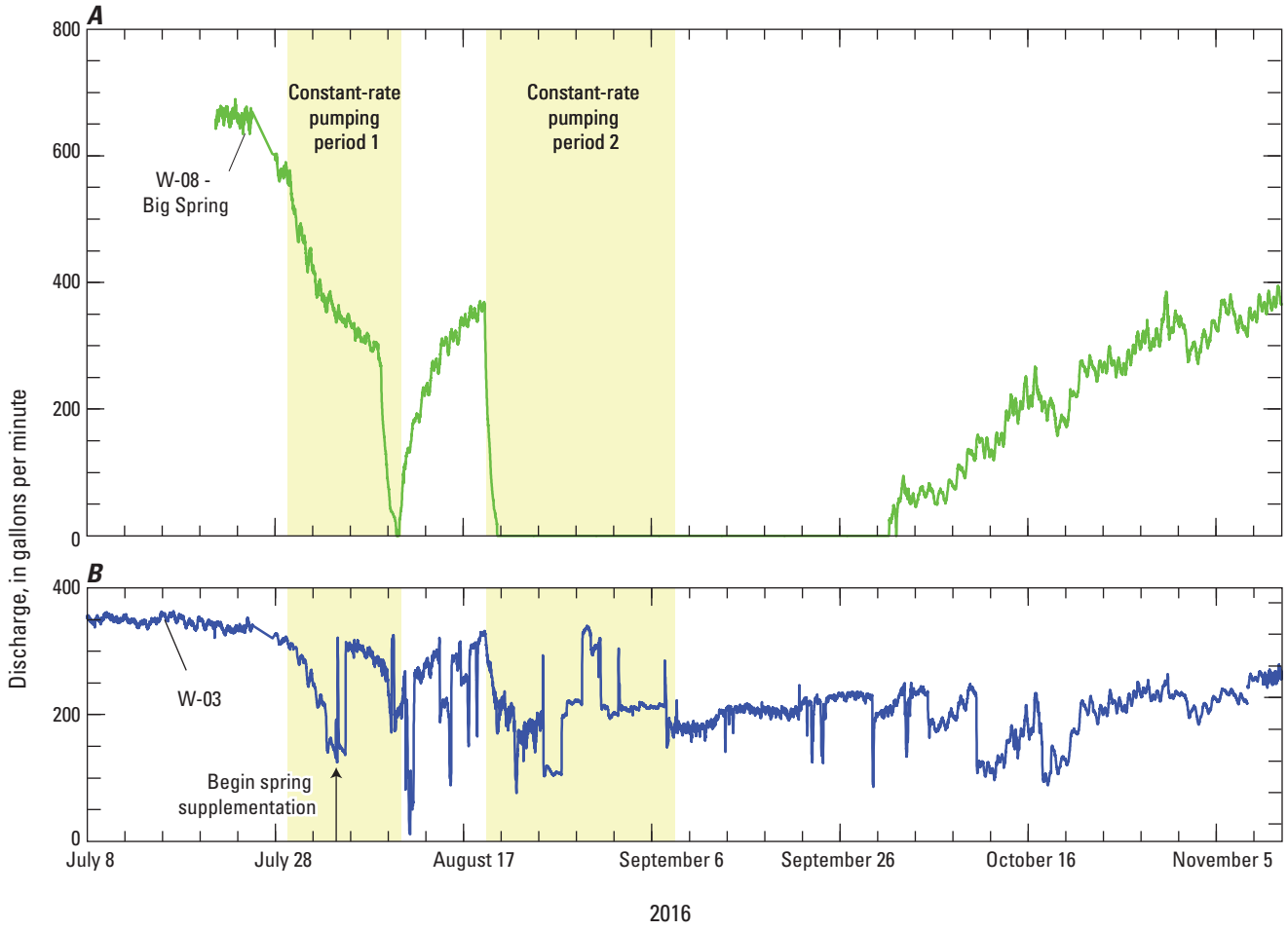

Figure 19. Measured spring discharge rates at weirs (*A*) W-08 (Big Spring) and (*B*) W-03 during the 2016 carbonate-rock aquifer test, Long Canyon Mine project area, northeastern Nevada, July–September 2016. Discharge measured in weir W-03 represents a fraction of the water discharged from Big Spring prior to August 4, 2016, and water from Big Spring and spring supplementation thereafter.

during May–July 2016 in response to winter 2015–16 precipitation or snowmelt (similar to LCP-36B in fig. 8), whereas monitoring sites completed in the deep Pogonip Group and Notch Peak Formation rose a few feet at most during the same period (see LCMW-02D in fig. 8). A steep response to winter precipitation or snowmelt might be indicative of lower permeability rocks open to the LCP-52 monitoring well or compartmentalization of hydrogeologic units (see section, "Groundwater Levels").

Drawdown at monitoring sites completed in valley fill was classified as ambiguous or not detected (fig. 20; Smith and others, 2021, appendixes 2 and 3). Drawdown detection in valley-fill wells along the western valley floor most likely was obscured by rising water levels from ditch leakage, which offset drawdown from pumping wells LCW-6 and LCPW-1. Additional drawdown-limiting factors for wells and piezometers completed in valley fill include contrasting permeabilities between coarse-grained basin-fill deposits along the alluvial fan and fine-grained deposits on the valley floor and (or) a vertical low-permeability barrier such as the Hardy fault, which intervenes between alluvial-fan and valley-fill deposits (figs. 2 and 20).

Declines in spring stage were detected at Big Spring (W-08), at W-03 downgradient from Big Spring, at the northernmost spring in the JSWC (NS-5), and at flumes F-01 and F-04, located downgradient from spring NS-05 (fig. 21). Maximum stage decline at these springs ranged from 0.05 to 0.4 ft. A stage decline of 0.4 ft at Big Spring (W-08) corresponded with 100 percent capture of the initial discharge, 680 gal/min (SRK Consulting, 2017). Stage decline at NS-5 represented a more than 10 percent capture of discharge from multiple northern springs (SRK Consulting, 2017). Stage decline was ambiguous at south spring SS-16 and at W-07 and was not detected at other continuously monitored spring sites located between Big Spring and the northernmost spring sites. Based on mean discharge rates during the days prior to aquifer testing, total capture of spring discharge was about 700 gal/min out of about 1,100 gal/min, (see section, "Groundwater Discharge"), or just more than 60 percent.

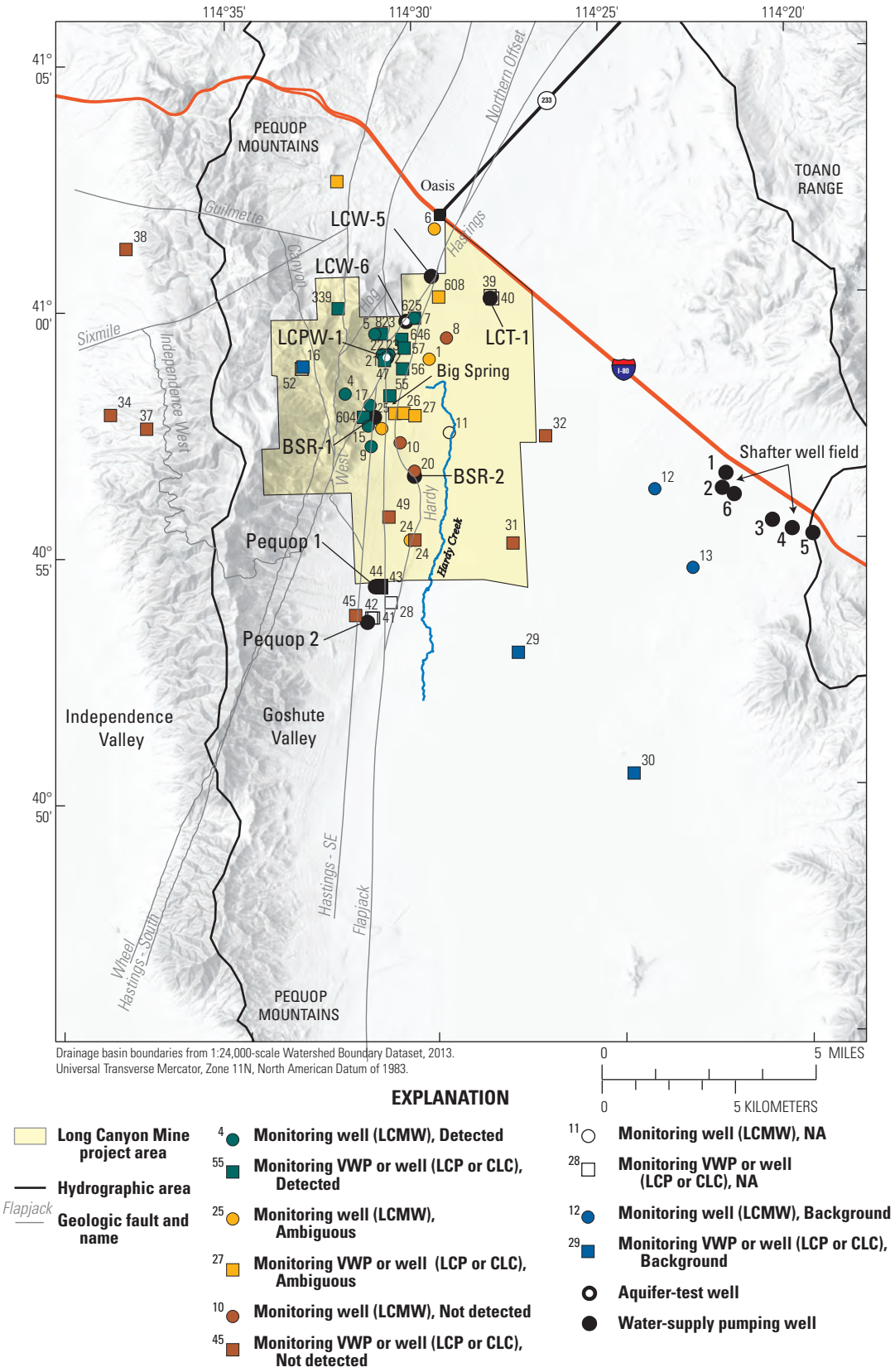

Figure 20. Water-level drawdown classifications at monitoring sites from the carbonate-rock aquifer test, Long Canyon, Goshute Valley, northeastern Nevada, 2016. Drawdown is classified as detected, ambiguous, and not detected. Sites with nested wells or piezometers are shown as detected if at least one water-level drawdown was detected. VWP, vibrating-wire piezometer. Well and VWP name prefixes are shown in parentheses.

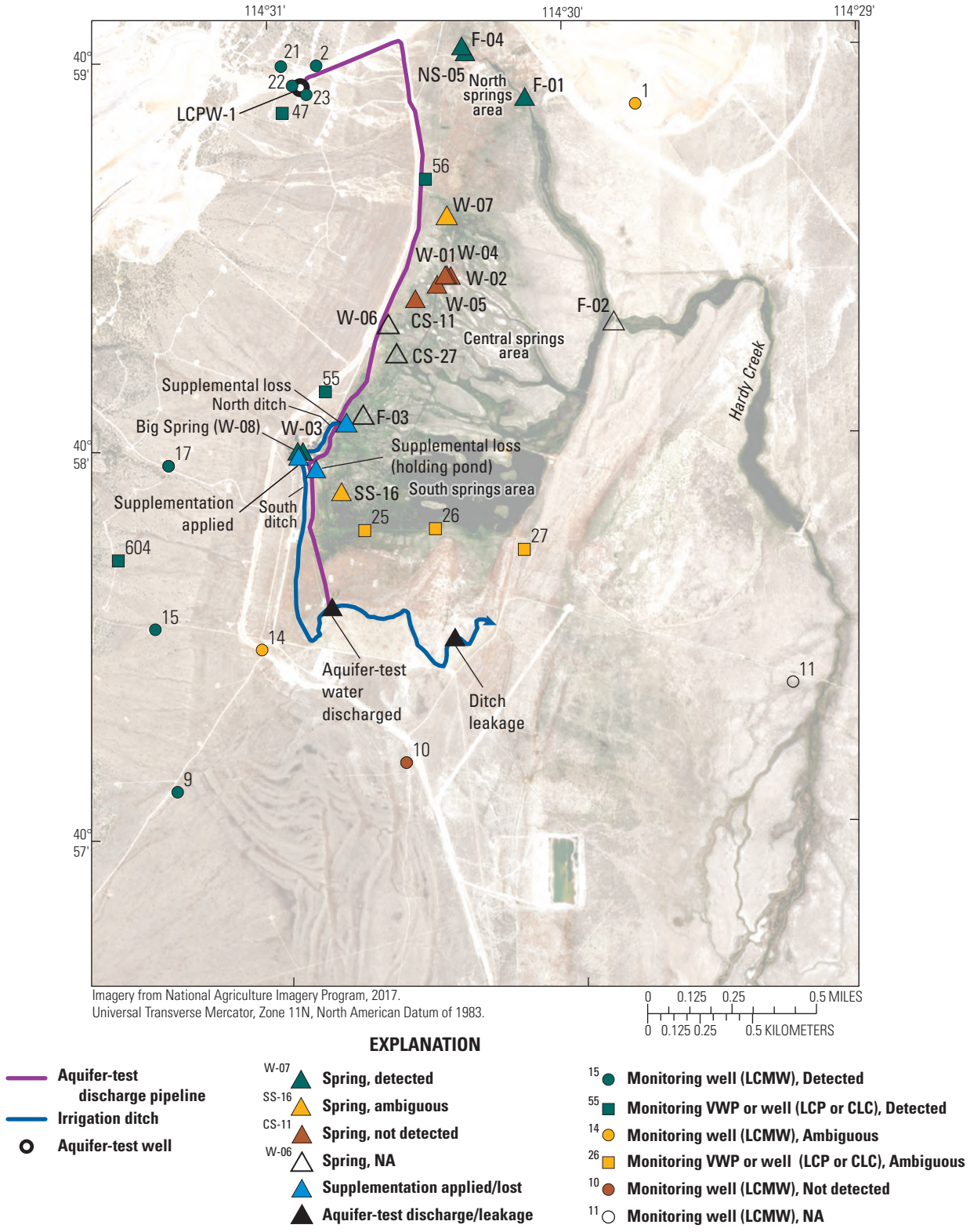

Figure 21. Water-level drawdown classifications at spring monitoring sites from the carbonate-rock aquifer test, Long Canyon, Goshute Valley, northeastern Nevada, 2016. Drawdown is classified as detected, ambiguous, and not detected. Sites with nested wells or piezometers are shown as detected if at least one water-level drawdown was detected. VWP, vibrating-wire piezometer. Well and VWP name prefixes are shown in parentheses.

The area of drawdown detection extends northeast-to-southwest over more than 3 mi (from sites LCMW-07 to LCMW-09) and northwest-to-southeast over more than 2 mi (extending from sites CLC-339 to LCP-57) (fig. 20). The extent of drawdown detection south of site LCMW-09 is unknown. The nearest carbonate-rock (LCP-45A) and alluvial-fan (LCP-41–44) monitoring sites are more than 3 mi south of LCMW-09 and had either poor precision in the water-level record or were affected by unmeasured water-supply pumping in adjacent wells (figs. 20 and 22). In LCP-45A (fig. 22) and LCP-45B (not shown), poor transducer precision (± 0.5 ft) precluded detection of pumping-induced, water-level changes. North of LCMW-07, representing the northern extent of detected drawdown, carbonate-rock and alluvial-fan monitoring wells do not exist. However, the area of drawdown likely was bounded by the volcanic rocks open to monitoring site LCP-36, where drawdown was ambiguous or not detected. Steep water-level responses to winter 2015–16 precipitation (or snowmelt) at the LCP-36 site likely indicate that adjacent volcanic rocks have low permeability (for example, LCP-36B in fig. 8).

Similar drawdown in carbonate rocks within the drawdown detection area suggest that all wells penetrate a highly transmissive zone (HTZ) that is bounded by low-permeability rocks. Drawdown in carbonate rocks within the detection area averaged 3.5 ft and varied little spatially (standard deviation of ±0.9 ft). Similar drawdown responses indicate a high degree of connection among wells within the area of drawdown detection. The similarity of carbonate-rock drawdowns in the HTZ suggests that the area is bounded by low-permeability rocks or structural features; otherwise, maximum drawdown in a well would decrease with distance from the pumping wells. Potential bounding features are the Canyon fault to the west and Hardy fault or lower-permeability basin fill to the east (fig. 20).

The quality of drawdown estimates and detection classifications are indicated by responses in monitoring well LCMW-22S and VWPs LCP-56B, CLC-339B, and LCP-45A (fig. 22). Drawdown estimate quality was limited by superimposed short- and long-term environmental fluctuations and measurement precision. Drawdown was detected with a high degree of certainty in well LCMW-22S because three discrete pumping intervals can be discerned, recovery is observed, and the signal-to-noise ratio is 115 (Smith and others, 2021, appendix 3). Drawdown was detected in VWP LCP-56B with lesser certainty because discrete pumping intervals are more obscured, observed recovery is limited, and the signal-to-noise ratio is 14. Drawdown detection in VWP CLC-339B was ambiguous because no recovery was observed (fig. 22) and water levels had a long-term (several-year) decline (similar to LCMW-02D in fig. 8). Drawdown was not detected in VWP LCP-45A, the most distant carbonate-rock site monitored to the south of aquifer-test wells. Measurement precision at LCP-45A was limited to 0.5 ft or more, masking any potential pumping signal that might otherwise have been observed more than 6 mi from the nearest test well. Plots and individual Microsoft Excel® files for measured and simulated water levels, residuals, and drawdown (and rise) estimates for all wells, piezometers, and springs are available in Smith and others (2021).

Rise Observations

Water-level rise from ditch leakage and supplementation loss was detected at nine monitoring sites and ranged from 0.43 ft in LCMW-08 to 3.29 ft in LCP-27A (fig. 23; Smith and others, 2021, appendix 3). The absolute magnitude of rise detections at sites LCMW-01, LCP-26, and LCP-27 is uncertain because rise is inversely correlated with drawdown, such that an increase in water-level rise can be offset by an equal and opposite increase in drawdown (for example, LCP-27A in fig. 23). Water-level rise was classified as ambiguous at nine monitoring sites, extending as far south as LCP-00049A. Springs with an ambiguous rise in stage of less than 0.05 ft include CS-11 and SS-16 (Smith and others, 2021, appendix 3).

The area of rise detection extends about 3 mi from north to south (from LCMW-08 to LCMW-20) and at least 1 mi from southwest to northeast (from LCP-26 to LCMW-08) (fig. 24). Rise detection over this expansive area indicates the presence of an underlying low-permeability unit that inhibits downward percolation and promotes lateral flow. The top of this low-permeability unit likely exists between depths of 100 and 300 ft bls based on monitoring well screen and vibrating-wire transducer locations. Rise detection north and south of the JSWC indicates that the shallow alluvium underlying the wetland area likely is composed of a thin layer of permeable sediments underlain by impermeable sediments.

The quality of detected water-level rise estimates is shown for monitoring sites LCP-27A and LCMW-08 (fig. 23). Estimate quality was characterized by the rise magnitude relative to measurement precision. Water-level rise was detected with a high degree of certainty in VWP LCP-27A, located less than one-half mile from the ditch leakage point, because two discrete ditch leakage intervals (indicating constant rate pumping periods) can be discerned, recovery is observed, and the signal-to-noise ratio is 37 (fig. 23; Smith and others, 2021, appendix 3). Water-level rise in well LCMW-08, located more than 2 mi from the ditch leakage point, was detected with a lesser degree of certainty because discrete ditch leakage intervals were not clearly observed, observed recovery was limited, and the signal-to-noise ratio was 14 (fig. 23; Smith and others, 2021, appendix 3).

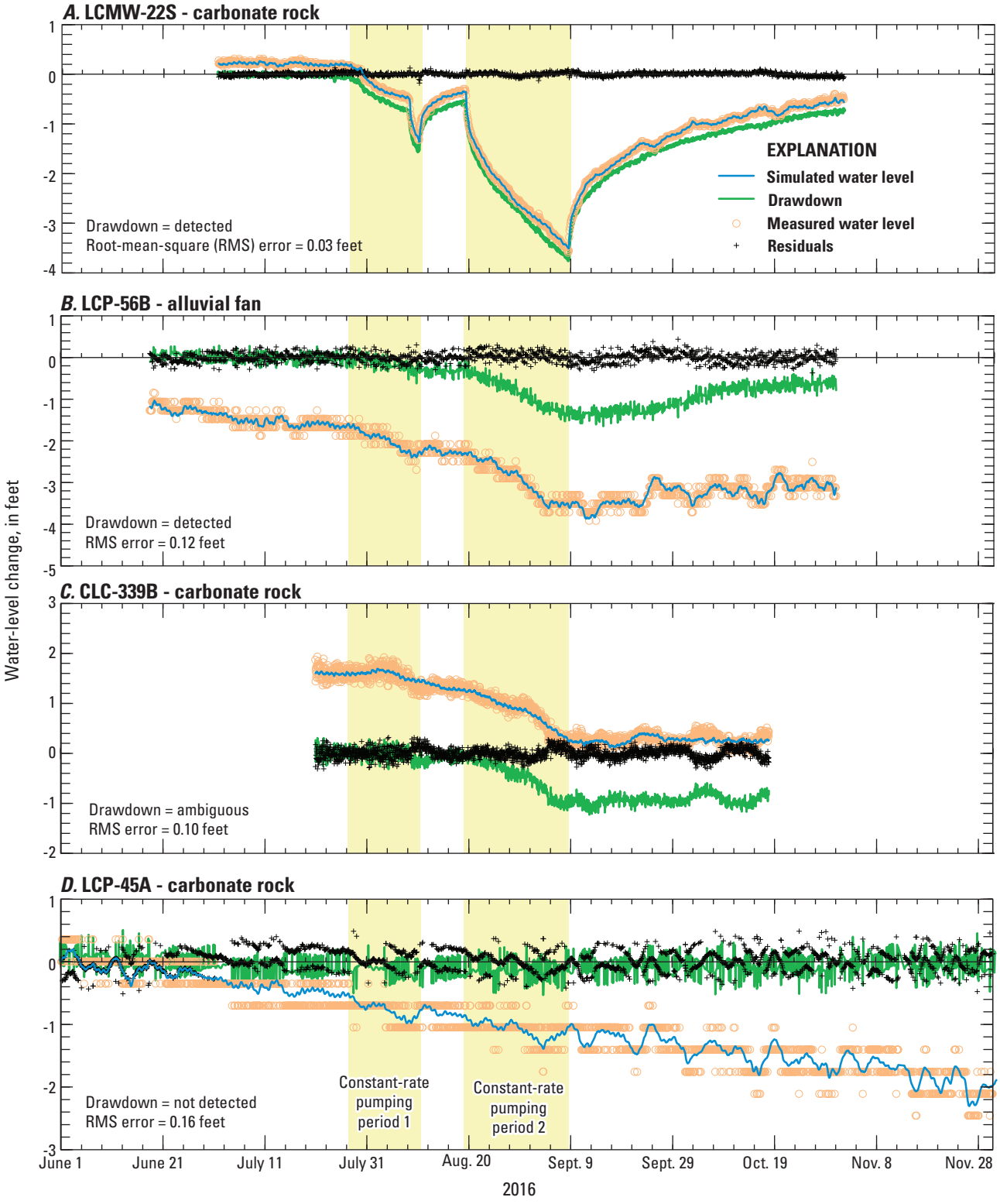

Figure 22. Examples of measured and simulated water levels and drawdown estimates showing detected, ambiguous, and not detected responses at four monitoring sites, Long Canyon, Goshute Valley, northeastern Nevada, June–November 2016. Drawdown resulted from pumping in wells LCW-6 and LCPW-1 during the 2016 carbonate-rock aquifer test.

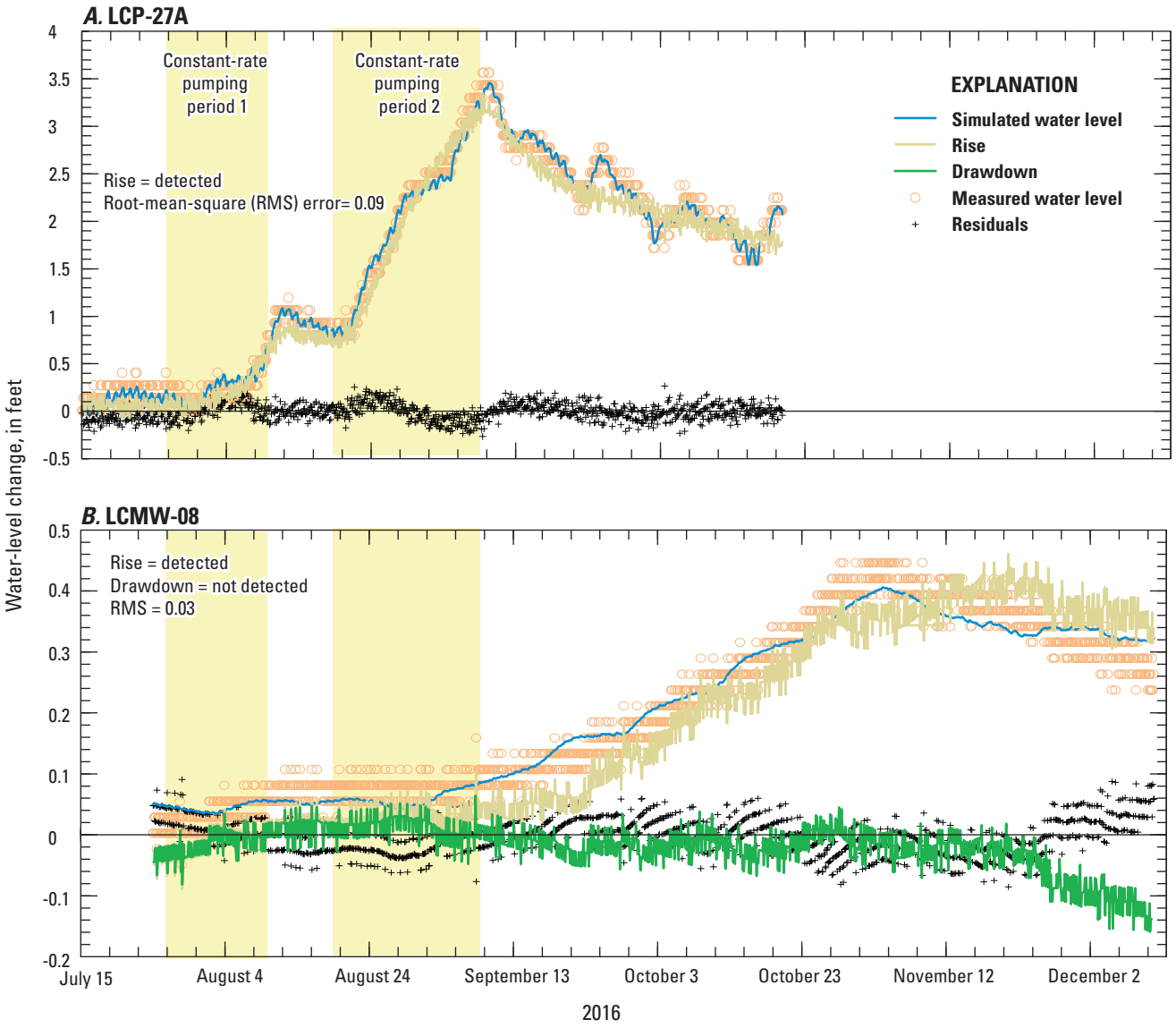

Figure 23. Examples of measured and simulated water levels and water-level rise estimates at two monitoring sites showing detected responses, Long Canyon, Goshute Valley, northeastern Nevada, July–December 2016. Water-level rise resulted from shallow subsurface loss of pumped discharge in an unlined channel and spring supplementation water during the 2016 carbonate-rock aquifer test.

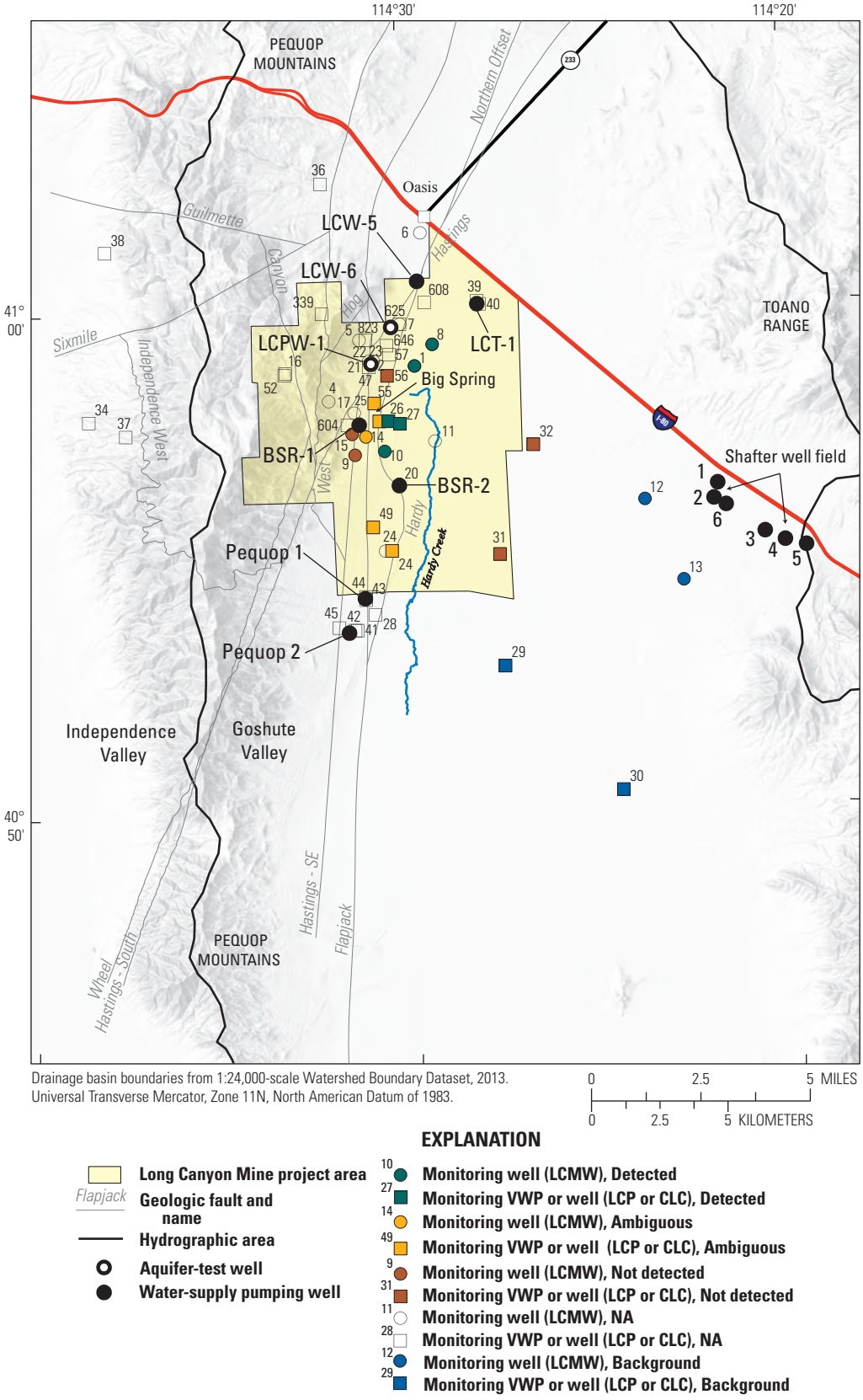

Figure 24. Water-level rise classifications at monitoring sites from subsurface loss of pumped water discharged into an unlined irrigation ditch and loss of supplementation water discharged at Big Spring during the carbonate-rock aquifer test, Long Canyon, Goshute Valley, northeastern Nevada, 2016. Water-level rise is classified as detected, ambiguous, and not detected. Sites with nested wells or piezometers are shown as detected if at least one water-level rise was detected. VWP, vibrating-wire piezometer. Well and VWP name prefixes are shown in parentheses.

Integrated Estimation of Recharge and Hydraulic-Property Distributions with Numerical Models

Hydraulic-property and recharge distributions were estimated by simultaneously calibrating two three-dimensional numerical groundwater models of the area of interest (fig. 1). Steady-state flow under predevelopment conditions was simulated with the *Long Canyon Steady State* (LC-SS) model. Changes in groundwater levels and springflows from the 2016 carbonate-rock aquifer test were simulated with the *Long Canyon Multiple-Well Aquifer Test 2016* (LC-MWAT2016) model. When the LC-SS and LC-MWAT2016 models are coupled for calibration, the integrated model is referred to as the integrated LC model.

Steady-state flow and changes from the 2016 carbonate-rock aquifer test were simulated with two models because multiple observed conditions can be better specified in separate models. For example, steady-state discharge from Big Spring averaged 1,100 gal/min with a pool altitude of 5,680 ft. With multiple models, steady-state discharge from Big Spring was simulated as a specified discharge of 1,100 gal/min and as a head-dependent boundary during the 2016 carbonate-rock aquifer test. Multiple models helped to prevent discrepancies between simulated and measured pool altitudes from affecting simulated capture during the 2016 carbonate-rock aquifer test.

Groundwater-flow equations were solved using the USGS Modular Three-Dimensional Finite-Difference Groundwater Flow Model (MODFLOW) (Harbaugh, 2005). The two coupled (stress-response) groundwater models were calibrated simultaneously using the Parameter ESTmation (PEST) code, (Doherty, 2010a). Archives of the Long Canyon models containing executable files, PEST calibration files, stress-response models, and information on drawing maps, creating MODFLOW packages, and simulating groundwater-flow paths and velocities are available in Nelson and others (2021).

Both groundwater-flow models developed for the study shared a common domain, spatial and temporal discretization, hydrogeologic framework, and hydraulic properties. Model domains extended laterally to no-flow boundaries along the edges of the area of interest (figs. 1 and 25). Each model was divided areally into 143 rows and 139 columns of variably spaced, rectangular cells with side lengths that ranged from 250 to 2,500 ft. Finer discretization was used in a 16 mi^2 area (fig. 25) centered on the area surrounding the 2016 carbonate-rock aquifer-test pumping wells and springs in the JSWC. The model grid is oriented north-south using the same coordinate system as Newmont Mining Corporation, referred to as mine coordinates, which are rotated 0.9291 degrees clockwise from Universal Transverse Mercator (UTM), zone 11, North American Datum of 1983 (NAD 83) projection. Easting and northing of the model grid's northwest corner are 897,500, 570,000 ft in mine coordinates and 692,458, 4,555,425 m in UTM zone 11.

A single grid was defined for all groundwater-flow models. This grid extended vertically from the water table to 2,000 ft above the North American Vertical Datum of 1988 (NAVD 88), and was divided into 11 layers. The water table was assumed to equal the potentiometric surface (fig. 7) for defining the top of saturated rocks and upper model boundaries. Layer 1 of the groundwater-flow models was 1-ft thick to better simulate groundwater/surface-water interaction and drainage at the water table. The tops of layers 3–11 nominally occurred at depths of 100, 150, 200, 250, 360, 450, 850, 1,250, and 1,750 ft below the water table (fig. 26). The bottom of layer 11 was set at an arbitrary elevation of 2,000 ft above NAVD 88 and was designated as a no-flow boundary in both groundwater-flow models.

Saturated thicknesses of all model layers were specified and did not change in response to simulated pumping. Therefore, the simulated water table does not deform or move through layers. Saturated thicknesses were specified to improve model performance because models converge consistently and execute quickly when simulating transmissivity as a function of head (Sheets and others, 2015). Specifying saturated thicknesses also better approximates fractured-rock aquifers where flowing fractures occur below the maximum change in saturated thickness (Sheets and others, 2015). For example, water levels ranged from 189 to 233 ft bls in well LCPW-1 during the 2016 carbonate-rock aquifer test, whereas flow logs showed that the highest transmissivity occurred at depths greater than 1,000 ft bls.

Hydrogeologic Framework

A hydrogeologic framework was developed from geologic mapping and hydraulic testing to distribute hydraulic properties in saturated rocks throughout the area of interest. Hydrogeologic units were simplified from geologic units, while maintaining spatial locations of hydraulically significant units and major structural features. Hydrogeologic units in the study area were consistent with Basin and Range normal faulting, where northeast-trending deep fault-blocked basin fill is bounded by mountain ranges of primarily carbonate-clastic rocks. (fig. 26).

The grid of the hydrogeologic framework coincided with groundwater-flow model grids. Groundwater-flow model layers 2–11 coincided with hydrogeologic framework layers 1–10. Hydrogeologic units in groundwater-flow model layers 1 and 2 were identical. A single hydrogeologic unit was assigned uniquely to each cell in the hydrogeologic framework.

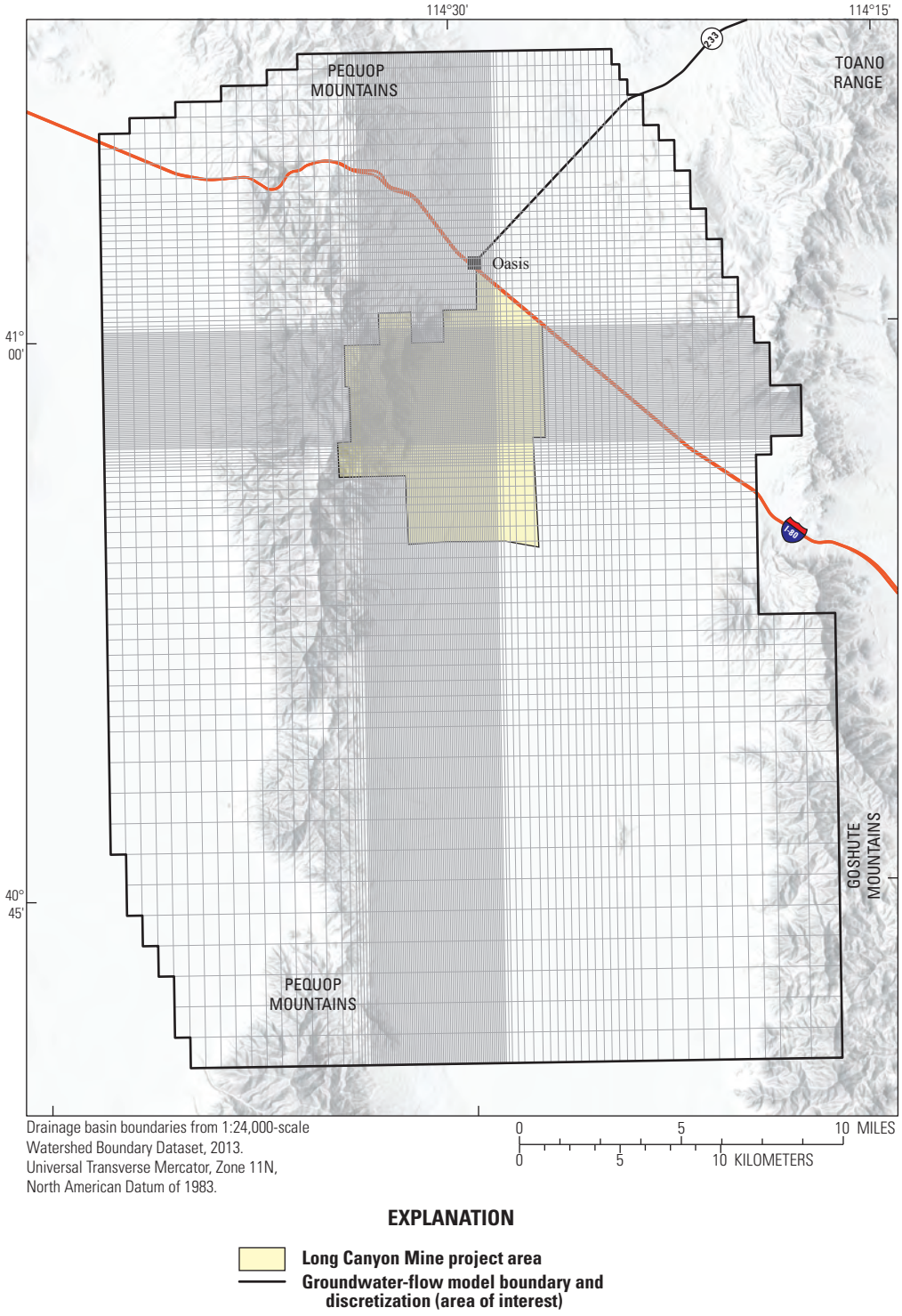

Figure 25. Boundary of Long Canyon groundwater-flow models and area of finer discretization near Johnson Spring wetland complex, Long Canyon, Goshute Valley, northeastern Nevada.

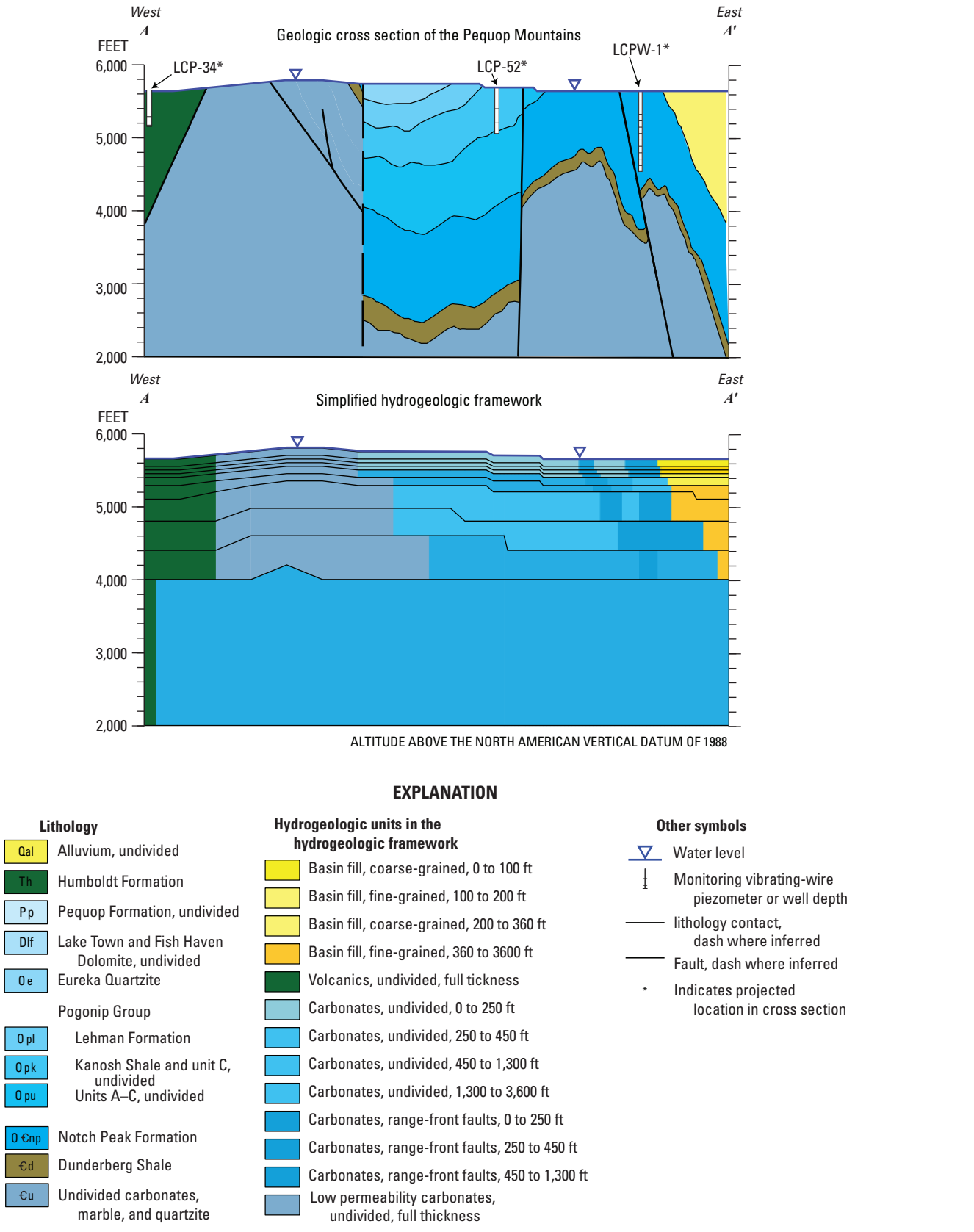

Figure 26. Example geologic and hydrogeologic framework cross sections through saturated rocks, Long Canyon, Goshute Valley, northeastern Nevada. Trace of cross section *A*–*A*′ is shown in figure 2.

Thickness, extent, and geometric relations of hydrogeologic units and major structural features were inferred from 77 geologic coring holes and monitoring wells completed by the Long Canyon Mine and mapped structural features of Camilleri (2010). The model framework is a synthesis of geologic data from maps and cross sections (Camilleri, 2010; Golder Associates Inc., 2012; Newmont Mining Corporation, 2018, written commun.), lithologic descriptions and interpretations (Thorman, 1970; Coats, 1987; Ketner, 1997), and gravity survey data (Paul Pettit and Stephanie Douglas, Newmont Mining Corporation, written commun., 2017).

Geologic units initially were reduced to four hydraulically unique rock types: (1) carbonate rocks, (2) basin fill, (3) volcanic rocks, and (4) low-permeability rocks (Halford and Jackson, 2020). Carbonate rocks included dolomite and limestone sequences such as Notch Peak and Lehman Formations, respectively. Basin fill was composed of all unconsolidated sediments including unconsolidated volcanic sediments. Volcanic rocks were rhyolite ash-flow tuffs, andesite ash-flow breccia, and other hard rock units. Low-permeability rocks were composed principally of quartzite and shale.

The four hydraulically unique rock types were divided into 13 hydrogeologic units to simulate structural features and depth-dependent changes in hydraulic conductivities (table 11). Carbonate rocks were differentiated with depth because flow logs measured depth-dependent hydraulic-conductivity contrasts. Carbonate rocks nominally were subdivided 250, 450, and 1,300 ft below the water table (table 11). A 1-mi-wide section of carbonate rocks along the eastern flank of the Pequop Mountains through the Long Canyon Mine project area was differentiated from other carbonate rocks to simulate bulk effects of range-front faults (fig. 26) that include Flapjack, Hastings, and Hardy faults. Basin fill nominally was subdivided 100, 200, and 360 ft below the water table to accommodate known hydrologic variability (table 11).

Distributing Hydraulic Properties and Recharge

Heterogeneous hydraulic-property and recharge distributions were estimated with PEST using pilot points. Log-values of hydraulic conductivity, specific yield, and specific storage were estimated at pilot points (RamaRao and others, 1995), where the locations of pilot points were user-specified. In this study, pilot points were used throughout the model extent but more pilot points were placed in areas with more observation data to constrain hydraulic-property estimates. Estimated hydraulic properties at user-specified locations were translated into continuous hydraulic-property fields by interpolation with kriging (Doherty, 2010b).

Table 11. Hydrogeologic units, groundwater-flow model layers, and preferred hydraulic properties in the hydrogeologic framework, Long Canyon, Goshute Valley, northeastern Nevada.

[**Hydrogeologic unit:** Identifier used in groundwater-flow models. **Preferred hydraulic properties**, or prior information (Doherty, 2010a), were determined from aquifer-test results and lithology. **Abbreviations:** ft²/d. feet squared per day; 1/ft, 1 per foot]

Rock type	Description and nominal depths below water table (feet)	Hydrogeologic unit	Layers	Preferred hydraulic property		
				Transmissivity (ft²/d)	Specific yield (unitless)	Specific storage (1/ft)
Carbonate rocks	Undivided, 0–250	204	1–5	5,000	0.01	2.0×10^{-7}
	Undivided, 250–450	206	5–7	5,000	0.01	2.0×10^{-7}
	Undivided, 450–1,300	208	7–9	20,000	0.01	2.0×10^{-7}
	Undivided, 1,300–3,600	210	9–11	20,000	0.01	2.0×10^{-7}
	Range-front faults, 0–250	304	1–5	20,000	0.01	2.0×10^{-7}
	Range-front faults, 250–450	306	5–7	20,000	0.01	2.0×10^{-7}
	Range-front faults, 450–`1,300	308	7–9	20,000	0.01	2.0×10^{-7}
Volcanic rocks	Undivided, full thickness	1010	1–11	10	0.01	2.0×10^{-7}
Basin fill	Coarse-grained, 0–100	1501	1–2	3,000	0.08	1.5×10^{-6}
	Fine-grained, 100–200	1503	2–4	10	0.08	1.5×10^{-6}
	Coarse-grained, 200–360	1505	4–6	3,000	0.08	1.5×10^{-6}
	Fine-grained, 360–3,600	1510	6–11	0.1	0.08	1.5×10^{-6}
Low-permeability rocks	Undivided, full thickness	1910	1–11	0.1	0.01	2.0×10^{-7}

Isotropic, exponential variograms defined spatial variability of log-hydraulic properties for kriging, where spatial correlation was specified with user-defined ranges (distances). Spatial correlation is assumed to be non-existent where distances between interpolated location (cell center) and known value (pilot point) exceed the range. A hydraulic-property value at a cell functionally was an inverse-distance, weighted average of the eight nearest pilot-point values if all distances between cell center and pilot points were less than the range. A hydraulic-property value at a cell approaches a simple average if distances between a cell center and the eight nearest pilot points all exceed the range.

Interpolated hydraulic properties varied laterally but were uniform with depth in multiple-layer hydrogeologic units. For example, consider the distribution of hydraulic-conductivity values within a hypothetical framework consisting of basin fill, volcanic rocks, and carbonate rocks (fig. 27). Carbonate rocks vary in thickness and intersect multiple MODFLOW model layers. Hydraulic conductivity is distributed laterally in the mapped extent of the hydrogeologic unit without regard for depth (fig. 27). Each hydrogeologic unit is a unique volumetric zone in MODFLOW and interpolation from pilot points occurred exclusively within each hydrogeologic unit. Hydraulic conductivities are interpolated laterally from three pilot points within the hypothetical carbonate rocks (fig. 27) The estimated hydraulic-conductivity values at each lateral (X,Y) location in the carbonate rocks are assigned to all model layers where the carbonate rocks occur. Therefore, hydraulic properties are estimated at pilot points, interpolated laterally within each hydrogeologic unit, and then assigned the same value for all layers where the hydrogeologic unit occurs. Map extents of hydrogeologic units and pilot points for each hydrogeologic unit are provided as spatial coverages in the accompanying USGS data release (Nelson and others, 2021).

A uniform lateral-to-vertical anisotropy of 10:1 for hydraulic conductivity was assigned and assumed to be reasonable for basin fill but has limited significance in carbonate and volcanic rocks. Dip and orientation of bedding varies markedly within lithologic units that are disrupted by faults (Camilleri, 2010; Heilweil and Brooks, 2011). Flow logs show extreme anisotropy or heterogeneity across intervals of less than 10 ft in carbonate rocks. For example, flow logging across 700 ft of saturated rocks in borehole LCP-74 indicated that 50 percent of the transmissivity occurred in a 5-ft interval (Nelson and others, 2021). Transmissive intervals in wells LCPW-1 and LCW-6 also were limited to a few, thin intervals. Anisotropic characteristics are not visually apparent in the hydrogeologic units, which are featureless groups of rocks. Moreover, heterogeneity is simulated entirely by contrasts in hydraulic properties within and between hydrogeologic units. Lateral contrasts within units largely were simulated by adding pilot points to hydrogeologic units, where greater pilot-point density allows for increased heterogeneity. Vertical contrasts were simulated exclusively as differences in hydraulic properties between hydrogeologic units (fig. 26). Carbonate rocks in the HTZ were subdivided laterally and vertically into multiple hydrogeologic units to simulate the effects of range-front faults and depth-dependent hydraulic conductivity (fig. 26; table 11). Basin fill was differentiated with depth into four units to simulate observed depth-dependent water-level changes (fig. 26). Heterogeneity and anisotropy are correlated, where large degrees of anisotropy can be simulated with large contrasts in hydraulic properties between hydrogeologic units.

Hydraulic Conductivity

Hydraulic conductivities and layer thicknesses define simulated transmissivities and were assigned with the Layer-Property Flow package in MODFLOW (Harbaugh, 2005). Laterally heterogeneous hydraulic-conductivity distributions were estimated for each hydrogeologic unit. Hydraulic conductivities are estimable in data-rich areas such as the HTZ. However, in areas of minimal data such as southern Goshute Valley and the Toano Range, hydraulic-conductivity estimates are defined primarily by preferred transmissivities based on prior information. A preferred transmissivity was estimated for each hydrogeologic unit from aquifer-test results and lithology (table 11). Hydraulic conductivities assigned to each hydrogeologic unit prior to model calibration were estimated by dividing the preferred transmissivity (table 11) by unit thicknesses represented in the model.

Hydraulic conductivities were specified with 563 pilot points, where pilot-point density increased as water-level measurements, spring discharges, and transmissivity estimates were more prevalent (fig. 28). Data density was greatest through the HTZ, around the ore body (not shown on fig. 28), and the JSWC, where model discretization was finest (fig. 25). Ranges of variograms were less than 2 mi in areas of greater pilot-point and observation data densities to permit more variability in interpolated hydraulic conductivities. Pilot-point density at the water table adequately represents variations in pilot-point density with depth even though only 31 percent of pilot points were positioned at the water table (fig. 28). Additional pilot points assigned to deeper hydrogeologic units at a single spatial location are obscured by pilot points assigned to the water table.

Hydraulic conductivities were specified with additional pilot points in areas where observations are limited and surface lithology was an adequate indicator of hydraulic properties. For example, playas on the floors of Independence and Goshute Valleys are classified as basin fill in the hydrogeologic framework (fig. 28), and these sediments primarily are salt and clay where hydraulic conductivities are expected to be less than 0.0001 ft/d (Jackson and others, 2018). Preferred hydraulic conductivities were assigned and fixed (not estimated) during model calibration.

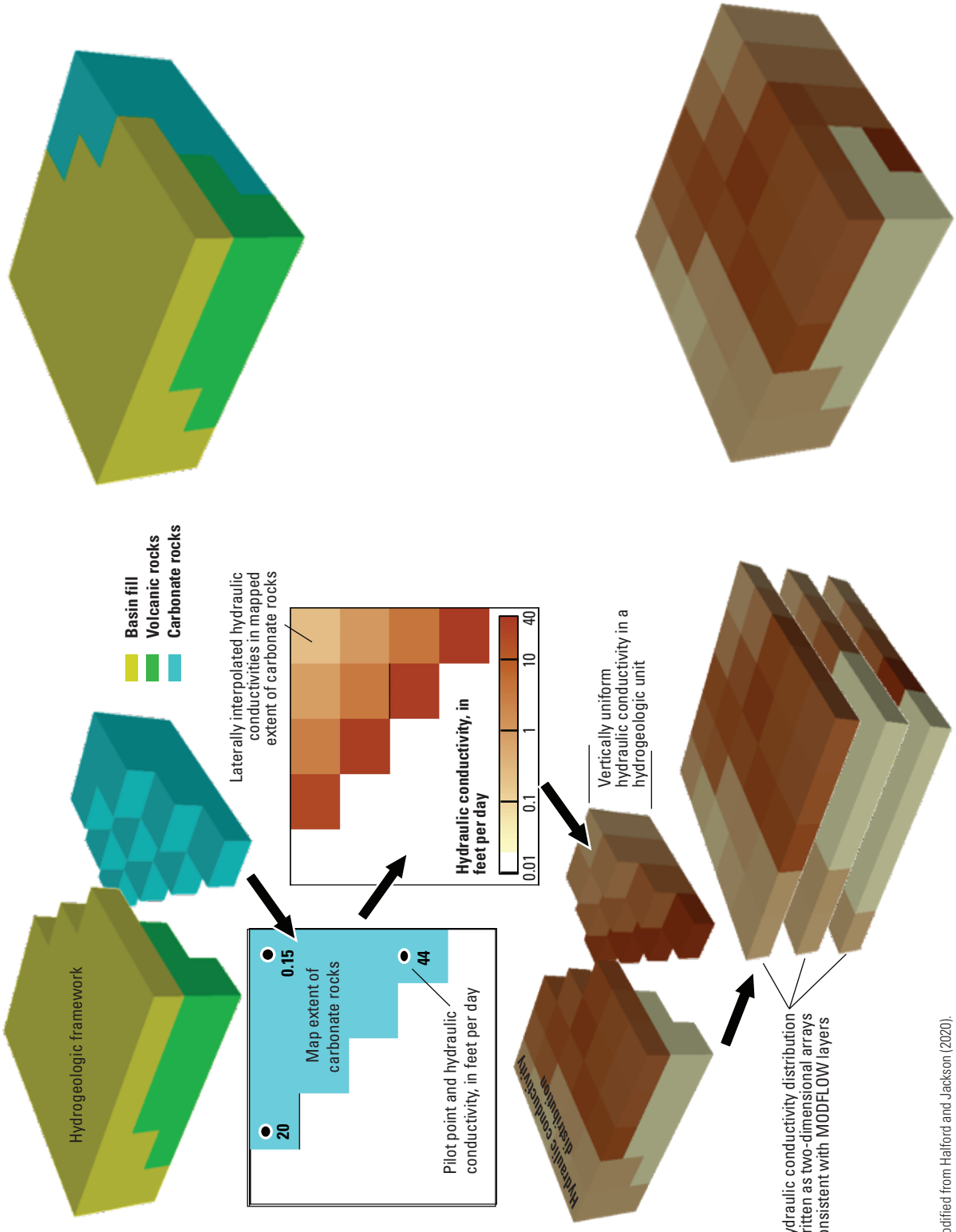

Modified from Halford and Jackson (2020).

Figure 27. Process for distributing hydraulic conductivities from pilot points to Modular Three-Dimensional Finite-Difference Groundwater Flow Model (MODFLOW) layers through hydrogeologic units in a hydrogeologic framework.

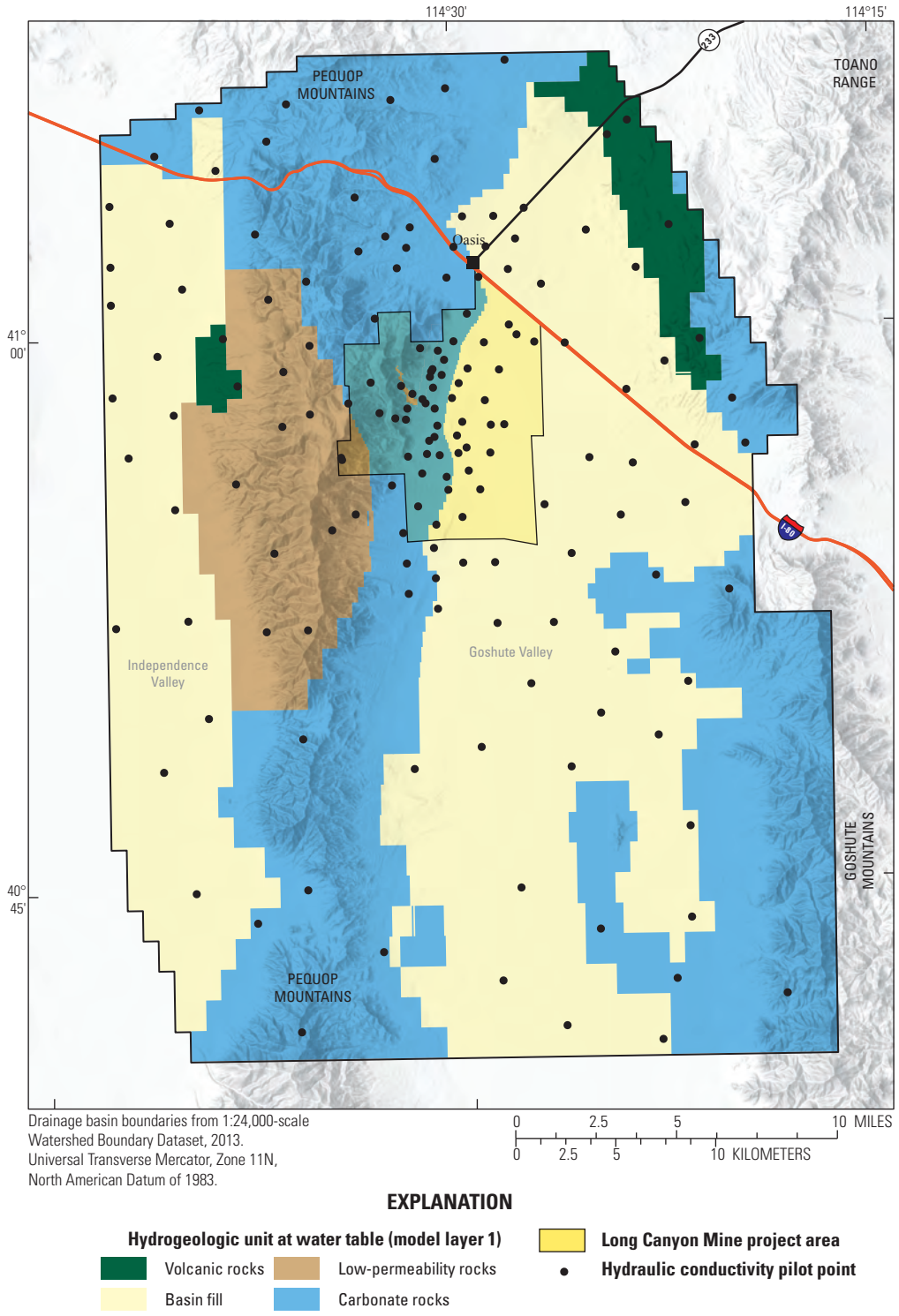

Figure 28. Extents of all hydrogeologic units and hydraulic-conductivity pilot points at the water table, Long Canyon, Goshute Valley, northeastern Nevada.

Specific Yield and Specific Storage

Storativity distributions were estimated for hydrogeologic units using a simplified framework consisting of basin fill and consolidated rocks (as specific storage and specific yield, table 11). A simplified framework was used because storativities are less variable than hydraulic conductivities. Storativity is approximately equal to specific yield for unconfined aquifers and specific storage times thickness for confined aquifers. Specific yields typically range from 0.05 to 0.25 in basin fill and from 0.005 to 0.05 in consolidated rocks. Specific-storage values typically range from 1×10^{-7} and 5×10^{-6} 1/ft, regardless of hydrogeologic unit. Specific-storage values less than 1×10^{-6} 1/ft typically occur in fractured rocks where much of the rock mass is poorly connected to permeable fractures. Preferred values of specific yield and specific storage (table 11) were assigned and fixed during calibration where basin fill and consolidated rocks were not affected by the 2016 carbonate-rock aquifer test (figs. 20 and 23).

Storativities were estimated and assigned with 48 pilot points as either specific yield or specific storage so that spatial variability could be simulated. Storativities in model layer 1 were equivalent to specific yields because layer 1 is unconfined and only 1-ft thick. Storativities varied laterally within basin fill and consolidated rocks. Specific storages were distributed in layers 2–11 and reported as storage coefficients, which is specific storage times thickness. Like hydraulic conductivities, interpolated specific storages varied laterally in model layers 2–11, but were uniform with depth. All variograms for distributing storativity values between pilot points were isotropic and exponential with a range of 9.5 mi. Arrays of specific yield and specific storages were only used in the transient LC-MWAT2016 model.

Recharge

Recharge was distributed throughout the LC-SS predevelopment flow model with a total of 57 pilot points (fig. 29). Recharge rates initially were assigned using the conceptual recharge distribution (fig. 6) and then were calibrated with PEST. Calibrated plot-point values were interpolated to model cells with kriging, similar to the interpolation method used for distributing hydraulic properties (Doherty, 2010b). Spatial variability of recharge was defined using an isotropic, exponential variogram with a range of 6 mi.

Stress-Response Models

Predevelopment conditions and the 2016 carbonate-rock aquifer test were simulated with two separate, but coupled, stress-response models. The LC-SS model simulated predevelopment conditions at steady state and informed estimates of recharge rates and hydraulic conductivities. The LC-MWAT2016 model simulated drawdowns from pumping during the 2016 carbonate-rock aquifer test, and informed estimates of hydraulic conductivity, specific yield, and storage coefficients through the Pequop Mountains and adjacent basin fill in Goshute Valley between well Pequop-2 and the Shafter well field. The area informed by the 2016 aquifer test was defined between wells where drawdowns were detected and not detected such as wells LCMW-9 and LCMW-10, respectively (fig. 20).

Predevelopment, LC-SS Model

Steady-state flow during predevelopment conditions was simulated so that recharge, hydraulic conductivities of low-permeability rocks, and the contributing area of springs in the JSWC could be estimated. Initial recharge volumes were defined primarily by available recharge estimated with the conceptual recharge distribution (fig. 6). Elevated water levels in areas of limited recharge identified low-permeability rocks, such as in the northern Pequop Mountains and Toano Range (fig. 7). The combined contributing area of Big Spring and other springs in the JSWC were estimated for comparison to geochemical interpretation.

Most discharges occurred from phreatophyte areas on the floors of Independence and Goshute Valleys (fig. 29) and were simulated with specified heads in layer 1. Phreatophyte and playa areas had been delineated previously (Nichols, 2000), but estimated groundwater-discharge rates were not accurate. Water-table altitudes in these areas were specified because water levels are better known than discharge rates.

Locations and discharges of small springs in the JSWC between Big Spring (W-08) and spring NS-05 were estimated from measurements at weirs and flumes (table 12; Smith and others, 2021, appendix 1). Stages were measured and discharges were estimated in channels downgradient from the small springs (table 12). Small spring locations were estimated from satellite imagery and paired with measured stages (table 12). Small spring and downgradient stage locations differed by as much as 1,000 ft, which is the width of four model cells. Discharge from small springs totaled 810 acre-ft/yr (500 gal/min) and was simulated as 25 gal/min per small spring.

Discharges from springs in the JSWC were specified in the LC-SS model using the well package in MODFLOW (Harbaugh, 2005) and totaled 2,740 acre-ft/yr (1,700 gal/min). Discharge from small springs likely varies more than was simulated in the model, but small spring discharge is only 30 percent of all discharge from JSWC; therefore, differences between actual and modeled discharges were considered negligible. Groundwater recharge and discharge from the LC-SS model area totaled 8,000 acre-ft/yr (4,960 gal/min) based on estimates from the conceptual recharge map of Independence, Goshute, and Antelope Valleys (fig. 6).

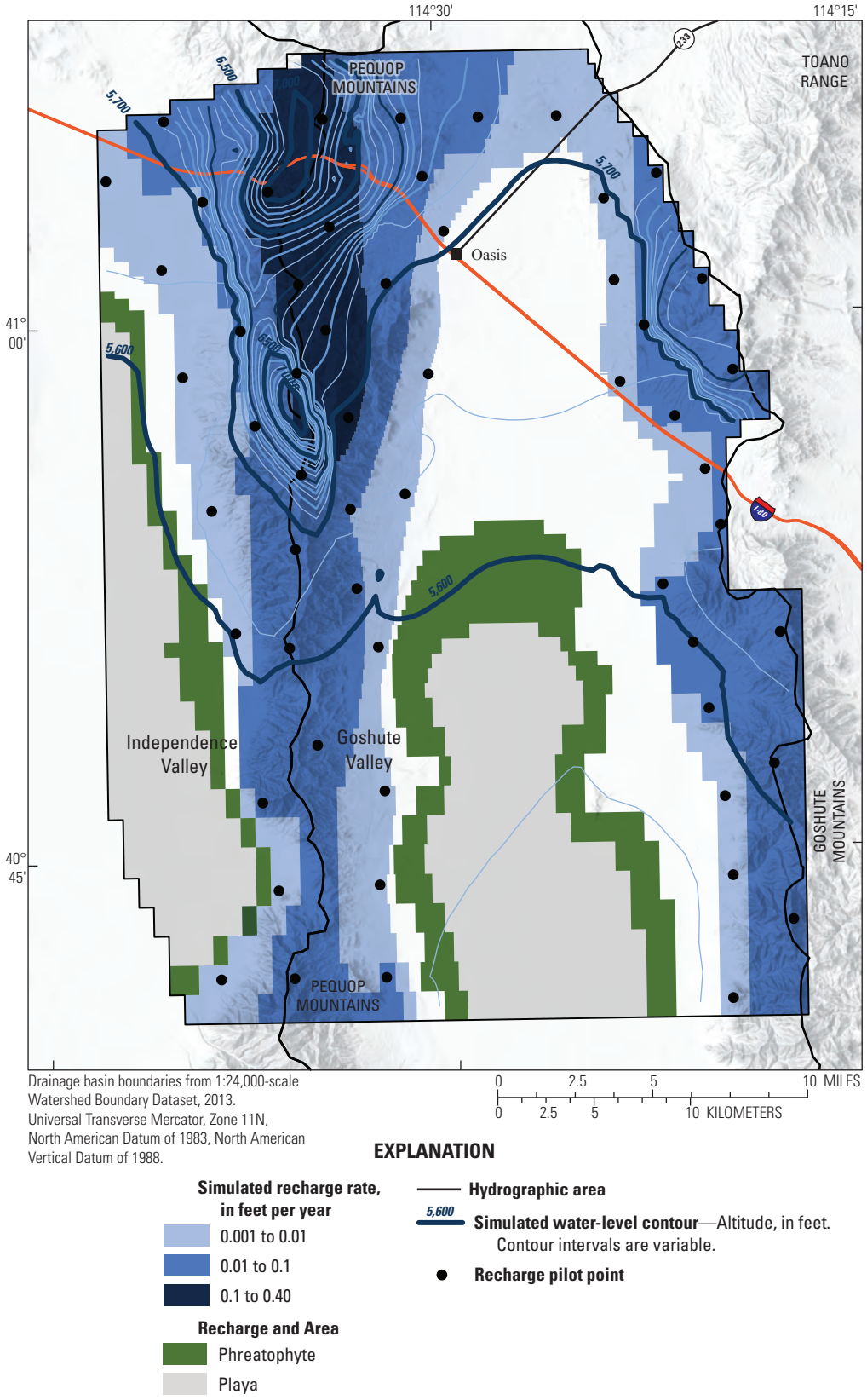

Figure 29. Simulated recharge distribution from Long Canyon Steady State (LC-SS) model, recharge pilot points, simulated potentiometric surface (layer 6), and groundwater-discharge areas, Long Canyon, Goshute Valley, northeastern Nevada.

Table 12. Pairing between measured stages and estimated locations of small springs, spring-pool altitude, steady-state discharge, and calibration weight used in numerical models, Long Canyon, Goshute Valley, northeastern Nevada.

Site name	Spring identifier	Spring-pool altitude (feet)	Steady-state discharge (gallons per minute)	Weight (feet per gallons per minute)
W-08	BigS	5,680	1,000	0.1
F-04	NS05	5,675	200	0.1
CS-11	CS11	5,660	25	0.01
	SCS11	5,660	25	0.01
	MCS11	5,659	25	0.01
CS-27	NCS27	5,654	25	0.01
	2CS27	5,653	25	0.01
	1CS27	5,652	25	0.01
	0CS27	5,651	25	0.01
F-03	6CS27	5,655	25	0.01
	3CS27	5,653	25	0.01
	4CS27	5,652	25	0.01
	5CS27	5,652	25	0.01
SS-16	DBS2	5,660	25	0.01
	DBS1	5,658	25	0.01
W-01	Eiso	5,651	25	0.0001
W-02	W-02	5,665	25	0.01
W-04	UW04	5,662	25	0.01
W-05	UW05	5,665	25	0.01
W-07	W07	5,677	25	0.1
	UW-01	5,664	25	0.01
	DW07	5,657	25	0.0001

2016 Carbonate-Rock Aquifer Test, LC-MWAT2016 Model

The LC-MWAT2016 model simulated changes in water levels and spring discharges from the 2016 carbonate-rock aquifer test to better constrain transmissivity and storativity estimates. An irregular 2-mi-wide by greater than 4-mi-long area of transmissive carbonate rocks west of Big Spring (fig. 20) cannot be interpreted analytically. Hydraulic properties of this broad area of carbonate rocks and adjacent hydrogeologic units were interpreted from 2016 carbonate-rock aquifer-test results and the LC-SS steady-state (predevelopment) flow model. The 2016 carbonate-rock aquifer test was simulated with seven stress periods that matched well development, initial pumping of well LCW-6, adding supplementation water to Big Spring, additional pumping from well LCPW-1, and simultaneous changes in pumping from wells LCPW-1 and LCW-6 (fig. 30). The pumping changes defined the first recovery, second pumping period, and second recovery in observed drawdowns during the 2016 carbonate-rock aquifer test (fig. 22).

Pumping from wells LCPW-1 and LCW-6 was simulated with the multi-node well (MNW) package (Halford and Hanson, 2002), because both wells were open to multiple MODFLOW layers. Return flow from ditch leakage and spring supplementation also were simulated with the MNW package.

Stress changes from the 2016 carbonate-rock aquifer test were simulated using the LC-MWAT2016 model. Initial heads were set to zero, which represented no drawdown prior to the start of pumping in wells LCPW-1 and LCW-6. Discharges from Big Spring and other springs in the JSWC that were simulated as specified discharges in the LC-SS model were simulated as capture-limited boundaries (Halford and Plume, 2011, p. 35) in the LC-MWAT2016 model.

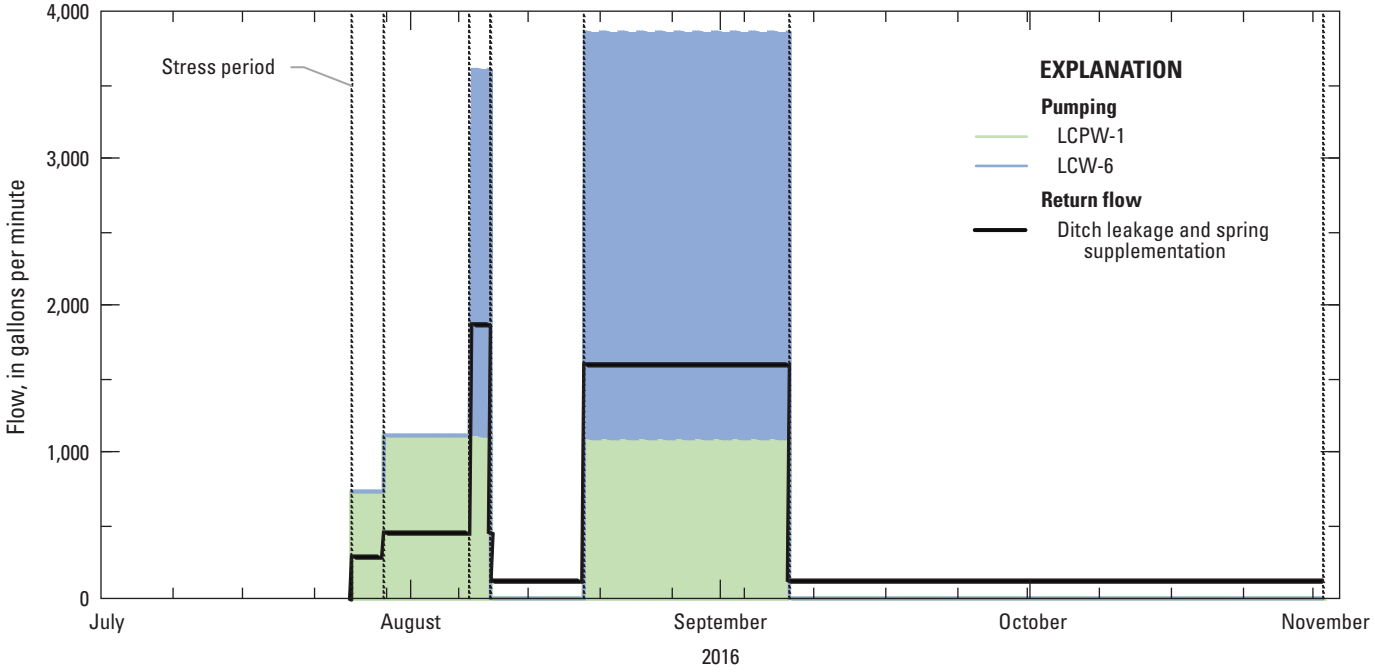

Figure 30. Pumping rates from wells LCPW-1 and LCPW-6, return flow rates from ditch leakage and spring supplementation, and stress periods that were simulated with the Long Canyon Multiple-well Aquifer Test 2016 (LC-MWAT2016) model, Long Canyon, Goshute Valley, northeastern Nevada, July–November 2016.

A capture-limited boundary restricts the total capture of discharge from springs to predevelopment-discharge estimates. MODFLOW does not have a boundary-condition package that simulates limited capture. Therefore, two MODFLOW packages were combined in each model cell where discharge occurs that simulate limited capture. One package simulates the injection of water into the model cell and the other package simulates the removal of water from the model cell. The water injected during each stress period is the predevelopment discharge. The water removed is controlled by a head-dependent boundary package, such as the drain package (Harbaugh, 2005). In the drain package, the elevation is equal to the extinction depth and the conductance is equal to the predevelopment discharge divided by the extinction depth. The extinction depth is the depth below the predevelopment water level at which the spring will go dry (Halford and Plume, 2011).

Capture-limited boundaries were simulated with a combination of the river and drain packages in MODFLOW (Harbaugh, 2005). Discharge prior to pumping was injected with the river package, instead of the well package, so that only pumping was simulated and tracked with the well package. The river package only simulated and tracked the injection component of capture when using the MODFLOW ZONEBUDGET utility (Harbaugh, 1990). Riverbed conductance was the discharge prior to pumping divided by the difference between the river stage and river bottom. The river-stage parameter was set equal to 1 ft above the river-bottom altitude so that riverbed conductance equaled discharge prior to pumping. River stages and bottom altitudes were sufficiently high above the top of the model (water table) so that the river cells always behaved as losing river cells, which allowed simulated river leakage to be a constant injection rate. Drain elevations equaled extinction depths and drain conductances equaled discharges prior to pumping divided by extinction depths. Groundwater capture was limited by simulated differences between injected and drained water, so that simulated captures did not exceed measured discharges prior to pumping.

Extinction depths were estimated empirically by trial and error to approximate discharge differences between Big Spring and other springs in the JSWC. Discharge from Big Spring responds quickly to recharge events (fig. 4) and pumping from carbonate rocks (fig. 19). Big Spring was simulated as capture-limited because it ceased flowing in response to pumping wells LCPW-1 and LCW-6. An extinction depth of 0.5 ft was specified to model cells representing Big Spring and adequately replicated observed changes in discharge during the 2016 carbonate-rock aquifer test. Discharge from other springs in the JSWC changed minimally in response to recharge events and during the aquifer test. Extinction depths of 16 and 25 ft were assigned to spring NS-05 and all other springs, respectively.

Discharges from phreatophyte and playa areas that were simulated as specified heads in the LC-SS model (fig. 29) also were simulated as specified heads in the LC-MWAT2016 model with a value of zero. The specified heads simulated unconstrained no-drawdown boundaries on the floors of

Independence and Goshute Valleys. Specified heads were not converted to capture-limited boundaries because capture was small in these areas and never exceeded 0.1 acre-ft/yr relative to simulated predevelopment discharges of 5,250 acre-ft/yr in the LC-SS model.

Calibration

Hydraulic conductivity, specific yield, storage coefficient, and recharge distributions were estimated by minimizing a weighted composite, sum-of-squares objective function. The objective function defines misfit between measured data and simulated equivalents and is minimized by changing parameters. Adjustable parameters include hydraulic conductivities, specific yields, specific storages, and recharge rates. Parameters are estimable at pilot points in areas where simulated results are sensitive to parameter changes, and data exist to judge goodness of fit. However, parameter estimation is not effective at pilot points where data are unavailable.

Hydraulic-property and recharge distributions were defined with 668 pilot points, where about 70 percent of the pilot points were adjusted with PEST (Doherty, 2010a). Differences between measured observations and simulated values formally defined the goodness of fit or improvement of calibration. Calibration quality also was assessed by qualitative assessment of estimated hydraulic-property distributions and biases in residuals.

Stress responses were simulated with the integrated LC model, which was called by PEST (fig. 31). The integrated LC model initially translated estimated hydraulic conductivities, specific yields, storage coefficients, and recharge rates at pilot points into two-dimensional MODFLOW arrays. Stress-response models were executed sequentially, where each model read the same hydraulic-property arrays from a common directory (fig. 31). Simulated responses from both groundwater-flow models were compared to measured observations. Results from all models simultaneously informed PEST, and parameter changes were estimated iteratively until the objective function had been minimized. The objective function was informed by measurement and regularization observations.

Calibration with regularization was used to improve simulated hydraulic properties where limited observation data are available. Tikhonov regularization informs the objective function of conceptual models for parameters relatively insensitive to measurement observations and is specified as prior information. Tikhonov regularization provides information in the form of either preferred values of parameters or preferred relations between parameters (Doherty, 2010a). These preferred values or relations are regularization observations, which are added as prior information to the PEST control file (Doherty, 2010a). A hypothetical example of a preferred condition is the assumption of a homogeneous transmissivity of 1,000 ft^2/d in a hydrogeologic unit. For each hydraulic-conductivity pilot point in the hydrogeologic unit, the regularization observation would be the transmissivity (1,000 ft^2/d) divided by the hydrogeologic unit thickness. During calibration with PEST, measurement and regularization objective functions are minimized simultaneously by allowing measurement observations to inform parameters where data are present and regularization observations (preferred conditions) to inform parameters where measured observations are absent.

Measurement Observations

Measurement observations characterized steady-state flow and pumping effects. Observations used for modeling steady-state flow included water-level altitudes, transmissivities, and annual volumes of recharge and groundwater discharge (table 13). Measured water-level altitudes included groundwater levels in wells, spring-pool altitudes, and land-surface altitudes. Land-surface altitudes were used to maintain awareness of areas where simulated water-level altitudes exceeded land surface. Transmissivity observations include single-well aquifer-test results and transmissivity estimates from specific capacities. Annual volumes of recharge and groundwater discharge based on the conceptual distributions were included as preferred estimates of water availability but were minimally weighted during parameter estimation. Drawdowns and changes in spring discharges in response to the 2016 carbonate-rock aquifer test characterized pumping effects (table 13).

Weights were assigned to observations to represent observation accuracy and importance of each observation to model fit. For example, water-level altitude observations were weighted progressively less as observations were more uncertain, which resulted in weighting water levels from drillers' logs less than water levels in wells measured by other sources. Weights also were adjusted to ensure that equal consideration was given to observation groups considered to have the same accuracy. For example, log-transmissivities from 48 sites ranged from 0.2 to 4.9 $\log(ft^2/d)$, whereas water-level altitudes in 189 wells ranged from 5,425 to 7,225 ft above NAVD 88. Transmissivity observations would not affect calibration if log-transmissivities from aquifer tests and water-level altitudes in wells were weighted equally.

Weights were adjusted iteratively so all observation groups affected model calibration. Mismatches in scatter plots of water-level altitudes and transmissivities, spatial distributions of water-level residuals, profiles of predevelopment water levels, and hydrographs of drawdowns and spring captures directly informed the relative importance of observation groups on model calibration. Simulated water levels, drawdown extents, transmissivity, specific yield,

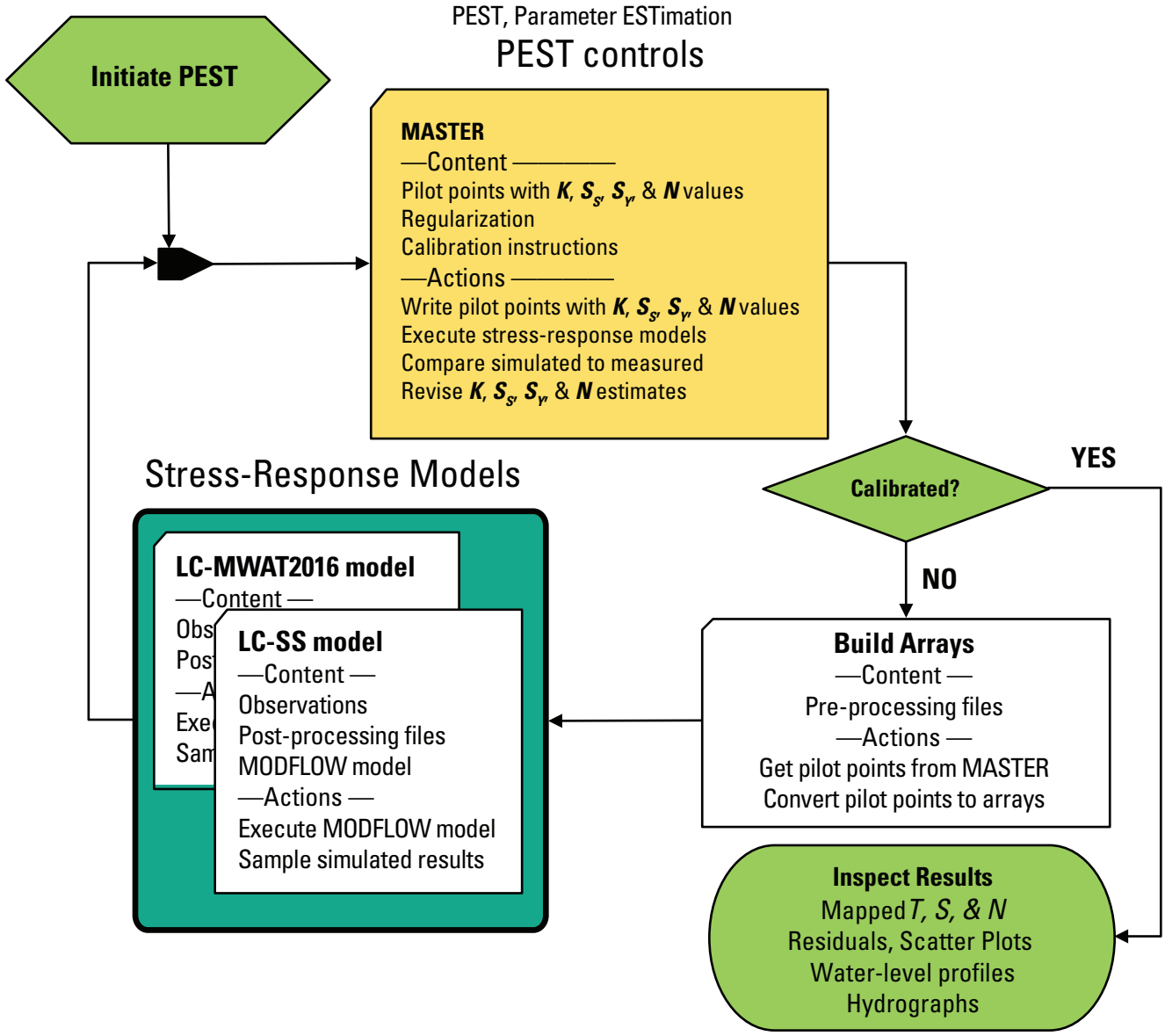

Figure 31. Integrated stress-response model, where K is hydraulic conductivity, S_s is specific storage, S_y is specific yield, N is recharge, T is transmissivity, and S is storativity.

specific storage, and recharge distributions were examined for conceptual inconsistencies. For example, simulated transmissivities exceeding 1,000 ft²/d in low-permeability rocks are conceptually inaccurate. This problem typically identified a misclassified hydrogeologic unit, a compensating error, or an insensitive parameter that drifted to an upper limit. Influence of each observation group on calibration was best summarized by sum-of-squares (table 13) because the weighted sum-of-squares residuals for each observation group integrates the number of observations, range of measurement values, and relative weighting.

Water Levels in Wells and Spring Pools

Simulated water levels in wells and spring pools were sampled from a single MODFLOW layer for comparison to measured water-level altitudes and changes. For 184 of 189 wells and piezometers with open intervals less than 100 ft in length, a single MODFLOW layer was assigned. For the remaining five wells and piezometers penetrating multiple MODFLOW layers, water levels were assigned to the most transmissive layer as conceptualized in the hydrogeologic framework. The most transmissive layer was used because water levels in wells most closely represent water levels in the most transmissive interval of a formation.

Table 13. Summary of observations and fit to simulated comparisons of models LC-SS and LCMWAT2016, Long Canyon, Goshute Valley, northeastern Nevada.

[**Model:** LC-SS, Long Canyon Steady State model; LCWAT2016, Long Canyon Multiple-well Aquifer Test 2016 model. **RMS error:** Root-mean-square error. **Abbreviations:** acre-ft/yr, acre-feet per year**;** ft, feet; $(ft/[acre\text{-}ft/yr])^2$, feet per acre-feet per year squared; $(ft/ft)^2$, foot per foot squared; $(ft/[gal/min])^2$, foot per gallon per minute squared; $(ft/log[ft^2/d])^2$, foot per log of foot squared per day squared; gal/min, gallon per minute; $log(ft^2/d)$, log of foot squared per day; –, not applicable]

Model	Observation group	Count	Sum-of-squares of weighted residuals (feet squared)	Sum-of-weights squared	RMS error
LC-SS	Regional water level altitude	42	13,342	$2.\times10^{1}$ $(ft/ft)^2$	23 ft
	Local water level altitude	147	11,220	$6.\times10^{11}$ $(ft/ft)^2$	13.6 ft
	Spring pool altitude	22	2,373	$2.\times10^{1}$ $(ft/ft)^2$	10.4 ft
	Water-table comparison to land surface	502	646	$1.\times10^{0}$ $(ft/ft)^2$	23 ft
	Transmissivity from slug tests	22	608	$2.\times10^{2}$ $(ft/log[ft^2/d])^2$	1.8 $log(ft^2/d)$
	Transmissivity from aquifer tests	6	21,417	$1.\times10^{5}$ $(ft/log[ft^2/d])^2$	0.4 $log(ft^2/d)$
	Transmissivity from specific capacities	20	1,665	$7.\times10^{3}$ $(ft/log[ft^2/d[)^2$	0.5 $log(ft^2/d)$
	Conceptual discharge volumes	17	991	$2.\times10^{5}$ $(ft/[acre\text{-}ft/yr])^2$	70 acre-ft/yr
	Conceptual recharge volumes	10	7,285	$1.\times10^{5}$ $(ft/[acre\text{-}ft/yr])^2$	210 acre-ft/yr
LC-MWAT2016	2016 aquifer-test drawdowns	7,395	27,655	$1.\times10^{5}$ $(ft/ft)^2$	0.5 ft
	2016 aquifer-test spring captures	2,090	442	$2.\times10^{0}$ $(ft/[gal/min])^2$	13 gal/min
	All observations	10,273	87,643	–	–

Simulated water levels in wells and spring pools were interpolated laterally from model cell centers to measured locations in assigned layers (fig. 32). Simulated water levels mostly were interpolated from nodes of surrounding cells to points of measurement with the PEST utility MOD2OBS (Doherty, 2010b). Well locations of a small number of wells on the edge of the model domain were shifted from their true locations to the model cell centers in MOD2OBS input files. Locations of Big Spring and spring NS-05 pools were shifted to cell centers because simulated discharges exceeded 100 gal/min. Shifted locations are shown in spatial coverages of model results (Nelson and others, 2021).

Water-Table Altitude Comparison to Land Surface

Simulated water-table altitudes were compared to land-surface altitudes to maintain awareness of where the simulated water table exceeded land surface. Land-surface altitudes were defined with a Digital-Elevation Model (DEM) that sampled 1:24,000-scale maps every 30 m and reported to the nearest whole meter (Gesch and others, 2009). Land-surface altitudes were sampled from the DEM at 502 locations (fig. 32). Simulated water levels that were below land surface were replaced with the land-surface altitude so the residual difference between the water level and land surface equaled zero and did not affect model calibration. For example, a simulated water-table altitude that initially equaled 5,700 ft would be changed to 6,000 ft, where land-surface altitude is 6,000 ft, and the residual would be 0 ft. Alternatively, a simulated water-table altitude that initially equaled 6,500 ft at the same location would not be changed and the residual would be 500 ft. Water-table altitude comparisons to land surface were weighted much less than measured water levels in wells.

Transmissivity Comparisons

Transmissivity estimates from single-well aquifer tests, specific capacities, and slug tests were compared to simulated transmissivities. Simulated transmissivities were defined by the area investigated by each aquifer test (fig. 32). Simulated transmissivities were averaged by model layer within the area investigated (Halford, 2016). The area of investigation was the radial distance from the pumped well where drawdowns exceeded 0.1 ft at the end of each aquifer test, but the radial distance was not allowed to exceed 7,000 ft (fig. 32). Contributing thickness was limited to the well screen length if transmissivity was less than 1,000 ft^2/d or small volumes of water were displaced, as occurs with slug tests. For aquifer tests where transmissivity exceeded 1,000 ft^2/d or large volumes (more than 100,000 gal) of water were pumped (Halford and others, 2006), the contributing thickness was the aquifer thickness from the hydrogeologic framework model. Simulated transmissivities summed all layer-averaged transmissivities investigated by each aquifer test (Halford, 2016, p. 10). Estimated transmissivities from aquifer tests, specific capacities, and slug tests (table 10) are discussed herein as measured transmissivities for comparison to simulated transmissivities from the LC-SS model.

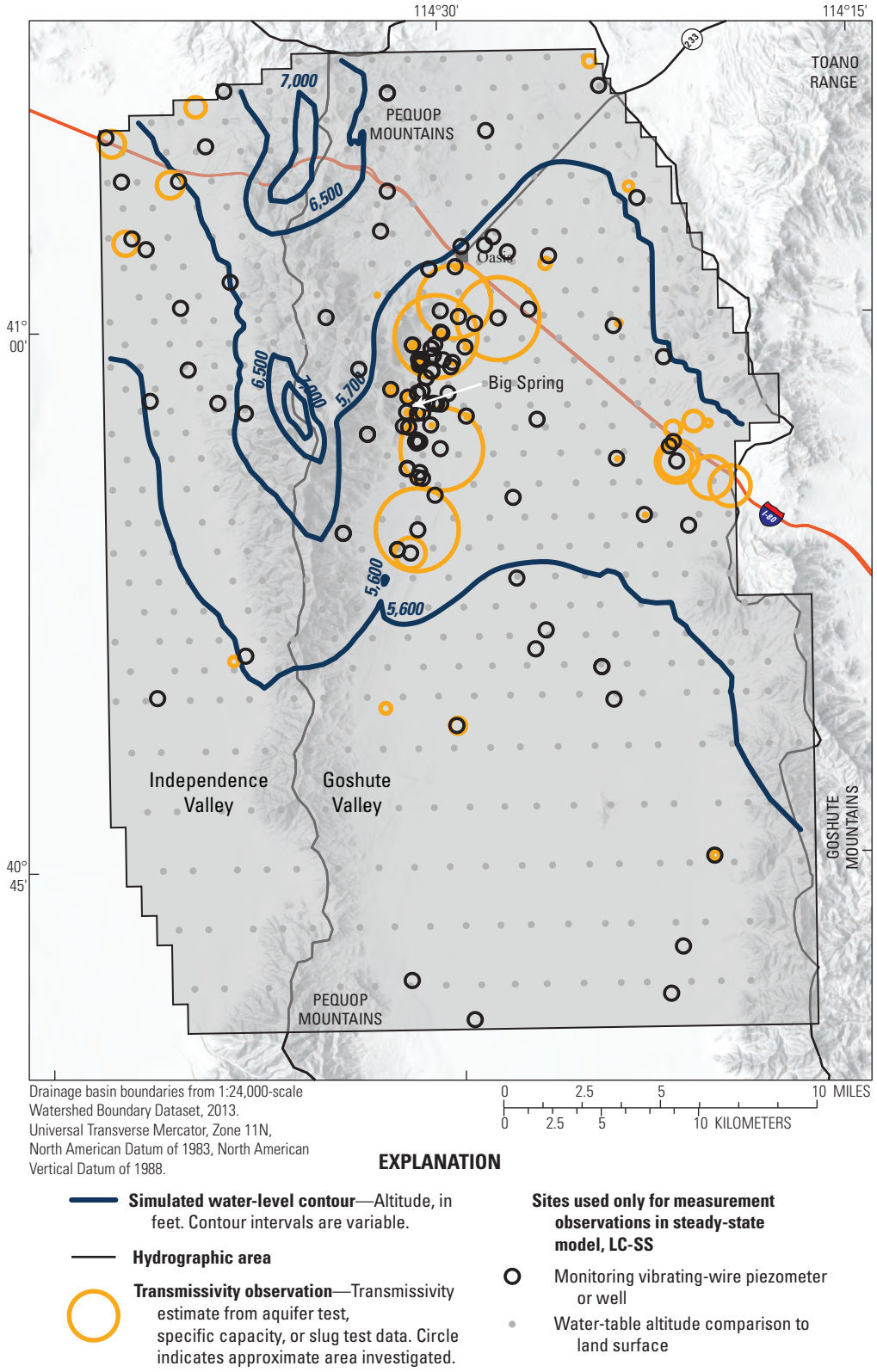

Figure 32. Locations and types of measurement observations used in the Long Canyon Steady State (LC-SS) model that simulated predevelopment conditions, Long Canyon, Goshute Valley, northeastern Nevada.

Measured transmissivities were considered more representative as pumping volumes increased because greater volumes of aquifer were investigated. Measured transmissivities from aquifer tests were most representative with millions of gallons pumped during each test. Measured transmissivities from slug tests were least representative where each test displaced less than 10 gal. Measured and simulated transmissivity comparisons for slug tests were discounted further because investigated volumes were small relative to any cell in the LC-SS model. Transmissivity observations were weighted accordingly with weights ranging from 3 ft/log(ft²/d) for slug tests to 305 ft/log(ft²/d) for the BSR-2 aquifer test.

Annual Volumes of Recharge and Groundwater Discharge

The model area was divided into ten zones to calibrate annual volumes of groundwater recharge and discharge (fig. 33). Zone boundaries were small enough to capture spatial variability between zones, but remained large enough to balance local recharge and discharge within each zone. Zones were delineated along no-flow boundaries as interpreted from the potentiometric surface (fig. 7) and water-quality interpretations (figs. 9 and 11–13) so that groundwater discharge should equal recharge within zones. Three zones in the Pequop Mountains generated about two-thirds of all recharge (fig. 29). Playa areas were differentiated with an annual discharge of 0 acre-ft (fig. 33). Simulated annual volumes of recharge and groundwater discharge were sampled from the LC-SS model using ZONEBUDGET (Harbaugh, 1990).

The "Johnson Springs Catchment Area" compares reasonably well with the "high-altitude carbonate recharge area" (fig. 9) proposed as the source of water to the JSWC. The simulated "Johnson Springs Catchment Area" extends somewhat farther north and northeast and includes some areas below 7,200 ft in altitude compared to the proposed "high-altitude carbonate recharge area," which partly explains the simulated recharge being about 30-percent larger than expected (table 14).

Annual volumes of recharge and groundwater discharge were conceptual observations that are well understood, but quantified poorly. These observations were included in the objective function in part to formally influence parameter estimation, but primarily to maintain awareness of departures between numerical and conceptual models. Conceptual observations were weighted minimally because values were uncertain.

Drawdown and Water-Level Rises

Drawdowns and water-level rises caused by the 2016 carbonate-rock aquifer test were differentiated from environmental water-level fluctuations; test-induced aquifer stresses were attributed to pumping wells LCPW-1 and LCW-6, ditch leakage, and spring supplementation (fig. 30). Comparable drawdowns and water-level rises from these stresses were simulated in the LC-MWAT2016 model. Simulated drawdowns and water-level rises were compared with point measurements by interpolating node values from cells surrounding point locations with MOD2OBS (Doherty, 2010b) as occurred with steady-state water levels. Simulated hydrographs were compared in 83 wells and piezometers (fig. 20, Smith and others, 2021, appendix 3)

Drawdowns and water-level rises were condensed to daily averages for comparison with simulated equivalents in the objective function. These daily averages are discussed as measured drawdowns and water-level rises where compared to simulated equivalents. Averaging eliminated noisy drawdown estimates from VWPs (fig. 34*A*, well CLC-608A) and high-frequency fluctuations that were not simulated (fig. 34*B*, well LCMW-22S).

Spring Capture

Measured spring capture (differences in measured discharge or stage) and simulated capture were compared at 22 springs in the JSWC (fig. 21, table 12, Smith and others, 2021, appendix 3). Limited capture was simulated by combining the river and drain packages in MODFLOW (Harbaugh, 2005). Simulated spring capture was computed by subtracting the predevelopment discharge injected in the river package from the water removed in the drain package. Simulated flow rates from the river and drain packages were extracted with a variation of ZONEBUDGET (Harbaugh, 1990) to compute capture. Simulated capture could not be computed directly from ZONEBUDGET because this utility only reports flows across zone faces and flows from individual MODFLOW packages for each zone, and rates from multiple packages are not combined. The modified program, MOD2BUD, computed capture by reading flows from the cell-by-cell output file from MODFLOW. MOD2BUD sums rates from multiple packages, converts units, interpolates rates between time steps, and reports time series values for each zone. Source code for MOD2BUD is provided in the USGS data release for this report (Nelson and others, 2021).

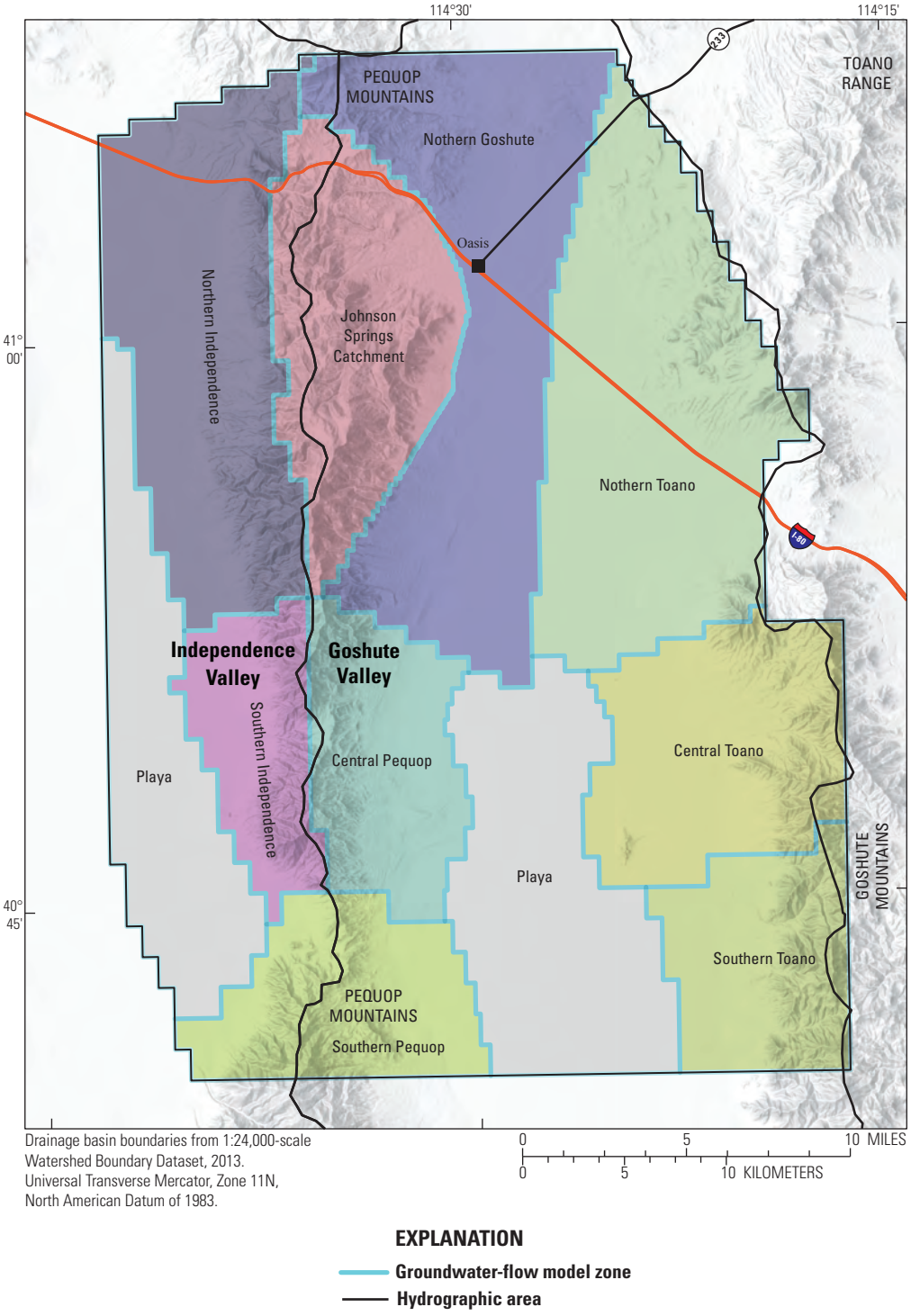

Figure 33. Groundwater-flow model zones for comparing annual volumes of recharge and groundwater discharge, Long Canyon, Goshute Valley, northeastern Nevada.

Table 14. Observed and simulated annual volumes of recharge and groundwater-discharge, Long Canyon, Goshute Valley, northeastern Nevada.

[All values are in acre-feet]

Area	Annual recharge			Annual discharge		
	Observed	Simulated	Residual	Observed	Simulated	Residual
Northern Goshute	1,220	1,500	280	1,220	1,290	70
Johnson Springs catchment	2,750	3,570	820	2,760	2,740	-20
Northern Independence	1,380	1,120	-260	1,370	1,360	-10
Southern Independence	290	270	-20	290	230	-60
Central Pequop	550	340	-210	550	540	-10
Southern Pequop	400	210	-190	400	310	-90
Southern Toano	320	170	-150	320	260	-60
Central Toano	380	320	-60	380	410	30
Northern Toano	700	460	-240	700	560	-140
Playa	0	0	0	0	260	260
Totals	7,990	7,960	-30	7,990	7,960	-30

Regularization Observations

Tikhonov regularization informed hydraulic conductivity, specific yield, specific storage, and recharge-rate parameters that were insensitive to measurement observations during model calibration (Doherty, 2010a). Tikhonov regularization observations were equations that defined preferred relations between pilot points. These relations were ratios between preferred values at each pilot point. For example, preferred hydraulic conductivities of 0.3 and 30 ft/d at two pilot points would specify a preferred ratio of 100. Hydraulic-conductivity estimates of 5 and 500 ft/d at the two pilot points would perfectly agree with the preferred relation because the ratio is 100.

If the preferred relation is homogeneity, then pilot points within a zone are assigned the same initial preferred value and the preferred ratio between pilot points is 1. By invoking homogeneity, Tikhonov regularization limits differences between pilot points by penalizing sharp differences, and thereby ensuring relatively continuous distributions (Doherty and Johnston, 2003). Contrasts within hydrogeologic units and the recharge distribution were penalized minimally in areas where data informed the objective function.

The preferred relation between pilot points for the recharge distribution was based on the conceptual average annual recharge (fig. 6). Initial recharge estimates at pilot points were sampled from the conceptual recharge distribution (fig. 6). Recharge rates were estimated independently at all pilot points, but preferred ratios of conceptual recharge rates did not change between pilot points during calibration. A maximum of 1,500 regularization observations initially constrained recharge estimates using preferred relations.

Each hydrogeologic unit was conceptualized with a homogeneous transmissivity (table 11) so that preferred hydraulic conductivities differed because of differences in thickness. Preferred hydraulic conductivity equaled preferred transmissivity of a hydrogeologic unit divided by thickness of the hydrogeologic unit at a pilot point. About 8,000 regularization observations initially constrained hydraulic-conductivity estimates using preferred relations.

Homogeneity was the preferred relation between pilot points for specific yield and specific storage. Preferred values of specific yield for basin fill and carbonate rocks were 0.08 and 0.01, respectively (table 11). Preferred values of specific storage for basin fill and consolidated rocks were 2×10^{-7} and 1.5×10^{-6} 1/ft, respectively. About 300 regularization observations initially constrained specific-yield and specific-storage values using preferred relations.

Regularization observations were weighted so that preferred relations were emphasized where measurement observations were few. Regularization observations were weighted relative to distances between pilot points and nearest measurement sites. Weights between pilot-point pairs were equal to 1 where the distance between the two pilot points was less than the distance between the points and the nearest measured water level. Weights decreased as the distance between the two pilot points exceeded the distance between the points and the nearest measured water level. Distances between measurement sites were less than 1 mi through the Long Canyon Mine project area and exceeded 3 mi in northern Toano Range and southern extents of the area of interest (fig. 7).

Unrealistic hydraulic-property distributions were minimized during calibration by preventing over-fitting of the measurement observations (Fienen and others, 2009). Goodness of

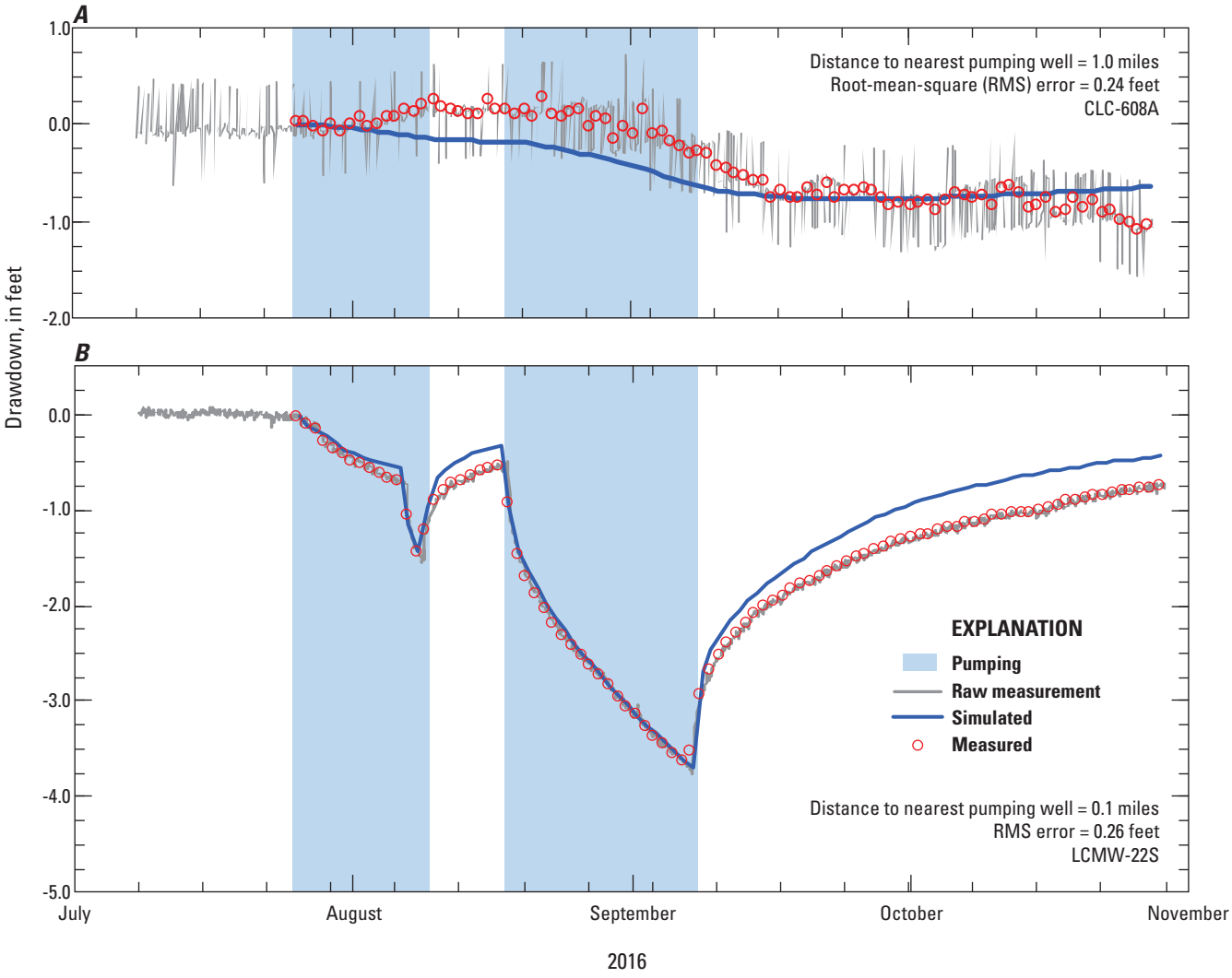

Figure 34. Periods when wells LCPW-1 and LCW-6 were pumped, and simulated and measured drawdowns in (*A*) vibrating-wire piezometer CLC-608A, and (*B*) well LCMW-22S, Long Canyon, Goshute Valley, northeastern Nevada, July–November 2016. Simulated drawdowns are from the Long Canyon Multiple-well Aquifer Test 2016 (LC-MWAT2016) model and measured drawdowns are estimated from water-level models.

fit between measured and simulated values was limited so that the weighted, sum-of-squares error could not subceed measurement and numerical model errors. The variable PHIMLIM in a PEST control file (Doherty, 2010a) is the expected weighted, sum of squares error representing the average allowable misfit between measured and simulated values at each well or piezometer. A PHIMLIM of 85,000 ft^2 was specified, which is equivalent to an RMS error of about 17 ft for water-level measurements.

Goodness of Fit

Goodness of fit was evaluated with scatter plots, a map of residuals (simulated minus measured), water-level profiles, hydrographs, and hydraulic-property distributions. Steady-state calibration was evaluated with scatter plots of simulated and measured water-level altitudes and transmissivities. A map of predevelopment (steady-state) water-level residuals identified systematic spatial biases. Agreement between vertical and lateral gradients was checked with profiles of measured and simulated water levels. Calibration of the 2016 carbonate-rock, aquifer-test model, LC-MWAT2016, was evaluated by agreement between measured and simulated hydrographs of water-level changes (drawdown or rise) in each well and agreement between measured and simulated changes in spring discharges (table 13). Significant hydrologic features have been identified in conceptual models from water-level profiles, hydrographs, transmissivity estimates, and a refined hydrogeologic framework. Simulation of these hydrologic features was evaluated qualitatively by comparing measured water-level profiles and hydrographs to simulated equivalents and examining simulated hydraulic-property distributions.

Predevelopment Steady-State Observations

Simulated water levels compare favorably to measured water levels in the LC-SS model (fig. 35). Average and RMS water-level errors of –2 and 17 ft, respectively, are not large relative to the 1,100-ft range of measured water levels (fig. 35). Measured water-level altitudes range from 5,546 to 6,645 ft from the floor of Goshute Valley to the Pequop Mountains north of I-80, respectively. Simulated spring-pool altitudes were biased low and averaged 6 ft less than measured spring-pool altitudes in the LC-SS model (fig. 35). The RMS spring-pool altitude error was 10 ft. Simulated and measured ranges in spring-pool altitude were similar at 33 and 29 ft, respectively.

Mapped water-level residuals show little spatial patterns of significance, suggesting a good overall fit between simulated and measured water levels (fig. 36). Water-level residuals average about 15 ft through the Long Canyon Mine project area. Water-level residuals exceed 60 ft in high-altitude, high-relief, low-transmissivity areas such as northern Pequop Mountains, but have little positive or negative spatial bias (fig. 36). Water-level residuals of more than 60 ft are expected in high-relief areas because simulated water levels are sensitive to small amounts of recharge across low-permeability rocks. Additionally, simulated water levels computed at cell centers represent averages that are being compared to average land-surface altitudes that can vary by more than 1,200 ft within a model cell.

Simulated water-table altitudes exceed land surface in the northern Pequop Mountains, where land-surface altitudes exceed 6,900 ft (fig. 36). Simulated water levels exceeded land surface primarily because of well 410341114315301 and piezometer LCP-58C with measured water levels of 6,231 and 6,645 ft, respectively. Measured water levels are within 100 ft of land surface at both sites and at well NDWR126309, which supports simulated water levels being similar to land-surface altitudes. Maximum exceedance was less than 200 ft, which is small relative to greater than 1,200 ft of change in land-surface altitude within a cell.

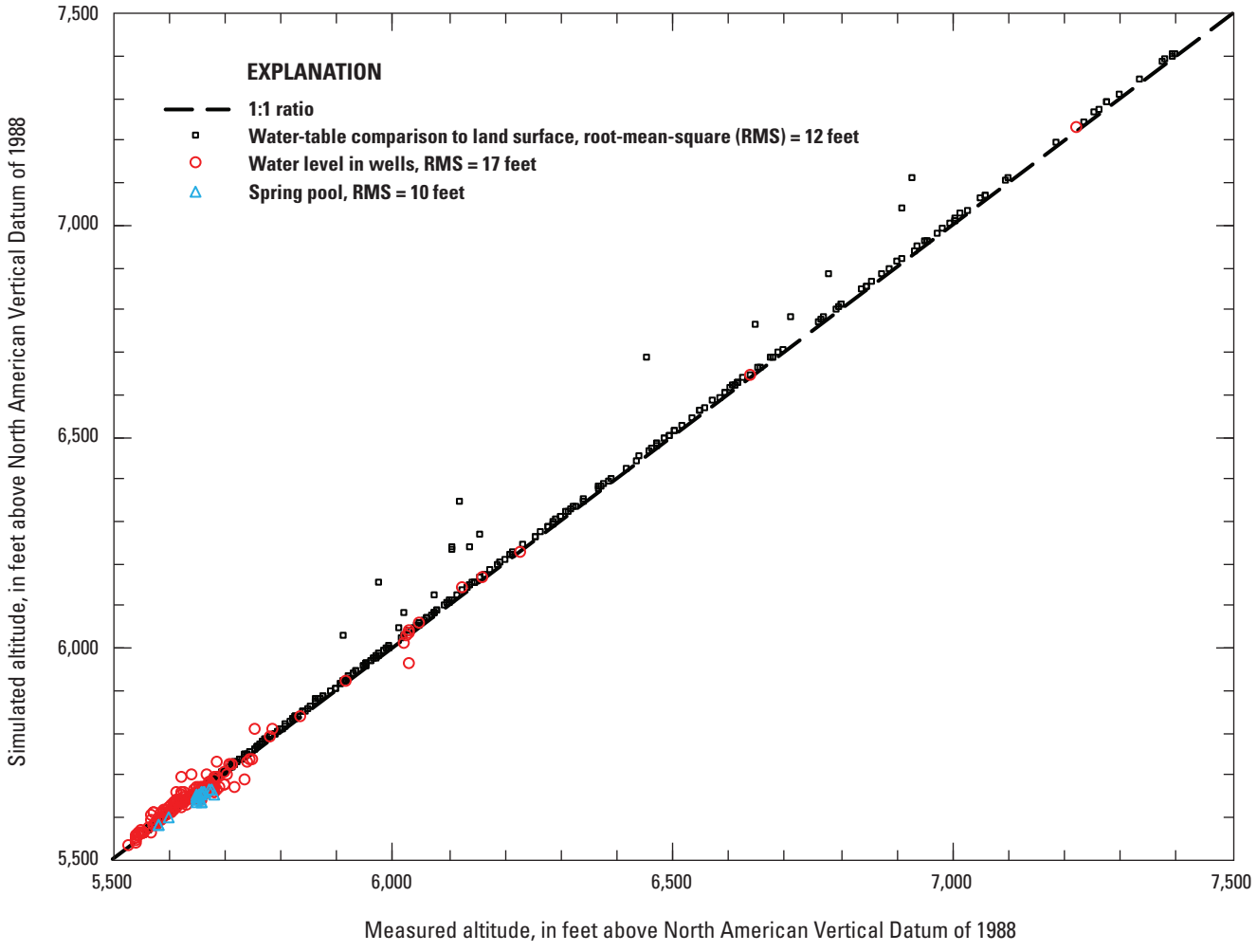

Figure 35. Comparison of simulated water-level altitudes from the calibrated Long Canyon Steady State (LC-SS) model to estimated land-surface altitudes, spring pool altitudes, and measured water-level altitudes in wells, Long Canyon, Goshute Valley, northeastern Nevada.

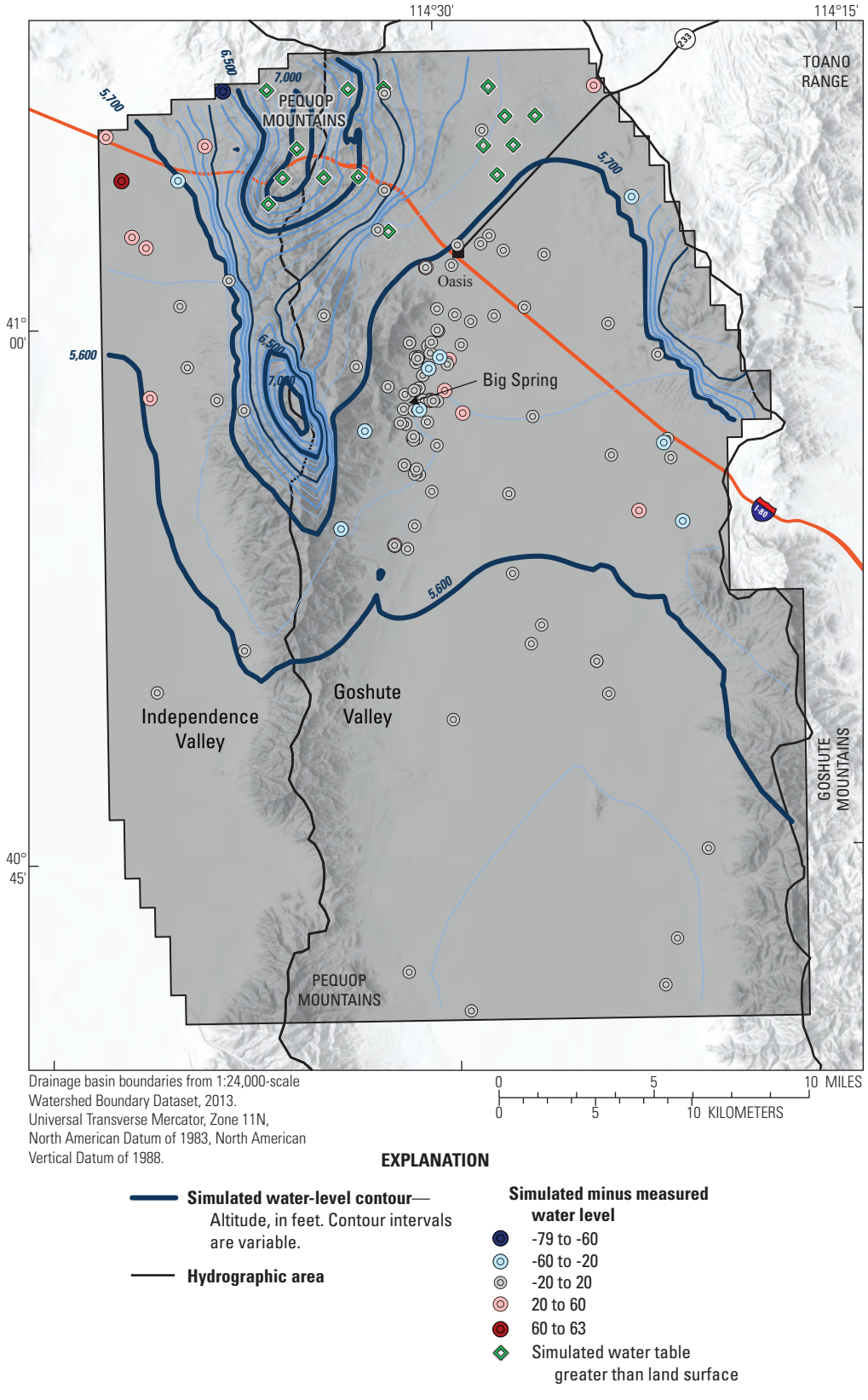

Figure 36. Simulated steady-state water-level contours and water-level altitude residuals (simulated minus measured water level) in the Long Canyon Steady State (LC-SS) model, Long Canyon, Goshute Valley, northeastern Nevada.

Simulated and measured transmissivities from single-well aquifer tests and specific capacities generally agree, with 88 percent of sites within the 95-percent confidence interval (fig. 37). Simulated and measured transmissivities from aquifer tests and specific capacities geometrically average 900 and 1,140 ft²/d, respectively. The log standard deviation of residuals from just aquifer-test transmissivity observations is 0.8, which represents a multiplier of 7. Measured transmissivities from slug tests geometrically average 270 ft²/d, which is an order of magnitude less than simulated transmissivities with a geometric mean of 2,400 ft²/d. Measured transmissivities from slug tests represent the maximum transmissivity that was estimable from the test and are considered a lower bound. Large differences between simulated and measured transmissivities are consistent with small investigated volumes of slug tests and the difficulty of estimating large representative transmissivities (Frus and Halford, 2018). Simulated transmissivities range from 5 to 300,000 ft²/d, or about five orders of magnitude. This is similar to measured transmissivities that range from 2 to 80,000 ft²/d, also about five orders of magnitude.

Annual volumes of simulated and expected groundwater discharge differ by only 30 acre-ft, where simulated discharge totals 7,960 acre-ft and expected discharge totals 7,990 acre-ft (table 14). Simulated and expected annual volumes of recharge and groundwater discharge largely agree in rate and location (table 14). The largest discrepancy was for annual volumes of recharge to the JSWC, where simulated and measured volumes totaled 3,570 and 2,750 acre-ft, respectively. Conceptual and simulated catchment areas differed because Lower simulated recharge rates than conceptual recharge rates indicate that simulated and conceptual catchment areas differed. The simulated catchment area was smaller than the conceptual catchment area to match measured annual volumes of groundwater discharge for JSWC (table 14). Simulated and measured annual volumes of groundwater discharge for Johnson Springs catchment agree because discharge was specified.

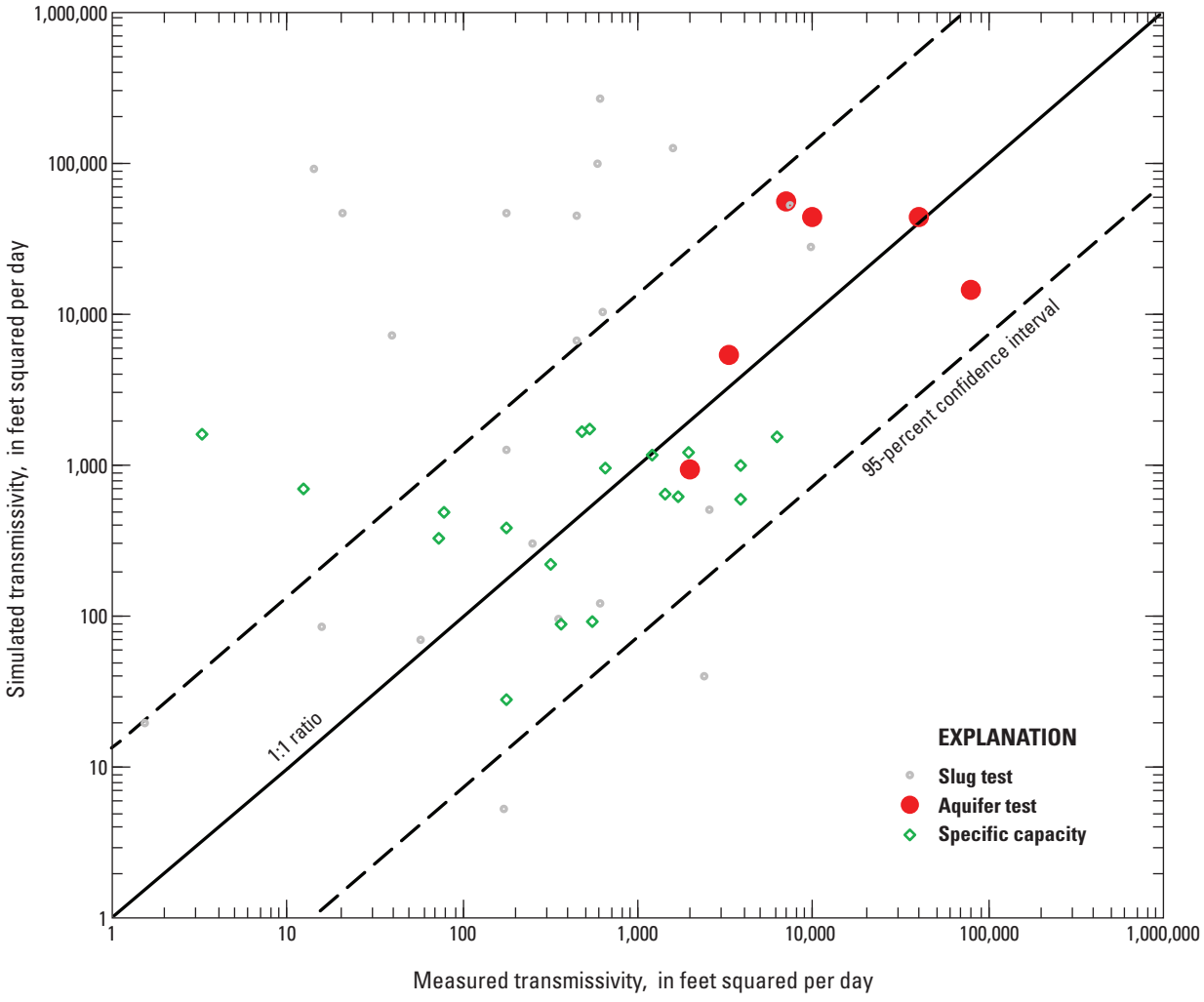

Figure 37. Comparison of simulated and measured transmissivities from the calibrated Long Canyon Steady State (LC-SS) model, Long Canyon, Goshute Valley, northeastern Nevada.

2016 Carbonate-Rock Aquifer Test

Heterogeneous transmissivity and specific-yield distributions were estimated in the Long Canyon Mine project area to match drawdowns and water-level rises from the 2016 carbonate-rock aquifer test. Transmissivities in the HTZ ranged from 10,000 to 23,000,000 ft^2/d with the most transmissive areas occurring around Big Spring (fig. 38). Simulated drawdowns in the HTZ matched measured values with little attenuation or delay between changes in pumping rates and pumping wells (fig. 34, well LCMW-22S). The northernmost drawdown measurement of about 1 ft at piezometer CLC-608A was simulated with an RMS error of 0.24 ft (fig. 34). Westernmost drawdown measurements of about 4 and 1 ft in piezometers CLC-339A and CLC-339B, respectively (Smith and others, 2021, appendix 3), were simulated with an RMS error of 1.7 and 0.39 ft. Simulated drawdowns in wells CLC-339A and CLC-339B differed little with depth with a maximum drawdown of 2 ft.

Simulated drawdowns in carbonate rocks were well constrained in all directions except to the south (fig. 38). Southernmost drawdown measurements occurred in well LCMW-09D, S, located 2.2 miles from the nearest pumping well (fig. 39*B*). Maximum drawdown in well LCMW-09S was 2.8 ft with responses similar to drawdowns in well CLC-625D (fig. 39*C*), which is within 0.2 mi of pumping well LCW-6. Simulated and measured drawdowns in wells LCMW-09S and CLC-625D agreed, with RMS errors of 0.20 and 0.24 ft, respectively (fig. 39). Simulated responses to pumping changes show little attenuation or delay, which suggests that drawdown propagated south of well LCMW-09S in carbonate rocks. This is consistent with simulated drawdowns of 1 ft extending 3 mi south of well LCMW-09S when pumping ceased (fig. 38).

Water-level rises from ditch leakage and spring supplementation during the 2016 carbonate-rock aquifer test were not simulated as accurately as pumping-induced drawdowns with the LC-MWAT2016 model (fig. 40). Significant mismatches between simulated and measured water-level rises are indicated in RMS errors that ranged from 0.43 to 1.19 ft. These errors are expected because the magnitude and distribution of ditch leakage and spring supplementation were defined poorly, unlike pumping from wells LCPW-1 and LCW-6 (fig. 30). Water-level rises in well LCMW-20 were underestimated by 0.8 ft, with the nearest ditch leakage specified 1.3 mi away

Observed maximum water-level rises of 3.1 and 1.7 ft in wells LCP-27A and LCP-27B, respectively, separated by a 42-ft depth, were not accurately simulated with the LC_MWAT2016 model (fig. 40) because the shallowest simulated hydrogeologic units are 100-ft thick. However, greater water-level rises in LCP-27A than LCP-27B are atypical because LCP-27A, which is completed at 92 ft bls, is 42 ft deeper than well LCP-27B, completed at 50 ft bls. Greater water-level rises at depth suggest that piezometer LCP-27A is completed in more permeable material and better connected to the water table than LCP-27B.

Simulated and measured spring discharges were closely matched in the JSWC, where pumping affected discharge from spring NS-05 and Big Spring (fig. 41). Measured and simulated spring discharges in spring NS-05 and Big Spring agreed with RMS errors of 21 and 5 gal/min, respectively. The RMS errors are small relative to pre-pumping discharges of 700 and 160 gal/min, respectively. Simulated discharges from Big Spring closely matched rapid declines and prolonged recovery in measured discharges (fig. 41). Discharge declines mostly were affected by pumping well LCPW-1 (fig. 30). Simulated and measured periods of no discharge from Big Spring totaled 37 and 36 days, respectively. Discharges from all springs in the JSWC, other than Big Spring and NS-05 springs, were minimally affected by pumping and the LC-MWAT2016 model accurately simulated negligible changes in these springs.

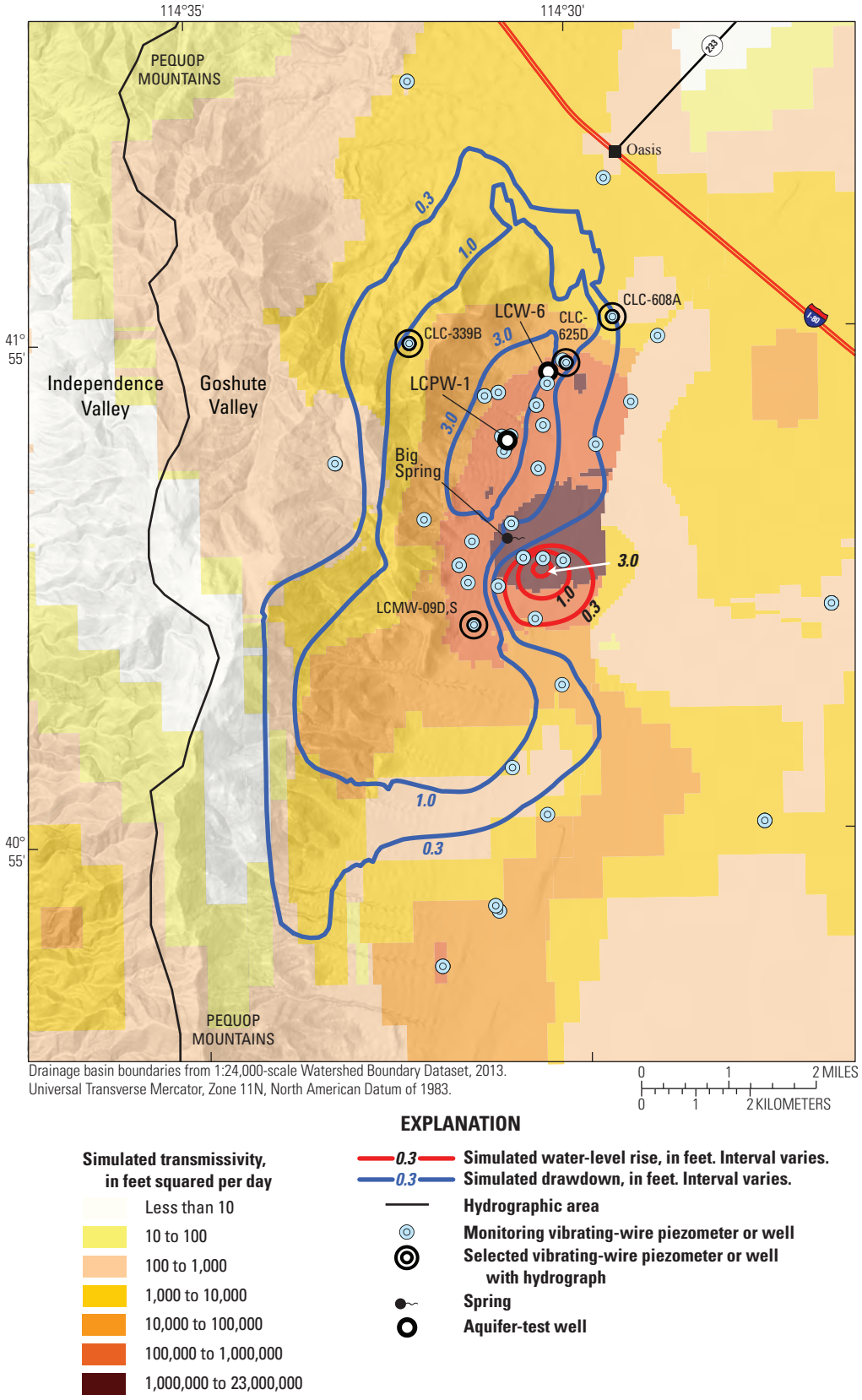

Figure 38. Simulated transmissivity distribution from integrated LC model, hydrograph sites, and simulated drawdowns and water-level rises in layer 4 when wells LCPW-1 and LCW-6 ceased pumping, Long Canyon, Goshute Valley, northeastern Nevada.

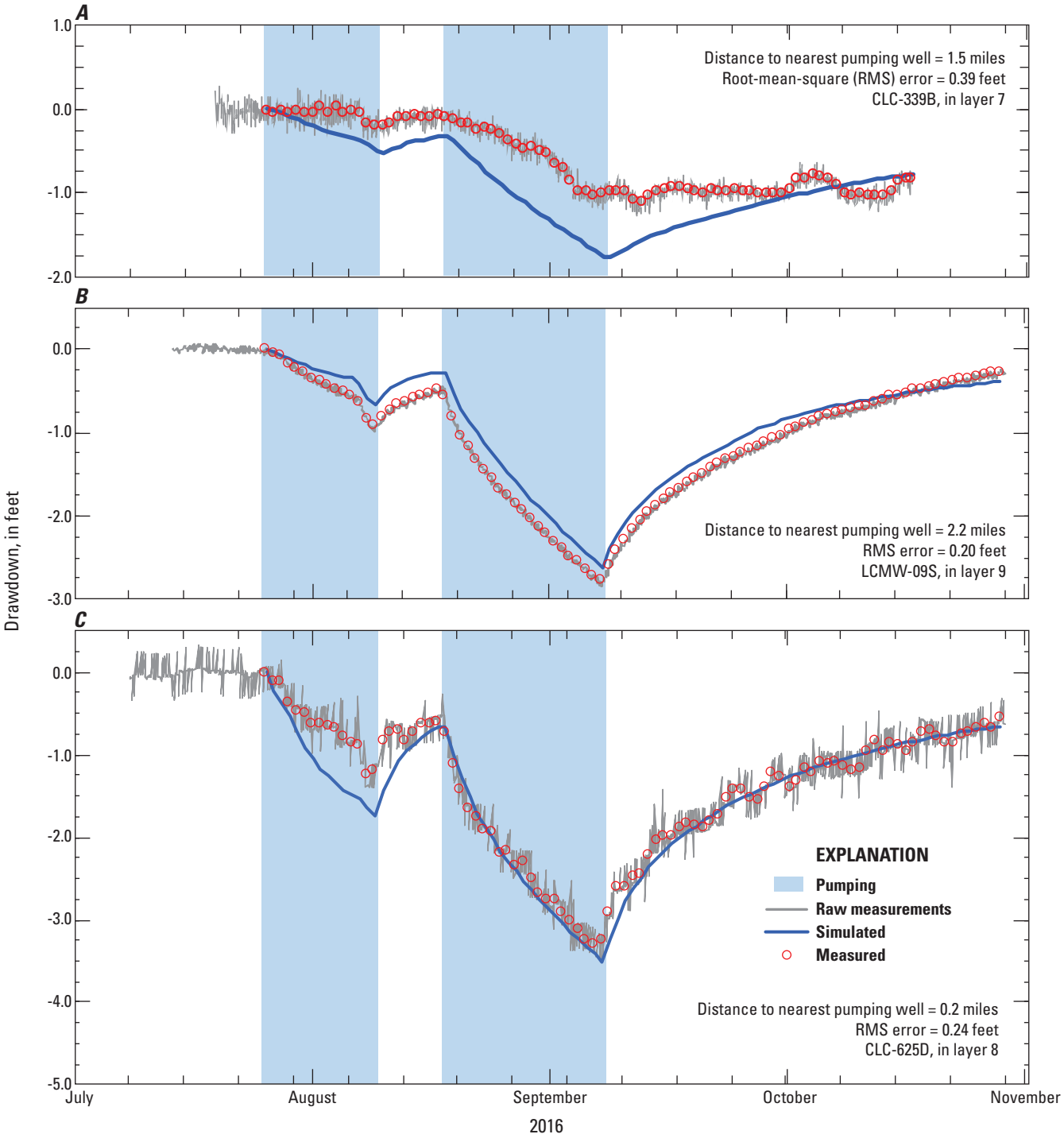

Figure 39. Periods when wells LCPW-1 and LCW-6 were pumped, simulated drawdowns from Long Canyon Multiple-well Aquifer Test 2016 (LC-MWAT2016) model, and measured drawdowns in wells (*A*) CLC-339B, (*B*) LCMW-09S, and (*C*) CLC-625D, Long Canyon, Goshute Valley, northeastern Nevada, July–November 2016.

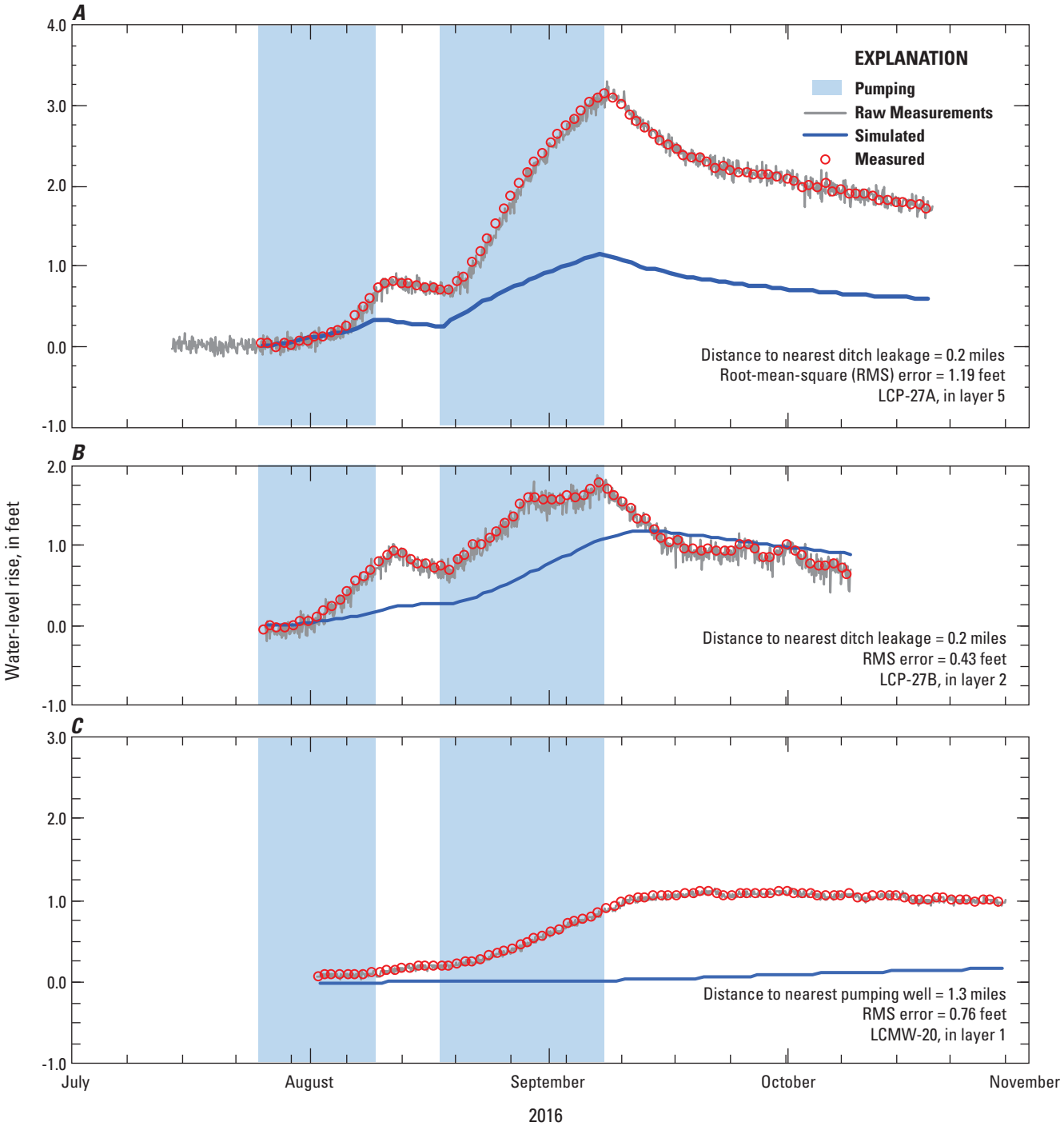

Figure 40. Periods when wells LCPW-1 and LCW-6 were pumped, simulated water-level rises from Long Canyon Multiple-well Aquifer Test 2016 (LC-MWAT2016) model, and measured water-level rises (estimated from water-level models) in wells (*A*) LCP-27A, (*B*) LCP-27B, and (*C*) LCMW-20, Long Canyon, Goshute Valley, northeastern Nevada, July–November 2016.

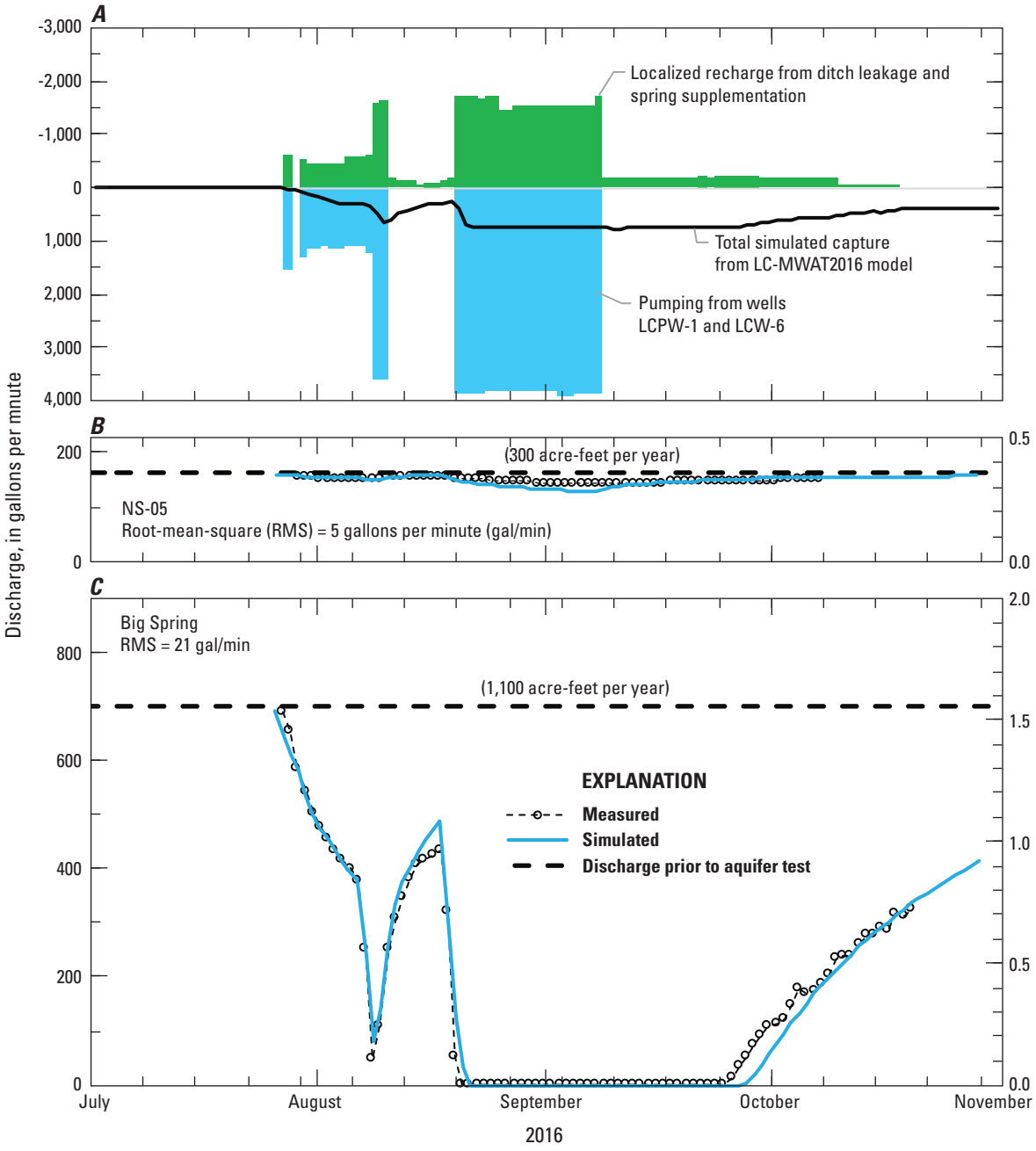

Figure 41. Periods when wells LCPW-1 and LCW-6 were pumped, periods of localized recharge from ditch leakage and spring supplementation, and total simulated capture from Long Canyon Multiple-well Aquifer Test 2016 (LC-MWAT2016) model (*A*); and effects of pumping and localized recharge shown in graph (*A*) on measured and simulated discharges at spring NS-05 (*B*) and at Big Spring (*C*), Long Canyon, Goshute Valley, northeastern Nevada, July–November 2016.

Hydraulic-Property Estimates

Transmissivity, specific yield, and storage coefficient distributions in carbonate-rock and basin-fill aquifers were estimated with the integrated LC model. Bulk hydraulic properties distributed across the Long Canyon area of interest were well constrained by hydraulic testing where drawdowns were detected during the 2016 carbonate-rock aquifer test. Transmissivity estimates also were constrained by single-well aquifer tests, primarily in basin fill.

The transmissivity distribution in carbonate rocks was estimated reliably in a limited extent of the Pequop Mountains. The extent of reliably estimated transmissivity ranged south to north from about 1 mi south of Big Spring to I-80, and ranged west to east from the western edge of Goshute Valley to the eastern edge of carbonate rocks in the Long Canyon Mine project area (figs. 2 and 42). A maximum drawdown of about 3 ft in well LCMW-09S was the southernmost observed detection in carbonate rocks during the 2016 aquifer test (fig. 20). Carbonate rocks extending several miles south of well LCMW-09S likely are transmissive, but this has not been confirmed directly (fig. 42). Northward, about a mile south of I-80, drawdown observations in piezometer LCP-36B were classified as not detected (fig. 20), which is consistent with a maximum simulated drawdown of 0.08 ft. Westernmost drawdowns were bounded between sites CLC-339 and LCP-38 (fig. 20) where drawdowns were detected in Goshute Valley and not detected in Independence Valley.

Relatively low transmissivities were estimated for carbonate rocks of the Pequop Mountains north of I-80. These estimates primarily were informed by steady-state water levels that are 500 to 1,000 ft higher than water levels in the HTZ (fig. 43, cross section B–B′). Simulated recharge rates are similar from the HTZ to the northern extent of the area of interest (fig. 29). Water-level gradients are steepest north of well LCP-75D, indicating that along the B–B′ profile, groundwater flow is least between LCP-58C and LCP-75D and greatest to the south near Big Spring (fig. 43). These conditions require transmissivities north of well LCP-75D to be markedly less than in the HTZ (fig. 43).

Transmissivities of carbonate rocks in the Toano Range and Goshute Mountains are defined poorly (fig. 42). Low transmissivity in the Toano Range north of I-80 is consistent with low recharge rates and elevated water levels in well 405852114215701, which has a water-level altitude of 6,130 ft. This water-level altitude is 400 ft greater than water-level altitudes in the Shafter well field less than 3 mi away. Neither water levels nor specific-capacity data are available for carbonate rocks of the Toano Range south of I-80 or Goshute Mountains.

Transmissivity of basin fill along the eastern flank of the Pequop Mountains through the Long Canyon Mine project area was informed primarily from aquifer tests where pumping wells were open to basin fill (fig. 44). Greater than 80,000,000 gallons were pumped from wells BSR-2, LCT-1, Pequop-1, and Pequop-2 (fig. 2) at rates of 850–2,900 gal/min during the four aquifer tests. Transmissivity estimates of 40,000 and 80,000 ft^2/d from the BSR-2 and Pequop-1 tests, respectively, are consistent with simulated transmissivities in the basin fill (figs. 2 and 44). Simulated transmissivities about 2 mi southeast of Oasis and south of I-80 agree with a 2,000 ft^2/d estimate from LCT-1 (fig. 44). Transmissivities in basin fill were minimally constrained by the 2016 carbonate-rock aquifer test during calibration because poorly known ditch leakage affected water levels more so than pumping (fig. 23).

Basin-fill transmissivity through northern Goshute and Independence Valleys outside the Long Canyon Mine project area was informed largely from specific capacities (fig. 44; table 10). Transmissivity estimates of 1,000 to 7,000 ft^2/d in the Shafter well field along the eastern edge of the area of interest (fig. 2) are more representative than most estimates from specific capacities because large volumes of water were pumped during testing. Transmissivity estimates from specific capacities in all other areas are more uncertain than estimates from the Shafter well field because pumping periods were substantially shorter (fig. 44).

Transmissivity distributions of volcanic and low-permeability rocks were combined because these rocks collectively occupy less than 20 percent of the geologic framework (fig. 45). Direct hydraulic testing of volcanic and low-permeability rocks was minimal. Low transmissivities in the Pequop Mountains, north of I-80 were informed by steady-state water levels (figs. 36 and 43). Drawdowns were not observed in wells LCP-38A and LCP-37A in Independence Valley during the 2016 carbonate-rock aquifer test (fig. 20). This observation is consistent with intervening low-permeability rocks, but not conclusive because drawdowns were not detected. Transmissivity estimates from specific capacities were limited to two sites in the northern Toano Range (fig. 45), where less than 2,000,000 gallons were pumped from both wells.

Estimated specific-yield and specific-storage distributions primarily were informed by sites with continuous water-level hydrograph data (hydrograph wells) (figs. 46 and 47). Specific-yield estimates of 0.002 within the HTZ (figs. 42 and 46) likely were low for fractured rocks, but storativity, the sum of specific yield and storage coefficient, averaged 0.01. The pilot point with the greatest storage coefficient in the HTZ was 0.01, which was the product of a specific storage of 2.6×10^{-6} 1/ft times a 3,700-ft thickness in layers 2–11. Total storativity in the HTZ is reasonable for carbonate rocks, but the partitioning between specific yield and specific storage likely is incorrect. Differentiating specific yield from specific storage within the HTZ is complicated by the heterogeneity and high transmissivity of carbonate rocks in this area. Specific-yield estimates of nearly 0.3 in the JSWC likely are overestimated and are a compensating error for not simulating Hardy Creek and the higher specific-yield areas surrounding it in the LCMWAT2016 model. For areas without hydrograph wells, specific-yield estimates primarily were informed by preferred hydraulic properties (table 11). Storage coefficients ranged from 0.001 to 0.050 (fig. 47).

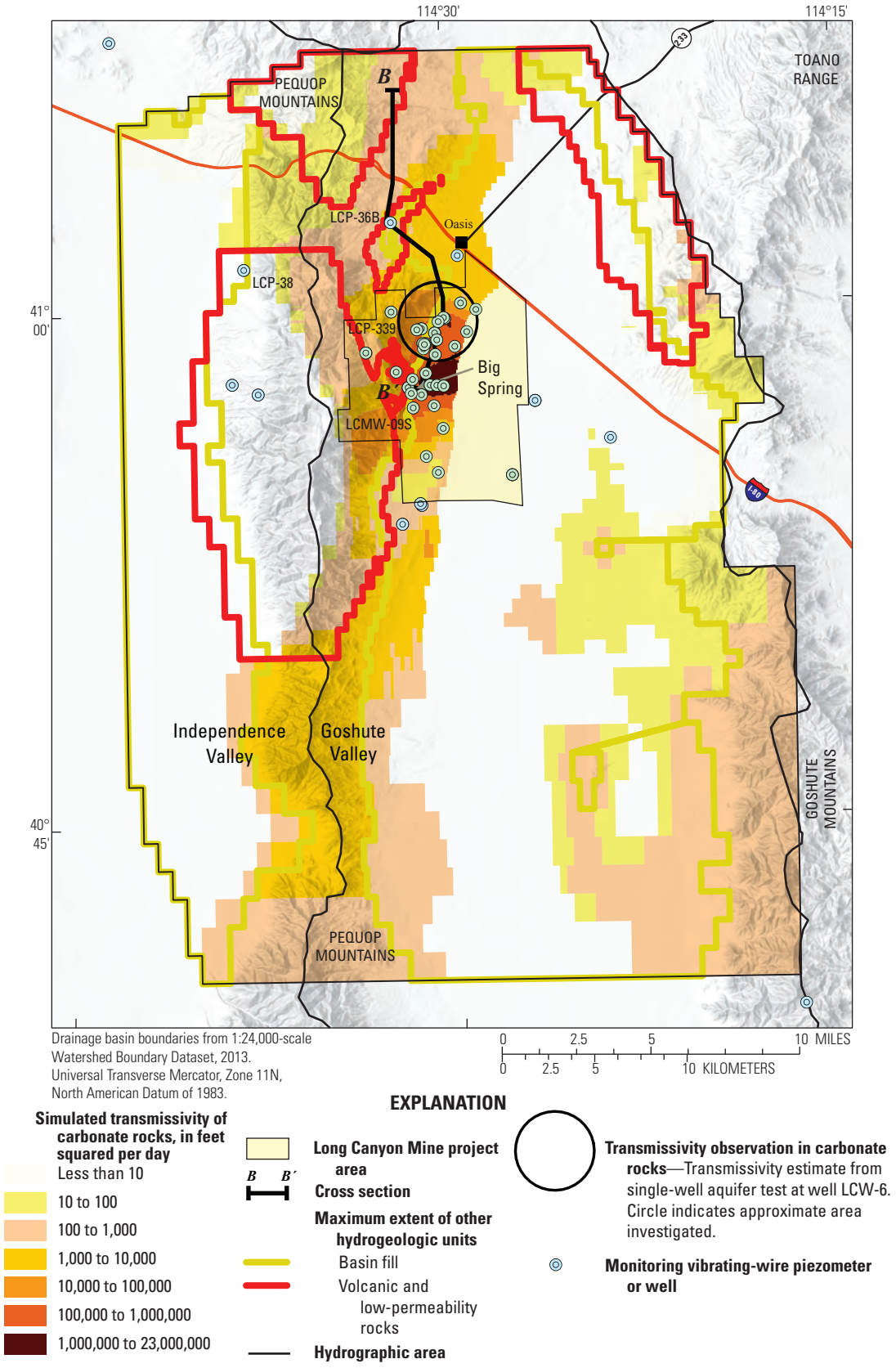

Figure 42. Simulated transmissivity distribution in carbonate rocks from integrated LC model and the maximum extent of simulated basin fill and volcanic and low-permeability rocks, Long Canyon, Goshute Valley, northeastern Nevada. See figure 43 for cross section *B–B'*.

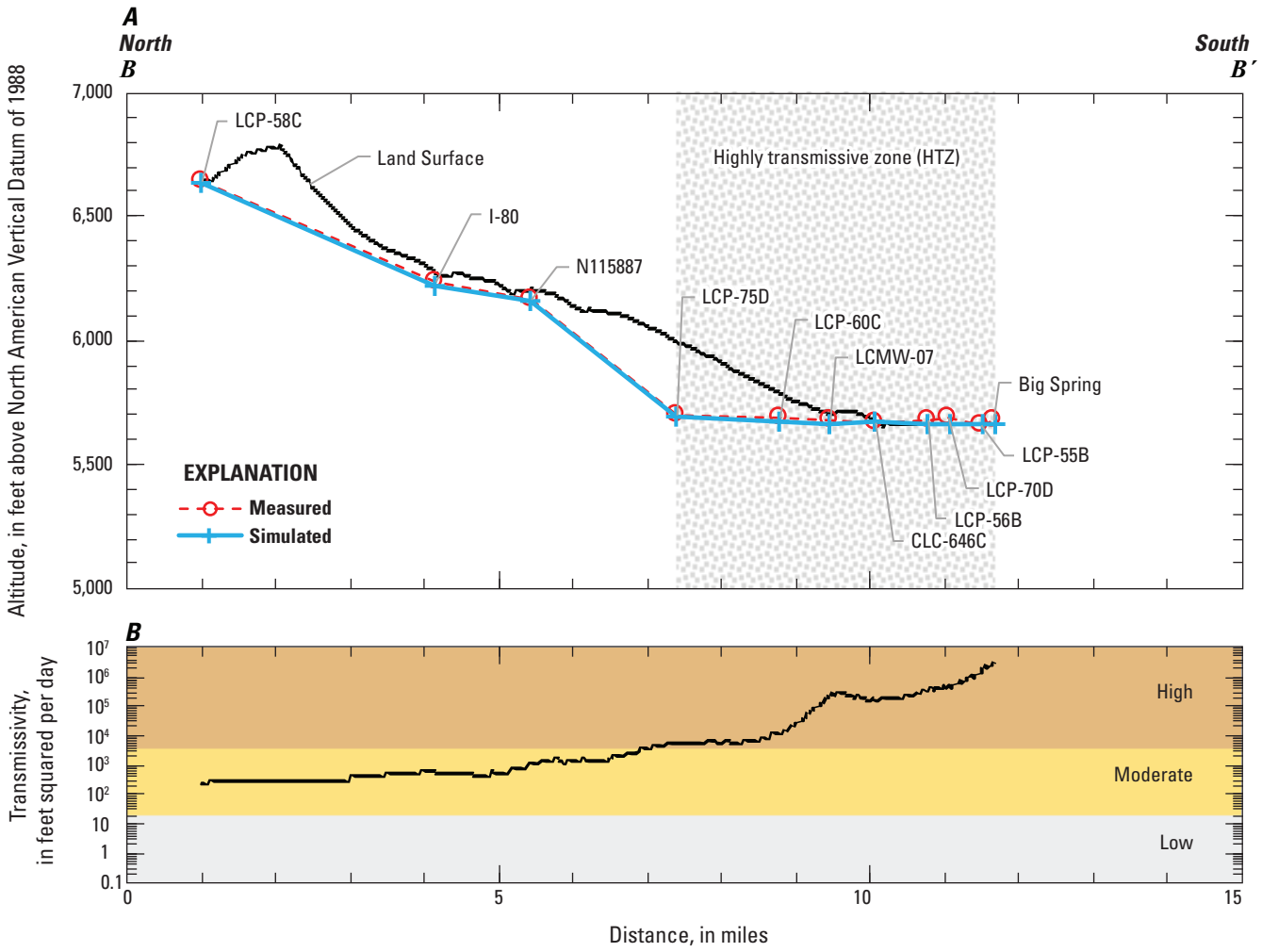

Figure 43. Measured and simulated water-levels (*A*), and transmissivity profiles along cross section *B–B′* from Northern Pequop Mountains to Big Spring (*B*), Long Canyon, Goshute Valley, northeastern Nevada. Trace of cross section *B–B′* is shown in figure 42.

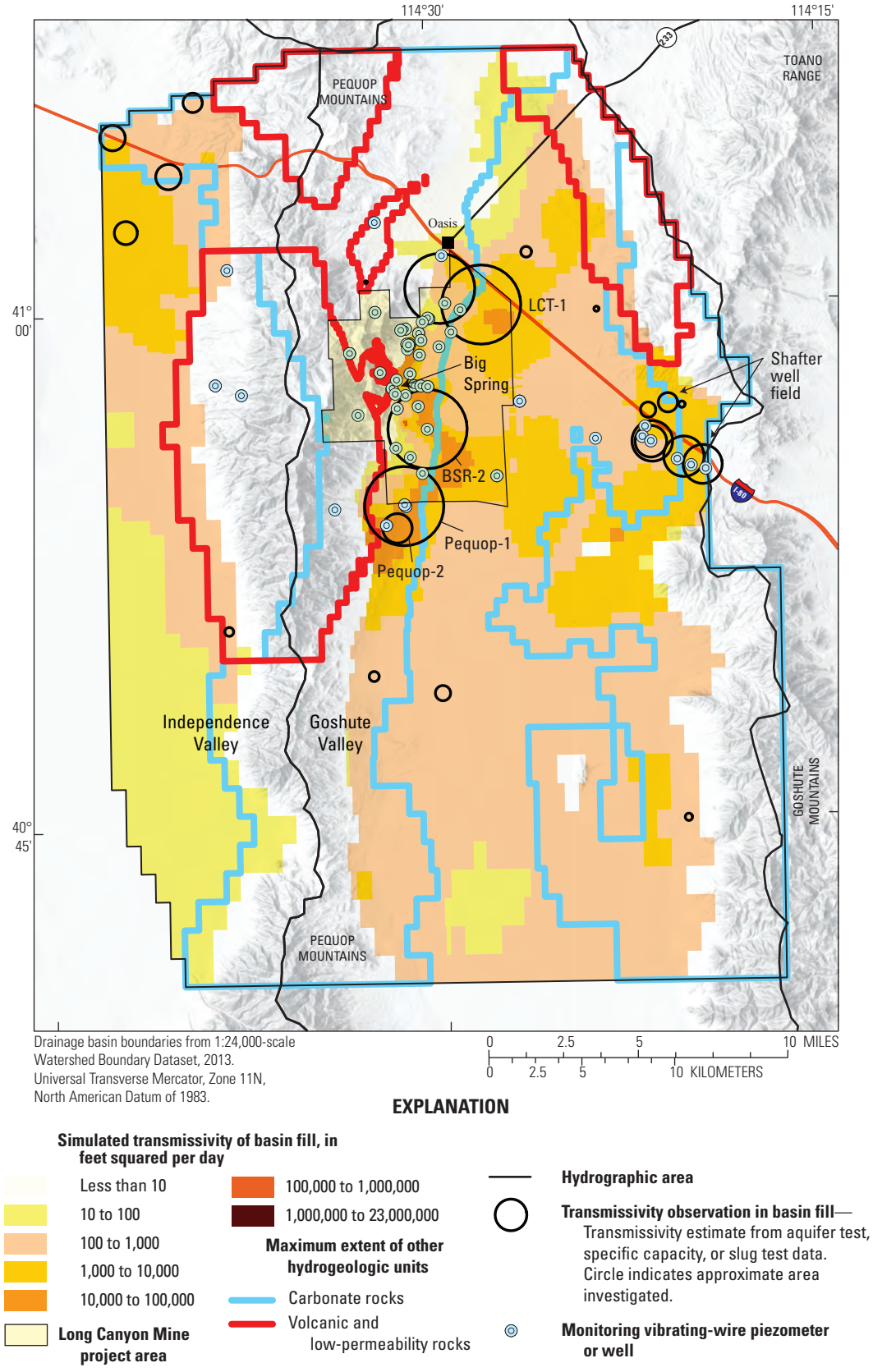

Figure 44. Simulated transmissivity distribution in basin fill from integrated LC model and the maximum extent of simulated carbonate and volcanic and low-permeability rocks, Long Canyon, Goshute Valley, northeastern Nevada.

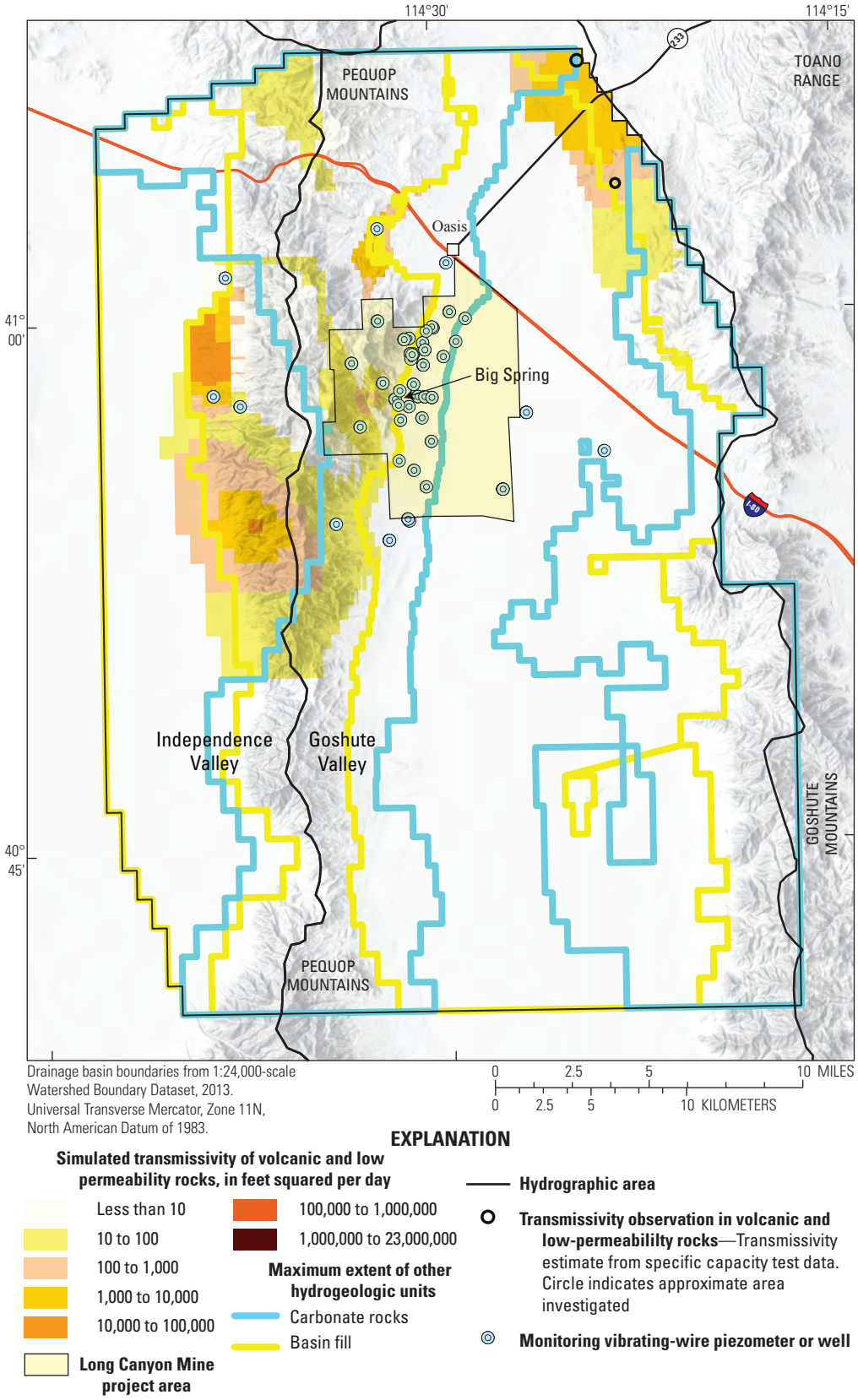

Figure 45. Simulated transmissivity distribution in volcanic and low-permeability rocks from integrated LC model and the maximum extent of simulated carbonate rocks and basin fill, Long Canyon, Goshute Valley, northeastern Nevada.

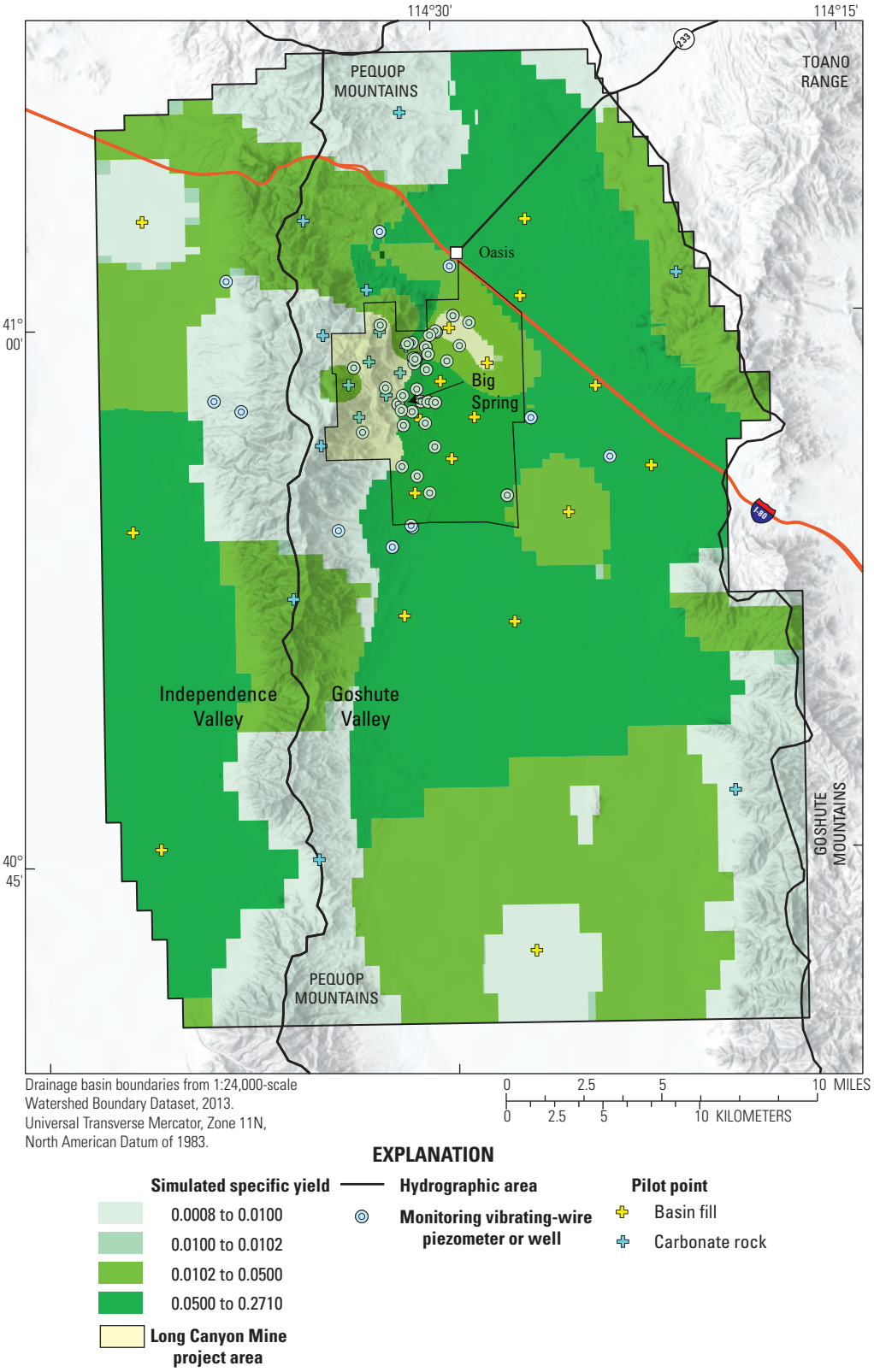

Figure 46. Simulated specific-yield distribution and pilot points from integrated LC model, Long Canyon, Goshute Valley, northeastern Nevada.

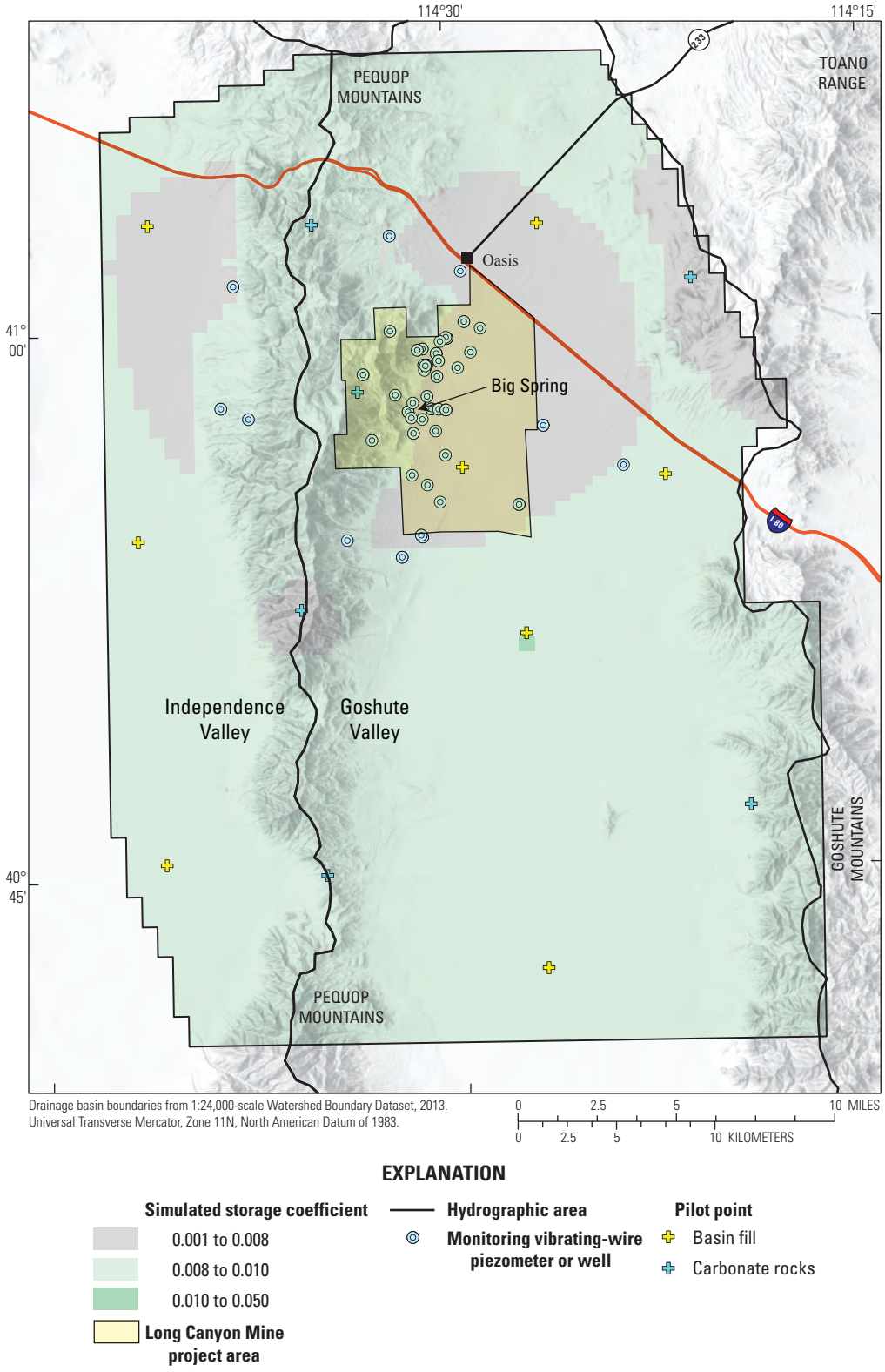

Figure 47. Simulated storage-coefficient distribution and pilot points from integrated LC model, Long Canyon, Goshute Valley, northeastern Nevada.

Model Limitations

Numerical groundwater-flow models provide simplified representations of natural systems and rely on assumptions made during model construction and calibration that lead to limitations for their use and uncertainty in their results. The integrated LC model addresses questions about predevelopment groundwater flow and groundwater development in the area of interest but has several limitations. Veracity of simulated results depends on how well the integrated LC model approximates the actual system. The most notable limitations include groundwater flow conceptualization, insufficient observations, and model discretization. Simplification of underlying conceptual models and uncertainty in estimates of predevelopment groundwater discharges are substantial limitations. Conceptual model limitations result from insufficient measurements to fully account for variations in hydraulic properties and stresses throughout the area of interest. Spatial and temporal discretization also affect results, but these numerical limitations are minor relative to data limitations.

Predevelopment groundwater discharge affected numerical model results because the quantities and volumes remain uncertain. Although groundwater discharge from Independence, Goshute, and Antelope Valleys is not well defined, uncertainty is less than that suggested by Nichols (2000). Similarities between recent spring discharge measurements and reported discharges from Big Spring (Eakin and others, 1951) suggest that discharge from Independence, Goshute, and Antelope Valleys totals about 20,000 acre-ft/yr (table 3). Groundwater discharge from Big Spring in the Long Canyon Mine project area is well defined. Discharges from other springs in the JSWC are less certain, but account for less than 40 percent of total discharge from the JSWC.

Measured groundwater levels and discharges were not matched perfectly by their simulated equivalents, even after calibration, because errors cumulatively affect model results. These irreducible errors result from simplification of the conceptual model, grid scale, and insufficient measurements. Simulated and measured quantities should be compared to estimate uncertainty of specific simulated results. Plausibility of predicted drawdowns in a well should be gaged by similarity between simulated and measured water-level changes prior to prediction.

Lateral discretization of the study area into a rectangular grid of cells and vertical discretization into layers forced an averaging of hydraulic properties. Each cell is assumed to represent a homogeneous block or some volumetric average of the aquifer medium. Discretization errors occurred in every model cell, which includes the smallest model cells. Bedding structures in the alluvium and fracture networks in the bedrock were averaged even in the smallest cells, which were 250 ft on a side and 50-ft thick.

Summary

Estimated hydraulic-property distributions and presence and absence of hydraulic connections among hydrogeologic units improves the characterization and representation of groundwater flow near the Long Canyon Mine, in northwestern Goshute Valley, northeastern Nevada, where groundwater development is expected over the next decade. Hydraulic properties of carbonate-rock and basin-fill aquifers near and downgradient from the Long Canyon Mine project area were estimated with stress-response models that simulated steady-state flow and responses to a large-scale aquifer test. Simulated hydrologic components included groundwater recharge and discharge, the predevelopment contributing area to Big Spring and the Johnson Springs wetland complex (JSWC), and water-level and spring-discharge changes from a 2016 carbonate-rock multiple-well aquifer test. Multiple hydrologic components were simulated simultaneously with two three-dimensional numerical groundwater-flow models of the area of interest.

Recharge and groundwater discharge from Goshute, Antelope, and Independence Valleys are similar and each total about 19,000 acre-feet per year (acre-ft/yr) based on previous studies. Estimated, long-term average discharge from all springs in the JSWC of 1,700 gallons per minute (2,740 acre-ft/yr) is similar to previous estimates, providing support for basin-wide discharge estimates. Recharge principally is derived from cool-season (October–March) precipitation during years with greater-than-average accumulation.

A 27-square-mile, high-altitude carbonate recharge area was delineated using water chemistry data and a potentiometric surface. Dissolved major-ion and trace-mineral concentrations and strontium isotopic compositions identify a group of waters with chemistry similar to Big Spring, including sites LCMW-15, LCMW-09S, BSR-2, Central Spring, LCMW-07, LCMW-19, and LCMW-17. Stable isotope compositions of oxygen-18 and deuterium ($\delta^{18}O$ and $\delta^{2}H$) and noble-gas recharge temperatures confined the recharge area to altitudes above 7,200 feet (ft). The recharge area consists mostly of permeable carbonate rock and fractured quartzite. The western edge of the recharge area is bounded by the Dunderberg Shale and a thick sequence of marbleized carbonate rocks, whereas the southeastern edge of the recharge area is bounded by the Chainman Shale and siliciclastic Diamond Peak Formation, all presumed to be low-permeability hydrogeologic units. Groundwater-age data indicate that source waters for the JSWC flow system are from within the high-altitude carbonate recharge area. Groundwater flow from this recharge area is substantially more active to the JSWC than to other areas of Goshute Valley. The increase in groundwater age from modern to premodern in western Goshute Valley and to Pleistocene in eastern Goshute Valley, coupled with groundwater-flow directions toward the central valley from surrounding upland areas, indicates that interbasin flow through the Toano Range is unlikely.

Transmissivities around individual wells were estimated at 48 sites with 7 single-well aquifer tests, 19 specific-capacity estimates, and 22 slug tests. Transmissivities from single-well aquifer tests ranged from 7,000 to 400,000 feet squared per day (ft^2/d) in carbonate rocks and from 2,000 to 80,000 ft^2/d in basin fill, where estimates increased from the valley floor to the alluvial fan. The most transmissive carbonate rocks tested were dolomite and limestone in the Notch Peak Formation, open to LCPW-1, whereas the most transmissive basin fill was alluvial-fan material open to Pequop-2, located along the eastern front of the Pequop Mountains, south of the JSWC.

Water-level and spring-discharge changes from the 2016 carbonate-rock multiple-well aquifer test were differentiated from environmental water-level fluctuations with analytical models. The multiple-well aquifer-test included a combined pumpage of 140 million gallons (gal) from carbonate-rock wells LCW-6 and LCPW-1 during summer 2016 and simultaneous unintentional leakage of about 58 million gal to the adjacent (or overlying) basin-fill aquifer. Leakage was generated by discharge of pumped water into a leaky irrigation ditch south of the JSWC and water supplementation to Big Spring to maintain fish habitat.

Drawdown was detected at 42 of the 93 sites monitored and as far as 3 miles (mi) from the nearest pumping well. For monitoring sites more than 500 ft from the pumping wells, maximum detected drawdown estimates ranged from 1.0 to 5.5 ft in monitoring wells, 1.2 to 4.8 ft in vibrating-wire piezometers, and 0.05 to 0.4 ft at springs. Drawdown or capture was detected definitively at all carbonate-rock monitoring sites east of the Canyon fault and north of the Long Canyon Mine project area boundary, at all but two (LCP-55B and LCP-49A) basin-fill monitoring sites completed in alluvial-fan material, at the single monitoring site completed in Ordovician and Cambrian Dunderberg Shale (CLC-604A), and at five springs issuing near Big Spring and spring NS-05. Drawdown at monitoring sites completed in valley fill (basin-fill deposits on the valley floor) was classified as ambiguous or not detected.

Water-level rise from leakage into basin fill was detected at nine monitoring sites, ranging from 0.43 ft in LCMW-08 to 3.29 ft in LCP-27A. The area of rise detection extends laterally at least 3 mi from north to south from LCMW-08 to LCMW-20 and at least 1 mi from west to east from LCP-25 to LCMW-08. Rise detection over this expansive area indicates the presence of an underlying low-permeability unit from about 100 to 300 ft below land surface that inhibits downward percolation and promotes lateral flow.

Hydraulic-property and recharge distributions were estimated by simultaneously calibrating two three-dimensional numerical groundwater models of the area of interest. Steady-state flow during predevelopment conditions was simulated with the Long Canyon Steady State (LC-SS) model so that recharge, hydraulic conductivities of low-permeability rocks, and the contributing area of springs in the JSWC could be estimated. Changes in groundwater levels and springflows from the 2016 carbonate-rock aquifer test were simulated with the Long Canyon Multiple-well Aquifer Test 2016 (LC-MWAT2016) model to better constrain transmissivity and storativity estimates. The LC-SS and LC-MWAT2016 models were calibrated simultaneously as a single integrated model.

Simulated and measured values compare favorably in the LC-SS model. Small root-mean-square water-level errors of 17 ft were simulated relative to the 1,100-ft range of measured water levels, and residuals showed little spatial pattern of significance, suggesting a good overall fit between simulated and measured water levels. Simulated and measured transmissivities from single-well aquifer tests and specific capacities generally agree, with 88 percent of sites being within the 95-percent confidence interval. Simulated and measured transmissivities from aquifer tests and specific capacities geometrically average 900 and 1,400 ft^2/d, respectively. Simulated and expected annual volumes of recharge and groundwater discharge largely agreed in rate and location, except for the Johnson Springs catchment. Simulated recharge exceeded conceptual estimates by 30 percent in the JSWC catchment area, indicating that the conceptual catchment area likely was overestimated.

Simulated transmissivities, drawdowns, and spring discharge matched measured values in the LC-MWAT2016 model, but substantial mismatches exist between simulated and measured water-level rises because of uncertainty in leakage rates and coarse model resolution in the upper 100 ft where leakage occurred. In a highly transmissive zone (HTZ) near the JSWC, simulated transmissivities ranged from 10,000 to 23,000,000 ft^2/d, with the most transmissive areas occurring around Big Spring. Little attenuation or delay between changes in pumping rates and water-level declines at monitoring sites occurred in the HTZ, resulting in extensive simulated drawdown several miles south of site LCMW-09, which represented the southern extent of carbonate-rock monitoring during the 2016 multiple-well carbonate-rock aquifer test. Simulated and measured spring discharges agree in the JSWC, where pumping affected discharge from Big Spring and spring NS-05.

The transmissivity distribution in carbonate rocks was estimated reliably in a limited extent of the Pequop Mountains extending from about 1 mi south of Big Spring to I-80 northward, and from the western Goshute Valley divide to basin fill in the Long Canyon Mine project area. Carbonate rocks extending several miles south of well LCMW-09 likely are transmissive, but analysis of carbonate-rock transmissivities south of well LCMW-09 in Goshute Valley were not confirmed in this study. Northward, about 1 mi south of I-80, drawdown observations in piezometer LCP-36B were classified as not detected, which is consistent with a maximum simulated drawdown of 0.08 ft. Transmissivities of less than 3,000 ft^2/d were estimated in carbonate rocks of the Pequop Mountains north of I-80 and were informed by steady-state water levels that are 500 to 1,000 ft higher than water levels in the HTZ.

Transmissivity of basin fill along the eastern flank of the Pequop Mountains through the Long Canyon Mine project area was informed primarily from aquifer tests where pumping wells were open to basin fill. Transmissivity estimates of 40,000 and 80,000 ft^2/d from the BSR-2 and Pequop-2 tests, respectively, are consistent with simulated transmissivities in the basin fill. Simulated transmissivities about 2 mi southeast of Oasis and south of I-80 agree with a 2,000 ft^2/d estimate for well LCT-1. Transmissivities in basin fill were minimally constrained by the 2016 carbonate-rock aquifer test because ditch leakage affected water levels more so than pumping. Simulated transmissivities of volcanic and low-permeability rocks are mostly less than 1,000 ft^2/d and were constrained by steep water-level gradients in the Pequop Mountains north of I-80 and two specific-capacity estimates in the Toano Range.

The integrated LC model adequately simulates predevelopment groundwater flow and groundwater development in the area of interest but has several limitations. Predevelopment groundwater discharge remains uncertain for Independence, Goshute, and Antelope Valleys, but measurements constrain uncertainties in developed areas. Measured groundwater levels and discharges were not matched perfectly by their simulated equivalents because of cumulative errors; therefore, simulated quantities should be compared to estimate uncertainty of specific simulated results. Lateral discretization of the study area into a rectangular grid of cells and vertical discretization into layers forced an averaging of hydraulic properties in bedding structures in alluvium and bedrock fracture networks.

References Cited

Aeschbach-Hertig, W., Peeters, F., Beyerle, U., and Kipfer, R., 2000, Paleotemperature reconstruction from noble gases in ground water taking into account equilibration with entrapped air: Nature, v. 405, no. 6790, p. 1040–1044. [Also available at https://doi.org/10.1038/35016542.]

Allander, K.K., Smith, J.L., and Johnson, M.J., 2009, Evapotranspiration from the Lower Walker River Basin, West-Central Nevada, Water Years 2005–07: U.S. Geological Survey Scientific Investigations Report 2009–5079, 62 p. [Also available at https://doi.org/10.3133/sir20095079.]

Barker, J.A., and Black, J.H., 1983, Slug tests in fissured aquifers: Water Resources Research, v. 19, no. 6, p. 1558–1564.

Barnett Intermountain Water Consulting, Global Hydrologic Services Inc., and Aqua Engineering, 2011, Report on the Long Canyon bedrock well aquifer test, Goshute Valley, Elko County, Nevada: Prepared for Fronteer Development (USA) Inc., Elko, Nevada.

Berger, D.L., Mayers, C.J., Garcia, C.A., Buto, S.G., and Huntington, J.M., 2016, Budgets and chemical characterization of groundwater for the Diamond Valley flow system, central Nevada, 2011–12: U.S. Geological Survey Scientific Investigations Report 2016–5055, 83 p. [Also available at https://doi.org/10.3133/sir20165055.]

Bouwer, H., and Rice, R.C., 1976, A slug test for determining hydraulic conductivity of unconfined aquifers with completely or partially penetrating wells: Water Resources Research, v. 12, no. 3, p. 423–428. [Also available at https://agupubs.onlinelibrary.wiley.com/doi/10.1029/WR012i003p00423.]

Bredehoeft, J., 2007, It is the discharge: Ground Water, v. 45, p. 523, https://doi.org/10.1111/j.1745-6584.2007.00305.x.

Brooks, L.E., Masbruch, M.D., Sweetkind, D.S., and Buto, S.G., 2014, Steady-state numerical groundwater flow model of the Great Basin carbonate and alluvial aquifer system: U.S. Geological Survey Scientific Investigations Report 2014–5213, 124 p., 2 pls. [Also available at https://doi.org/10.3133/sir20145213.]

Brooks, W.E., Thorman, C.H., Snee, L.W., Nutt, C.J., Potter, C.J., and Dubiel, R.F., 1995, Summary of chemical analyses and $^{40}Ar/^{39}Ar$ age-spectra data for Eocene volcanic rocks from the central part of the northeast Nevada volcanic field: U.S. Geological Survey Bulletin, v. 1988-K, p. K1–K33.

Bureau of Land Management, 2014, Newmont Mining Corporation's Long Canyon Mine draft environmental impact statement, March 21, 2014: Document prepared for Bureau of Land Management [variously paged], accessed September 17, 2015, at https://www.blm.gov/nv/st/en/fo/elko_field_office/blm_information/nepa/long_canyon_eis__7.html.

Butler, J.J., Jr., 1998, The design, performance, and analysis of slug tests: Washington, D.C., Lewis Publishers, 252 p.

Butler, J.J., Jr., and Garnett, E.J., 2000, Simple procedures for analysis of slug tests in formations of high hydraulic conductivity using spreadsheet and scientific graphics software: Lawrence, Kansas, Kansas Geological Survey Open-File Report 2000–40. [Also available at http://www.kgs.ku.edu/Hydro/Publications/OFR00_40/.]

Camilleri, P.A., 2010, Geologic map of the northern Pequop Mountains, Elko County, Nevada: Nevada Bureau of Mines and Geology Map 171, 15 p. [Also available at https://pubs.nbmg.unr.edu/Geol-N-Pequop-Mts-map-txt-p/m171.htm.]

Camilleri, P.A., and Chamberlain, K.R., 1997, Mesozoic tectonics and metamorphism in the Pequop Mountains and Wood Hills region, northeast Nevada—Implications for the architecture and evolution of the Sevier orogeny: Geological Society of America Bulletin, v. 109, no. 1, p. 74–94. [Also available at https://pubs.geoscienceworld.org/gsa/gsabulletin/article/109/1/74/183182/mesozoic-tectonics-and-metamorphism-in-the-pequop.]

Cerling, T.E., Solomon, D.K., Quade, J., and Bowman, J.R., 1991, On the isotopic composition of carbon in soil carbon dioxide: Geochimica et Cosmochimica Acta, v. 55, no. 11, p. 3403–3405. [Also available at https://doi.org/10.1016/0016-7037(91)90498-T.]

Clarke, W.B., Jenkins, W.J., and Top, Z., 1976, Determination of tritium by mass spectrometric measurement of ^{3}He: The International Journal of Applied Radiation and Isotopes, v. 27, no. 9, p. 515–522. [Also available at https://doi.org/10.1016/0020-708X(76)90082-X.]

Coats, R.R., 1987, Geology of Elko County, Nevada: Nevada Bureau of Mines and Geology Bulletin 101, 112 p.

Cooper, H.H., Jr., and Jacob, C.E., 1946, A generalized graphical method for evaluating formation constants and summarizing well field history: Eos (Washington, D.C.), v. 27, no. 4, p. 526–534. [Also available at https://agupubs.onlinelibrary.wiley.com/doi/10.1029/TR027i004p00526.]

Coplen, T.B., 1994, Reporting of stable hydrogen, carbon, and oxygen isotopic abundances: Pure and Applied Chemistry, v. 66, no. 2, p. 273–276. [Also available at https://doi.org/10.1351/pac199466020273.]

Craig, H., 1961b, Isotopic variations in meteoric waters: Science, v. 133, no. 3465, p. 1702–1703. [Also available at https://doi.org/10.1126/science.133.3465.1702.]

Craig, H., 1961a, Standard for reporting concentrations of deuterium and oxygen-18 in natural waters: Science, v. 133, no. 3467, p. 1833–1834. [Also available at https://doi.org/10.1126/science.133.3467.1833.]

Daly, C., Neilson, R.P., and Phillips, D.L., 1994, A statistical-topographic model for mapping climatological precipitation over mountainous terrain: Journal of Applied Meteorology, v. 33, p. 140–158. [Also available at https://doi.org/10.1175/1520-0450(1994)033%3C0140:ASTMFM%3E2.0.CO;2.]

DeMeo, G.A., Laczniak, R.J., Boyd, R.A., Smith, J.L., and Nylund, W.E., 2003, Estimated ground-water discharge by evapotranspiration from Death Valley, California, 1997–2001: U.S. Geological Survey Water-Resources Investigations Report 2003–4254, 27 p. [Also available at http://pubs.er.usgs.gov/publication/wri034254.]

de Vries, H., 1958, Variation in concentration of radiocarbon with time and location on Earth: Proceedings of the Koninklijke Nederlandse Akademie van Wetenschappen, v. B61, p. 1–9.

Doherty, J., 2010b, Addendum to the PEST manual: Brisbane, Australia, Watermark Numerical Computing, 235 p.

Doherty, J., 2010a, PEST, Model-independent parameter estimation—User manual (5th ed., with slight additions): Brisbane, Australia, Watermark Numerical Computing, 336 p.

Doherty, J., and Johnston, J.M., 2003, Methodologies for calibration and predictive analysis of a watershed model: Journal of the American Water Resources Association, v. 39, no. 2, p. 251–265.

Eakin, T.E., Maxey, G.B., Robinson, T.W., Fredricks, J.C., and Loeltz, O.J., 1951, Contributions to the hydrology of eastern Nevada—Nevada State Engineer: Water Resources Bulletin, v. 12, p. 17–34. [Also available at http://images.water.nv.gov/images/publications/water%20resources%20bulletins/Bulletin12.pdf.]

Elliott, P.E., and Fenelon, J.M., 2010, Database of groundwater levels and hydrograph descriptions for the Nevada Test Site area, Nye County, Nevada: U.S. Geological Survey Data Series 533, version 7.0, October 2016, 16 p. [Also available at https://pubs.usgs.gov/ds/533/.]

Epstein, B.J., Pohll, G.M., Huntington, J.L., and Carroll, R.W.H., 2010, Development and uncertainty analysis of an empirical recharge prediction model for Nevada's desert basins: Journal of the Nevada Water Resources Association, v. 5, no. 1., 22 p. [Also available at https://www.researchgate.net/publication/288753211_Development_and_uncertainty_analysis_of_an_empirical_recharge_prediction_model_for_Nevada's_desert_basins.]

Fenelon, J.M., 2000, Quality assurance and analysis of water levels in wells on Pahute Mesa and vicinity, Nevada Test Site, Nye County, Nevada: U.S. Geological Survey Water-Resources Investigations Report 2000–4014, 68 p. [Also available at https://doi.org/10.3133/wri004014.]

Fienen, M., Muffels, C., and Hunt, R., 2009, On constraining pilot point calibration with regularization in PEST: Ground Water, v. 47, no. 6, p. 835–844. [Also available at https://onlinelibrary.wiley.com/doi/10.1111/j.1745-6584.2009.00579.x.]

Friedman, I., Smith, G.I., Johnson, C.A., and Moscati, R.J., 2002, Stable isotope compositions of waters in the Great Basin, United States—2, Modern precipitation: Journal of Geophysical Research, v. 107, p. ACL15.1–ACL15.22. [Also available at https://pubs.er.usgs.gov/publication/70023926.]

Frus, R.J., and Halford, K.J., 2018, Documentation of single-well aquifer tests and integrated borehole analyses, Pahute Mesa and vicinity, Nevada: U.S. Geological Survey Scientific Investigations Report 2018–5096, 22 p. [Also available at https://doi.org/10.3133/sir20185096.]

Garcia, C.A., Halford, K.J., and Fenelon, J.M., 2013, Detecting drawdowns masked by environmental stresses using Theis transforms: Ground Water, v. 51, no. 3, p. 322–332. [Also available at https://doi.org/10.1111/gwat.12042.]

Garcia, C.A., Huntington, J.M., Buto, S.G., Moreo, M.T., Smith, J.L., and Andraski, B.J., 2015, Groundwater discharge by evapotranspiration, Dixie Valley, west-central Nevada, March 2009–September 2011 (ver. 1.1, April 2015): U.S. Geological Survey Professional Paper 1805, 90 p. [Also available at https://doi.org/10.3133/pp1805.]

Gardner, P.M., and Heilweil, V.M., 2014, A multiple-tracer approach to understanding regional groundwater flow in the Snake Valley area of the eastern Great Basin, USA: Applied Geochemistry, v. 45, p. 33–49. [Also available at https://doi.org/10.1016/j.apgeochem.2014.02.010.]

Gesch, D., Evans, G., Mauck, J., Hutchinson, J., and Carswell, W.J., Jr., 2009, The national map—Elevation: U.S. Geological Survey Fact Sheet 2009–3053, 4 p. [Also available at https://doi.org/10.3133/fs20093053.]

Global Hydrologic Services, Inc., 2010, Hydrology baseline data report for northern Goshute Valley, Elko County: NV, Global Hydrologic Services, Inc., 161 p.

Golder Associates Inc., 2012, Hydrogeologic characterization—Long Canyon, Newmont USA Limited: Golder Associates Inc., Project No. 113-81813, p. 48.

Halford, K., Garcia, C.A., Fenelon, J., and Mirus, B., 2012, Advanced methods for modeling water-levels and estimating drawdowns with SeriesSEE, an Excel add-in: U.S. Geological Survey Techniques and Methods, book 4, chap. F4, 28 p. [Also available at https://doi.org/10.3133/tm4F4.]

Halford, K.J., 2016, T-COMP—A suite of programs for extracting transmissivity from MODFLOW models: U.S. Geological Survey Techniques and Methods, book 6, chap. A54, 17 p. [Also available at https://doi.org/10.3133/tm6A54.]

Halford, K.J., and Hanson, R.T., 2002, User guide for the drawdown-limited, Multi-node well (MNW) package for the U.S. Geological Survey's modular three-dimensional finite-difference ground-water flow model, versions MODFLOW–96 and MODFLOW–2000: U.S. Geological Survey Open-File Report 02–293, 33 p. [Also available at https://pubs.usgs.gov/of/2002/ofr02293/text.html.]

Halford, K.J., and Jackson, T.R., 2020, Groundwater characterization and effects of pumping in the Death Valley regional groundwater flow system, Nevada and California, with special reference to Devils Hole: U.S. Geological Survey Professional Paper 1863, 178 p. [Also available at https://doi.org/10.3133/pp1863.]

Halford, K.J., and Plume, R.W., 2011, Potential effects of groundwater pumping on water levels, phreatophytes, and spring discharges in Spring and Snake Valleys, White Pine County, Nevada, and adjacent areas in Nevada and Utah: U.S. Geological Survey Scientific Investigations Report 2011–5032, 52 p. [Also available at https://pubs.usgs.gov/sir/2011/5032/.]

Halford, K.J., Weight, W.D., and Schreiber, R.P., 2006, Interpretation of transmissivity estimates from single-well pumping aquifer tests: Ground Water, v. 44, p. 467–471. [Also available at https://doi.org/10.1111/j.1745-6584.2005.00151.x.]

Han, L.F., and Plummer, L.N., 2013, Revision of Fontes and Garnier's model for the initial ^{14}C content of dissolved inorganic carbon used in groundwater dating: Chemical Geology, v. 351, p. 105–114. [Also available at https://doi.org/10.1016/j.chemgeo.2013.05.011.]

Han, L.F., Plummer, L.N., and Aggarwal, P., 2012, A graphical method to evaluate predominant geochemical processes occurring in groundwater systems for radiocarbon dating: Chemical Geology, v. 318–319, p. 88–112. [Also available at https://doi.org/10.1016/j.chemgeo.2012.05.004.]

Harbaugh, A.W., 1990, A computer program for calculating subregional water budgets using results from the U.S. Geological Survey modular three-dimensional ground-water flow model: U.S. Geological Survey Open-File Report 90–392, 46 p. [Also available at https://doi.org/10.3133/ofr90392.]

Harbaugh, A.W., 2005, MODFLOW-2005, the U.S. Geological Survey modular ground-water model—The ground-water flow process: U.S. Geological Survey Techniques and Methods, book 6, chap. A16. [Also available at https://doi.org/10.3133/tm6A16.]

Hardman, G., 1936, Nevada precipitation and acreages of land by rainfall zones: University of Nevada, Reno, Agricultural Experiment Station report, 10 p. plus map.

Harrill, J.R., Gates, J.S., and Thomas, J.M., 1988, Major ground-water flow systems in the Great Basin region of Nevada, Utah, and adjacent states: U.S. Geological Survey Hydrologic Atlas 694-C, pls. 1–2.

Hart, R., Nelson, S.T., and Eggett, D., 2010, Uncertainty in ^{14}C model ages of saturated zone waters—The influence of soil gas in terranes dominated by C3 plants: Journal of Hydrology, v. 392, nos. 1–2, p. 83–95. [Also available at https://doi.org/10.1016/j.jhydrol.2010.08.001.]

Heilweil, V.M., and Brooks, L.E., eds., 2011, v. 2010–5193. Conceptual model of the Great Basin carbonate and alluvial aquifer system, U.S. Geological Survey Scientific Investigations Report 2010–5193, 191 p. [Also available at https://doi.org/10.3133/sir20105193.]

Henry, C.D., and Thorman, C.H., 2015, Preliminary geologic map of the Pequop Summit Quadrangle, Elko County, Nevada: Nevada Bureau of Mines and Geology Open-File Report 15–8, 12 p.

Hyder, Z., Butler, J.J., Jr., McElwee, C.D., and Liu, W., 1994, Slug tests in partially penetrating wells: Water Resources Research, v. 30, no. 11, p. 2945–2957. [Also available at https://doi.org/10.1029/94WR01670.]

Jackson, T.R., and Fenelon, J.M., 2018, Conceptual framework and trend analysis of water-level responses to hydrologic stresses, Pahute Mesa–Oasis Valley groundwater basin, Nevada, 1966–2016: U.S. Geological Survey Scientific Investigation Report 2018–5064, 89 p. [Also available at https://doi.org/10.3133/sir20185064.]

Jackson, T.R., Halford, K.J., Gardner, P.M., and Garcia, C.A., 2018, Evaluating micrometeorological estimates of groundwater discharge from Great Basin desert playas: Ground Water, v. 56, no. 6, p. 909–920. [Also available at https://doi.org/10.1111/gwat.12647.]

Kennedy, C.D., and Genereux, D.P., 2007, ^{14}C groundwater age and the importance of chemical fluxes across aquifer boundaries in confined Cretaceous aquifers of North Carolina, USA: Radiocarbon, v. 49, no. 3, p. 1181–1203. [Also available at https://doi.org/10.1017/S0033822200043101.]

Ketner, K.B., 1997, Geologic maps showing structural modes in the Goshute Mountains and Toano Range, Elko County, Nevada: U.S. Geological Survey Miscellaneous Geologic Investigations Map I-2546. [Also available at https://ngmdb.usgs.gov/Prodesc/proddesc_13050.htm.]

Ketner, K.B., Day, W.C., Elrick, M., Vaag, M.K., Zimmermann, R.A., Snee, L.W., Saltus, R.W., Repetski, J.E., Wardlaw, B.R., Taylor, M.E., and Harris, A.G., 1998, An outline of tectonic, igneous, and metamorphic events in the Goshute-Toano Range between Silver Zone Pass and White Horse Pass, Elko County, Nevada—A history of superposed contractional and extensional deformation: U.S. Geological Survey Professional Paper 1593, 12 p. [Also available at https://pubs.usgs.gov/pp/p1593/p1593.pdf.]

Kipfer, R., Aeschbach-Hertig, W., Peeters, F., and Stute, M., 2002, Noble gases in lakes and ground waters, *in* Porcelli, D., Ballentine, C.J., and Wieler, R., eds., Noble gases in geochemistry and cosmochemistry—Reviews in mineralogy and geochemistry 47: Chantilly, Virginia, Mineralogical Society of America, p. 615–700. [Also available at https://doi.org/10.1515/9781501509056-016.]

Laczniak, R.J., DeMeo, G.A., Reiner, S.R., Smith, J.L., and Nylund, W.E., 1999, Estimates of ground-water discharge as determined from measurements of evapotranspiration, Ash Meadows Area, Nye County, Nevada: U.S. Geological Survey Water-Resources Investigations Report 99–4079, 70 p. [Also available at http://pubs.er.usgs.gov/publication/wri994079.]

Laczniak, R.J., Flint, A.L., Moreo, M.T., and others, 2008, Ground-water budgets, *in* Welch, A.H., Bright, D.J., and Knochenmus, L.A., eds., Water resources of the Basin and Range carbonate-rock aquifer system, White Pine County, Nevada, and adjacent areas in Nevada and Utah: U.S. Geological Survey Scientific Investigations Report 2007–5261, 96 p. [Also available at http://pubs.er.usgs.gov/publication/sir20075261.]

Laczniak, R.J., Smith, J.L., Elliot, P.E., DeMeo, G.A., Chatigny, M.A., and Roemer, G.J., 2001, Ground-water discharge determined from estimates of evapotranspiration, Death Valley regional flow system, Nevada and California: U.S. Geological Survey Water-Resources Investigations Report 01–4195, 51 p. [Also available at http://pubs.er.usgs.gov/publication/wri014195.]

Lawrence, A.O., Roberts, L., and Potter, C.J., 2007, Geologic assessment of undiscovered oil and gas in the Paleozoic–Tertiary composite total petroleum system of the eastern Great Basin, Nevada, and Utah, chap. 2 *of* U.S. Geological Survey Eastern Great Basin Province Assessment Team—Geologic assessment of undiscovered oil and gas resources of the Eastern Great Basin Province, Nevada, Utah, Idaho, and Arizona: U.S. Geological Survey Digital Data Series DDS–69–L, 50 p.

Lohman, S.W., 1972, Ground-water hydraulics: U.S. Geological Survey Professional Paper 708, 70 p. [Also available at https://doi.org/10.3133/pp708.]

Manning, A.H., 2011, Mountain-block recharge, present and past, in the eastern Española Basin, New Mexico, USA: Hydrogeology Journal, v. 19, no. 2, p. 379–397. [Also available at https://doi.org/10.1007/s10040-010-0696-8.]

Manning, A.H., and Solomon, D.K., 2003, Using noble gases to investigate mountain-front recharge: Journal of Hydrology, v. 275, nos. 3-4, p. 194–207. [Also available at https://doi.org/10.1016/S0022-1694(03)00043-X.]

Maxey, G.B., and Eakin, T.E., 1949, Ground water in White River Valley, White Pine, Nye, and Lincoln Counties, Nevada: Nevada State Engineer, Water Resources Bulletin 8, 59 p.

Maxey, G.B., and Eakin, T.E., 1951, Ground water in Railroad, Hot Creek, Reveille, Kawich, and Penoyer Valleys, Nye, Lincoln, and White Pine Counties, Nevada, *in* Eakin, T.E., Maxey, G.B., Robinson, T.W., Fredricks, J.C., and Loeltz, O.J., Contributions to the hydrology of eastern Nevada—Nevada State Engineer: Water Resources Bulletin, v. 12, p. 129–171.

Mayo and Associates, 2013, Isotopic characterization of groundwaters in the Long Canyon mine area, Nevada: Consultant report prepared for JBR Environmental Consultants, Inc., Sandy, Utah. 20 p.

McCollum, L.B., and Miller, D.M., 1991, Cambrian stratigraphy of the Wendover area, Utah and Nevada: U.S. Geological Survey Bulletin 1948, 43 p. [Also available at https://pubs.er.usgs.gov/publication/b1948.]

McElwee, C.D., and Zenner, M., 1998, A nonlinear model for analysis of slug-test data: Water Resources Research, v. 34, no. 1, p. 55–66. [Also available at https://doi.org/10.1029/97WR02710.]

McKenna, G.T., 1995, Grouted-in installation of piezometers in boreholes: Canadian Geotechnical Journal, v. 32, no. 2, p. 355–363. [Also available at https://doi.org/10.1139/t95-035.]

Mikkelsen, P.E., and Green, G.E., 2003, Piezometers in fully grouted boreholes, *in* Myrvoll, F., ed., Field measurements in geomechanics—Proceedings of the 6th International Symposium, Oslo, Norway, September, 23–26, 2003: Boca Raton, Florida, CRC Press, p. 545–553, https://www.zeminas.com.tr/docs/ZET_2.pdf.

Moreo, M.T., Laczniak, R.J., and Stannard, D.I., 2007, Evapotranspiration rate estimates of vegetation typical of ground-water discharge areas in the Basin and Range Carbonate-Rock aquifer system, Nevada and Utah, September 2005–August 2006: U.S. Geological Survey Scientific Investigations Report 2007–5078, 36 p. [Also available at http://pubs.er.usgs.gov/publication/sir20075078.]

National Climatic Data Center, 2017, 1981–2010 U.S. climate normals—Data access: National Oceanic and Atmospheric Administration National Climatic Data Center web page, accessed July 2017, at https://www.ncdc.noaa.gov/data-access/land-based-station-data/land-based-datasets/climate-normals/1981-2010-normals-data.

Nelson, N.C., Halford, K.J., and Garcia, C.A., 2021, MODFLOW-2005 and PEST models used to simulate the 2016 carbonate-rock aquifer test and characterize hydraulic properties of carbonate-rock and basin-fill aquifers near Long Canyon, Goshute Valley, northeastern Nevada: U.S. Geological Survey data release, https://doi.org/10.5066/P9JI8NQF.

Nevada Division of Water Resources, 2017, Well driller's report—Well LCP-66: Nevada Division of Water Resources, accessed March 22, 2019, at http://images.water.nv.gov/images/well_logs/129000/129536.pdf.

Nichols, W.D., 2000, Regional ground-water evapotranspiration and ground-water budgets, Great Basin, Nevada: U.S. Geological Survey Professional Paper 1628. [variously paged]. [Also available at https://pubs.er.usgs.gov/publication/pp1628.]

Paces, J.B., and Wurster, F.C., 2014, Natural uranium and strontium isotope tracers of water sources and surface water–groundwater interactions in arid wetlands—Pahranagat Valley, Nevada, USA: Journal of Hydrology (Amsterdam), v. 517, p. 213–225. [Also available at https://doi.org/10.1016/j.jhydrol.2014.05.011.]

Penman, A.D.M., 1961, A study of the response time of various types of piezometers, *in* British National Society of the International Society of Soil Mechanics and Foundation Engineering, eds., Pore pressure and suction in soils: London, Butterworths, British Geotechnical Society, p. 53–58.

Plummer, L.N., and Sprinkle, C.L., 2001, Radiocarbon dating of dissolved inorganic carbon in groundwater from confined parts of the Upper Floridian aquifer, Florida, USA: Hydrogeology Journal, v. 9, no. 2, p. 127–150. [Also available at https://doi.org/10.1007/s100400000121.]

PRISM Climate Group, 2012, PRISM climate data, 30-year normal—Norm81m data set: Oregon State University PRISM Climate Group web page, accessed May 2014, at http://prism.oregonstate.edu

RamaRao, B.S., de Marsily, G., and Marietta, M.G., 1995, Pilot point methodology for automated calibration of an ensemble of conditionally simulated transmissivity fields—1. Theory and computational experiments: Water Resources Research, v. 31, no. 3, p. 475–493.

Reimer, P.J., Bard, E., Bayliss, A., and others, 2013, IntCal13 and Marine09 radiocarbon age calibration curves 0–50,000 years cal BP: Radiocarbon, v. 55, no. 4, p. 1869–1887. [Also available at https://doi.org/10.2458/azu_js_rc.55.16947.]

Reiner, S.R., Laczniak, R.J., DeMeo, G.A., Smith, J.L., Elliott, P.E., Nylund, W.E., and Fridrich, C.J., 2002, Ground-water discharge determined from measurements of evapotranspiration, other available hydrologic components, and shallow water-level changes, Oasis Valley, Nye County, Nevada: U.S. Geological Survey Water-Resources Investigations Report 01–4239, 65 p. [Also available at http://pubs.er.usgs.gov/publication/wri014239.]

Renard, P., 2005, The future of hydraulic tests: Hydrogeology Journal, v. 13, p. 259–262. [Also available at https://doi.org/10.1007/s10040-004-0406-5.]

Sheets, R.A., Hill, M.C., Haitjema, H.M., Provost, A.M., and Masterson, J.P., 2015, Simulation of water-table aquifers using specified saturated thickness: Ground Water, v. 53, p. 151–157. [Also available at https://doi.org/10.1111/gwat.12164.]

Smith, D.W., Garcia, C.A., Halford, K.J., and Gardner, P.M., 2021, Appendixes and supplemental data—Hydraulic characterization of carbonate-rock and basin-fill aquifers near Long Canyon, Goshute Valley, northeastern Nevada, 2011–16: U.S. Geological Survey data release, https://doi.org/10.5066/P9P1P7QV.

Smith, D.W., Moreo, M.T., Garcia, C.A., Halford, K.J., and Fenelon, J.M., 2017, A process to estimate net infiltration using a site-scale water-budget approach, Rainier Mesa, Nevada National Security Site, Nevada, 2002–05: U.S. Geological Survey Scientific Investigations Report 2017–5078, 22 p. [Also available at https://doi.org/10.3133/sir20175078.]

Smith, G.I., Friedman, I., Veronda, G., and Johnson, C.A., 2002, Stable isotope compositions of waters in the Great Basin, United States—3, Comparison of groundwaters with modern precipitation: Journal of Geophysical Research, v. 107, p. ACL16.1–ACL16.15. [Also available at https://pubs.er.usgs.gov/publication/70023854.]

Smith, J.L., Laczniak, R.J., Moreo, M.T., and Welborn, T.L., 2007, Mapping evapotranspiration units in the Basin and Range carbonate-rock aquifer system, White Pine County, Nevada, and adjacent areas in Nevada and Utah: U.S. Geological Survey Scientific Investigations Report 2007–5087, 20 p.

Smith, M., Gray, J., Lee, C., and Simmons, G., 2011, Updated technical report on the Long Canyon Project, Elko County: Nevada, USA, Prepared by Frontier Gold, Inc., 192 p.

Solomon, D.K., 2000a, ^{3}H and ^{3}He, *in* Cook, P.G., and Herczeg, A.L., eds., Environmental tracers in subsurface hydrology: Boston, Kluwer Academic Publishers, p. 397–424. [Also available at https://doi.org/10.1007/978-1-4615-4557-6_13.]

Solomon, D.K., 2000b, ^{4}He in groundwater, *in* Cook, P.G., and Herczeg, A.L., eds., Environmental tracers in subsurface hydrology: Boston, Kluwer Academic Publishers, p. 425–439. [Also available at https://doi.org/10.1007/978-1-4615-4557-6_14.]

Springer, R.K., and Gelhar, L.W., 1991, Characterization of large-scale aquifer heterogeneity in glacial outwash by analysis of slug tests with oscillatory response, Cape Cod, Massachusetts, *in* Mallard, G., and Aronson, D., eds., Toxic substances hydrology program—Proceedings of the technical meeting, Monterey, California, March 11–15, 1991: U.S. Geological Survey Water Resources Investigations Report 91-4034, p. 36–40.

SRK Consulting, 2017, 2016 carbonate aquifer test report—Long Canyon Mine: Nevada, SRK Consulting, 256 p.

Stute, M., and Schlosser, P., 2000, Atmospheric noble gases, *in* Cook, P.G., and Herczeg, A.L., eds., Environmental tracers in subsurface hydrology: Boston, Kluwer Academic Publishers, p. 349–377. [Also available at https://doi.org/10.1007/978-1-4615-4557-6_11.]

Sweetkind, D.S., Cederberg, J.R., Masbruch, M.D., and Buto, S.G., 2010, Hydrogeologic framework, chap. B *of* Heilweil, V.M., and Brooks, L.E., eds., Conceptual model of the Great Basin carbonate and alluvial aquifer system: U.S. Geological Survey Scientific Investigations Report 2010–5193, p. 15–50. [Also available at https://pubs.usgs.gov/sir/2010/5193/.]

Theis, C.V., 1935, The relation between the lowering of the piezometric surface and the rate and duration of discharge of a well using groundwater storage: Eos—Transactions, American Geophysical Union, v. 16, no. 2, p. 519–524. [Also available at https://doi.org/10.1029/TR016i002p00519.]

Thorman, C.H., 1970, Metamorphosed and nonmetamorphosed Paleozoic rocks in the Wood Hills and Pequop Mountains, northeast Nevada: Geological Society of America Bulletin, v. 81, no. 8, p. 2417–2448. [Also available at https://doi.org/10.1130/0016-7606(1970)81[2417:MANPRI]2.0.CO;2.]

U.S. Geological Survey, 2018, General introduction for the "National field manual for the collection of water-quality data" (ver. 1.1, June 2018): U.S. Geological Survey Techniques and Methods, book 9, chap. A0, 4 p. [Also available at https://doi.org/10.3133/tm9A0.]

U.S. Geological Survey, 2019, USGS National Water Information System—Web interface: U.S. Geological Survey National Water Information System database, accessed December 2019, at https://dx.doi.org/10.5066/F7P55KJN.

Walton, W.C., 2008, Upgrading aquifer test analysis: Ground Water, v. 46, p. 660–662. [Also available at https://doi.org/10.1111/j.1745-6584.2008.00442.x.]

Welch, A.H., Bright, D.J., and Knochenmus, L.A., eds., 2007, Water resources of the Basin and Range carbonate-rock aquifer system, White Pine County, Nevada, and adjacent areas in Nevada and Utah, U.S. Geological Survey Scientific Investigations Report 2007–5261, 96 p.

Welch, A.H., and Preissler, A.M., 1986, Aqueous geochemistry of the Bradys Hot Springs geothermal area, Churchill County, Nevada, *in* Selected papers in the hydrological sciences: U.S. Geological Survey Water-Supply Paper, v. 2290, p. 17–36.

Western Regional Climate Center, 2019, Pequop, Nevada (266148) and Oasis, Nevada (265722): Western Regional Climate Center database, accessed December 22, 2019, at https://wrcc.dri.edu/cgi-bin/cliMAIN.pl?nv6148 and https://wrcc.dri.edu/cgi-bin/cliMAIN.pl?nv5722.

Wildlife Action Plan Team, 2012, Nevada wildlife action plan: Reno, Nevada Department of Wildlife.

Yobbi, D.K., and Halford, K.J., 2008, Numerical simulation of aquifer tests, west-central Florida (revised): U.S. Geological Survey Scientific Investigations Report 2005–5201, 85 p. [Also available at https://pubs.usgs.gov/sir/2005/5201/.]

Publishing support provided by the U.S. Geological Survey
Science Publishing Network, Tacoma Publishing Service Center

For more information concerning the research in this report, contact the
Director, Oregon Water Science Center
U.S. Geological Survey
2130 SW 5th Avenue
Portland, Oregon 97201
https://www.usgs.gov/centers/or-water

ISSN 2328-0328 (online)
https://doi.org/10.3133/sir20215021